Dynamic Analysis of Steel Confined Concrete Tubular Columns against Blast Loads

Fangrui Zhang
Bachelor of Engineering (Civil & Structural) (Hons)

Thesis submitted for the degree of Doctor of Philosophy at The University of Adelaide, Australia

The School of Civil, Environmental and Mining Engineering

January 2017

Table of Contents

Abstract

The use of composite construction has drawn more and more attention in recent decades. This thesis contains a number of journal articles which aim to enrich the knowledge of the performance of concrete filled tubular columns when subjected to blast loading. Experimental investigations are used in conjunction with numerical analysis to provide a thorough assessment of the blast-resistance of concrete filled tubular columns.

The first chapter mainly focuses on the experimental study on concrete filled tubular columns under blast loading. A large-scale blast experimental program is carried out on concrete filled double-skin steel tube (CFDST) columns. The blast experiment aims to examine the blast-resistance of ten CFDST specimens, including five with square cross-section and the other five with circular cross-section. The parameters that are investigated during the blast experiment include: cross-sectional geometry, explosive charge weight and magnitude of axial load. After the experiment, several damaged test specimens are then transported back to the laboratory for residual axial load-carrying capacity tests. The proposed CFDST columns are able to retain more than 60% of its axial load-carrying capacity even after being subjected to close-range explosion.

As blast experiments are often costly and associated with potential safety concerns, numerical tools have been adopted by more and more researchers. In the second chapter of the thesis, numerical approaches in modelling the dynamic behaviour of concrete filled steel tube (CFST) columns and CFDST columns under blast loading are presented. The numerical models are validated against the results of the blast experiment as described in the first chapter and good agreement is achieved. Parametric studies on the effect of column dimensions and material properties are also discussed through intensive numerical simulations.

In the last chapter, a numerical method to generate pressure-impulse diagrams for CFDST columns is proposed which uses a damage criterion involving the residual axial

load-carrying capacity. Based on the numerical method, pressure-impulse diagrams for different column configurations are derived and analytical expressions of deriving pressure-impulse diagrams for CFDST columns are also developed through regression analysis.

Statement of Originality

I certify that this work contains no material which has been accepted for the award of any other degree or diploma in my name, in any university or other tertiary institution and, to the best of my knowledge and belief, contains no material previously published or written by another person, except where due reference has been made in the text. In addition, I certify that no part of this work will, in the future, be used in a submission in my name, for any other degree or diploma in any university or other tertiary institution without the prior approval of the University of Adelaide and where applicable, any partner institution responsible for the joint-award of this degree.

I give consent to this copy of my thesis when deposited in the University Library, being made available for loan and photocopying, subject to the provisions of the Copyright Act 1968.

The author acknowledges that copyright of published works contained within this thesis resides with the copyright holder(s) of those works.

I also give permission for the digital version of my thesis to be made available on the web, via the University's digital research repository, the Library Search and also through web search engines, unless permission has been granted by the University to restrict access for a period of time.

I acknowledge the support I have received for my research through the provision of an Australian Government Research Training Program Scholarship.

……	……	……..……
Print Name	Signature	Date

List of publications

1. Zhang, F., Wu, C., Zhao, X.-L., Xiang, H., Li, Z.-X., Fang, Q., Liu, Z., Zhang, Y., Heidarpour, A. & Packer, J. A. 2016. Experimental study of CFDST columns infilled with UHPC under close-range blast loading. *International Journal of Impact Engineering*.
   Status: Published

2. Zhang, F., Wu, C., Li, Z.-X. & Zhao, X.-L. 2015. Residual axial capacity of CFDST columns infilled with UHPFRC after close-range blast loading. *Thin-Walled Structures,* 96**,** 314-327.
   Status: Published

3. Zhang, F., Wu, C., Wang, H. & Zhou, Y. 2015. Numerical simulation of concrete filled steel tube columns against BLAST loads. *Thin-Walled Structures,* 92**,** 82-92.
   Status: Published

4. Zhang, F., Wu, C., Zhao, X.-L., Li, Z.-X., Heidarpour, A. & Wang, H. 2015. Numerical modeling of concrete-filled double-skin steel square tubular columns under blast loading. *Journal of Performance of Constructed Facilities,* 29**,** B4015002.
   Status: Published

5. Zhang, F., Wu, C., Zhao, X.L., Heidarpour, A. and Li, Z., 2016. Experimental and numerical study of blast resistance of square CFDST columns with steel-fibre reinforced concrete. *Engineering Structures*.
   Status: Published

6. Numerical derivation of pressure-impulse diagrams for square UHPCFDST columns
   Status: Submitted to *Thin-walled Structures*

Acknowledgements

My sincerest gratitude goes to Professor Chengqing Wu, whose knowledge in the field of structural responses to blast loadings knows no bounds. For his willingness to provide guidance and assistance, no matter what day of the week it is, I am also extremely grateful for.

I would also like to thank Dr Terry Bennet and Professor Xiao-Ling Zhao, who were always willing to provide their expertise when needed. Also, my friends and family deserve my thanks and much more, for their patience and support. Finally, I dedicate this thesis to my wife, Ye Xia, who has provided me with the confidence and support to complete this thesis to the best of my abilities.

Introductory Background

CFST & CFDST columns

The concept of concrete filled steel tubular (CFST) columns can be traced back to as early as 1960s [1-3]. However, the use of CFST columns in actual construction was very limited due to the fact that concrete casting for CFST columns during that time was laborious and costly. Therefore, CFST columns were rarely considered until 1980s when the concrete pumping technique was matured. Nowadays, CFST columns have been widely used in the construction industry across the world. Some typical examples of using CFST columns include the Latitude building in Sydney, the SEG Plaza in Shenzhen and the Otemachi tower in Tokyo.

(a) (b)

Fig. 1: The typical cross section of (a) a circular CFST (left) and (b) a circular CFDST (right)

CFST columns, as shown in Fig. 1(a), have a number of advantages in comparison to conventional RC columns or steel columns [4]: 1) the confining pressure provided by the steel tube put the concrete filler under a tri-axial stress state therefore the strength and ductility of concrete can be significantly enhanced; 2) Local buckling of the steel tube is delayed by the concrete filler and on the other hand, concrete spalling is delayed by the steel tube; 3) The steel tube is able to develop its full strength under bending since it is located at the outermost of the cross-section; 4) The steel tube can be directly used as formwork and concrete casting is done by pumping method which leads to a cleaner construction site and a reduction in project length and cost.

A large number of studies have been carried out to investigate the behaviours of CFST columns under a variety of loading conditions through experimental, analytical or numerical methods.

Extensive experimental studies have been carried out to investigate the behaviour of CFST columns under axial compression [5-7]. Parameters such as the cross-section shapes, diameter-to-thickness (D/t) ratio, concrete and steel strengths were discussed thoroughly and based on the results, a number of finite element models and analytical formulae were proposed to predict the axial load-carrying capacity of CFST columns.

Elchalakani et al. [8] subjected 12 circular CFST specimens to pure bending. The bond between concrete filler and steel tube was studied and reported to have little effect on the strength of CFST columns under flexure. A simplified formula to determine the ultimate bending capacity of circular CFSTs was also derived based on plastic stress blocks and was shown to agree with experimental results.

Uy et al. [9] compared some test data to the predictions made by the four commonly used international design codes. It was reported that all four codes underestimated the load-carrying capacity of CFST columns both under axial compression and combined loading condition. There is therefore, a need for a new standard or some modifications of existing codes.

A unified theory was presented by [10-14] which can be used to predict the behaviours of CFST columns under axial compression, flexural bending or combined loading condition. In this theory, a confinement factor (ξ), which is a function of cross-section area and material strength, was introduced to describe the composite action between the steel tube and concrete filler. When validated against some test results, good correlation was achieved.

Prichard [15] conducted a series of axial-direction drop hammer tests, with impact velocity ranging from 3.2 m/s to 6.3 m/s, on concrete cylinders, passively confined by

sleeves of steel, aluminium and plastic. CFST cylinders were found to have higher strength and better crack control over the other two types. Xiao [16] further explored the effectiveness of using carbon fibre reinforced polymer as the additional external confining layer to improve the performance of CFSTs under axial impact loads.

Bambach et al. [17] presented an experimental and analytical investigation of hollow and CFST square beams subjected to transverse impacts with cross-section width ranging from 20 mm to 50 mm. It was reported that concrete filler precluded the formation of local buckling beneath/near the impactor and thus significantly increased the section moment capacity. Deng et al. [18] investigated simply-supported circular CFST under impact loading and the failure mode was carefully observed. It was reported that failure mode for steel tubes was mainly tensile facture along the circumference and for concrete filler was mainly crushing under compression and spalling under tension around the impact area.

Han [19] proposed a simplified analytical formulae to calculate the dynamic flexural capacity for circular CFST columns based on results from an experimental program and numerical parametric studies.

In addition to CFST columns, concrete filled double-skin steel tube (CFDST) columns (as shown in Fig. 1(b)), which was developed based on the concept of CFST, has also gained much attention in recent years. CFDST columns are structurally similar to CFST columns except it is made from two concentrically placed steel tubes, instead of one in CFST columns, filled with concrete in-between. Extensive studies have also been undertaken in terms of the static and dynamic behaviours of CFDST columns under different loads and the behaviours of CFDST columns are very similar to those of CFST columns.

Wei et al. [20] reported the investigation of 26 circular CFDST stub columns under axial compression and it was found that the axial load capacity of a CFDST stub column

was usually 10%-30% larger than the simply superposed capacity of steel tubes and concrete filler when acting alone.

Uenaka et al. [21] and Zhao et al. [22] also undertook a series of tests on circular CFDST stub columns subjected to axial compression with different D/t ratios, slenderness ratios, hollow section areas and material strengths. The main failure mode of CFDST columns under axial compression was found to be multiple buckling of steel tubes associated with concrete cracks due to shear compression failure. Analytical equations were also derived to predict the ultimate axial capacity of CFDST columns and good agreement was achieved between the test results and the estimated strengths.

Comprehensive studies of the flexural capacity of CFDST beam-columns with circular and square cross-sections have also been carried out [23, 24]. It was reported that the energy-absorbing ability of CFDST columns with circular cross-sections was superior to that of the specimens with square cross-sections and the behaviour of CFDST columns during the experiment is very similar to that of CFST columns as discussed in [12, 14]. From the test results, an analytical formula was developed to predict the response of CFDST beam-columns under combined axial load and cyclically increasing flexural load.

A lot of effort was also made to probe into the tensile behaviour [25, 26], torsional behaviour [27] and fire resistance [28] of CFDST columns. Experiments and numerical analysis were conducted to explore the behaviour of tapered CFDST columns under concentric and eccentric axial compression as well [29, 30].

The use of UHPFRC

The previously mentioned studies indicate that CFDST members inherit the advantages of CFST columns while having a smaller self-weight and that they exhibit very ductile behaviour under axial compressive as well as transverse loading. However, the concrete filler used in most of the existing literatures and design codes of either CFST or CFDST members are limited to normal strength concrete only, and the topic of using

ultra-high performance fibre-reinforced concrete (UHPFRC) has been barely discussed. It is well known that UHPFRC has been more and more commonly used in the field of civil engineering applications due to its superior high strength. Since CFDST members are widely used in constructing super high-rise buildings, underground tunnels and bridge piers, where large axial load-carrying capacity is required, replacing the normal-strength concrete filler by UHPFRC can lead to a significant reduction in the self-weight of CFDST members. In addition, owing to the presence of fibres, crushing and spalling damage of the concrete can be better restrained thus can further delay the local buckling of steel tubes. Although several studies have investigated CFST members filled with high-strength concrete [31, 32], very little information can be found in regard to CFDST members filled with UHPFRC.

The investigation of blast loading

Furthermore, over the past few decades, terrorist attacks, such as the infamous 9/11 world trade centre attack and the most recent Brussels airport attack, on structures has led engineers and researchers to put more effort in assessing the vulnerability of buildings and important infrastructures under hazardous loadings, and in this context, explosions. While most research focus has been placed on the conventional structures, namely reinforced concrete (RC) structures and steel structures, little resources have been allocated to other structure types. Therefore, there exists a need to investigate into the blast-resistance of the newly developed structure types and in this context, concrete filled tubular columns.

Various methods exist for analysing the dynamic response of structural members subjected to blast loading and among which, experimental investigation, single degree of freedom (SDOF) analysis and numerical analysis are the three most popular.

The simplest method is SDOF analysis since it converts the entire structural member into a SDOF system, relying on various transformation factors, and only provides the deflection response of the mid-span of the member. Many studies have shown that SDOF

analysis provides an easy means to predict the structural response under blast loading [33-35]. However, SDOF analysis cannot accurately incorporate the strain-rate effect therefore is likely to underestimate the structural damage under impulsive loading, and is incapable of accounting for different failure modes since its damage criterion is either based on the maximum structural deflection or end rotation.

Experimental investigations are able to provide more intuitive observation of structural members subjected to blast loading. However, as experiments are often associated with issues such as safety concern, budget control and time constraints, normally only a limited number of parameters can be investigated. As a result, the findings discovered by one researcher often cannot be directly used by another if a different column dimension or material property is adopted.

The third common method, namely numerical analysis, uses three-dimensional meshes to determine the dynamic response of a structural member over time. Nowadays, numerical tools are widely used to analyse situations where complex loading conditions and/or interaction between materials are involved. This method has demonstrated its ability to provide robust predictions of the dynamic response of different structural members subjected to blast loading, especially when used in conjunction with experimental results [36-43].

The pressure-impulse diagram, as shown in Fig. 2, is usually used to quickly assess whether a structural member fails or survives a blast event in preliminary design. It represents a group of loading histories (e.g. blast load) that cause the same level of damage to a structural component. It can be used to assess the damage in a structural component or even the blast-induced human injury [44, 45].

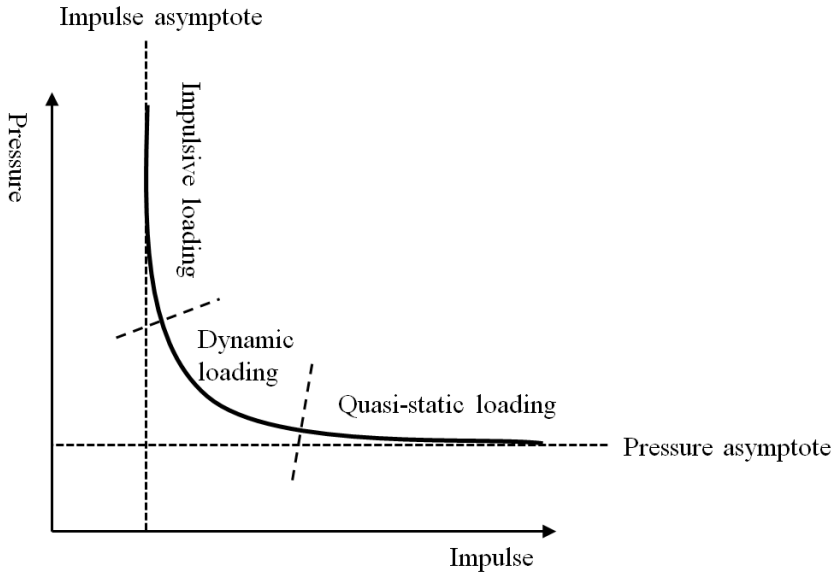

Fig. 2: A typical pressure-impulse diagram

Although the use of a pressure-impulse diagram is efficient, the derivation of a pressure-impulse diagram is usually very difficult since it involves a significantly time-consuming trial and error process as shown in Fig. 3, which makes it almost unrealistic to be experimentally derived. Therefore, analytical and numerical methods are commonly used to obtain the pressure-impulse diagrams for a structural component.

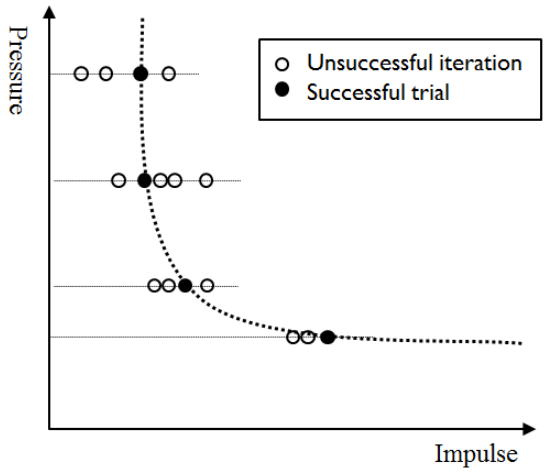

Fig. 3: The method to generate a pressure-impulse diagram

Fallah and Louca [46] proposed a SDOF model based on a bi-linear resistance-deflection function which can be used to derive Pressure-impulse diagrams. Dragos et al. [47] developed a finite element model to predict the pressure-impulse diagram of UHPC members. The model was validated against blast tests and the results showed reasonably good agreement. Shi et al. [48] derived pressure-impulse diagrams

numerically for RC columns with different parameters. Based on a regression analysis of the numerical results, mathematical formulas were proposed to predict the pressure-impulse diagrams of RC columns at different damage levels.

Research gaps and objectives

It can be concluded from the literature review that there are several key knowledge gaps in CFST and CFDST columns that need to be filled:

- Most existing open literature only investigate the behaviours of CFST and CFDST columns under static loading (e.g. uniaxial compression test, flexural test), the knowledge of their behaviours under dynamic loading, especially blast loading, is still relatively lacking.
- Most CFST and CFDST columns are filled with normal strength concrete, and the use of UHPC is very rare which requires more investigation as UHPFRC is becoming more and more popular in the construction industry.
- Although there are a number of numerical studies of CFST columns under transverse impact loading, there is a lack of numerical investigations of CFST and CFDST columns under blast loading, especially when filled with UHPFRC.
- There is a lack of efficient means (i.e. pressure-impulse diagram) to quickly assess the vulnerability/survivability of CFST and CFDST columns under blast loading.

This thesis aims to address those identified knowledge gaps. It contains a number of manuscripts which have been published in, or accepted in, or submitted to, internationally recognised journals. Each chapter contains an introduction, explaining the aims and how the papers fit together, and each manuscript.

Chapter 1 contains two journal articles which report a series of laboratory and field experiments on ultra-high performance concrete filled double-skinned tube (UHPCFDST) columns. Firstly, a number of laboratory tests are carried out to obtain the material

properties, namely compressive strength and flexural tensile strength of UHPC, yield and ultimate strength of steel tubes. Also, uniaxial compression tests and three point bending tests are also conducted to investigate the behaviours of UHPCFDST under axial and flexural loading, respectively. Furthermore, a field experiment is then carried out to examine the blast-resistance of ten UHPCFDST specimens, including five with square cross-section and the other five with circular cross-section. In addition, one square and one circular ultra-high performance concrete filled steel tube (UHPCFST) specimens are also included to check the dissimilarities when compared with their double-skinned counterparts. The parameters that are investigated in the blast tests include: cross-sectional geometry, explosive charge weight and magnitude of axial load. Finally, some of the specimens used in the blast experiment are transported back to the lab for residual axial load-carrying capacity test.

Chapter 2 contains four journal papers which present numerical studies on CFST and CFDST columns under blast loading. Numerical models for CFST and CFDST columns are developed by using the finite element tool LS-DYNA. These numerical models are then validated against the blast experiments as mentioned in Chapter 1 and good agreement is achieved. Moreover, a parametric study is carried out to investigate the influence of the geometrical properties on the blast-resistance of CFDST columns.

Based on the numerical model proposed within chapter 2, chapter 3 presents a numerical method to generate pressure-impulse diagrams for UHPCFDST columns. Analytical expressions for pressure-impulse diagrams of UHPCFDST columns are also developed through regression analysis.

References

[1] Furlong, RW, *Strength of steel-encased concrete beam columns.* Journal of the Structural Division, 1967. **93**(5): p. 113-124.

[2] Gardner, NJ and Jacobson, ER, *Structural behavior of concrete filled steel tubes.* ACI Structural Journal, 1967. **64**(7): p. 404-413.

[3] Knowles, RB and Park, R, *Strength of concrete filled steel tubular columns.* Journal of the Structural Division, 1969. **95**(12): p. 2565-2588.

[4] Morino, S and Tsuda, K, *Design and construction of concrete-filled steel tube column system in Japan.* Earthquake Engineering and Engineering Seismology, 2003. **4**(1): p. 51-73.

[5] Schneider, SP, *Axially loaded concrete-filled steel tubes.* Journal of Structural Engineering, 1998. **124**(10): p. 1125-1138.

[6] Zhao, X-L, Grzebieta, R, and Lee, C, *Void-filled cold-formed rectangular hollow section braces subjected to large deformation cyclic axial loading.* Journal of Structural Engineering, 2002. **128**(6): p. 746-753.

[7] Sakino, K, Nakahara, H, Morino, S, and Nishiyama, I, *Behavior of centrally loaded concrete-filled steel-tube short columns.* Journal of Structural Engineering, 2004. **130**(2): p. 180-188.

[8] Elchalakani, M, Zhao, X-L, and Grzebieta, R, *Concrete-filled circular steel tubes subjected to pure bending.* Journal of Constructional Steel Research, 2001. **57**(11): p. 1141-1168.

[9] Uy, B, Tao, Z, and Han, L-H, *Behaviour of short and slender concrete-filled stainless steel tubular columns.* Journal of Constructional Steel Research, 2011. **67**(3): p. 360-378.

[10] Han, L-H, Zhao, X-L, and Tao, Z, *Tests and mechanics model for concrete-filled SHS stub columns, columns and beam-columns.* Steel and Composite Structures, 2001. **1**(1): p. 51-74.

[11] Han, L-H, *Tests on stub columns of concrete-filled RHS sections.* Journal of Constructional Steel Research, 2002. **58**(3): p. 353-372.

[12] Han, L-H, Yang, Y-F, and Tao, Z, *Concrete-filled Thin-walled Steel SHS and RHS Beam-columns Subjected to Cyclic Loading.* Thin-Walled Structures, 2003. **41**(9): p. 801-833.

[13] Han, L-H, Yao, G-H, and Zhao, X-L, *Behavior and calculation on concrete-filled steel CHS (Circular Hollow Section) beam-columns.* Steel and Composite Structures, 2004. **4**(3): p. 169-188.

[14] Han, L-H and Yang, Y-F, *Cyclic Performance of Concrete-filled Steel CHS Columns under Flexural Loading.* Journal of Constructional Steel Research, 2005. **61**(4): p. 423-452.

[15] Prichard, S and Perry, S, *The impact behaviour of sleeved concrete cylinders.* Structural Engineer, 2000. **78**(17): p. 23-7.

[16] Xiao, Y and Shen, Y, *Impact Behaviors of CFT and CFRP Confined CFT Stub Columns.* Journal of Composites for Construction, 2012. **16**(6): p. 662-670.

[17] Bambach, M, Jama, H, Zhao, X, and Grzebieta, R, *Hollow and concrete filled steel hollow sections under transverse impact loads.* Engineering Structures, 2008. **30**(10): p. 2859-2870.

[18] Deng, Y, Tuan, CY, and Xiao, Y, *Flexural behavior of concrete-filled circular steel tubes under high-strain rate impact loading.* Journal of Structural Engineering, 2011. **138**(3): p. 449-456.

[19] Han, L-H, Hou, C-C, Zhao, X-L, and Rasmussen, KJ, *Behaviour of high-strength concrete filled steel tubes under transverse impact loading.* Journal of Constructional Steel Research, 2014. **92**: p. 25-39.

[20] Wei, S, Mau, S, Vipulanandan, C, and Mantrala, S, *Performance of New Sandwich Tube under Axial Loading: Experiment.* Journal of Structural Engineering, 1995. **121**(12): p. 1806-1814.

[21] Uenaka, K, Kitoh, H, and Sonoda, K, *Concrete Filled Double Skin Circular Stub Columns under Compression.* Thin-Walled Structures, 2010. **48**(1): p. 19-24.

[22] Zhao, X-L, Tong, L-W, and Wang, X-Y, *CFDST stub columns subjected to large deformation axial loading.* Engineering Structures, 2010. **32**(3): p. 692-703.

[23] Han, L-H, Huang, H, Tao, Z, and Zhao, X-L, *Concrete-filled Double Skin Steel Tubular (CFDST) Beam–columns Subjected to Cyclic Bending.* Engineering Structures, 2006. **28**(12): p. 1698-1714.

[24] Han, L-H, Huang, H, and Zhao, X-L, *Analytical behaviour of concrete-filled double skin steel tubular (CFDST) beam-columns under cyclic loading.* Thin-Walled Structures, 2009. **47**(6): p. 668-680.

[25] Li, W, Han, L-H, and Chan, T-M, *Tensile behaviour of concrete-filled double-skin steel tubular members.* Journal of Constructional Steel Research, 2014. **99**: p. 35-46.

[26] Li, W, Han, L-H, and Chan, T-M, *Numerical investigation on the performance of concrete-filled double-skin steel tubular members under tension.* Thin-Walled Structures, 2014. **79**: p. 108-118.

[27] Huang, H, Han, L-H, and Zhao, X-L, *Investigation on concrete filled double skin steel tubes (CFDSTs) under pure torsion.* Journal of Constructional Steel Research, 2013. **90**: p. 221-234.

[28] Lu, H, Zhao, X-L, and Han, L-H, *Testing of self-consolidating concrete-filled double skin tubular stub columns exposed to fire.* Journal of Constructional Steel Research, 2010. **66**(8): p. 1069-1080.

[29] Li, W, Ren, Q-X, Han, L-H, and Zhao, X-L, *Behaviour of tapered concrete-filled double skin steel tubular (CFDST) stub columns.* Thin-walled structures, 2012. **57**: p. 37-48.

[30] Li, W, Han, L-H, Ren, Q-X, and Zhao, X-L, *Behavior and calculation of tapered CFDST columns under eccentric compression.* Journal of Constructional Steel Research, 2013. **83**: p. 127-136.

[31] Varma, AH, Ricles, JM, Sause, R, and Lu, L-W, *Experimental behavior of high strength square concrete-filled steel tube beam-columns.* Journal of Structural Engineering, 2002. **128**(3): p. 309-318.

[32] Liew, J and Xiong, D, *Experimental investigation on tubular columns infilled with ultra-high strength concrete.* 2010.

[33] Ye, Z and Ma, G, *Effects of Foam Claddings for Structure Protection against Blast Loads.* Journal of Engineering Mechanics, 2007. **133**(1): p. 41-47.

[34] Ma, G and Ye, Z, *Analysis of Foam Claddings for Blast Alleviation.* International Journal of Impact Engineering, 2007. **34**(1): p. 60-70.

[35] Xia, Y, Wu, C, and Li, Z-X, *Optimized Design of Foam Cladding for Protection of Reinforced Concrete Members under Blast Loading.* Journal of Structural Engineering, 2014. **141**(9): p. 06014010.

[36] Qu, H, Li, G, Chen, S, Sun, J, and Sozen, MA, *Analysis of Circular Concrete-Filled Steel Tube Specimen under Lateral Impact.* Advances in

Structural Engineering, 2011. **14**(5): p. 941-952.
[37] Deng, Y and Tuan, CY, *Design of Concrete-Filled Circular Steel Tubes under Lateral Impact.* ACI Structural Journal, 2013. **110**(4): p. 691.
[38] Wang, R, Han, L-H, and Hou, C-C, *Behavior of concrete filled steel tubular (CFST) members under lateral impact: Experiment and FEA model.* Journal of Constructional Steel Research, 2013. **80**: p. 188-201.
[39] Yousuf, M, Uy, B, Tao, Z, Remennikov, A, and Liew, J, *Transverse impact resistance of hollow and concrete filled stainless steel columns.* Journal of Constructional Steel Research, 2013. **82**: p. 177-189.
[40] Mao, L, Barnett, S, Begg, D, Schleyer, G, and Wight, G, *Numerical simulation of ultra high performance fibre reinforced concrete panel subjected to blast loading.* International Journal of Impact Engineering, 2014. **64**: p. 91-100.
[41] Ngo, T, Mohotti, D, Remennikov, A, and Uy, B, *Numerical simulations of response of tubular steel beams to close-range explosions.* Journal of Constructional Steel Research, 2015. **105**: p. 151-163.
[42] Li, J, Wu, C, and Hao, H, *An experimental and numerical study of reinforced ultra-high performance concrete slabs under blast loads.* Materials & Design, 2015. **82**: p. 64-76.
[43] Xia, Y, Wu, C, Zhang, F, Li, Z-X, and Bennett, T, *Numerical Analysis of Foam-Protected RC Members Under Blast Loads.* International Journal of Protective Structures, 2014. **5**(4): p. 367-390.
[44] Baker, WE, Cox, P, Kulesz, J, Strehlow, R, and Westine, P, *Explosion hazards and evaluation*. 2012: Elsevier.
[45] Mays, G, *Blast effects on buildings: design of buildings to optimize resistance to blast loading*. 1995: Thomas Telford.
[46] Fallah, AS and Louca, L, *Pressure–impulse diagrams for elastic-plastic-hardening and softening single-degree-of-freedom models subjected to blast loading.* International Journal of Impact Engineering, 2007. **34**(4): p. 823-842.
[47] Dragos, J, Wu, C, Haskett, M, and Oehlers, D, *Derivation of Normalized Pressure Impulse Curves for Flexural Ultra High Performance Concrete Slabs.* Journal of Structural Engineering, 2012. **139**(6): p. 875-885.
[48] Shi, Y, Hao, H, and Li, Z-X, *Numerical Derivation of Pressure–Impulse Diagrams for Prediction of RC Column Damage to Blast Loads.* International Journal of Impact Engineering, 2008. **35**(11): p. 1213-1227.

Chapter 1 – Experimental Investigation of CFDST Columns under Close-range Blast Loading

Introduction

In this chapter, experimental investigations are carried out to report a series of laboratory and field experiments on ultra-high performance concrete filled double-skinned tube (UHPCFDST) columns.

Firstly, in the paper entitled "Experimental study of CFDST columns infilled with UHPC under close-range blast loading", a field experiment is carried out to examine the blast-resistance of ten UHPCFDST specimens, including five with square cross-section and the other five with circular cross-section. In addition, one square and one circular ultra-high performance concrete filled steel tube (UHPCFST) specimens are also included to check the dissimilarities when compared with their double-skinned counterparts. The parameters that are investigated in the blast tests include: cross-sectional geometry, explosive charge weight and magnitude of axial load.

Within the paper entitled "Residual axial capacity of CFDST columns infilled with UHPFRC after close-range blast loading", static tests, such as uniaxial compression tests and three point bending tests, are conducted to investigate the behaviours of UHPCFDST under axial and flexural loading. In addition, some of the specimens used during the blast experiment are transported back to the lab for residual axial load-carrying capacity test.

Statement of Authorship

Title of Paper	Experimental study of CFDST columns infilled with UHPC under close-range blast loading
Publication Status	☑ Published ☐ Accepted for Publication ☐ Submitted for Publication ☐ Unpublished and Unsubmitted w ork w ritten in manuscript style
Publication Details	Zhang, F., Wu, C., Zhao, X.-L., Xiang, H., Li, Z.-X., Fang, Q., Liu, Z., Zhang, Y., Heidarpour, A. & Packer, J. A. 2016. Experimental study of CFDST columns infilled with UHPC under close-range blast loading. *International Journal of Impact Engineering*.

Principal Author

Name of Principal Author (Candidate)	Fangrui Zhang		
Contribution to the Paper	The author helped conduct tests, processed and analysed test data and prepared manuscript.		
Overall percentage (%)	60%		
Certification:	This paper reports on original research I conducted during the period of my Higher Degree by Research candidature and is not subject to any obligations or contractual agreements with a third party that would constrain its inclusion in this thesis. I am the primary author of this paper.		
Signature		Date	

Co-Author Contributions

By signing the Statement of Authorship, each author certifies that:

i. the candidate's stated contribution to the publication is accurate (as detailed above);

ii. permission is granted for the candidate in include the publication in the thesis; and

iii. the sum of all co-author contributions is equal to 100% less the candidate's stated contribution.

Name of Co-Author	Chengqing Wu		
Contribution to the Paper	This co-author supervised research and tests, provided critical manuscript evaluation and acted as corresponding author.		
Signature		Date	6/6/2016

Name of Co-Author	Xiao-Ling Zhao		
Contribution to the Paper	This co-author provided critical manuscript evaluation		
Signature		Date	05/06/16

Name of Co-Author	Hengbo Xiang		
Contribution to the Paper	This co-author helped design and conduct tests.		
Signature		Date	June. 6. 2016

Name of Co-Author	Zhong-Xian Li		
Contribution to the Paper	This co-author helped design and conduct tests.		
Signature		Date	2016. 6. 6

Name of Co-Author	Qin Fang		
Contribution to the Paper	This co-author helped design and conduct tests.		
Signature		Date	June 6. 2016

Name of Co-Author	Zhongxian Liu		
Contribution to the Paper	This co-author helped design and conduct tests.		
Signature		Date	2016. 6. 5

Name of Co-Author	Yadong Zhang		
Contribution to the Paper	This co-author helped design and conduct tests.		
Signature		Date	June. 6. 2016

Name of Co-Author	Amin Heidarpour		
Contribution to the Paper	This co-author helped design and conduct tests.		
Signature		Date	5. Jun. 2016

Name of Co-Author	Jeffrey A. Packer
Contribution to the Paper	This co-author helped design and conduct tests, provided manuscript evaluation.
Signature	Date: June 5, 2016

EXPERIMENTAL STUDY OF CFDST COLUMNS INFILLED WITH UHPC UNDER CLOSE-RANGE BLAST LOADING

Fangrui Zhang, Chengqing Wu, Xiao-Ling Zhao, Hengbo Xiang, Zhong-Xian Li, Qin Fang, Zhongxian Liu, Yadong Zhang, Amin Heidarpour, Jeffrey A. Packer

Abstract

Concrete-filled double-skin tubes (CFDST) have been increasingly popular in the field of engineering in recent years. A lot of research has been carried out to investigate the behaviour of CFDST members under a variety of loading conditions. This paper presents an experimental investigation on ultra-high performance concrete infilled double-skin tube columns subjected to close-in blast loading. Two types of CFDST columns were investigated in the experiments – one with both inner and outer tubes circular and the other one with both square. The main test parameters included the explosive charge weight and the magnitude of axial load. After the blast tests, there was no visible buckling nor ruptures found on the steel tubes and only minor cracks, of no more than 1mm width, were observed in the core concrete when the outer steel tube was removed. Based on the findings of the experiments, it is evident that CFDST column has excellent blast resistance. This feature has the potential to be used in high-value structures which may be the targets of terrorist attacks, such as embassies, government buildings and critical infrastructures.

***Keywords**:* CFDST columns, Ultra-high-performance concrete, Blast loading

1. Introduction

In the past decades, thousands of lives have been lost all over the world due to terrorist activities. Much research has been carried out, aiming to improve the reliability of vulnerable structures so as to reduce the number of human casualties. A number of studies have discussed retrofitting techniques to protect existing structures [1-3] while others have

proposed the use of innovative structures and materials of higher strength to construct new buildings [4-7]. In recent years, a new steel-concrete composite member, known as a concrete-filled double-skin steel tube (CFDST), has gained interest in the construction industry due to its attractive properties such as ease of construction, light weight, high strength and good seismic resistance.

A CFDST member is simply made from two concentrically placed steel skins filled with concrete in between and it utilises the advantages of both steel and concrete. Under axial compression, due to the different Poisson's ratio of steel and concrete, the concrete of a CFDST column is normally in a tri-axially confined state and consequently the confining pressures can effectively enhance the strength and the ductility of the concrete which is known as the confinement effect. Wei et al. [8] reported the investigation on 26 circular CFDST stub columns under axial compression and it was found that the axial load capacity of a CFDST stub column was usually 10%–30% larger than the simply superposed capacity of the steel tubes and core concrete when acting alone. Following references [9, 10] the failure mode of CFDST stub columns under axial compression was also investigated: the most dominant failure mode was found to be local buckling of the outer steel tube associated with concrete shear failure; also, the outer diameter to steel-tube-thickness ratio had the most significant influence on the failure mode. Analytical models have also been derived, based on a large number of experiments, to predict the behaviour of CFDST members under axial compression and these have showed good agreement with the test results [11-13].

On the other hand, studies have also been carried out to examine the performance of CFDST members under transverse cyclic load [14, 15]. In the experiments, different cross-sectional geometries were compared and it was found that the energy-absorbing ability of the CFDST columns with circular cross-sections was superior to those of the specimens with square cross-sections. From the test results, an analytical model was also

developed to predict the response of CFDST beam-columns under combined axial load and cyclically increasing flexural load. Efforts were also put into studying the tensile behaviour [16, 17], torsional behaviour [18] and fire resistance of CFDST columns [19]. Experiments and numerical analyses were also carried out to explore the behaviour of tapered CFDST members under concentric and eccentric axial compression [20, 21].

All of the previously mentioned studies indicate that CFDST members inherit the advantages of both steel and concrete and that they exhibit very ductile behaviour under axial compressive as well as transverse loading. However, most existing studies are strictly limited to static loading only, thus the analytical models developed cannot be applied to evaluate situations where impact and blast loads are introduced. Therefore, there is a need to evaluate the performance of CFDST members subjected to impact and blast loads. Furthermore, as CFDST members has been more and more commonly adopted in the field of civil engineering applications, where large axial bearing capacity is required. Therefore, by replacing normal strength concrete by UHPC in CFDST members, the cross-section area as well as the self-weight of the structural members can be further reduced, owing to its much higher strength and ductility. In addition, for UHPC mixed with fibres, crushing and spalling damage of the concrete can be well restrained thus can further delay the buckling of the steel tubes. Moreover, CFDST columns are becoming more and more commonly seen in high rise buildings and bridge piers where large axial capacity is required; therefore, by replacing the normal strength concrete filler by ultra-high performance concrete (UHPC), the axial load capacity and ductility can be further enhanced whilst the cross-section area and the self-weight of the column can be reduced. Additionally, for UHPC mixed with fibres, crushing and spalling damage of the concrete can be also restrained; consequently the buckling of the steel tubes can be delayed or prevented.

Three types of how blast loading could be applied to a structure in terms of the distance from the explosives to the surface of the structure, i.e. near-field blast (e.g. [22, 23]), close-range blast (e.g. [1, 3]) and direct contact (e.g. [24, 25]). This paper presents an experimental investigation on ultra-high-performance concrete-filled double-skin tubes subjected to close-range blast loading. In total, 10 CFDST column specimens, including 5 specimens with SHS (square hollow section) outer and SHS inner, and 5 specimens with CHS (circular hollow section) outer and CHS (circular hollow section) inner, and 2 regular CFST column specimens for comparison purposes, were subjected to blast loads from a distance of 1.5 meters. All specimens were filled with ultra-high-performance concrete (UHPC) of compressive strength averaging 170 MPa. The parameters that were investigated in the blast tests included: cross-sectional geometry, explosive charge weight and magnitude of axial load.

2. Experimental Program

2.1 Specimen preparation

Ten CFDST specimens, including 5 specimens with SHS outer and SHS inner and 5 circular specimens with CHS outer and CHS inner were tested. In addition, one square and one circular concrete-filled steel tube (CFST) specimens were also investigated to check the dissimilarities, in terms of their structural response when subjected to blast loading, when compared with their double-skinned counterparts. All specimens had a span of 2500 mm. The tubes had outer-diameter/width $D_o = 210\,mm$, inner-diameter/width $D_i = 100\,mm$, and the steel tube thickness $t_{si} = t_{so} = 5\,mm$. Therefore, the hollow section ratio ($\chi = \frac{Di}{D_o - 2t_{so}}$) were 0.5. For ease of concrete pouring, a steel plate was first welded to one end of the empty steel tube prior to pouring concrete. The empty tube was then set up straight and concrete was poured from the top with concrete vibrators being used for the purpose of consolidation. Last, each specimen was maintained at room temperature for 28

days and then levelled and polished before any tests. Fig. 1 shows the typical cross sections of the CFDST specimens used in the blast tests and Table 1 presents detailed information for each of the tested specimens.

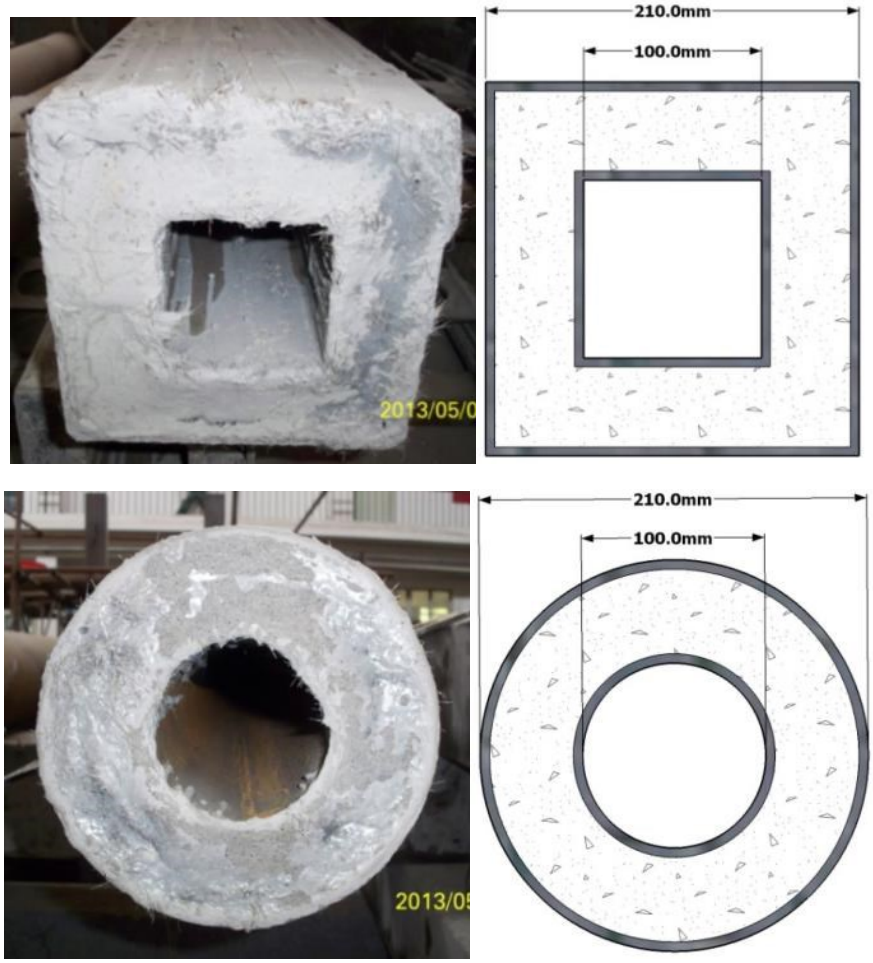

Fig. 1: Cross sections of a square and a circular CFDST specimen

Table 1: The characteristics of each test specimen

Cross section	Label	Test setup	L (mm)	Nominal outer dimensions (D x t_{so} mm)	Nominal inner dimensions (D x t_{io} mm)	χ	TNT (kg)*	Axial load (kN)	Maximum Δ (mm)	Residual Δ (mm)
Square	S1A	a	2500	210 x 5	110 x 5	0.5	35	-	41	16
	S1B	a	2500	210 x 5	110 x 5	0.5	50	-	49	22
	S2A	a	2500	210 x 5	110 x 5	0.5	35	1000	36	8
	S2B	a	2500	210 x 5	110 x 5	0.5	50	1000	-	14**
	S3A	a	2500	210 x 5	110 x 5	0.5	50	1000	41	8
	S3B	a	2500	210 x 5	-	-	50	1000	50	10
Circular	C1A	b	2500	210 x 5	110 x 5	0.5	35	-	98	65
	C1B	c	2500	210 x 5	110 x 5	0.5	35	-	50	20
	C2A	b	2500	210 x 5	110 x 5	0.5	35	1000	-	39**
	C2B	c	2500	210 x 5	110 x 5	0.5	17.2	-	35	12
	C3A	b	2500	210 x 5	110 x 5	0.5	50	1000	91	52
	C3B	b	2500	210 x 5	-	-	50	1000	83	43

*Note: TNT-equivalent charge, based on impulse

**Note: LVDT readings were lost for S2B and C2A, residual displacements were manually measured.

2.2 Material properties

The mechanical properties of the steel tubes were determined from two tensile coupons taken from the outer steel tube of a square CFDST specimen. The loading increment was 10 MPa/s before steel yielding and the pulling chuck pulled at a rate less than 0.5 L/min (L represents the total length of the specimen) after steel yielding. The average yield strength and ultimate strength of the steel tubes test are 360 MPa and 515 MPa, respectively with an elongation of 22%. Fig. 2 shows a typical stress–strain relationship of the tested steel tubes.

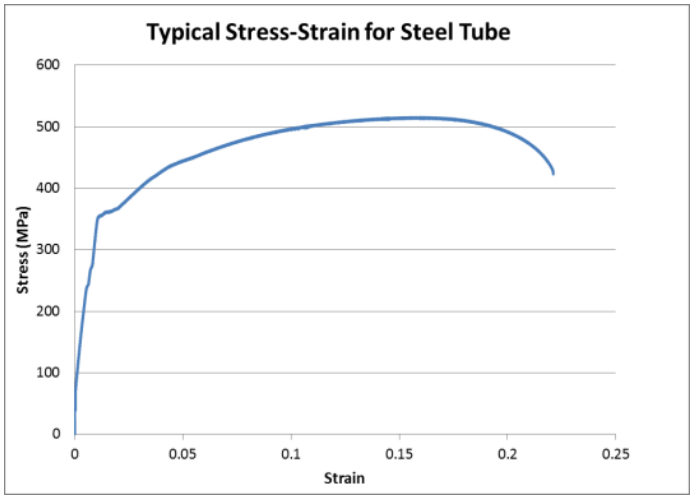

Fig. 2: A typical stress-strain relationship of steel tube material

Steel fibre reinforced self-consolidating concrete with nanoparticles was used as the concrete in all CFDST specimens. The nanoparticle, namely CaCO3, was used as a nano-scale additive to fill up the void existing in concrete as well as to enhance the hydration process. The mixture was produced by mixing silica fume, fine sand and powder materials, which consisted of cement and nanoparticles, in a laboratory concrete mixer. They were firstly mixed in dry condition for 5 minutes prior to pouring in additives. To fluidise the mix, approximately 70% water was then added and mixed for 3 minutes. Superplasticiser was added followed by the other 30% water. The mixing process was then continued for another 5 minutes and micro steel fibres were added afterwards which were manually dispersed and added to the mixer in order to avoid clumping.

Twenty-nine $100\text{mm} \times 100\text{mm} \times 100\text{mm}$ specimens were made for compressive tests and another twenty-nine $100\text{mm} \times 100\text{mm} \times 400\text{mm}$ specimens were made for flexural tensile tests as shown in Fig. 3. Prior to the compressive tests, each cube was properly levelled, sanded, polished, cleaned and dried to attain smooth surfaces. The average cube compressive strength and the flexural tensile strength of the concrete at 28 days were 170 MPa and 33.8 MPa, respectively, which are much higher than normal strength concrete.

Fig. 3: Concrete compression test (left) and flexural tensile test (right)

2.3 Data acquisition and measurement devices

The blast tests on CFDST columns were carried out by PLA University of Science and Technology in Nanjing, China. As shown in Fig. 4, a 3 m × 0.4 m × 1.5 m test pit was excavated for the placement of recording apparatus and corresponding data cables. The surface of the test pit was fully covered with 20 mm thick steel plates to prevent the test pit and the recording apparatus from being damaged by the incoming blast wave. A pneumatic jack was also installed and buried beneath the ground at one side of the test pit to apply an axial load to test specimens. The test specimen was simply-supported at both ends by rollers. Bolts were also used to provide an upward restraint against column rebound, thus making the effective span of the CFDST specimen 2300 mm. Emulsion explosive was used in the experiment which has an average TNT-equivalent value of 0.7 in terms of the magnitude of impulse [26].

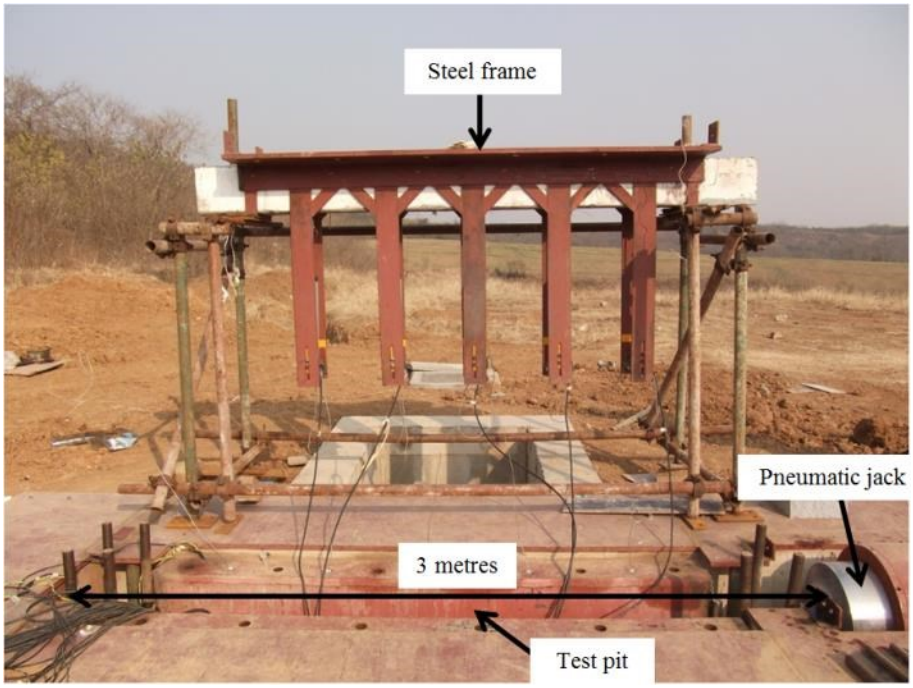

Fig. 4: Blast test setup

As shown in Figs. 5 and 6, three displacement gauges (LVDTs) spaced at 380 mm were attached to each test specimen to measure the displacement-time histories and each LVDT had a 120 mm measuring range for both upward and downward displacement.

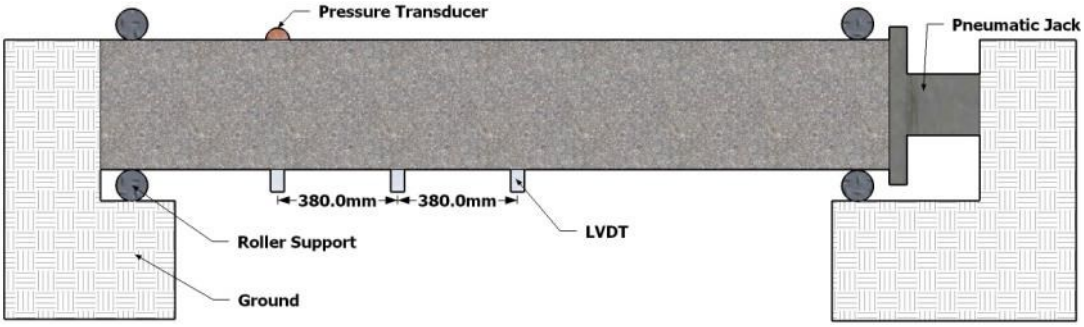

Fig. 5: Schematic view of the test setup

Fig. 6: The installation of LVDTs

To capture the pressure-time history of each blast event acting on a specimen, a pressure transducer was also used, considering the chances of the pressure transducer malfunctioning due to an excessive amount of blast pressure if directly placed under the explosive. Therefore, the pressure transducer was positioned 760 mm away from the centre of the specimen, as shown in Fig. 7.

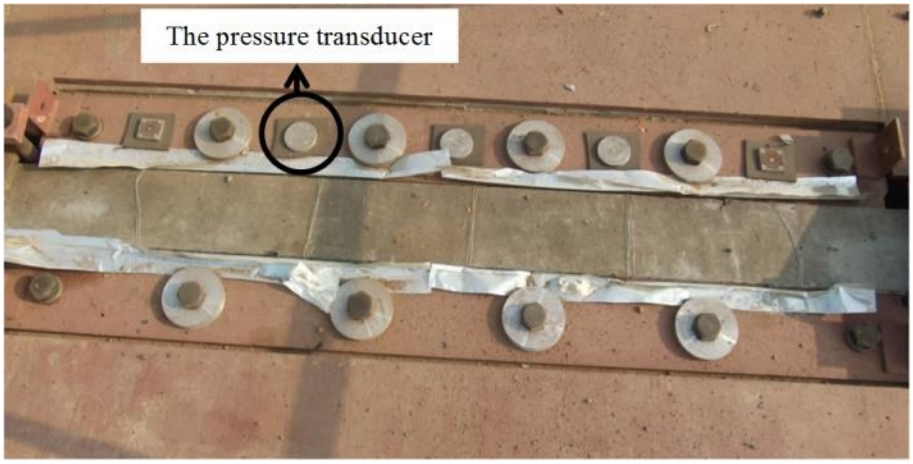

Fig. 7: Location of the pressure transducer

All data cables from the measurement devices were buried beneath the ground. The data-acquisition systems as well as the command console were placed inside a protected concrete bunker nearby.

2.4 Experiment setup

Three different test setups were used during the blast tests as depicted in Figs. 8 and 9. The test pit was designed in such a way that it was as wide as the test specimens; therefore, as shown in setup (a), when the square specimen was placed into it, its front side (the side which received the blast load) was levelled with the ground surface so that there would be no clearing effect nor would the incident wave damage the recording apparatus which were placed at the bottom of the pit. However, the same design cannot be directly applied to circular specimens due to the location of the pneumatic jack. The geometric centre of the pneumatic jack was aligned with that of the square specimen as shown in setup (a). Since the pneumatic jack cannot be moved upward nor downward, setup (b) had to be used for circular specimens if axial load needed to be applied. However, because of the circular cross section shape, the blast wave could now travel into the pit and get reflected & amplified within the narrow space (like a confined blast scenario). Therefore, setup (c) was then introduced for these circular specimens without axial load so that the loading condition would not be too complicated to analyse.

In summary, setup (a) was used for square CFDST columns with and without axial load: the specimen was put into the test pit with its top surface level with the ground surface to ensure that the blast wave could not travel into the pit. Setup (b) was used for circular CFDST columns with axial load: almost the entire specimen was placed beneath the ground with steel angles also being used to reduce the blast wave that travels into the pit. Setup (c) was used for circular CFDST columns without axial load: half of the specimen was above the ground surface.

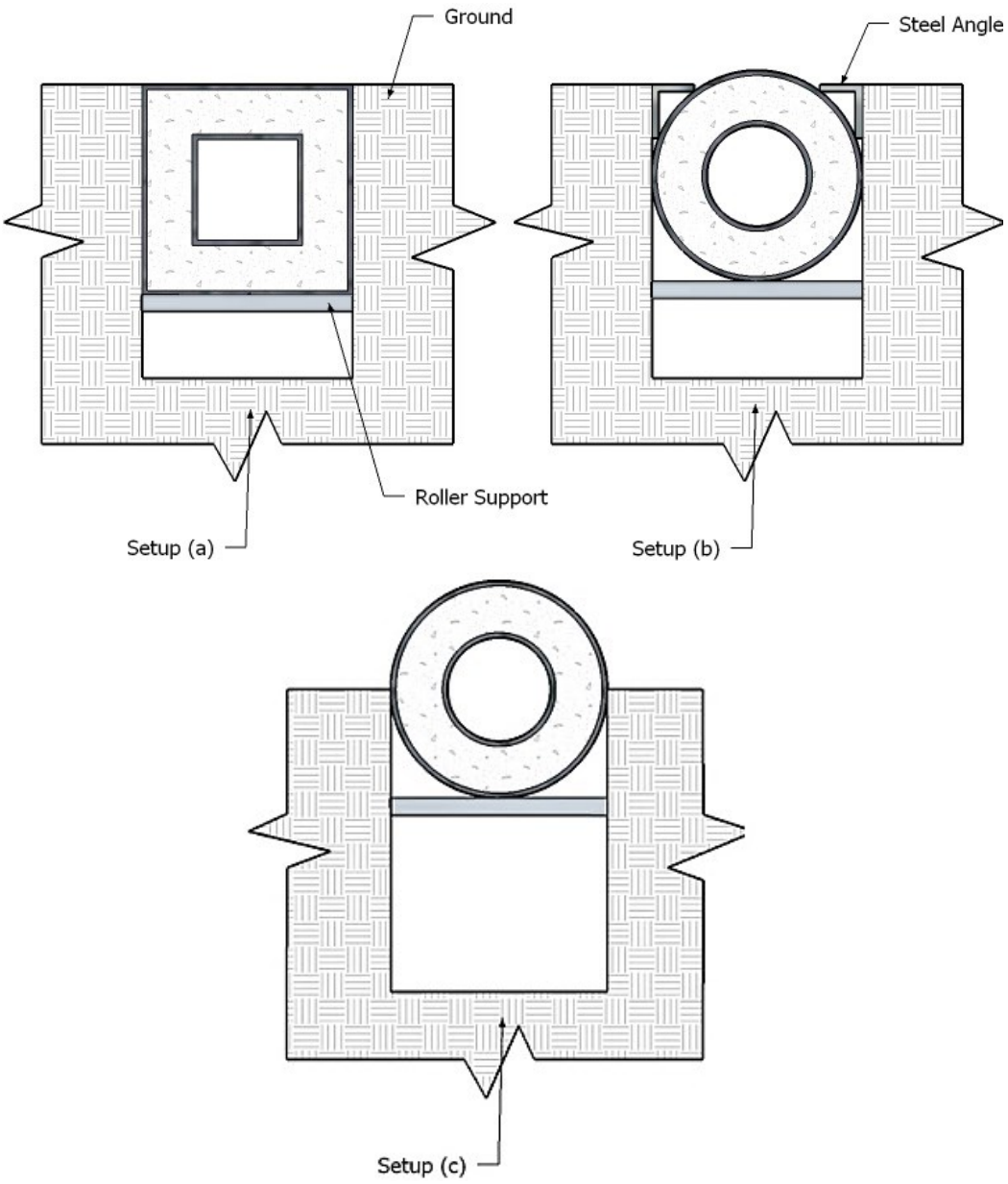

Fig. 8: Cross-sectional view of the test setups

3. Test Results

3.1 Pressure-time histories

Emulsion explosive was used in the blast test program. Simoens [26] reported that emulsion explosive generates a blast wave that has peak pressures of the same magnitude as an identical mass of TNT but for impulse, however, a mass of emulsion explosives equals about 70% of that mass in TNT. Under high strain rate impact load, structural response is mainly governed by the magnitude of impulse; thus in this study 1.4 kg of emulsion explosive was equated to 1 kg of TNT explosive (see Table 2). It should be noted

that Simoens [26] only tested relatively small amounts of emulsion explosive (i.e. 4.8kg); therefore the conversion factor may vary once a much larger charge weight is used.

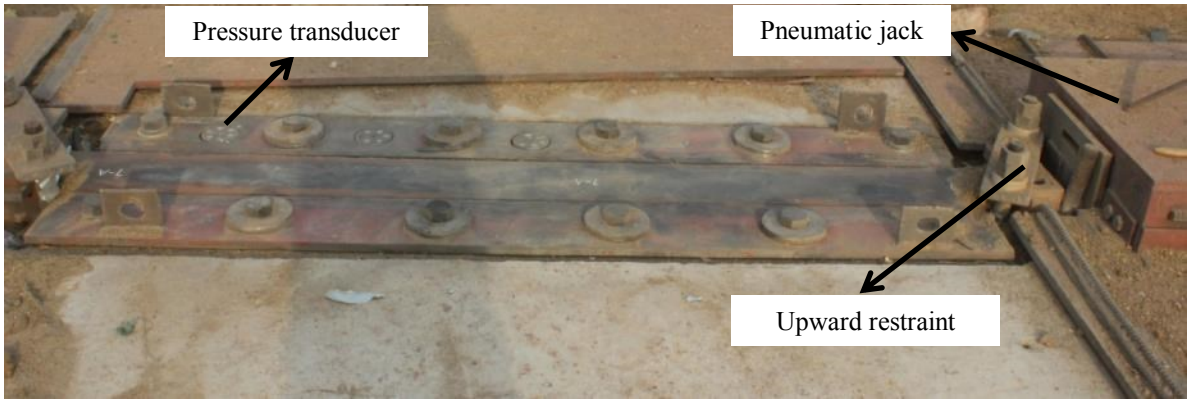

(a)

(b)

(c)

Fig. 9: Elevation of specimens: setup (a), setup (b) and setup (c) respectively

Since the explosive charge weight used in the blast experiment was large, the diameter of the emulsion explosive could be up to half a meter if made spherical, which would cause inconvenience for transportation and storage. As a result, several smaller

cylindrical explosives of identical mass and dimension were used as shown in Fig. 10(a). These smaller cylindrical explosives were firstly placed in a sack in such a way that they together assembled a larger cylindrical shape, and they were then lifted to a desired standoff distance as shown in Fig. 10(b). In addition to the explosive shape, the orientation also plays an important role in determining the magnitude of pressure and impulse of a blast event; therefore, the positioning of the explosive in every test was very carefully adjusted so that it was parallel to the test specimen in the axial direction. According to Wu et al. [27], the pressure and impulse that resulted from such experiment setup would be similar to that resulted from a spherical explosive of the same weight and standoff distance.

(a) (b)

Fig. 10: Shape and orientation of the explosive

In this study, CONWEP predictions of spherical explosive was used as benchmarks for calculation of the peak reflected pressure and impulse for TNT [28, 29]. Table 2 lists the comparisons between the measured and CONWEP-predicted peak reflected pressures and impulses. Errors between the measured and CONWEP-predicted peak reflected pressures and impulses are on average 20% and 18% respectively, without taking specimen S3B into consideration since it deviates from the average too significantly. Fig. 11 compares the measured pressure-time histories to the CONWEP-predicted ones of the

corresponding TNT equivalents. It is observed that except for Figs. 11 (a), (b), (f) and (g), the measured blast loads are generally in good agreement with the CONWEP predictions. Discrepancies are found in measured pressures and impulses between identical blasts and most measured pressure-time histories have multiple peaks rather than only having one peak pressure as found in the CONWEP-predicted cases. In the authors' opinions, these issues are mainly resulted from the following reasons: 1) first of all, when the blast wave travels toward a test specimen, a lot of sand and soil particles travel along with it which inevitably hit on the pressure transducer. As the pressure transducer is highly sensitive, the pressure resulted from the particle collision is therefore also regarded as part of the blast load; 2) secondly, the explosive charge weights used in the blast tests are relatively large; therefore, the accuracy and sensitivity of the pressure transducer can deteriorate over time. It is found that it is more likely to obtain more accurate results every time when a new pressure transducer is put to use such as specimens S2A and C3A; 3) last, the size of a 70kg emulsion explosive may be too large that the chemical reactions within the explosive compound were unthorough and incomplete at the initial detonation.

Table 2: Comparison between measured and CONWEP-predicted pressures & impulses

Specimen No.	Emulsion Explosive (Kg)	TNT Equivalent (Kg)	Standoff Distance (mm)	Peak Reflected Pressure (Mpa)			Peak Reflected Impulse (Mpa·ms)		
				Measured	CONWEP	Error (%)	Measured	CONWEP	Error (%)
S1A	48	35	1500	18.7	24.5	-24%	3.07	3.76	-18%
S1B	70	50	1500	18.6	32.2	-42%	4.20	4.98	-16%
S2A	48	35	1500	18.2	24.5	-26%	2.50	3.76	-34%
S2A	1.4	1	1500	1.05	1.2	-13%	0.29	0.28	+4%
S2B	70	50	1500	37.3	32.2	+16%	6.54	4.98	+31%
S3A	70	50	1500	18.6	32.2	-42%	3.50	4.98	-30%
S3B	70	50	1500	90.3	32.2	+180%	24.0	4.98	+382%
C2A	48	35	1500	23.4	24.5	-4%	3.85	3.76	+2%
C2B	24	17.2	1500	15.4	14.0	+10%	2.36	2.18	+8%
C3A	70	50	1500	37.4	32.2	+16%	5.90	4.98	+18%
C3B	70	50	1500	33.3	32.2	+3%	3.80	4.98	-24%

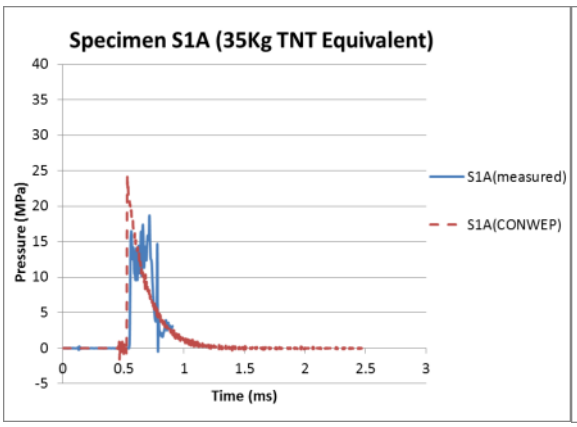
Specimen S1A (35Kg TNT Equivalent)
Pressure (MPa)
Time (ms)
S1A(measured)
S1A(CONWEP)

(a)

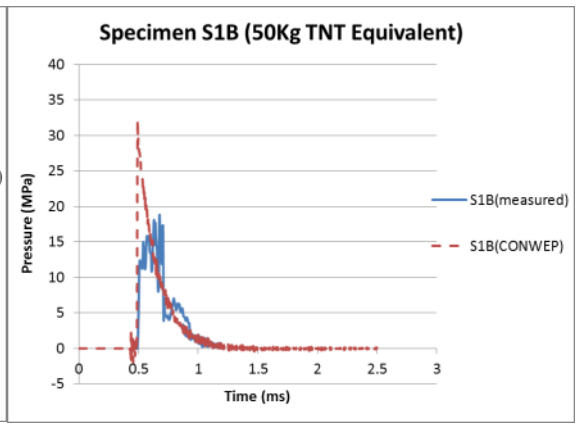
Specimen S1B (50Kg TNT Equivalent)
Pressure (MPa)
Time (ms)
S1B(measured)
S1B(CONWEP)

(b)

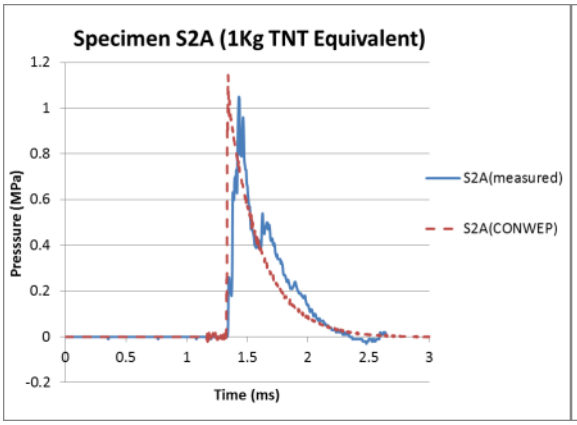
Specimen S2A (1Kg TNT Equivalent)
Presssure (MPa)
Time (ms)
S2A(measured)
S2A(CONWEP)

(c)

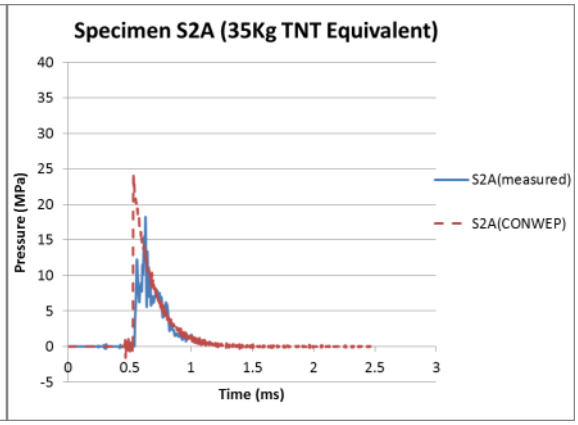
Specimen S2A (35Kg TNT Equivalent)
Pressure (MPa)
Time (ms)
S2A(measured)
S2A(CONWEP)

(d)

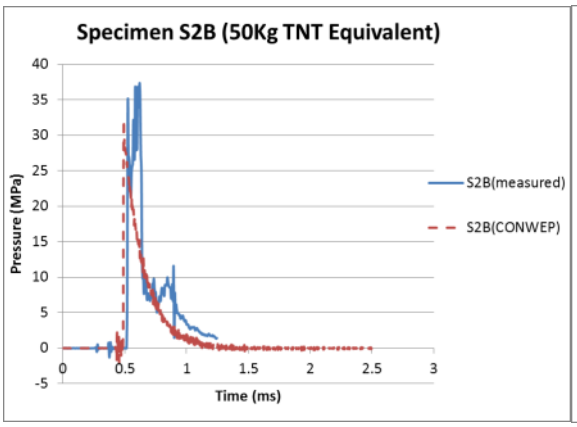
Specimen S2B (50Kg TNT Equivalent)
Pressure (MPa)
Time (ms)
S2B(measured)
S2B(CONWEP)

(e)

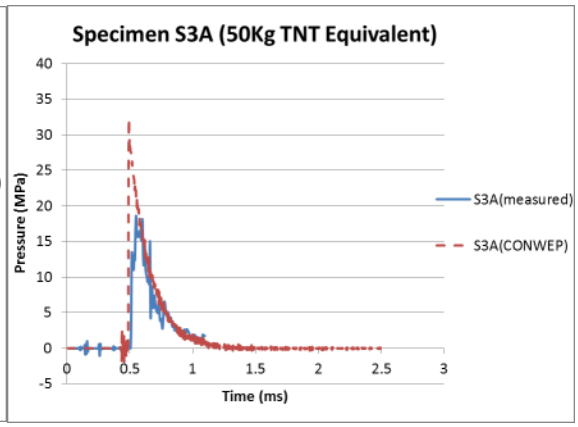
Specimen S3A (50Kg TNT Equivalent)
Pressure (MPa)
Time (ms)
S3A(measured)
S3A(CONWEP)

(f)

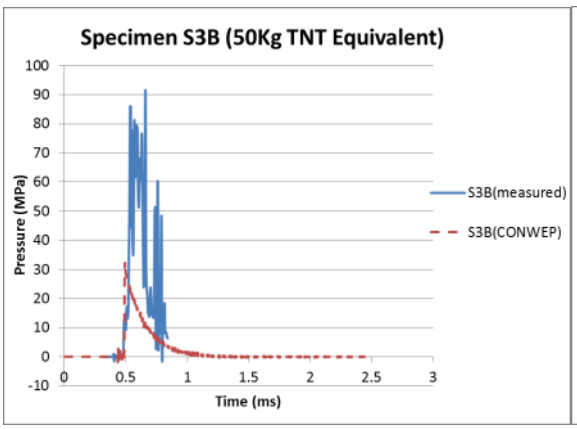
Specimen S3B (50Kg TNT Equivalent)
Pressure (MPa)
Time (ms)
S3B(measured)
S3B(CONWEP)

(g)

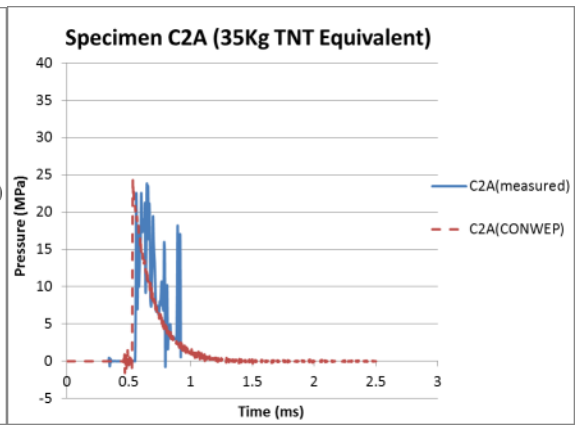
Specimen C2A (35Kg TNT Equivalent)
Pressure (MPa)
Time (ms)
C2A(measured)
C2A(CONWEP)

(h)

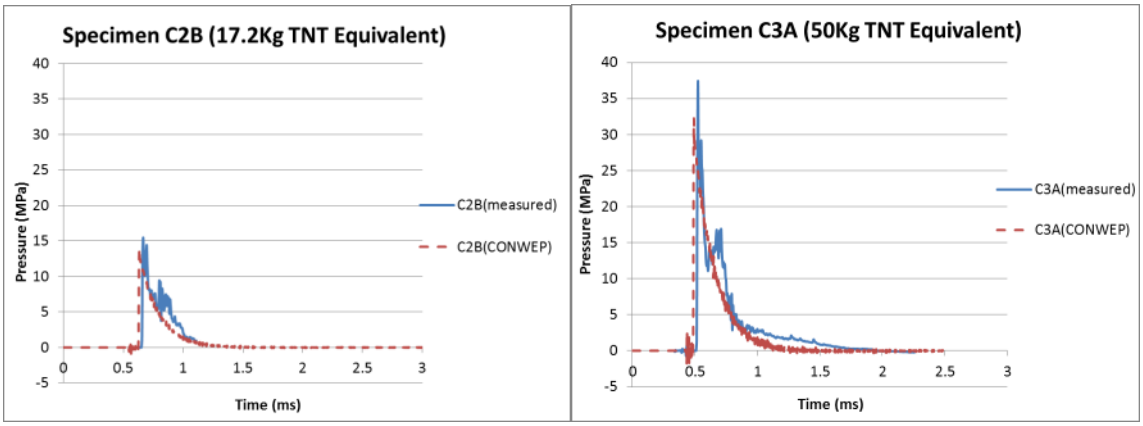

(i)

(j)

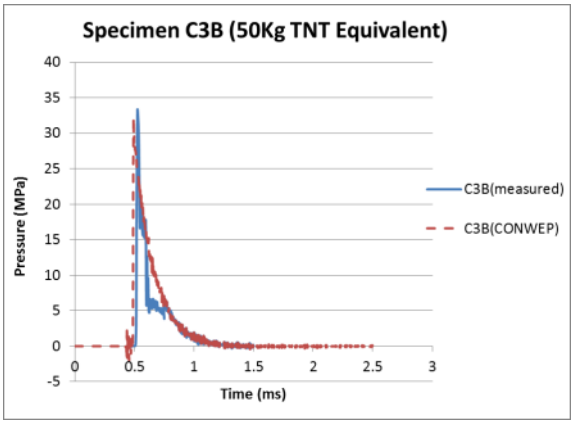

(k)

Fig. 11: Pressure-time histories for tested specimens

3.2 Displacement-time histories

Fig. 12 reports two of the typical displacement-time histories of the test specimens. All three LVDTs were aligned along the centreline of the member. LVDT1 was installed right below the centre of the specimen and LVDT2 and LVDT3 were installed 360 mm and 720 mm away from LVDT1, respectively. None of the displacement measurements reached the LVDT measuring range (120 mm). The mid-span residual displacements of the tested specimens were measured manually post-testing and they were also found to be in good agreement with the LVDT readings.

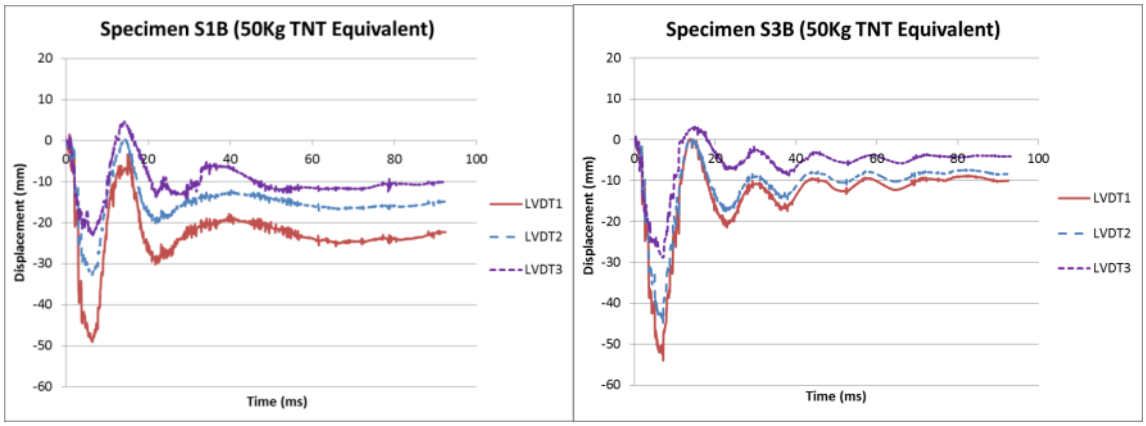

(a) (b)

Fig. 12: Typical displacement-time histories for tested specimens

4. Analysis and Discussion

4.1 The effect of charge weight

Fig. 13 compares the displacement-time histories of CFDST specimens subjected to different blast loads (LVDT1 recording at mid-span only). As expected, larger charge weight yields larger deflection. However, the test results also suggest that the effect of charge weight is more noticeable for the specimens without axial load than the axially-loaded ones. The differences between axially-loaded specimens S2A and S3A were small in Fig. 13(b) while for their axial-load-free counterparts in Fig. 13(a), S1B undergoes 25% larger peak displacement and 50% larger residual deflection than S1A.

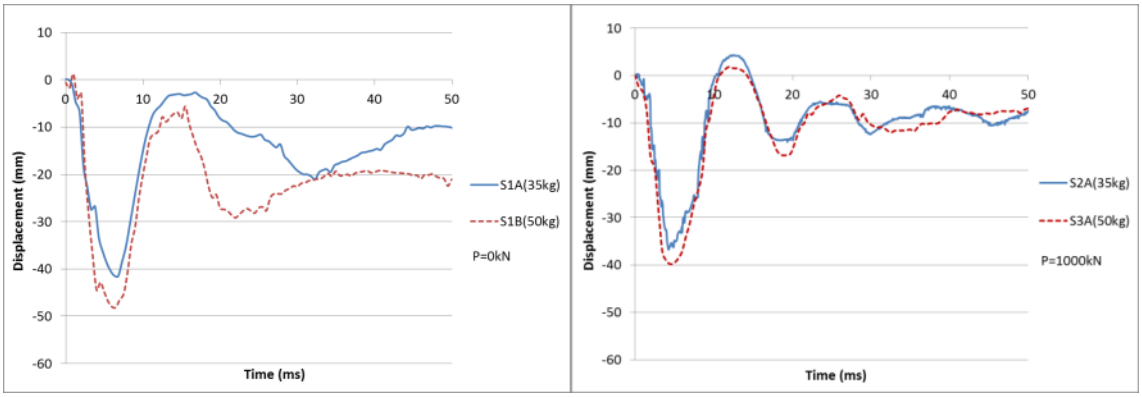

(a) (b)

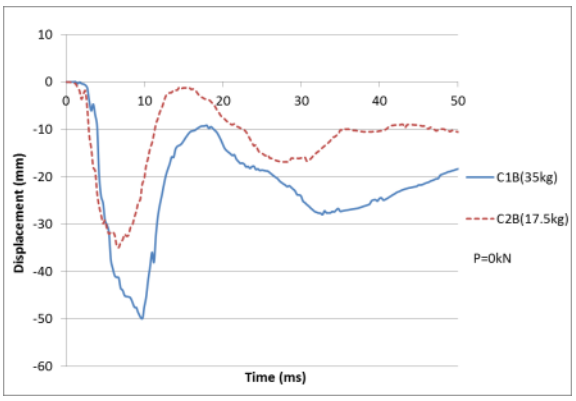

(c)

Fig. 13: Effect of charge weight

4.2 The effect of axial load

The effect of axial load was investigated by applying two different axial loads, namely 0 kN and 1000 kN, on several identical specimens and then comparing their displacement-time histories under the same blast loads. In both cases shown in Fig. 14, the application of 1000 kN axial load results in a reduction in the deflection. Similar results were also observed by Wang et al. [30] who discussed the relationship between the axial load ratio (i.e. applied axial load nominal axial load capacity) and the peak displacement. It was found that a small axial load ratio (e.g. less than 0.3) can effectively reduce the deflection while a large axial load ratio (e.g. more than 0.6) was likely to amplify the deflection. In the current research, the applied axial load (i.e. 1000 kN) corresponds to approximately an axial load ratio of 0.2.

Another possible reason is the membrane effect. In the present study, axial loads application provides lateral restrain to the column, and compressive membrane action may occur. Early age deflection may cause a migration of the neutral axis which is accompanied by in-plane expansion of the column at its boundaries. If this expansion is restrained, in this case by the axial load application, the development of arching action enhances the strength of the column. The compressive membrane effects can be accounted for the different column deflections under the same blast loading condition.

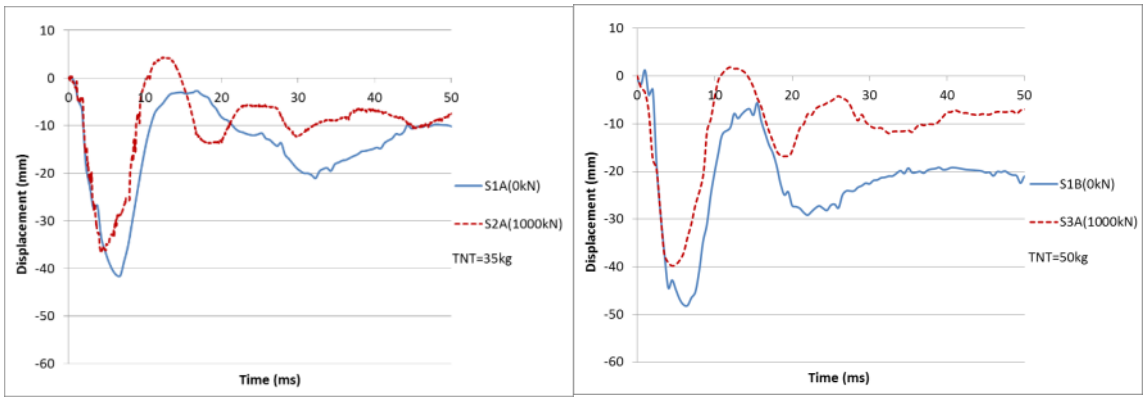

(a) (b)

Fig. 14: Effect of axial load

4.3 The effect of test setups

As mentioned previously, two different test setups were used on the circular CFDST specimens due to limitations of the pneumatic jack. If the test specimen was to be axially loaded, then setup (b) had to be used since the entire pneumatic jack was buried beneath the ground surface and it could not be moved up or down; otherwise, setup (c) was adopted.

Fig. 15 depicts the blast-pressure distributions on CFDST specimens by using the two different setups. Due to the presence of the steel angles, the pressure distribution in setup (b) is similar to the pressure acting on a square specimen: it reaches a peak at the middle and decays very slightly along its width. On the other hand, setup (c) exhibits the typical pressure distribution for circular columns: it reaches peak at the middle by the same magnitude as setup (b) and then decreases significantly along its circumference due to its roundness.

Fig. 16 compares setup (b) to setup (c) in terms of the displacement-time history. The deflection of the CFDST specimen in setup (b) yielded 100% more maximum deflection and 200% more residual deflection than that of the CFDST specimen in setup (c).

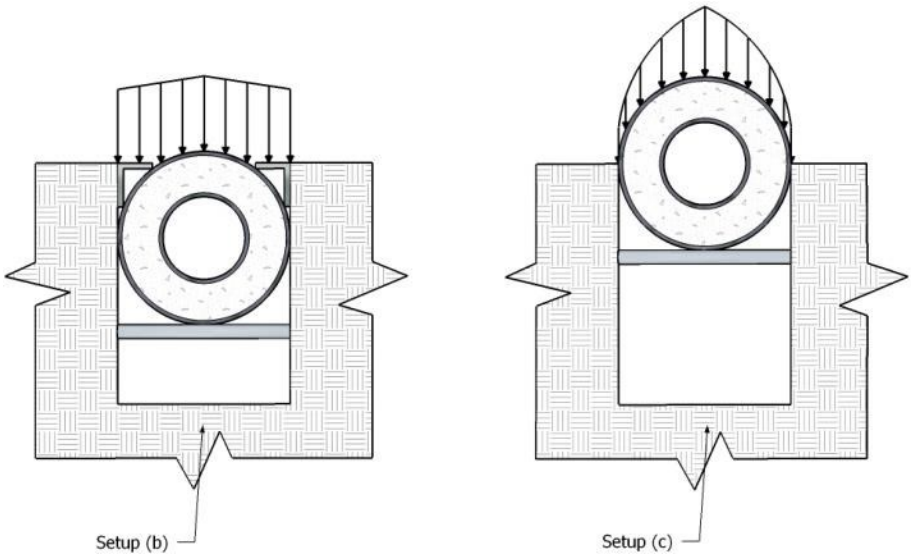

Fig. 15: Blast load distribution on setup (b) and (c)

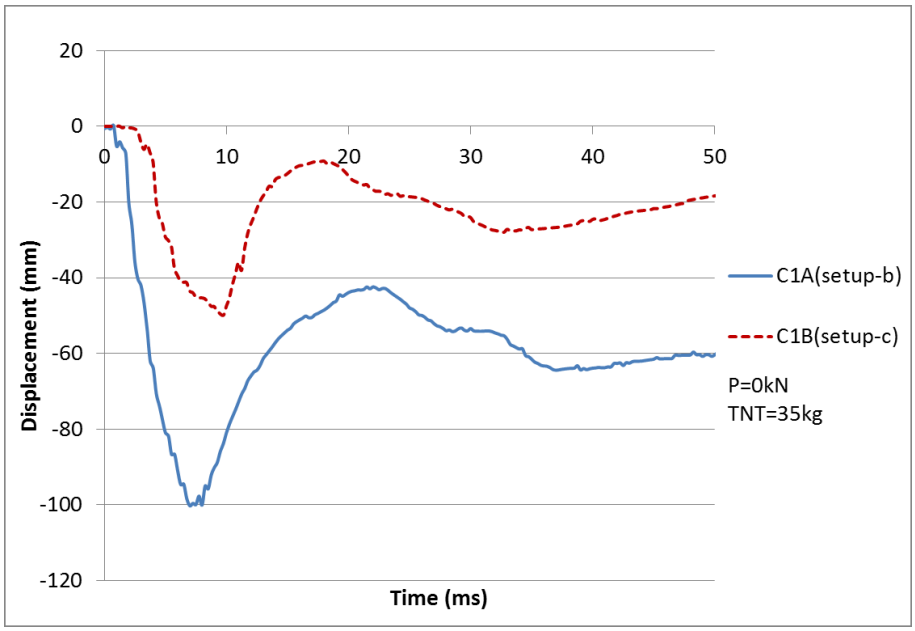

Fig. 16: Effect of different specimen setups

4.4 The effect of hollow core

By having a hollow core in the current study, the cross-sectional area and self-weight of the specimens (both the circular and square ones) was reduced by 23% relative to fully concrete-filled tubes. In prior research, not much effort has been put into investigating the difference caused by a hollow core versus a fully filled section. Han [15] studied this effect, with the area of hollow core ranging from 0 to 0.77 of the total cross-sectional area, for CFDST specimens under cyclic flexural load. It was then reported that most hollow

specimens exhibited a larger flexural load capacity and ductility than their solid counterparts if the hollow ratio can be kept under a certain value which is dependent on the amount of steel. For specimens with a hollow ratio of 0.77, a very significant decline in the flexural load capacity and ductility was observed.

However, during the blast test, it was found that both CFDST and CFST column specimens behaved in a very similar manner, regardless of the cross-sectional geometry. Despite of the difference in the maximum deflection, as shown in Fig. 17(a) and (b), the hollow area inside seems to have little effect on the overall structural responses as both types showed similar period of oscillation, maximum and residual deflection.

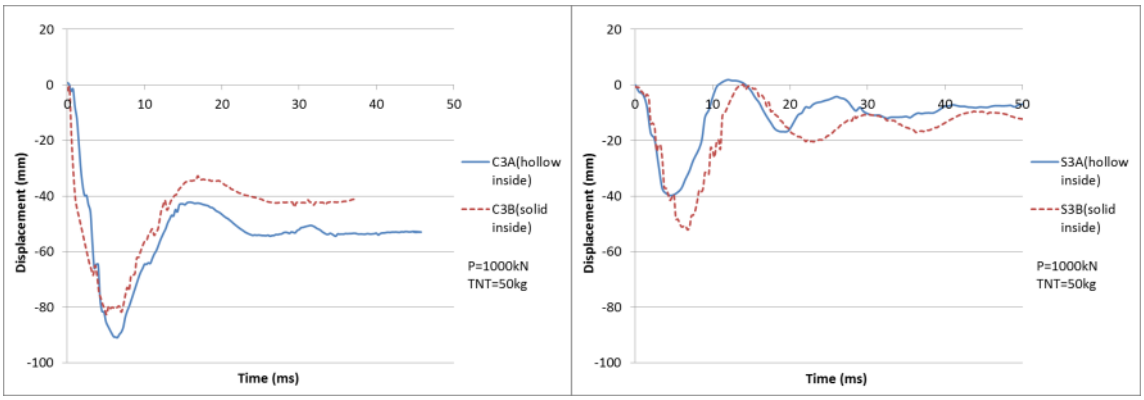

(a) (b)

Fig. 17: Effect of hollowness: S3A and C3A are CFDST and S3B and C3B are CFST

4.5 The deformed shape of and crack formation on CFDST specimens

For a CFDST specimen filled with normal strength concrete, its failure under flexural load is mainly due to the crushing of the concrete associated with local buckling of the steel tube, or even rupture, as shown in Fig. 18 [31-33].

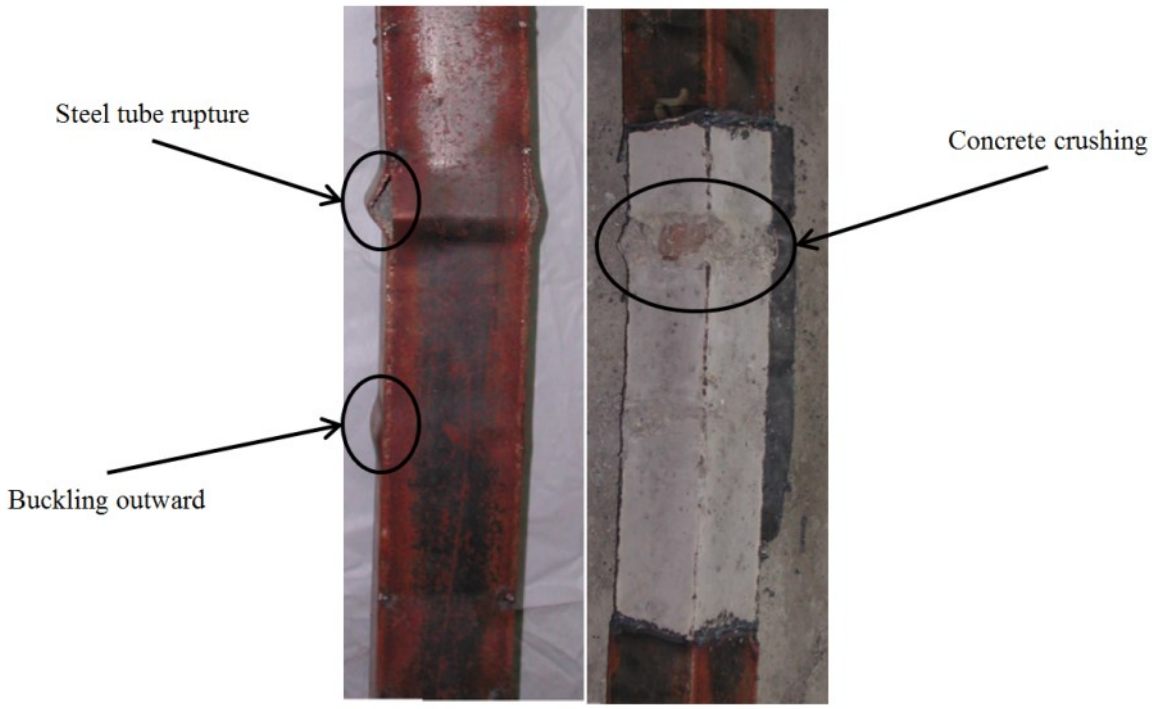

Fig. 18: Failure of CFDST [15] (courtesy of Prof. L.H. Han, Tsinghua University, China)

In the current study, the CFDST specimen is filled with steel-fibre reinforced UHPC; therefore its structural response is very different from those filled with normal strength concrete. Fig. 19 shows the deformed shapes of specimens S1A and C1A; no steel buckling or localised damage can be observed on both specimens which were subjected to 35 kg TNT equivalent despite specimen C1A yielded the largest maximum (98 mm) and residual deflection (65 mm) of all test specimens. Fig. 20 shows the crack propagation in the concrete after removing the outer steel skin from specimens S1A and C1A. There was no obvious sign of concrete crushing on both specimens, only minor flexural cracks of no more than 0.5 mm width on the tensile face of both specimens. Both figures show that the tested CFDST specimens were also able to remain overall of global flexural response as opposed to localised structural failure. This is one of the main advantages of using UHPC over conventional concrete in CFST/CFDST members: due to the higher compressive/ tensile strength and steel fibres, UHPC is very resistant to crushing or spalling. As mentioned previously, the steel tubes of a CFDST member normally only buckles after the

concrete filler at the same location crushes; therefore, compared to conventional concrete, UHPC can more effectively prevent or delay steel buckling.

(a) S1A

(b) C1A

Fig. 19: Deformed shapes of specimens S1A and C1A

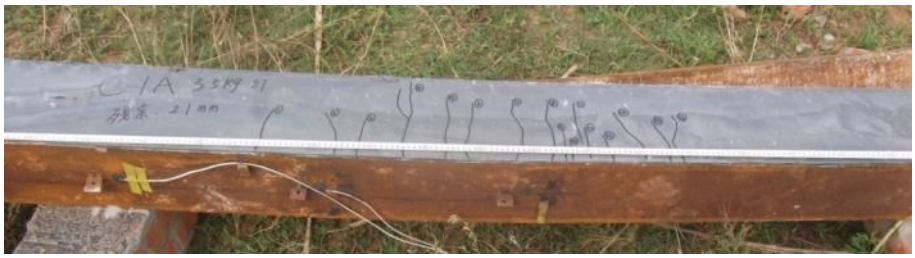

(a) S1A

(b) C1A

Fig. 20: Crack propagation in specimens S1A and C1A

5. Conclusions

This paper has presented an experimental study on the performance of concrete-filled double-skin steel tube (CFDST) columns under blast loading. The following conclusions can be drawn based on the test results and observations:

1) CFDST columns filled with UHPC can effectively withstand severe blast load without failure. Compared to normal strength concrete filled CFDST, the UHPC filled CFDST can better delay/prevent concrete crushing and steel buckling, and thus have an overall of global flexural response as opposed to localised structural failure.

2) The peak reflected pressures and impulses measured by the pressure transducer yield 18% and 20% error respectively compared to the CONWEP-predictions.

3) The increase in explosive charge weight caused a larger mid-span deflection, with this effect being more noticeable on axial-load-free specimens rather than axially-loaded specimens.

4) The presence of an axial compressive load, corresponding to approximately 20% of the squash load, led to a slight reduction in the peak deflection in two comparative cases.

5) In the current study, both CFDST and CFST specimens showed similar behaviours. The hollow area inside seems to have little effect on the overall structural responses as both types had similar period of oscillation, maximum and residual deflection.

Acknowledgement

The financial support of the Australian Research Council under ARC Discovery Projects DP130100181 and DP140103025, the Key Projects of Tianjin Science and Technology Support Plan 14ZCZDSF0016, and the Tsinghua Initiative Scientific Research Program (No. 20131089347) is gratefully acknowledged.

Reference

[1] Wu, C, Huang, L, and Oehlers, DJ, *Blast Testing of Aluminum Foam–Protected Reinforced Concrete Slabs.* Journal of Performance of Constructed Facilities, 2010. **25**(5): p. 464-474.

[2] Ma, G and Ye, Z, *Analysis of Foam Claddings for Blast Alleviation.* International Journal of Impact Engineering, 2007. **34**(1): p. 60-70.

[3] Hanssen, A, Enstock, L, and Langseth, M, *Close-Range Blast Loading of*

Aluminium Foam Panels. International Journal of Impact Engineering, 2002. **27**(6): p. 593-618.

[4] Wu, C, Oehlers, DJ, Rebentrost, M, Leach, J, and Whittaker, AS, *Blast Testing of Ultra-High Performance Fibre and FRP-Retrofitted Concrete Slabs.* Engineering Structures, 2009. **31**(9): p. 2060-2069.

[5] Dragos, J, Wu, C, Haskett, M, and Oehlers, D, *Derivation of Normalized Pressure Impulse Curves for Flexural Ultra High Performance Concrete Slabs.* Journal of Structural Engineering, 2012. **139**(6): p. 875-885.

[6] Mirmomeni, M, Heidarpour, A, Zhao, X-L, Hutchinson, CR, Packer, JA, and Wu, C, *Mechanical properties of partially damaged structural steel induced by high strain rate loading at elevated temperatures–An experimental investigation.* International Journal of Impact Engineering, 2015. **76**: p. 178-188.

[7] Gerlach, R, Kettenbeil, C, and Petrinic, N, *A new split Hopkinson tensile bar design.* International Journal of Impact Engineering, 2012. **50**: p. 63-67.

[8] Wei, S, Mau, S, Vipulanandan, C, and Mantrala, S, *Performance of New Sandwich Tube under Axial Loading: Experiment.* Journal of Structural Engineering, 1995. **121**(12): p. 1806-1814.

[9] Uenaka, K, Kitoh, H, and Sonoda, K, *Concrete Filled Double Skin Circular Stub Columns under Compression.* Thin-Walled Structures, 2010. **48**(1): p. 19-24.

[10] Zhao, X-L, Tong, L-W, and Wang, X-Y, *CFDST stub columns subjected to large deformation axial loading.* Engineering Structures, 2010. **32**(3): p. 692-703.

[11] Huang, H, Han, L-H, Tao, Z, and Zhao, X-L, *Analytical behaviour of concrete-filled double skin steel tubular (CFDST) stub columns.* Journal of Constructional Steel Research, 2010. **66**(4): p. 542-555.

[12] Yuan, W-b and Yang, J-j, *Experimental and Numerical Studies of Short Concrete-Filled Double Skin Composite Tube Columns under Axially Compressive Loads.* Journal of Constructional Steel Research, 2013. **80**: p. 23-31.

[13] Pagoulatou, M, Sheehan, T, Dai, X, and Lam, D, *Finite element analysis on the capacity of circular concrete-filled double-skin steel tubular (CFDST) stub columns.* Engineering Structures, 2014. **72**: p. 102-112.

[14] Han, L-H, Huang, H, and Zhao, X-L, *Analytical behaviour of concrete-filled double skin steel tubular (CFDST) beam-columns under cyclic loading.* Thin-Walled Structures, 2009. **47**(6): p. 668-680.

[15] Han, L-H, Huang, H, Tao, Z, and Zhao, X-L, *Concrete-filled Double Skin Steel Tubular (CFDST) Beam–columns Subjected to Cyclic Bending.* Engineering Structures, 2006. **28**(12): p. 1698-1714.

[16] Li, W, Han, L-H, and Chan, T-M, *Tensile behaviour of concrete-filled double-skin steel tubular members.* Journal of Constructional Steel Research, 2014. **99**: p. 35-46.

[17] Li, W, Han, L-H, and Chan, T-M, *Numerical investigation on the performance of concrete-filled double-skin steel tubular members under tension.* Thin-Walled Structures, 2014. **79**: p. 108-118.

[18] Huang, H, Han, L-H, and Zhao, X-L, *Investigation on concrete filled double skin steel tubes (CFDSTs) under pure torsion.* Journal of Constructional Steel

Research, 2013. **90**: p. 221-234.
[19] Lu, H, Zhao, X-L, and Han, L-H, *Testing of self-consolidating concrete-filled double skin tubular stub columns exposed to fire.* Journal of Constructional Steel Research, 2010. **66**(8): p. 1069-1080.
[20] Li, W, Ren, Q-X, Han, L-H, and Zhao, X-L, *Behaviour of tapered concrete-filled double skin steel tubular (CFDST) stub columns.* Thin-walled structures, 2012. **57**: p. 37-48.
[21] Li, W, Han, L-H, Ren, Q-X, and Zhao, X-L, *Behavior and calculation of tapered CFDST columns under eccentric compression.* Journal of Constructional Steel Research, 2013. **83**: p. 127-136.
[22] Langdon, G, Ozinsky, A, and Yuen, SCK, *The response of partially confined right circular stainless steel cylinders to internal air-blast loading.* International Journal of Impact Engineering, 2014. **73**: p. 1-14.
[23] Ritchie, C, Packer, J, Seica, M, and Zhao, X, *Field blast testing and FE modelling of concrete-filled RHS members*, in *The 3rd International Conference on Protective Structures (ICPS3)*2015: Newcastle, NSW.
[24] Jama, H, Nurick, G, Bambach, M, Grzebieta, R, and Zhao, X, *Steel square hollow sections subjected to transverse blast loads.* Thin-Walled Structures, 2012. **53**: p. 109-122.
[25] Bambach, M, Zhao, X, and Jama, H, *Energy absorbing characteristics of aluminium beams strengthened with CFRP subjected to transverse blast load.* International Journal of Impact Engineering, 2010. **37**(1): p. 37-49.
[26] Simoens, B, Lefebvre, MH, and Minami, F, *Influence of Different Parameters on the TNT-Equivalent.* Central European Journal of Energetic Materials, 2011. **8**(1): p. 53-67.
[27] Wu, C, Fattori, G, Whittaker, A, and Oehlers, DJ, *Investigation of air-blast effects from spherical-and cylindrical-shaped charges.* International Journal of Protective Structures, 2010. **1**(3): p. 345-362.
[28] Kingery, CN and Bulmash, G, *Air blast parameters from TNT spherical air burst and hemispherical surface burst*. 1984: Ballistic Research Laboratories.
[29] Hyde, D, *ConWep, conventional weapons effects program.* US Army Engineer Waterways Experiment Station, USA, 1991.
[30] Wang, R, Han, L-H, and Hou, C-C, *Behavior of concrete filled steel tubular (CFST) members under lateral impact: Experiment and FEA model.* Journal of Constructional Steel Research, 2013. **80**: p. 188-201.
[31] Tao, Z and Han, L-H, *Behaviour of concrete-filled double skin rectangular steel tubular beam–columns.* Journal of Constructional Steel Research, 2006. **62**(7): p. 631-646.
[32] Zhao, X-L and Grzebieta, R, *Strength and ductility of concrete filled double skin (SHS inner and SHS outer) tubes.* Thin-Walled Structures, 2002. **40**(2): p. 199-213.
[33] Zhang, F, Wu, C, Wang, H, and Zhou, Y, *Numerical simulation of concrete filled steel tube columns against BLAST loads.* Thin-Walled Structures, 2015. **92**: p. 82-92.

Statement of Authorship

Title of Paper	Residual axial capacity of CFDST columns infilled with UHPFRC after close-range blast loading
Publication Status	☑ Published ☐ Accepted for Publication ☐ Submitted for Publication ☐ Unpublished and Unsubmitted w ork w ritten in manuscript style
Publication Details	Zhang, F., Wu, C., Li, Z.-X. & Zhao, X.-L. 2015. Residual axial capacity of CFDST columns infilled with UHPFRC after close-range blast loading. *Thin-Walled Structures,* 96, 314-327.

Principal Author

Name of Principal Author (Candidate)	Fangrui Zhang		
Contribution to the Paper	The author helped conduct tests, processed and analysed test data and prepared manuscript.		
Overall percentage (%)	70%		
Certification:	This paper reports on original research I conducted during the period of my Higher Degree by Research candidature and is not subject to any obligations or contractual agreements with a third party that would constrain its inclusion in this thesis. I am the primary author of this paper.		
Signature		Date	

Co-Author Contributions

By signing the Statement of Authorship, each author certifies that:

i. the candidate's stated contribution to the publication is accurate (as detailed above);

ii. permission is granted for the candidate in include the publication in the thesis; and

iii. the sum of all co-author contributions is equal to 100% less the candidate's stated contribution.

Name of Co-Author	Chengqing Wu		
Contribution to the Paper	This co-author supervised research and tests, provided critical manuscript evaluation and acted as corresponding author.		
Signature		Date	6/6/2016

Name of Co-Author	Zhong-Xian Li		
Contribution to the Paper	This co-author helped design and conduct tests.		
Signature		Date	2016.6.6

Name of Co-Author	Xiao-Ling Zhao		
Contribution to the Paper	This co-author provided critical manuscript evaluation		
Signature		Date	05/06/16

RESIDUAL AXIAL CAPACITY OF CFDST COLUMNS INFILLED WITH UHPFRC AFTER CLOSE-RANGE BLAST LOADING

Fangrui Zhang, Chengqing Wu, Zhong-Xian Li, Xiao-Ling Zhao

Abstract

Concrete-filled double-skin tubes (CFDST) consist of two concentrically placed steel tubes with concrete filled in between and they have more and more commonly been used in the field of civil engineering in recent years. A number of recent researches evidenced the excellent performance of CFDST columns under a variety of loading conditions. However, very limited knowledge is known about the residual axial capacity of CFDST columns following severe blast loadings. This paper presents an experimental study on the residual behaviours of ultra-high performance concrete infilled double-skin steel tubular columns after close-in blast loading. In total, eight CFDST columns, including 3 square ones and 5 circular ones, were first tested under different blast loads with two axial load levels. After the blast tests, all CFDST columns were transported to the laboratory and each of them was then subjected to static axially compressive load until failure. It was found that the CFDST columns with smaller permanent displacement had larger peak residual axial capacity and the CFDST columns which were not subjected to axial load during the blast test exhibited more ductile behaviour than those which were axially loaded during the blast test exhibited more ductile behaviour than those which were axially loaded during the blast test.

Keywords: Concrete-filled double-skin tubes, Blast loading, Residual axial capacity

1. Introduction

Terrorist activities, especially blast attacks, have taken away thousands of innocent lives in the past decades. As a result, countless effort has been made to investigate and improve the reliability of vulnerable structures under blast loads. Progressive collapse, one

of the most common types of structural failure, is mainly triggered by failure of the key columns; therefore, the residual strength of these columns after blast loads has become one of the decisive factors when it comes to assessing the stability of a structure [1]. Although there is a large number of researches in regard to structural columns, very few of them are about the residual axial load capacity, let alone the fact that the majority of them are strictly limited to conventional reinforced concrete columns only [1-4]. In recent years, a new steel-concrete composite member, known as a concrete-filled double-skin steel tube (CFDST), has been more and more commonly used as load-bearing columns in the construction industry due to its attractive properties such as ease of construction, light weight and high strength. Therefore, there is a need to better understand the residual behaviours of CFDST columns after blast loads.

A CFDST member consists of two concentrically placed steel tubes with concrete filler poured in between them. One of the advantages of CFDST columns is the passive confinement which is attributed to the interaction between the steel tubes and concrete filler. Wei et al. [5] subjected 26 circular CFDST stub columns to axial compression and it was found that the axial load capacity of the CFDST stub column can be enhanced by up to 30% when compared to the simply superposed capacity of the steel tubes and concrete filler when acting alone. Furthermore, the failure mode of CFDST columns under axial load was reported predominantly to be local buckling of the steel tubes associated with concrete shear failure and the outer diameter-to-tube-thickness ratio affected the failure mode the most [6, 7]. On top of experimental investigations, a number of analytical models were also developed which could be used to predict the behaviour of CFDST members under different loads [8-13].

On the other hand, studies were also carried out to investigate the behaviours of CFDST members under transverse loading [14-16]. Different cross-sectional geometries were compared in terms of energy dissipation capacity and specimens of circular

cross-sections were found to have an advantage over those of the specimens of square cross-sections. Analytical models were also developed to predict the response of CFDST beam–columns under combined axial and flexural loading. Experimental efforts were also made to study the tensile behaviour [17, 18], torsional behaviour [19] and fire resistance of CFDST members [20], all of which have shown good results, recommending CFDST for building construction.

It is well known that ultra-high performance concrete (UHPC) has been more and more widely used in the field of civil engineering applications. Since CFDST members are mainly used in building underground tunnels, high-rise buildings or bridge piers, where large axial bearing capacity is required; therefore, by replacing normal strength concrete by UHPC in CFDST members, the cross-section area as well as the self-weight of the structural members can be significantly reduced, owning to its much higher strength. In addition, for UHPC mixed with fibres, crushing and spalling damage of the concrete can be well restrained by the fibres thus can further delay the buckling of the steel tubes. Despite several studies have investigated the behaviours of CFST members filled with high strength concrete [21-23], very little knowledge can be found in regard to CFDST members filled with ultra-high performance fibre reinforced concrete (UHPFRC).

In this research, an experimental study is presented to investigate the residual axial load capacity of CFDST columns infilled with UHPFRC. The experimental program mainly consists of three phases: the first phase includes experimentally determining the axial load capacity of undamaged CFDST columns by uniaxial compressive tests along with three point bending tests to determine the flexural capacity. The second phase includes conducting blast experiments on CFDST columns and then sending damaged columns back to laboratory for experiment phase three. The last phase includes conducting residual axial compressive tests on the blast-damaged CFDST columns from phase two. In total, 7 CFDST columns (including 4 with circular cross section and 3 with square cross section)

were used for phase one, 12 CFDST columns (including 6 with circular cross section and 6 with square cross section) were used for phase two and 8 CFDST columns (including 5 with circular cross section and 3 with square cross section) were used for phase three.

2. Test Specimens

All specimens measured 2500 mm in length with outer-diameter/width $D_o = 210\ mm$, inner-diameter/width $D_i = 100\ mm$ and both steel tubes' thickness $t_{si} = t_{so} = 5\ mm$. The steel tubes were made of hot-rolled seamless steel conforming to Chinese Standard GT/B 8162 – 2008 [24]. For ease of concrete pouring, a steel plate was first welded to one end of the empty steel tube prior to pouring concrete, making sure that both their geometric centres were aligned. The empty tube was then set up straight and concrete was poured from the top with concrete vibrators being used for compaction. All specimens maintained at room temperature for 28 days and then levelled and polished before any tests. Fig. 1 shows the typical cross sections of the CFDST specimens used in the blast tests.

The mechanical properties of the steel tubes were determined from tensile coupons taken from the outer steel tube of a square CFDST specimen in conformance with Chinese Standard GBT228-2010 [25]. The average yield strength and ultimate strength of the steel were 360 MPa and 515 MPa, respectively, with an average maximum elongation of 22%.

The cross sectional classification of the test specimens were determined in accordance with AS4100 [26]. A cross section can be classified as compact, non-compact or slender based on the section slenderness which can be calculated as:

$$\lambda = \frac{B - 2t}{t}\sqrt{\frac{f_y}{250}}\ for\ square\ cross\ section \qquad (1a)$$

$$\lambda = \frac{D}{t}\frac{f_y}{250}\ for\ circular\ cross\ section \qquad (1b)$$

where, B is the outer length of the square cross section, D is the outer diameter of the circular cross section, t is the thickness of the outer tube and f_y is the yield stress of the outer tube.

For unfilled square hollow tube, the plastic limit, λ_p, is 82 whereas for unfilled circular hollow tube, λ_p is 50. According to Elchalakani et al. [27], the concrete filler in CFST/CFDST specimens increases the plastic limit by about 50%. As a result, λ_p for the square and circular CFDST columns in this paper are 123 and 75, respectively. By using equations 1(a) and 1(b), the section slenderness for the square and circular cross sections are 48 and 60.5, respectively, which are both less than their corresponding plastic limits; therefore, the square and circular CFDST specimens used in this paper can be classified as compact sections.

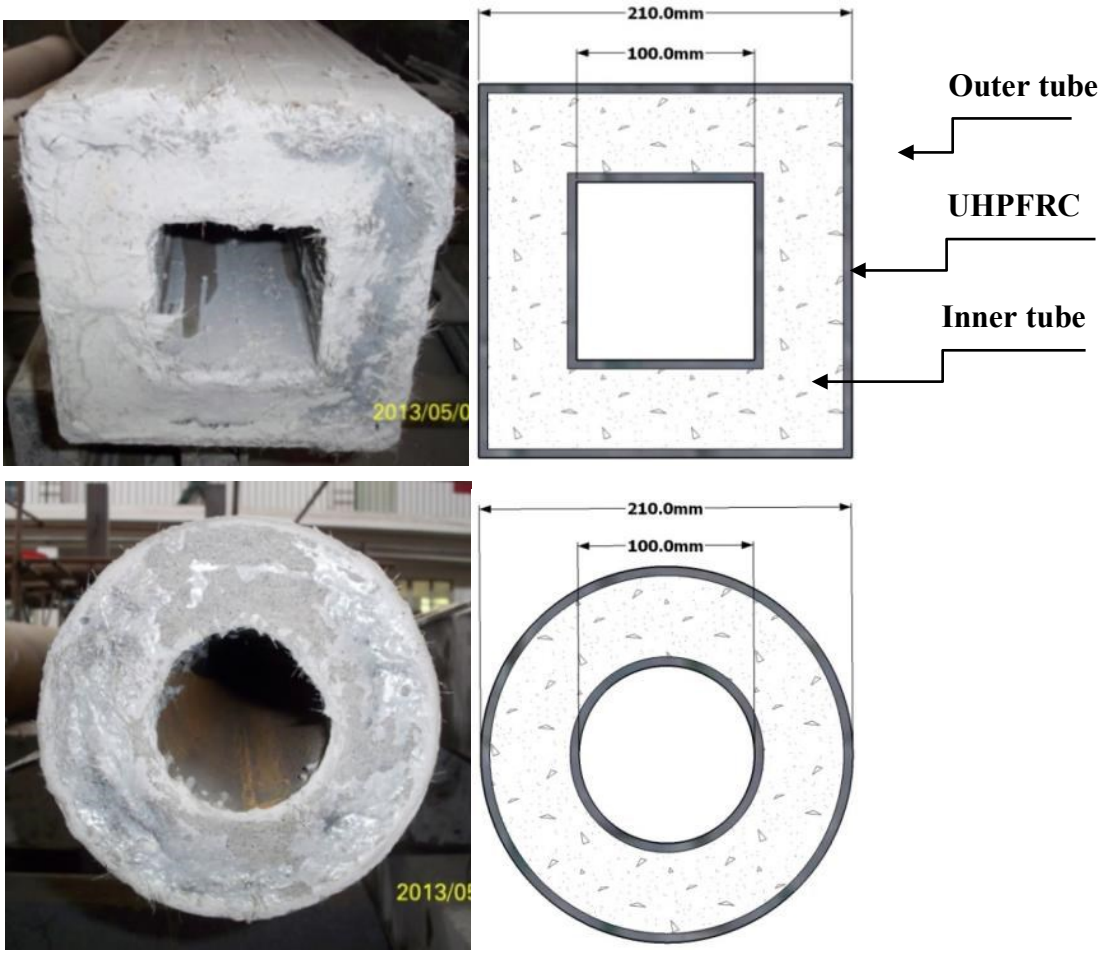

Fig. 1: Cross sections of a square and a circular CFDST specimen

All CFDST specimens used steel-fibre reinforced concrete as the concrete filler and nanoparticles, namely $CaCO_3$, were also added into the concrete mixture to fill the voids between cement grains as well as to improve the hydration process. The mixture was produced by mixing silica fume, fine sand and powder materials, which consisted of cement and nanoparticles, in a laboratory concrete mixer. They were firstly mixed in dry condition for 5 minutes prior to pouring in additives. Following that, approximate 70% of the water used in the entire process was added to fluidise the mix. Three minutes later, superplasticiser was then added followed by the other 30% of the water. The mixing process then continued for another 5 minutes and until then, micro steel fibres were poured into the mix and manually dispersed to avoid clumping.

To obtain the material properties, twenty-nine $100\text{mm} \times 100\text{mm} \times 100\text{mm}$ specimens were made for cube compressive tests and another twenty-nine $100\text{mm} \times 100\text{mm} \times 400\text{mm}$ specimens were made for flexural tensile tests. Prior to any tests, each specimen was properly levelled, sanded, polished, cleaned and dried to attain smooth surfaces. On average, the 28-day compressive strength and flexural tensile strength of the proposed concrete were 170 MPa and 33.8 MPa, respectively.

3. Experimental Program

3.1 Phase one: the static test

The axial compression tests and three point bending tests were carried out to investigate the behaviours of CFDST columns when subjected to axial compressive and transverse load, respectively. Those tests were carried out by using the experimental machineries as shown in Fig. 2. The test machine was displacement-controlled which mainly consisted of two fluid power systems: a horizontal hydraulic loading system for axial loading and a vertical hydraulic loading system for lateral loading. Both hydraulic jacks can carry up to 10,000 kN load and the test specimen length can be from 2000 mm to

3550 mm with the maximum displacement range of both hydraulic rams being 200 mm. As for support condition, the test specimen was simply supported near both ends and the location of supports can be adjusted accordingly to meet different experiment requirements

Tables 1 and 2 summarise the results of the axial compressive tests and three point bending tests, respectively. For comparison purpose, one circular and one square concrete-filled steel tube (CFST) specimens, namely TPB_C3 and TPB_S2, were also included to check the dissimilarities, in terms of their structural response, when compared with their double-skinned counterparts.

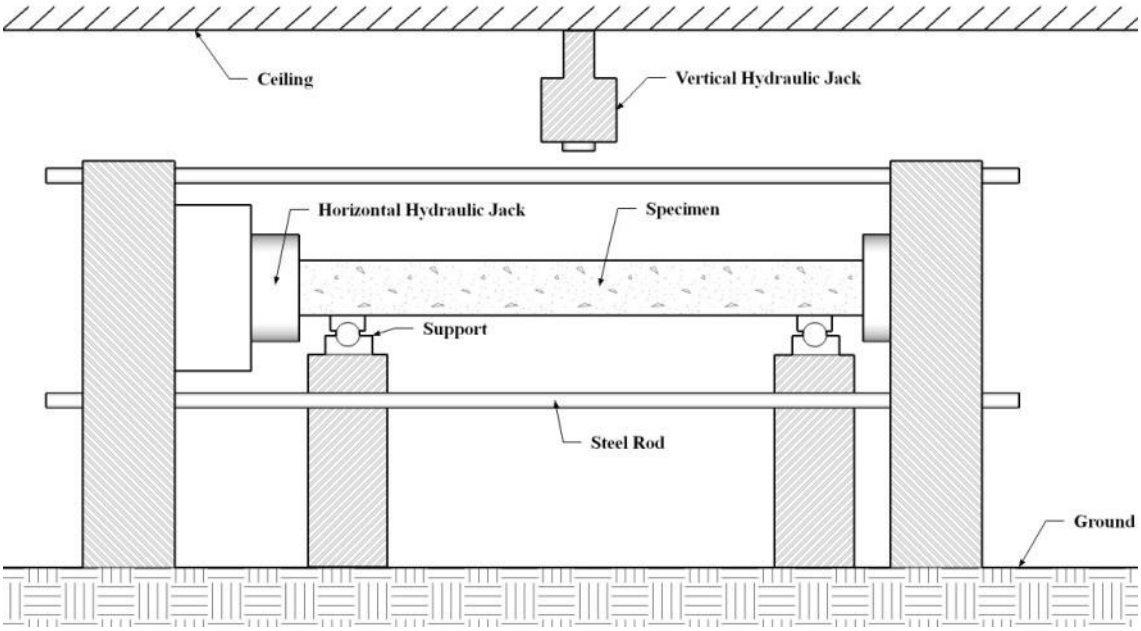

(a)

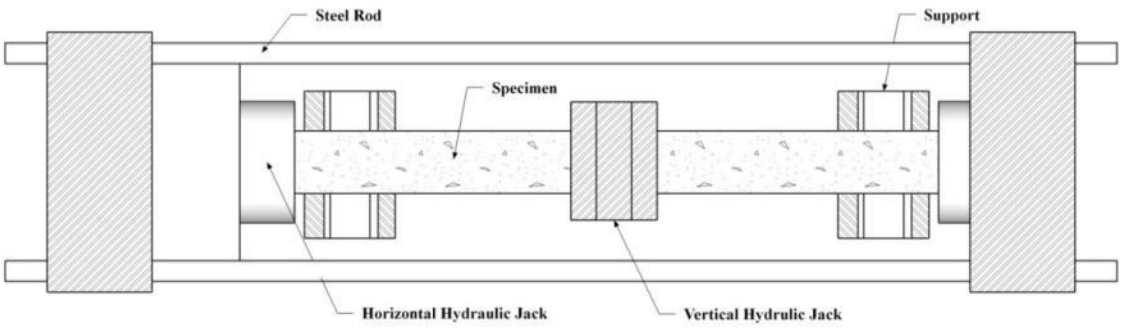

(b)

Fig. 2: The test machineries for the axial load test and three point bending tests: (a) elevation and (b) top view

Table 1: Axial compressive test

Specimen Label	Specimen Type	Nominal outer dimensions ($D \times t_{so}$)	Nominal inner dimensions ($D \times t_{io}$)	Axial Load (kN)
AC_C1	CFDST	210	100	4000
AC_S1	CFDST	210	100	4025

Note: "AC" means axial compression test

Table 2: Three point bending test

Specimen Label	Specimen Type	Nominal outer dimensions ($D \times t_{so}$)	Nominal inner dimensions ($D \times t_{io}$)	Axial Load (kN)	Peak Lateral Load (kN)
TPB_C1	CFDST	210	100	0	290.54
TPB_C2	CFDST	210	100	1000	484.03
TPB_C3	CFST	210	/	1000	412.52
TPB_S1	CFDST	210	100	1000	660.78
TPB_S2	CFST	210	/	1000	631.12

Note: "TPB" means three point bending test

Fig. 3 shows the axial load vs. axial shortening diagrams from the axial compressive tests. It can be seen that both specimens have similar peak axial load capacity although the specimen with square cross section has a larger cross sectional area. This verifies the theory that circular cross sections often result in better confinement under axial compression, thus larger axial capacity. Fig. 4 depicts the lateral load vs. lateral displacement diagrams from the three point bending tests.

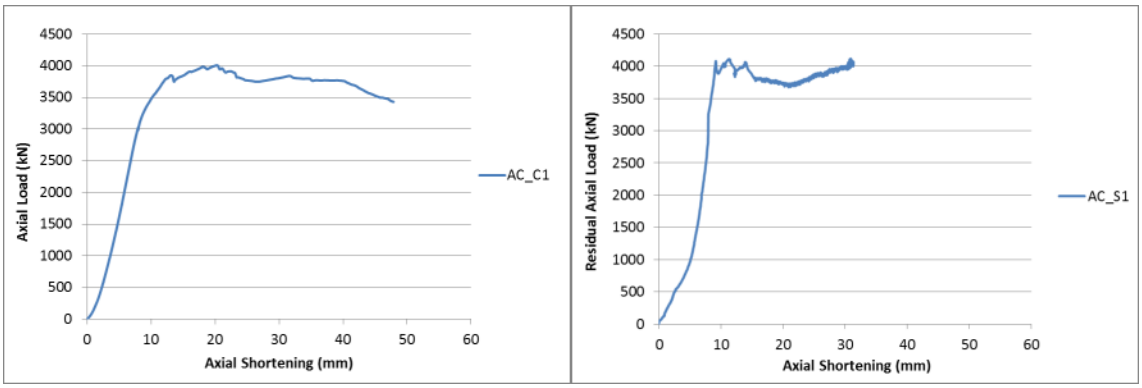

(a) (b)

Fig. 3: Axial compressive load vs. axial shortening curve: (a) circular CFDST and (b) square CFDST

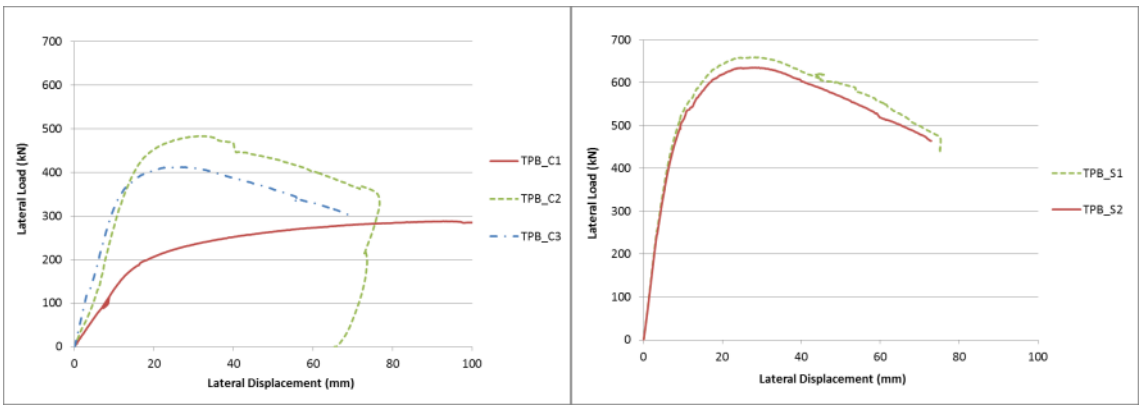

(a) (b)

Fig. 4: Load-displacement histories of three point bending tests for (a) circular and (b) square CFDST

3.1.1 Effect of axial load

Fig. 5 compares the axially loaded specimen TPB_C2 to the axial-load-free specimen TPB_C1. It is evident that the applied axial load on specimen TPB_C2 significantly increased the peak lateral load carrying capacity by 67%, compared to specimen TPB_C1 which was not axially loaded. However, in terms of ductility, specimen TPB_C1 behaved in a more ductile manner under flexural load while the load capacity of specimen TBP_C2 declined immediately after reaching its peak. The increase in the flexural load capacity due to axial loads can be well explained by the schematic moment–load interaction curve depicted in Fig. 6 where the moment capacity of a CFDST column can be enhanced by a low level of axial load (i.e. within branch BD). More details can be found in Zhao et al. [28] where an analytical model was also given to calculate the interaction curve for both CFST and CFDST columns.

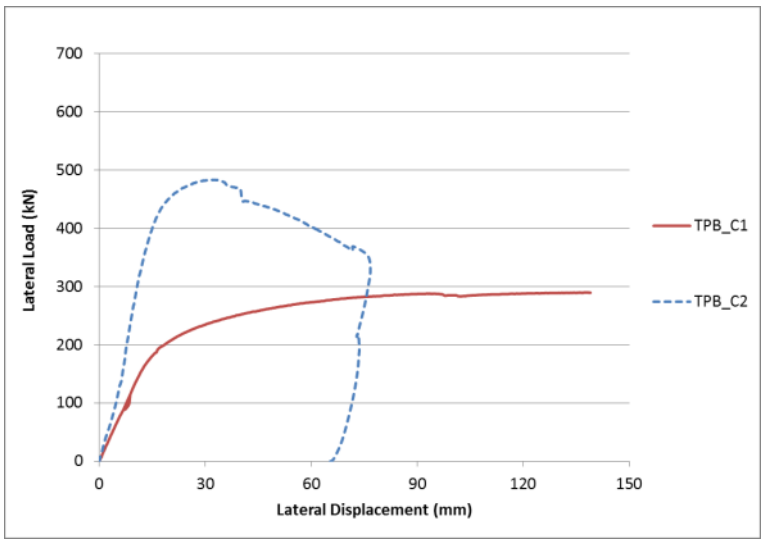

Fig. 5: Effect of axial load

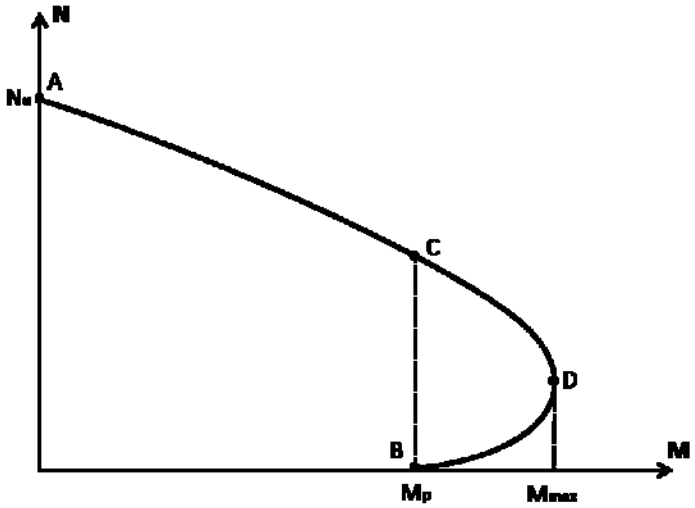

Fig. 6: Schematic view of M-N interaction diagram for CFST and CFDST [28]

In addition, the failure mode of axial-load-free specimen TPB_C1 was also found to be different from the rest axially loaded specimens. As shown in Figs. 7 and 8, the failure mode of the axial-load-free specimen was local buckling of the outer steel tube on the compression zone near the mid-span associated with noticeable outer steel tube crack on the tension zone near the mid-span whereas the failure mode of the axially loaded specimens was local buckling of the outer steel tube on the compression zone near the mid-span only.

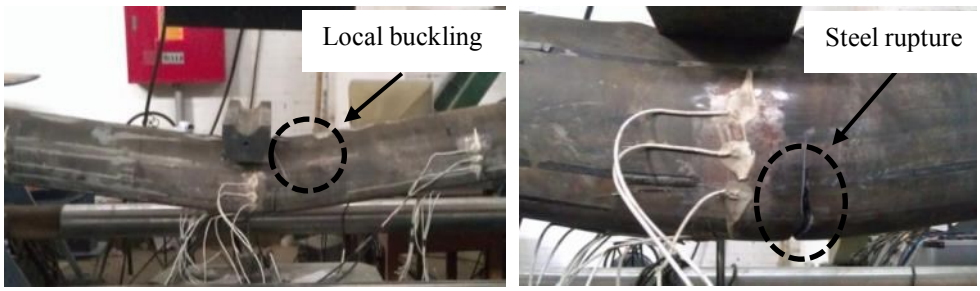

Fig. 7: Failure mode of TPB_C1

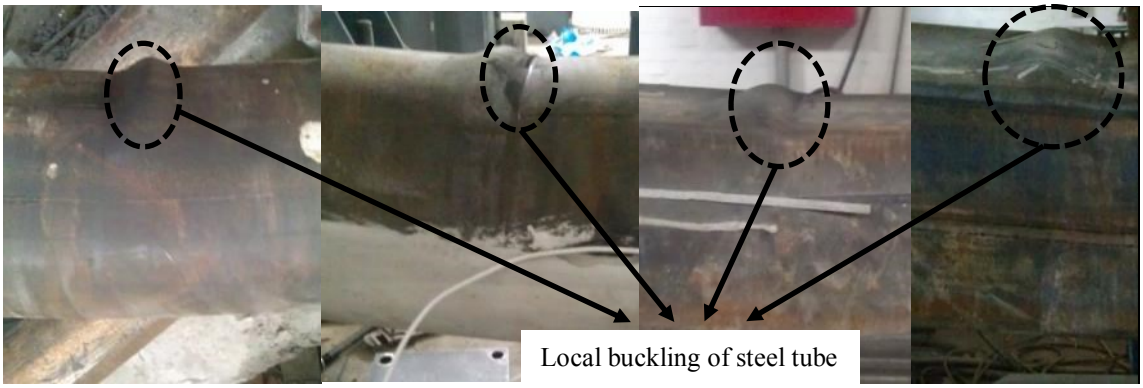

Fig. 8: Failure mode of other specimens (except TPB_C1)

3.1.2 Effect of the hollow core

Fig. 9 shows the effect of the hollow core on the circular and square cross sections. It was observed that the presence of the hollow cores in CFDST specimens does not impose a significant effect on the flexural behaviours as both curves showed very similar trend regardless of the cross section type. However, the presence of hollow cores caused a slight increase in the peak lateral load capacity, with this effect being more noticeable on circular specimens (i.e. 17%) rather than square specimens (i.e. 5%).

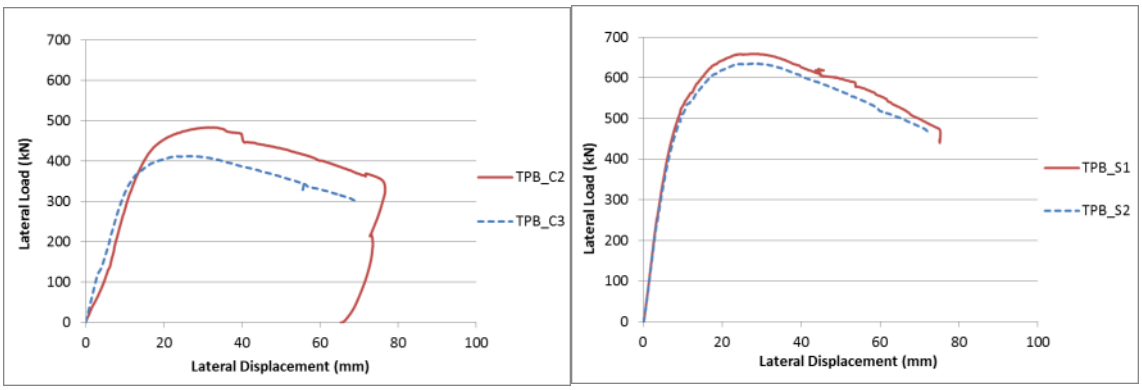

(a) (b)

Fig. 9: Effect of hollow core: (a) circular CFDST and (b) square CFDST

3.1.3 Effect of the cross section geometry

Fig. 10 shows the effect of the cross section geometry on the test specimens. It was shown that, although the overall behaviours of the circular and square specimens followed a similar pattern, the peak flexural load capacities of the square specimens were significantly larger than those of the circular specimens. In addition, the initial stiffness (i.e. the slope of the ascending branch) of the square specimens was also larger than those of the circular specimens. This finding indicates that the better confinement gained by the circular cross section does not significantly enhance the flexural load capacity as it does to the axial load capacity.

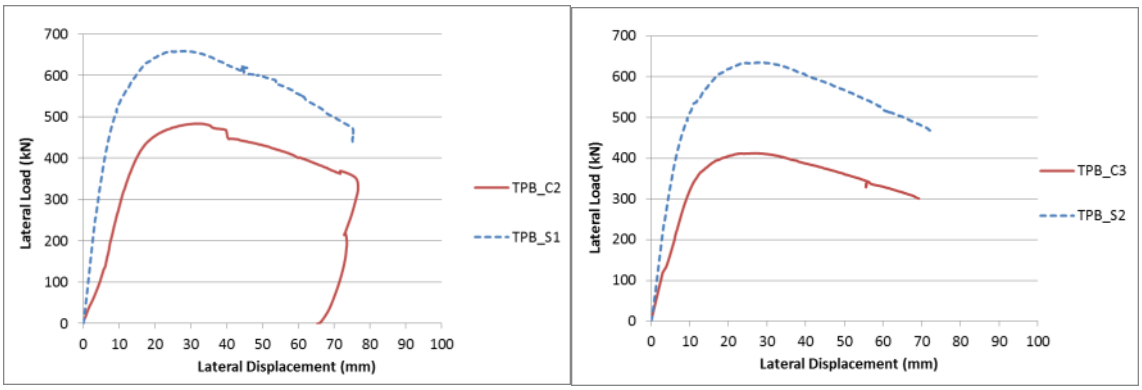

(a) (b)

Fig. 10: Effect of cross section geometry

3.2 Phase two: the blast experiment

As shown in Fig. 11(a), the test specimens and corresponding data cables were placed into the pre-excavated 3 m × 0.4 m × 1.5 m test pit during blast tests. It can be seen from Fig. 11(b) that the test pit was designed in such a way that it was as wide as the test specimens. As a result, once the test specimen was placed into the pit, the blast incident wave should be fully reflected thus preventing clearing effect from happening [29, 30]. A pneumatic jack was also installed at one side of the test pit to apply an axial load during the blast test. Important equipment (e.g. the pneumatic jack) was protected by 20 mm thick steel plates, preventing them from being disturbed or damaged by the blast wave. The test setup only allowed roller support at both ends and steel bolts were used to provide an

upward restraint against column rebound, thus making the effective span of the CFDST specimen 2300 mm.

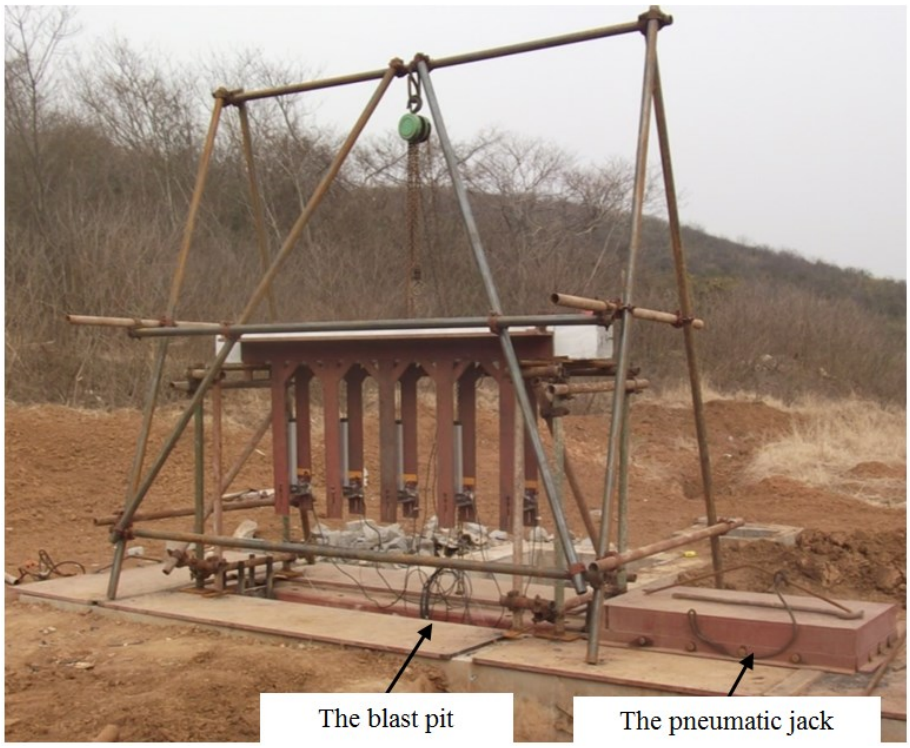

(a)

(b)

Fig. 11: Blast experiment setup

In terms of data acquisition, three displacement gauges (LVDTs) spaced at 380 mm, as shown in Fig. 12, were installed to measure the displacement–time histories along each test specimen. As for pressure–time histories, a pressure transducer was installed 760 mm away from the mid-span of the specimen; any closer positioning could significantly

increase the risk of damaging the pressure transducer due to the excessive amount of blast pressure.

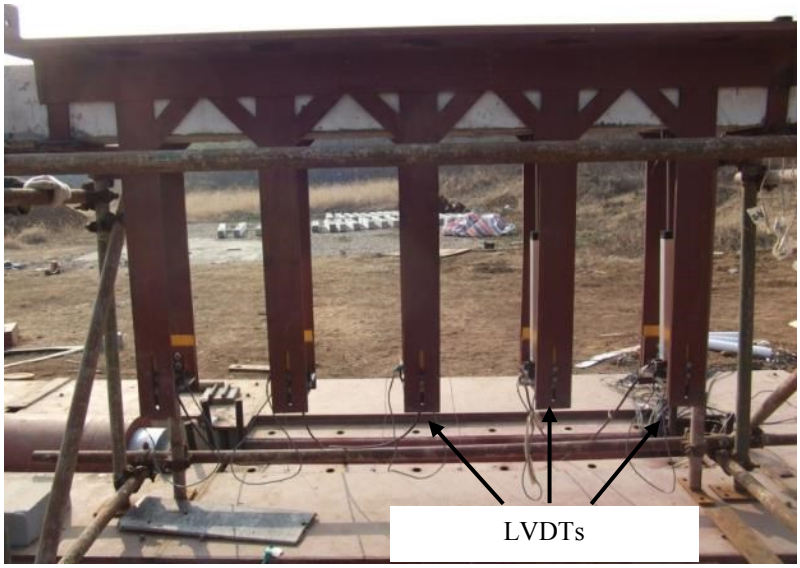

Fig. 12: Schematic view of the test setup

Since this paper mainly focuses on the residual performance of CFDST columns after blast loading, the blast test itself therefore is not discussed in great details. The results of the blast test are given in Table 3. The only thing that should draw extra attention was the differences in the test setups as shown in Fig. 13.

Table 3: Detailed information for each blast test specimen

Test series	Label	Speci-men setup	L (mm)	Nominal outer dimensions (D x t_{so})	Nominal inner dimensions (D x t_{io})	TNT (kg)	Axial load (kN)	Maximum Δ (mm)	Residual Δ (mm)
Square specimens	S1A	a*	2500	210 x 5	110 x 5	35	-	41	16
	S1B	a	2500	210 x 5	110 x 5	50	-	49	22
	S2A	a	2500	210 x 5	110 x 5	35	1000	36	8
	S2B	a	2500	210 x 5	110 x 5	50	1000	/	14*
	S3A	a	2500	210 x 5	110 x 5	50	1000	41	8
	S3B	a	2500	210 x 5	-	50	1000	50	10
Circular specimens	C1A	b	2500	210 x 5	110 x 5	35	-	98	65
	C1B	c	2500	210 x 5	110 x 5	35	-	50	20
	C2A	b	2500	210 x 5	110 x 5	35	1000	/	39*
	C2B	c	2500	210 x 5	110 x 5	17.2	-	35	12
	C3A	b	2500	210 x 5	110 x 5	50	1000	91	52
	C3B	b	2500	210 x 5	-	50	1000	83	43

Note: *the different experimental setups.

**LVDT readings were lost for S2B and C2A, residual displacements were manually measured.

In order to explore the relationship among the residual deflection, the blast load and the geometry of the specimen, a normalised parameter λ is introduced which is a dimensionless form of the initial kinetic energy of the CFDST specimen [31].

$$\lambda = \frac{\mathrm{m}v_0{}^2 L^2}{M_u H} \tag{2}$$

where, m is the mass per unit length, v_0 is the initial velocity of the specimen, L is half of the effective length of the specimen, M_u is the ultimate moment capacity, H is the depth of the specimen.

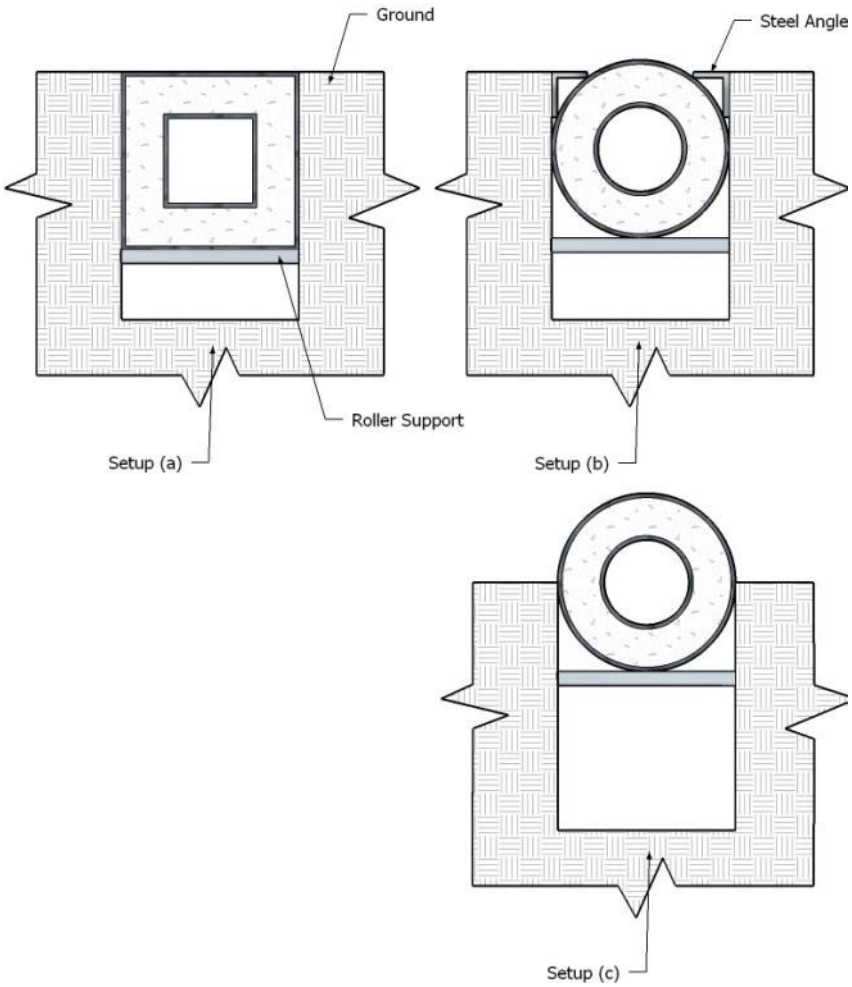

Fig. 13: Cross-sectional view of the specimen setups

Table 4 lists the parameters needed to calculate the value of λ for each CFDST specimen used in the blast experiment. The initial velocity was derived from differentiating the displacement-time history of each specimen. According to Zhao [28], when subjected to flexural loading, the outer steel of a CFDST column behaves in the same way as a CFST column whereas the inner steel tube behaves in a similar way as an empty steel tube. Therefore, the ultimate moment capacity of a CFDST column can be approximately by

simply superposing the section capacity of an inner tube and that of an outer tube filled with concrete:

$$M_{CFDST} = M_{inner\ tube} + M_{Outer\ tube\ with\ concrete} \quad (3)$$

The step by step calculations for M_{CFDST} have been demonstrated by Zhao and Choi [32] in detail thus only the results are given hereafter. It should be mentioned that since UHPFRC is used in the current research, its tensile strength shall not be ignored in calculation.

Table 4: Parameters of each specimen for λ

Specimen	TNT (kg)	Axial load (kN)	Mass per unit length (kg/m)	Initial velocity (m/s)	Half column length (m)	Ultimate moment capacity (N·m)	Cross section depth (m)	Residual deflection (mm)	λ
S1A	35	0	115.3	18.3	1.15	269200	0.21	16	0.90
S1B	50	0	115.3	28	1.15	269200	0.21	22	2.11
S2A	35	1000	115.3	13	1.15	269200	0.21	8	0.46
S2B	50	1000	115.3	/	1.15	269200	0.21	14	/
S3A	50	1000	115.3	22	1.15	269200	0.21	8	1.31
S3B	50	1000	128	33	1.15	230400	0.21	10	3.81
C1A	35	0	90.6	43.3	1.15	183800	0.21	65	5.82
C1B	35	0	90.6	24	1.15	183800	0.21	20	1.79
C2A	35	1000	90.6	/	1.15	183800	0.21	39	/
C2B	17.2	0	90.6	16	1.15	183800	0.21	12	0.79
C3A	50	1000	90.6	36.8	1.15	183800	0.21	52	4.20
C3B	50	1000	100.5	45.6	1.15	164000	0.21	43	8.02

It can be observed that specimens S3B and C3B deviated from the rest of the points quite significantly. This could be due to the fact that both S3B and C3B were CFST specimens (i.e. no hollow section inside) which were structurally different from the rest of the CFDST specimens. Fig. 14 also reveals that the residual deflection of a CFDST column increased linearly, regardless of the cross section geometry, and the relationship can be expressed as:

$$\text{Residual deflection} = 13.14\lambda + 1.18 \quad (4)$$

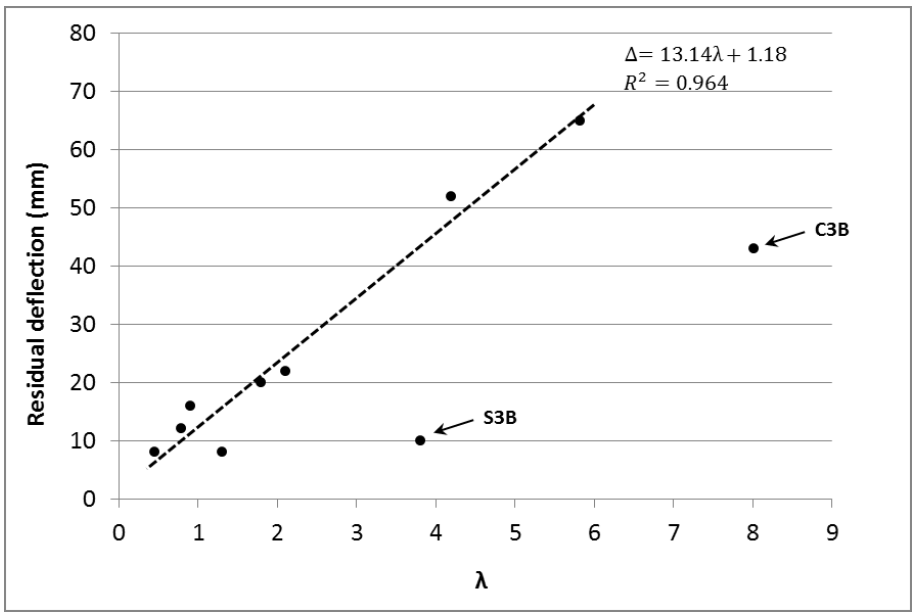

Fig. 14: Residual deflection vs. dimensionless parameter λ

3.3 Phase three: the residual performance test

The residual performance tests were carried out in the Joint Research Centre of Tianjin Chengjian University and The University of Adelaide. The same experiment machineries used for the previous static tests were also used for this test. During the experiment, instead of directly load specimens to their peak capacities, the loading schematic in Fig. 15 was introduced. At first, the specimen was gradually loaded axially to 500 kN, it was then maintained at this load level for 60 s to eliminate any the inhomogeneity in the specimen. This procedure was also repeated at 1000 kN and 2000 kN load level to achieve the best stability.

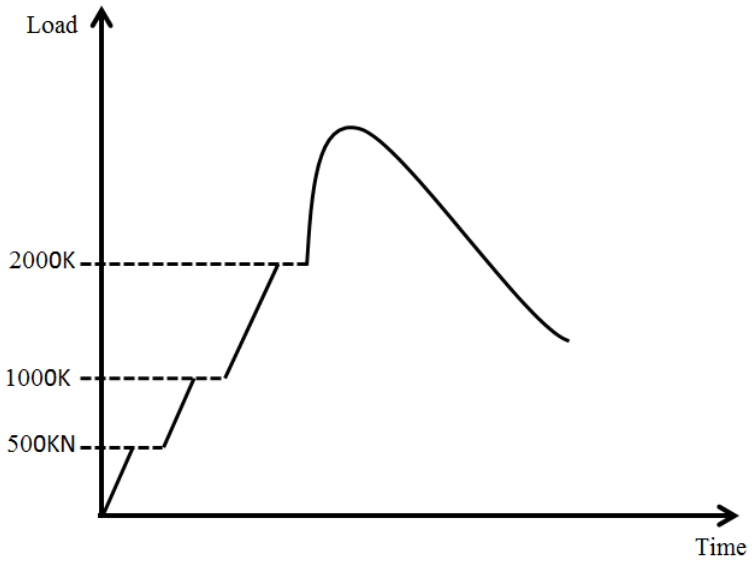

Fig. 15: The loading schematic for residual capacity test

Figs. 16 and 17 show the residual axial load vs. axial shortening diagrams of all test specimens and for comparison purpose, the curves of the undamaged specimens were also included. As a result of the damage accumulated during the blast test, none of the test specimens could carry as much axial load as before. In addition, all damaged specimens also behaved in a much less ductile manner under axial compressive load when compared to the undamaged control specimens.

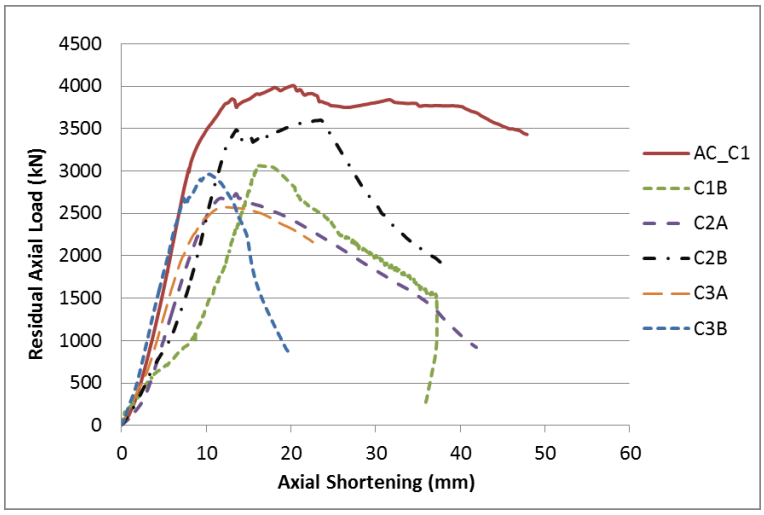

Fig. 16: The residual axial load vs. axial shortening histories for circular specimens

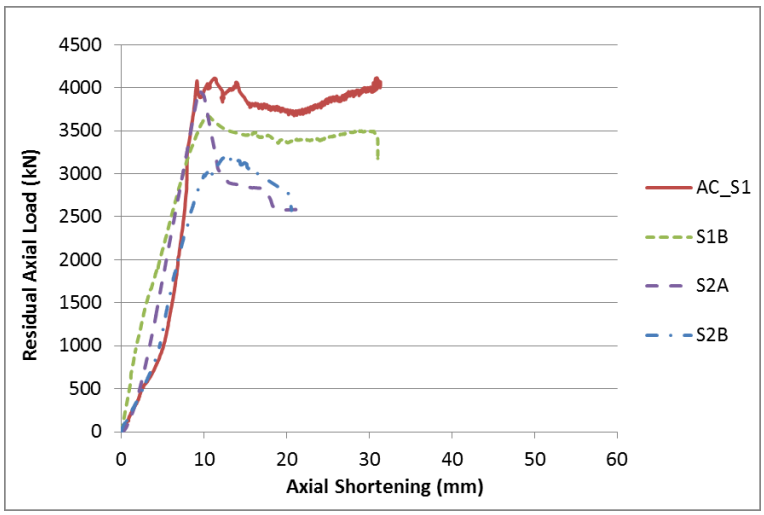

Fig. 17: The residual axial load vs. axial shortening histories for square specimens

The residual axial load capacities of the test specimens are listed in Table 4. The damage criterion is defined as the ratio between the residual axial load capacity and the designed axial load capacity of an undamaged specimen, known as the damage index D [2]:

$$\mathrm{D} = 1 - \frac{P_{N_{Residual}}}{P_{N_{Undamaged}}} \tag{5}$$

In order to calculate the damage index for the CFST specimen C3B, its designed axial load needs to be calculated. It was estimated by simply calculating the extra nominal axial capacity obtained by taking out the inner steel tube and then filling the hollow section by UHPFRC.

Table 5 indicates that, all damage indices of the test specimens were within 0.4, meaning only minor to moderate damage was done to the specimens during the blast test despite that large TNT equivalent charge weight was used and placed at a small standoff distance.

Table 5: Results of residual performance test

Specimen label	TNT (kg)	test setup	Applied axial load (kN)	Axial load capacity(kN)	Residual axial load (kN)	Residual Deflection (mm)	Max. Support rotation (degree)	Damage index
S1B	50	a	-	4025	3670	22	2.44	0.09
S2A	35	a	1000	4025	3970	8	1.79	0.01
S2B	50	a	1000	4025	3184	14	/	0.21
C1B	35	c	-	4000	3060	20	2.49	0.24
C2A	35	b	1000	4000	2733	39	/	0.32
C2B	17.2	c	-	4000	3594	12	1.74	0.10
C3A	50	b	1000	4000	2573	52	4.52	0.36
C3B	50	b	1000	4780	2962	43	4.13	0.38

3.3.1 Effect of the explosive charge weight

Fig. 18 shows the effect of explosive charge weight on the residual axial capacity. It is conclusive that, with the same applied axial load, specimens subjected to lesser explosive charge weight can always retain more residual axial capacity regardless of the cross section geometry, thus having a smaller damage index.

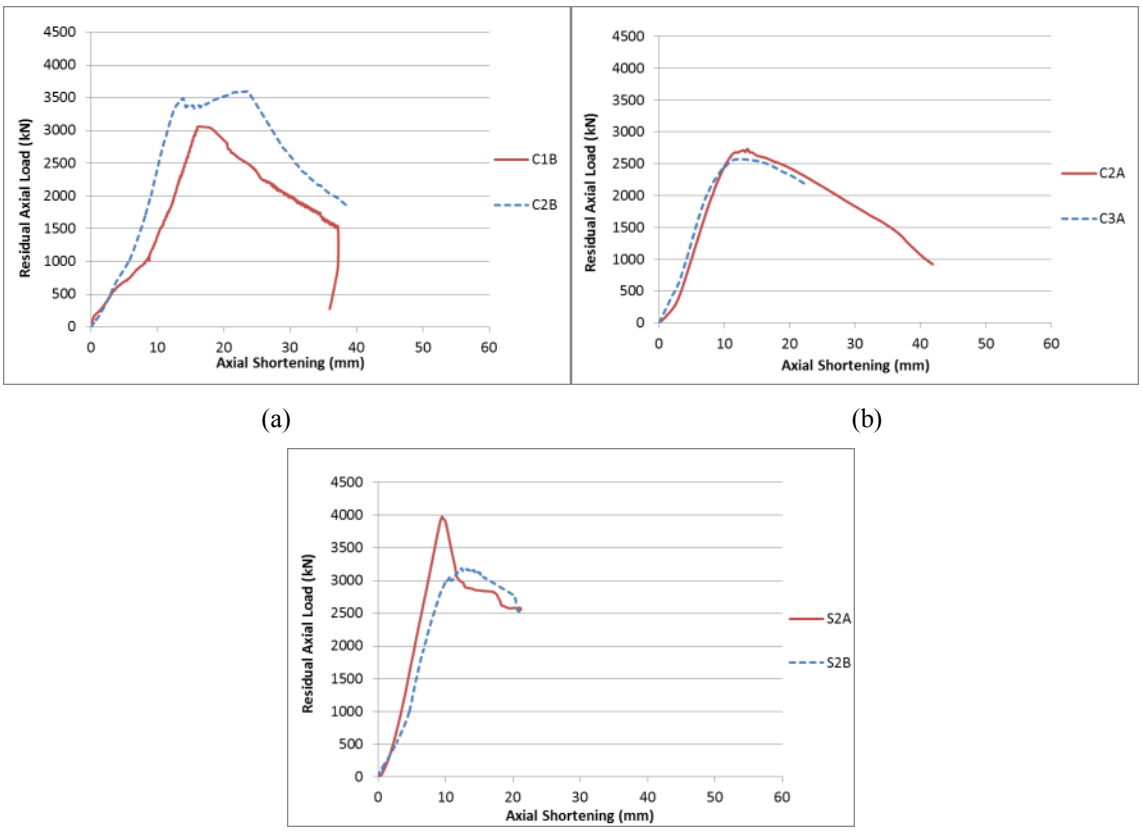

Fig. 18: Effect of explosive charge weight on residual performance

3.3.2 *Effect of the hollow core*

From Fig. 19, the CFST specimen C3B was able to retain a larger residual axial capacity than the CFDST specimen C3A under the same blast load. However, since specimen C3A had a smaller designed axial load capacity, the damage indices of both specimens were very similar. In addition, specimen C3A seems to have a more ductile behaviour over specimen C3B.

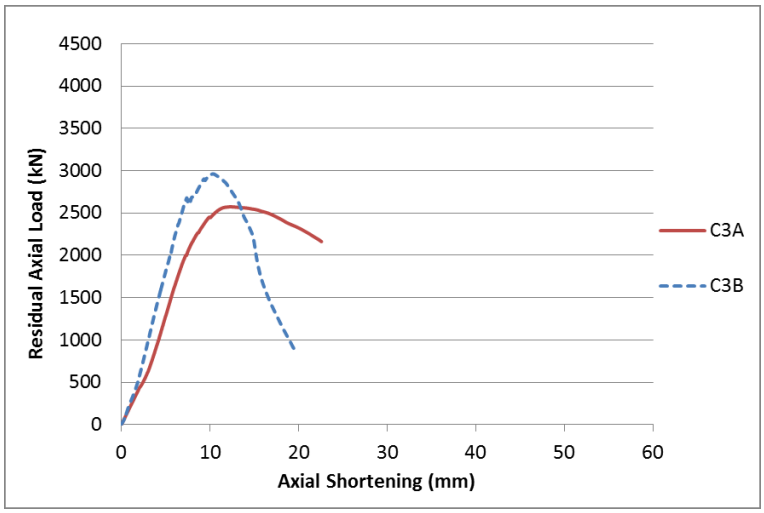

Fig. 19: Effect of hollow core on residual performance

3.3.3 *Effect of the axial load*

It can be noticed in the previous section that the axially loaded CFDST column (e.g. S2B) always had a smaller residual deflection than the axial-load-free column (e.g. S1B) under the same blast loads. However, as shown in Fig. 20, the CFDST specimen (e.g. S1B), which was not previously axially loaded in a blast event, can not only behave in a more ductile manner, but also retain a greater residual axial capacity, thus resulting in a smaller damage index, than an previously axially loaded CFDST specimen (e.g. S2B).

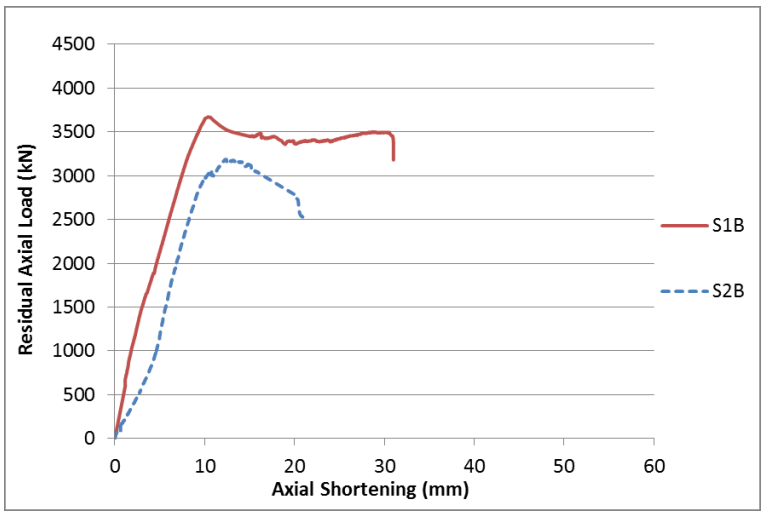

Fig. 20: Effect of axial load on residual performance

3.3.4 Failure Mode

Table 6 summaries the failure modes of all test specimens and Figs. 21 and 22 depict the deformed shape of the circular and square specimens, respectively.

For the circular CFDST columns, it was found that if the damage index was less than 0.3, local buckling of steel tube was more likely to happen (i.e. C1B & C2B); otherwise, steel rupture was more likely to happen (i.e. C2A & C3B). The only exception was specimen C3A, whose failure mode was global flexural failure despite having a damage index of 0.36. However, it can be found in Fig. 16 that the displacement curve of specimen C3A was very similar to that of specimen C2A (the latter was subjected to a lesser blast load during the blast test with the rest of the parameters being the same) except the loading somehow stopped when its axial shortening reached 23 mm whereas the rest of the circular specimens were normally loaded until column instability was observed; also, no obvious sign of local buckling of steel were seen on specimen C3A either. It is then reasonable to speculate that if specimen C3A was further loaded until failure, it would fail due to mid-span rupture just like C2A. Elchalakani et al. [33] also reported similar phenomenon (i.e. rupture of steel tube near mid-span) on CFST columns under large deformation cyclic loading.

On the other hand, for square specimens, local buckling at mid-span and/or column ends was the main failure mode with no signs of steel rupture. This type of local damage mode was also observed by [34] where they subjected square CFST columns to cyclic axial loading.

Table 6: failure modes of all specimens

Label	Failure Modes	Damage index
S1B	Local buckling at ends	0.09
S2A	Local buckling at mid-span	0.01
S2B	Local buckling at mid-span and ends	0.21
C1B	Local buckling at mid-span and ends	0.23
C2A	Outer steel rupture at mid-span	0.32
C2B	Local buckling at mid-span	0.10
C3A	Global flexural failure	0.36
C3B	Outer steel rupture at mid-span	0.38

(a): C1A

(b): C2A

(c): C2B

(d): C3A

(e): C3B

Fig. 21: Failure modes of circular specimens

(a): S1B

(b): S2A

(c): S2B

Fig. 22: Failure modes of square specimens

4. Conclusion

This paper has presented an experimental study on the static, dynamic and residual performance of concrete-filled double-skin steel tube (CFDST) columns filled with UHPFRC after close-range blast loading. The following conclusions can be drawn based on the test results and observations:

1. The axial load capacities of undamaged circular and square CFDST specimens were very similar, which were 4000 kN and 4025 kN, respectively, although square specimens had larger nominal cross sectional area. This is probably due to better confinement provided by the circular cross section.

2. Under static lateral load, the flexural load capacity of a square CFDST specimen was larger than its circular counterpart; also, an axially loaded CFDST specimen, with about 25% of its axial capacity, yielded a larger flexural load capacity than an axial-load-free counterpart, however this also led to a reduction in the ductility.

3. A dimensionless parameter λ was introduced to describe the relationship among the residual deflection, the blast load and the geometric dimension of the CFDST specimens. It was found that the residual deflection almost increased linearly with λ and the equation describing this linear relationship was also derived.

4. A damage index was used to assess the residual performance of CFDST specimens after blast loading and it was found that the damage indices of all CFDST specimens were less than 0.4, indicating that the CFDST specimens were able to retain more than 60% of its axial load capacity even after severe blast loading.

5. During the residual axial capacity tests after close-range blast loading, localised buckling failure of the outer steel tubes at mid-span and/or column ends always occurred for square CFDST; whereas for circular CFDST, localised buckling failure occurred when the damage level was low and steel rupture happened when the damage level was high. The failure modes were similar to those of CFST members subjected to damage caused by large deformation cyclic loading.

Acknowledgements

The research presented in this paper jointly supported by the National Key Technology R&D Program of the Ministry of Science and Technology of China of the People's Republic of China (2012BAJ07B05), the National Natural Science Foundation of China under Grant 51278326, and the ARC Discovery Grants DP130100181 and DP140103025, is gratefully acknowledged.

References

[1] Li, B, Nair, A, and Kai, Q, *Residual Axial Capacity of Reinforced Concrete Columns with Simulated Blast Damage.* Journal of Performance of Constructed Facilities, 2012. **26**(3): p. 287-299.

[2] Shi, Y, Hao, H, and Li, Z-X, *Numerical Derivation of Pressure–Impulse Diagrams for Prediction of RC Column Damage to Blast Loads.* International Journal of Impact Engineering, 2008. **35**(11): p. 1213-1227.

[3] Bao, X and Li, B, *Residual Strength of Blast Damaged Reinforced Concrete Columns.* International Journal of Impact Engineering, 2010. **37**(3): p. 295-308.

[4] Wu, K-C, Li, B, and Tsai, K-C, *Residual axial compression capacity of localized blast-damaged RC columns.* International Journal of Impact Engineering, 2011. **38**(1): p. 29-40.

[5] Wei, S, Mau, S, Vipulanandan, C, and Mantrala, S, *Performance of New Sandwich Tube under Axial Loading: Experiment.* Journal of Structural

Engineering, 1995. **121**(12): p. 1806-1814.
[6] Uenaka, K, Kitoh, H, and Sonoda, K, *Concrete Filled Double Skin Circular Stub Columns under Compression.* Thin-Walled Structures, 2010. **48**(1): p. 19-24.
[7] Zhao, X-L, Tong, L-W, and Wang, X-Y, *CFDST stub columns subjected to large deformation axial loading.* Engineering Structures, 2010. **32**(3): p. 692-703.
[8] Huang, H, Han, L-H, Tao, Z, and Zhao, X-L, *Analytical behaviour of concrete-filled double skin steel tubular (CFDST) stub columns.* Journal of Constructional Steel Research, 2010. **66**(4): p. 542-555.
[9] Yuan, W-b and Yang, J-j, *Experimental and Numerical Studies of Short Concrete-Filled Double Skin Composite Tube Columns under Axially Compressive Loads.* Journal of Constructional Steel Research, 2013. **80**: p. 23-31.
[10] Pagoulatou, M, Sheehan, T, Dai, X, and Lam, D, *Finite element analysis on the capacity of circular concrete-filled double-skin steel tubular (CFDST) stub columns.* Engineering Structures, 2014. **72**: p. 102-112.
[11] Han, LH, Tao, Z, Huang, H, and Zhao, XL, *Concrete-filled double skin (SHS outer and CHS inner) steel tubular beam-columns.* Thin-Walled Structures, 2004. **42**: p. 1329-1355.
[12] Tao, Z and Han, L-H, *Behaviour of concrete-filled double skin rectangular steel tubular beam–columns.* Journal of Constructional Steel Research, 2006. **62**(7): p. 631-646.
[13] Tao, Z, Han, L-H, and Zhao, X-L, *Behaviour of concrete-filled double skin (CHS inner and CHS outer) steel tubular stub columns and beam-columns.* Journal of Constructional Steel Research, 2004. **60**(8): p. 1129-1158.
[14] Han, L-H, Huang, H, and Zhao, X-L, *Analytical behaviour of concrete-filled double skin steel tubular (CFDST) beam-columns under cyclic loading.* Thin-Walled Structures, 2009. **47**(6): p. 668-680.
[15] Han, L-H, Huang, H, Tao, Z, and Zhao, X-L, *Concrete-filled Double Skin Steel Tubular (CFDST) Beam–columns Subjected to Cyclic Bending.* Engineering Structures, 2006. **28**(12): p. 1698-1714.
[16] Zhang, F, Wu, C, Zhao, X-L, Li, Z-X, Heidarpour, A, and Wang, H, *Numerical Modeling of Concrete-Filled Double-Skin Steel Square Tubular Columns under Blast Loading.* Journal of Performance of Constructed Facilities, 2015.
[17] Li, W, Han, L-H, and Chan, T-M, *Tensile behaviour of concrete-filled double-skin steel tubular members.* Journal of Constructional Steel Research, 2014. **99**: p. 35-46.
[18] Li, W, Han, L-H, and Chan, T-M, *Numerical investigation on the performance of concrete-filled double-skin steel tubular members under tension.* Thin-Walled Structures, 2014. **79**: p. 108-118.
[19] Huang, H, Han, L-H, and Zhao, X-L, *Investigation on concrete filled double skin steel tubes (CFDSTs) under pure torsion*. Journal of Constructional Steel Research, 2013. **90**: p. 221-234.
[20] Lu, H, Zhao, X-L, and Han, L-H, *Testing of self-consolidating concrete-filled double skin tubular stub columns exposed to fire.* Journal of Constructional Steel Research, 2010. **66**(8): p. 1069-1080.

[21] Han, L-H, Hou, C-C, Zhao, X-L, and Rasmussen, KJ, *Behaviour of high-strength concrete filled steel tubes under transverse impact loading.* Journal of Constructional Steel Research, 2014. **92**: p. 25-39.

[22] Varma, AH, Ricles, JM, Sause, R, and Lu, L-W, *Experimental behavior of high strength square concrete-filled steel tube beam-columns.* Journal of Structural Engineering, 2002. **128**(3): p. 309-318.

[23] Liew, J and Xiong, D, *Experimental investigation on tubular columns infilled with ultra-high strength concrete.* 2010.

[24] *GB/T 8162 - 2008: Seamless steel tubes for structural purposes*, 2008, National Standard of China.

[25] *GB/T 228.1 - 2010: Metallic materials - Tensile testing - Part 1: Method of test at room temperature*, 2010, National Standard of China.

[26] Australian Standard, *4100: 1990: Steel Structures.* Standards Australia, Sydney, 1998.

[27] Elchalakani, M, Zhao, X-L, and Grzebieta, R, *Concrete-filled circular steel tubes subjected to pure bending.* Journal of Constructional Steel Research, 2001. **57**(11): p. 1141-1168.

[28] Zhao, X-L, Han, L-H, and Lu, H, *Concrete-filled tubular members and connections*. 2010: Spon Press London.

[29] Wu, C, Oehlers, DJ, Wachl, J, Glynn, C, Spencer, A, Merrigan, M, and Day, I, *Blast testing of RC slabs retrofitted with NSM CFRP plates.* Advances in Structural Engineering, 2007. **10**(4): p. 397-414.

[30] Tyas, A, Warren, J, Bennett, T, and Fay, S, *Prediction of clearing effects in far-field blast loading of finite targets.* Shock Waves, 2011. **21**(2): p. 111-119.

[31] Jones, N, *Structural impact*. 2011: Cambridge university press.

[32] Zhao, X and Choi, A. *Moment capacity of concrete filled double skin tubes*. in *Tubular Structures XIII-Proceedings of the 13th International Symposium on Tubular Structures*. 2010. CRC Press/Balkema.

[33] Elchalakani, M, Zhao, X-L, and Grzebieta, R, *Concrete-filled steel circular tubes subjected to constant amplitude cyclic pure bending.* Engineering Structures, 2004. **26**(14): p. 2125-2135.

[34] Zhao, X-L, Grzebieta, R, and Lee, C, *Void-filled cold-formed rectangular hollow section braces subjected to large deformation cyclic axial loading.* Journal of Structural Engineering, 2002. **128**(6): p. 746-753.

Chapter 2 – Numerical Study of Concrete-filled Steel Columns under Close-range Blast Loading

Introduction

While the first chapter focuses only on experimental studies, the second chapter of this thesis presents numerical analysis of concrete filled steel columns under blast loading. Numerical models within this chapter are all developed by using the finite element tool LS-DYNA.

In the first journal paper entitled "Numerical simulation of concrete filled steel tube columns against blast loads", CFST columns filled with normal-strength concrete are investigated. In this paper, numerical studies are carried out to investigate the flexural behaviour of CFST columns under both static and blast loads. The proposed numerical models are validated against a number of experimental data where they showed reasonable agreement with the test results. The numerical models can be easily used to predict the performance of CFST columns under different loading conditions.

In the second journal paper, which is "Numerical modelling of concrete-filled double-skin steel square tubular columns under blast loading", numerical models of CFDST columns with two different cross sections are developed: one is with a CHS (circular hollow section) outer and CHS (circular hollow section) inner, and the other one is with SHS (square hollow section) outer and SHS (square hollow section) inner. Normal-strength concrete is filled in double-skin steel tubes. Different blast loads are applied to the surface of these columns for dynamic analysis and different axial loads are also applied to simulate combined load conditions.

Within the third paper entitled "Experimental and numerical study of the blast resistance of square CFDST columns with steel-fibre reinforced concrete", existing constitutive material model for concrete in LS-DYNA is tuned, based on a series of laboratory test results, in order to successfully simulate the behaviours of UHPC. The proposed numerical models of UHPCFDST columns are then validated against the flexural

and blast tests as discussed in chapter 1 previously and they are proven to be able to accurately predict the behaviours of UHPCFDST under various loading conditions.

Statement of Authorship

Title of Paper	Numerical simulation of concrete filled steel tube columns against blast loads
Publication Status	☑ Published ☐ Accepted for Publication ☐ Submitted for Publication ☐ Unpublished and Unsubmitted w ork w ritten in manuscript style
Publication Details	Zhang, F., Wu, C., Wang, H. & Zhou, Y. 2015. Numerical simulation of concrete filled steel tube columns against BLAST loads. *Thin-Walled Structures,* 92, 82-92.

Principal Author

Name of Principal Author (Candidate)	Fangrui Zhang		
Contribution to the Paper	The author developed numerical model, undertook data analysis and prepared manuscript.		
Overall percentage (%)	60%		
Certification:	This paper reports on original research I conducted during the period of my Higher Degree by Research candidature and is not subject to any obligations or contractual agreements with a third party that would constrain its inclusion in this thesis. I am the primary author of this paper.		
Signature		Date	

Co-Author Contributions

By signing the Statement of Authorship, each author certifies that:

i. the candidate's stated contribution to the publication is accurate (as detailed above);

ii. permission is granted for the candidate in include the publication in the thesis; and

iii. the sum of all co-author contributions is equal to 100% less the candidate's stated contribution.

Name of Co-Author	Chengqing Wu		
Contribution to the Paper	This co-author supervised research, provided critical manuscript evaluation and acted as corresponding author.		
Signature		Date	6/6/2016

Name of Co-Author	Hongwei Wang		
Contribution to the Paper	This co-author helped design and conduct tests.		
Signature		Date	2016. 6. 3

Name of Co-Author	Yun Zhou
Contribution to the Paper	This co-author helped design and conduct tests.
Signature	Date 2016.6.9

NUMERICAL SIMULATION OF CONCRETE FILLED STEEL TUBE COLUMNS AGAINST BLAST LOADS

Fangrui Zhang, Chengqing Wu, Hongwei Wang, Yun Zhou

Abstract

Concrete filled steel tubes (CFST) have been widely used in constructing high-rise buildings, arch bridges and factories for the past few decades. In this research, numerical studies were carried out to investigate the flexural behaviour of CFST columns under both static and dynamic loads. The numerical models were calibrated and validated against a number of experimental data where the proposed models showed very good agreement with the test results. The results indicated that CFST columns showed good resistance against flexural loads under both static and dynamic loading conditions and therefore it has the potential to be widely used in these areas where potential blast attacks or frequent earthquakes are expected. The verified numerical model can also be extended to predict performances of concrete-filled steel tubes under different loading conditions.

1. Introduction

A concrete filled steel tube (CFST) simply consists of one steel tube with concrete filled inside. In recent years, the use of CFST members has been increasingly popular in the field of construction due to the attractive properties such as ease of construction, high strength and excellent ductility [1-3]. For the past few decades, a large amount of research has been conducted to explore the performance of CFST columns under various loading conditions.

The main advantage of CFST columns is the passive confinement effect resulted from the interaction between the core concrete and the steel tube. Several studies have suggested that the overall axial load capacity of a CFST column can be much larger than

the combined ultimate capacity of the steel tube and the concrete when acting alone and the ductility of a CFST column under axial load as well as flexural load can be also significantly enhanced [4-8].

Although much effort has been put to study the behaviours of CFST columns under static load, the investigation on its structural behaviours under dynamic load is still relatively lacking. Prichard and Perry [9] carried out axial-direction drop hammer tests on CFST cylinders and compared them to unreinforced concrete cylinders. The test results suggested that unconfined concrete cylinders failed mainly by splitting axially into several sections while for CFST cylinders, only minor cracks were found on the contact surface at high velocity impact. Xiao and Shen [10] further explored the feasibility and effectiveness of using carbon fibre reinforced polymer (CFRP) as additional external confinement for CFST columns when subjected to axial impact load.

Recently, a number of tests on CFST members under transverse impact load have been also carried out. Han et al. [11] proposed a simplified method to calculate the dynamic flexural load capacity for circular CFST members. Yousuf et al. [12] studied the transverse impact resistance and failure mode of CFST columns made of stainless steel and compared the results with the Australian Standard. Their results suggested that the Australian Standard underestimates the strength of CFST columns when subjected to transverse impact load and it cannot account for the failure caused by the local buckling of steel tube neither. Deng et al. [13] experimentally studied the effectiveness of using post-tensioned or steel–fibre reinforced CFST columns to mitigate transverse impact load. The test results indicated that the use of pre-stressing strands and steel fibres reinforced concrete can effectively restrain the concrete tension cracks thus reducing the column deflection under transverse impact load. Wang et al. [14] carried out a number of experimental studies to investigate the influence of the axial load level (n) and the confinement factor (ξ) on CFST columns under different impact load. Remennikov et al.

[15] conducted some dynamic three point bending tests on foam- and concrete-filled square steel tubes. The concrete infill exhibited better energy-absorbing capacity while foam infill takes less time to become effective.

Numerical simulation has been widely adopted as an effective way to study the behaviours of CFST members under different loading conditions since the laboratory tests are often costly and time-consuming. A number of previous researches have demonstrated the ability of numerical simulations to deliver reliable predictions of CFST columns under transverse impact load [12, 14, 16, 17].

The previously mentioned research evidently demonstrated the outstanding performance of CFST members under static and dynamic loading conditions. However, due to the increasing threat of terrorist attack, the ability of a structural member to withstand and survive an explosion has never been more important. Blast loading is generally classified into three different types based on the distance from the explosives to the surface of the structure, including near-field blast [18], close-range blast [19, 20] and direct contact [21, 22]. This paper thus presents a numerical study on the performance of CFST columns under a variety of loading conditions including close-range blast loading. The proposed numerical models were validated against a number of three point bending tests and field blast tests which were undertaken by the Guangzhou University recently.

2. Finite Element Analysis of CFST Members

The finite element model was developed using steel and concrete elements in LS-DYNA [23]. In order to ensure the simulating accuracy and efficiency, the steel tube and the concrete were simulated by 8-node solid elements with single point integration algorithm. In this paper, LS-DYNA/Implicit Solver was used for used for the static analysis (i.e. the three point bending test) and LS-DYNA/Explicit Solver was used for the

dynamic analysis (i.e. the blast test). Viscos-type hourglass control was activated during the blast test simulation to prevent element distortion and zero energy modes.

2.1 Concrete model

The K&C concrete model (MAT CONCRETE DAMAGE REL3) was used herein because it is able to model the behaviours of concrete member subjected to active/passive confining stress and high strain rate effect which is particularly suitable for the simulation of blast experiment [24]. A number of previous studies have already demonstrated the ability of the K&C concrete model to provide a robust representation of the complex behaviours of concrete structures under blast load [25-28]. The material model provides a parameter self-generation function where the entire set of material properties is generated based on the unconfined compressive strength of the concrete. However, according to the recently released validation studies [24, 29], the K&C material model is mesh-size sensitive, especially for concrete under little to moderate confinement, where the default generated parameters are only valid for mesh size around 25.4mm (1 inch). In order to achieve an accurate representation of concrete element with, on average, 8 mm mesh size in the current study, necessary modifications have to be made to three parameters namely B1, B2 and Omega which governs the compressive damage evolution, tensile damage evolution and volume expansion respectively. The equations for calculating B1 and B2 are provided by Wu [29]:

$$\mathrm{B1} = 0.34 \times \mathrm{h} + 0.79 \tag{1a}$$

$$\mathrm{B2} = \left(0.09 \times w_{lz}^2 - 0.98 \times w_{lz} + 3.06\right) \times (1 - 0.004 \times f_c'^2 + 0.097 \times f_c' - 0.484) \tag{1b}$$

where h is the characteristic length of the element in the unit of inch; w_{lz} is the aggregate size in the unit of inch and w_{lz} must be set to smaller than the element regardless of the actual aggregate size; f_c' is the unconfined compressive strength in the unit of ksi.

Additionally, Omega, which controls the volume expansion, is suggested to be 0.75 for a case without confinement and 0.9 for a confined case. Table 1 summarises the key parameters of the K&C material model used in this paper.

Table 1: Key inputs for Material 72

Model parameter	Value
f_c'	40MPa
f_t	3.5MPa
Poisson's ratio	0.19
B1	0.92(default=1.6)
B2	2.68(default=1.35)
Omega	0.9(default=0.5)

It is well known that under high strain rate impact, the strength of concrete can significantly increase, by more than 100% for concrete in compression and by more than 600% for concrete in tension [26]. The dynamic increase factor (DIF) is usually used to represent the increase of the compressive and tensile strength of concrete under blast loading. For concrete in compression, the CEB Code [30], which has been widely used by most researchers as an accurate representation of actual behaviour, is adopted. The DIF of the concrete strength in compression is given by:

$$\frac{f_c}{f_{cs}} = \left(\frac{\dot{\varepsilon}}{\dot{\varepsilon}_s}\right)^{1.026\alpha_s} \qquad for\ \dot{\varepsilon}_s \leq 30\ s^{-1} \tag{2a}$$

$$= \gamma_s \left(\frac{\dot{\varepsilon}}{\dot{\varepsilon}_s}\right)^{1/3} \qquad for\ \dot{\varepsilon}_s > 30\ s^{-1} \tag{2b}$$

where f_c= dynamic compressive strength at $\dot{\varepsilon}$

f_{cs}= static compressive strength at $\dot{\varepsilon}_s$

$\dot{\varepsilon}$ = strain rate in the range of $30 \times 10^{-6}\ to\ 300\ s^{-1}$

$\dot{\varepsilon}_s$ = static strain rate which is 30×10^{-6}

$\log_{\gamma_s} = 6.156\alpha - 2$

$\alpha = 1/(5 + 9f_{cs}/f_{co})$

f_{co} =10MPa

The formulation used for concrete's DIF in tension was developed by Malvar and Crawford [31] which essentially is a modification to the CEB Code [30] and it is given by:

$$\frac{f_t}{f_{ts}} = \left(\frac{\dot{\varepsilon}}{\dot{\varepsilon}_s}\right)^{\delta} \quad for\ \dot{\varepsilon}_s \leq 1\ s^{-1} \tag{3a}$$

$$= \beta \left(\frac{\dot{\varepsilon}}{\dot{\varepsilon}_s}\right)^{1/3} \quad for\ \dot{\varepsilon}_s > 1\ s^{-1} \tag{3b}$$

where f_t = dynamic tensile strength at $\dot{\varepsilon}$

f_{ts} = static tensile strength at $\dot{\varepsilon}_s$

$\dot{\varepsilon}$ = strain rate in the range of $10^{-6}\ to\ 160\ s^{-1}$

$\dot{\varepsilon}_s$ = static strain rate which is 10^{-6}

$\log_{\beta} = 6\delta - 2$

$\delta = 1/(1 + 8f_{cs}/f_{co})$

f_{co} =10MPa

2.2 Steel model

Material model 24, namely MAT PIECEWISE LINEAR PLASTICITY, is used to represent the steel tube. It should be noted that an elasto-plastic stress–strain relationship for steel is assumed and the strain rate effect on the steel tube is incorporated by the Cowper and Symonds law which multiplies the yield stress by a factor given as:

$$DIF\ of\ steel = 1 + \left(\frac{\dot{\varepsilon}}{C}\right)^{\frac{1}{P}} \tag{4}$$

where $\dot{\varepsilon}$ = strain rate of steel.

Since the test required to obtain the exact values for parameter C and P is beyond the current research scope, the test results from a series of steel tube crush tests conducted in the past were directly adopted without modifications which suggested C = 808 s^{-1} and P = 3.585 are most suitable [32].

3. Experimental Program

3.1 Specimen preparation

In total, four CFST specimens were used for three point bending test and four CFST specimens were used for blast tests and the details are listed in Table 2. The steel tubes were straight welded with inside welding in Guangzhou University and the manufacture procedure was conforming to Chinese Standard the GB50017-2003. For ease of concrete pouring and specimen installation, two steel plates (400 mm x 500 mm x 16 mm) were manufactured for each CFST column. Before pouring concrete, one steel plate was firstly welded to one end of the empty steel tube, making sure that both their geometric centres were aligned. The tube was then set upstraight and concrete was poured from the top with concrete vibrators also being used for consolidation. At last, each specimen maintained at room temperature for 28 days and then levelled and polished by Gypsum before the other steel plate was welded to the end. Fig. 1 shows the CFST specimens that are used in the tests.

Table 2: Details of CFST members used in this paper

Three point bending tests			
Column No.	Cross Section	Span (mm)	D x t_s / B x t_s (mm)
S1	Square	2100	200 x 2.8
S2	Square	2100	200 x 2.8
C1	Circular	2100	194 x 2.8
C2	Circular	2100	194 x 2.8
Blast tests			
Column No.	Cross Section	Span (mm)	D x t_s / B x t_s (mm)
S3	Square	2500	200 x 2.8
S4	Square	2500	200 x 2.8
S5	Square	2500	200 x 3.8
C3	Circular	2500	200 x 3.8

Fig. 1: Square (right) and Circular (left) CFST specimens

3.2 Material test

3.2.1 Compressive test of concrete

C40 grade concrete was used for all specimens and the compression testing was conducted on 100 mm x 100 mm x 100 mm cubes. In total, four groups of laboratory tests were conducted, containing three concrete cubes in each group. From the test results listed in Table 3, the average cubic compressive strength obtained from the compression tests was 47.4MPa which is 37.9MPa if converted to cylindrical compressive strength.

Table 3: Concrete compressive test results

	Group 1	**Group 2**	**Group 3**	**Group 4**
Sample 1 (MPa)	46.7	45.9	48.4	44.3
Sample 2 (MPa)	49.8	46.4	48.4	48.3
Sample 3 (MPa)	50.9	46.9	48.9	44.6
Average (MPa)	49.1	46.4	48.6	45.7
Average of all (MPa)		47.4		

3.2.2. Tensile test of steel

The strengths of steel tubes were determined by direct tensile test using a high capacity hydraulic machine, in accordance with the Chinese Standard GBT228-2002. The specimen size used for direct tensile test was as shown in Fig. 2. The loading increment was 10 MPa/s before steel yielding and the pulling chuck pulled at a rate less than 0.5

L/min (L represents the total length of the specimen) after steel yielding. The average strengths of the steel tubes obtained from the direct tensile test are listed in Table 4.

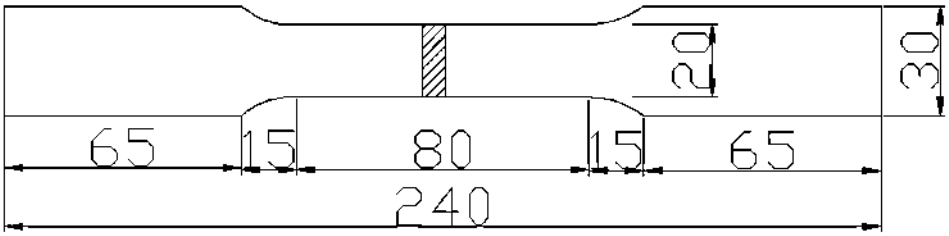

Fig. 2: Specimen size for direct tensile test

Table 4. The average steel strength

Geometry	Thickness (mm)	Yield Strength (MPa)	Ultimate Strength (MPa)	Young's Modulus (GPa)	Elongation (%)
Circular	2.8	311.5	414.0	203.6	22.1
Square	2.8	358.2	437.4	202.6	21.3
Circular	3.8	471.9	535.5	226.3	25.4
Square	3.8	484.7	535.3	215.8	20.8

3.3 Three Point Bending Tests

Three point bending tests were carried out to investigate the behaviours of CFST columns under static transverse load combined with axial load. The test machine was displacement-controlled and both ends of the specimen were simply supported and the axial load was only applied to one end of the specimen. The applied axial N_0 was roughly 20% of Nu (i.e. the axial load capacity) and the axial load capacities were calculated by using the following equations [33]:

$$N_{sc} = A_{sc}(1.212 + B\xi + C\xi^2)f_{ck} \quad (5)$$

where, A_{sc} is the cross sectional area of the CFST column; A_s and A_c are the cross sectional areas of the steel tube and the concrete, respectively; f_y and f_{ck} are the yield strength of the steel tube and the characteristic strength of the concrete, respectively.

$$\xi = \frac{A_s f_y}{A_c f_{ck}} \quad (6)$$

$$B = \begin{cases} 0.1759 f_y/235 + 0.974 \ (circular\ cross\ section) \\ 0.131 f_y/235 + 0.723 \ (square\ cross\ section) \end{cases} \quad (7)$$

$$C = \begin{cases} -0.1038 f_{ck}/20 + 0.0309 \ (circular\ cross\ section) \\ -0.07 f_{ck}/20 + 0.0262 \ (square\ cross\ section) \end{cases} \quad (8)$$

The calculated axial load capacities were 2200 kN and 2800 kN for the circular and square CFST columns, respectively, and the applied axial load was 404 kN on the circular CFST specimens and 514 kN on the square CFST specimens.

Prior to applying the lateral displacement, the specimen was gradually loaded axially to $0.5N_0$ and then unloaded to eliminate the inhomogeneity in the CFST specimen. The specimen was then loaded to N_0 followed by the lateral displacement. Fig. 3 shows the test setup of the three point bending test.

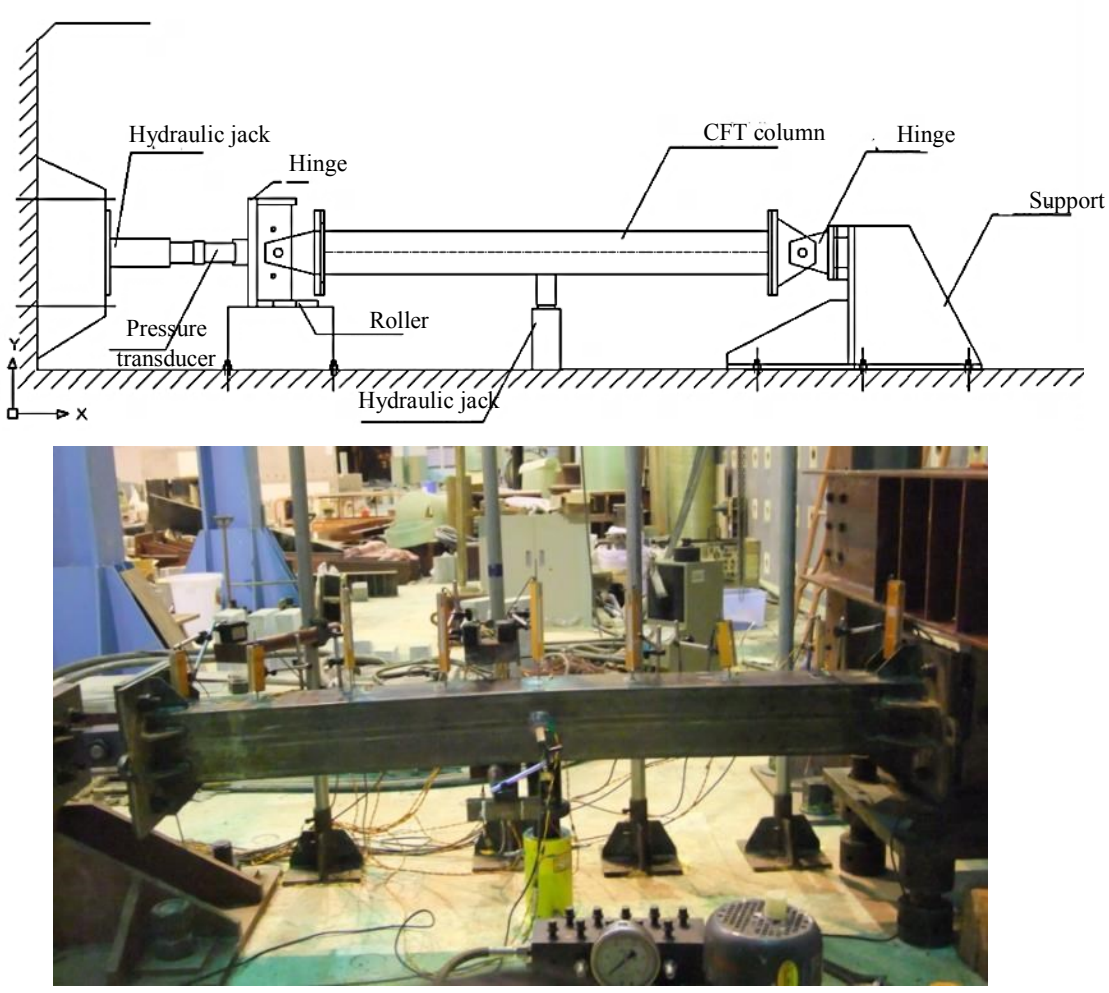

Fig. 3: The test setup for three point bending test

In total, 4 CFST columns were tested including 2 square CFST columns and 2 circular CFST columns; however, due to mechanical failure, the data of CFST column S1 were not recorded. Table 5 summarises the results of the three point bending tests. It is evident that the tested square specimen S2 exhibited a larger lateral load capacity than the circular specimen C2; moreover, the axially load specimen C2 also showed a slightly larger lateral load capacity than its axial-load free counterpart C1.

Table 5: Results of the three point bending tests

Column No.	Cross Section	Applied Axial Load (kN)	Maximum Lateral Load (KN)		Error (%)
			Test	LS-DYNA	
S1	Square (200mmx200mmx2.8mm)	0	/	/	/
S2	Square (200mmx200mmx2.8mm)	504	168	178	6%
C1	Circular (194mm Dia.x2.8mm)	0	88	87	0%
C2	Circular (194mm Dia.x2.8mm)	414	95	103	8.4%

3.4 Blast Tests

Blast tests on CFST columns were carried out by PLA University of Science and Technology in China. It is shown in Fig. 4 that a 3000 mm x 400 mm x 1500 mm test pit was excavated for the placement of the recording apparatus and corresponding data cables. The top of the test pit was covered with 20 mm thick steel plate to prevent the test pit itself as well as the recording apparatus from being damaged by the blast wave. A pneumatic jack was also installed and buried beneath the ground on side of the test pit to apply axial load on test specimens. During the test, the test specimen was firstly placed on a steel frame and then the steel frame was placed into the test pit.

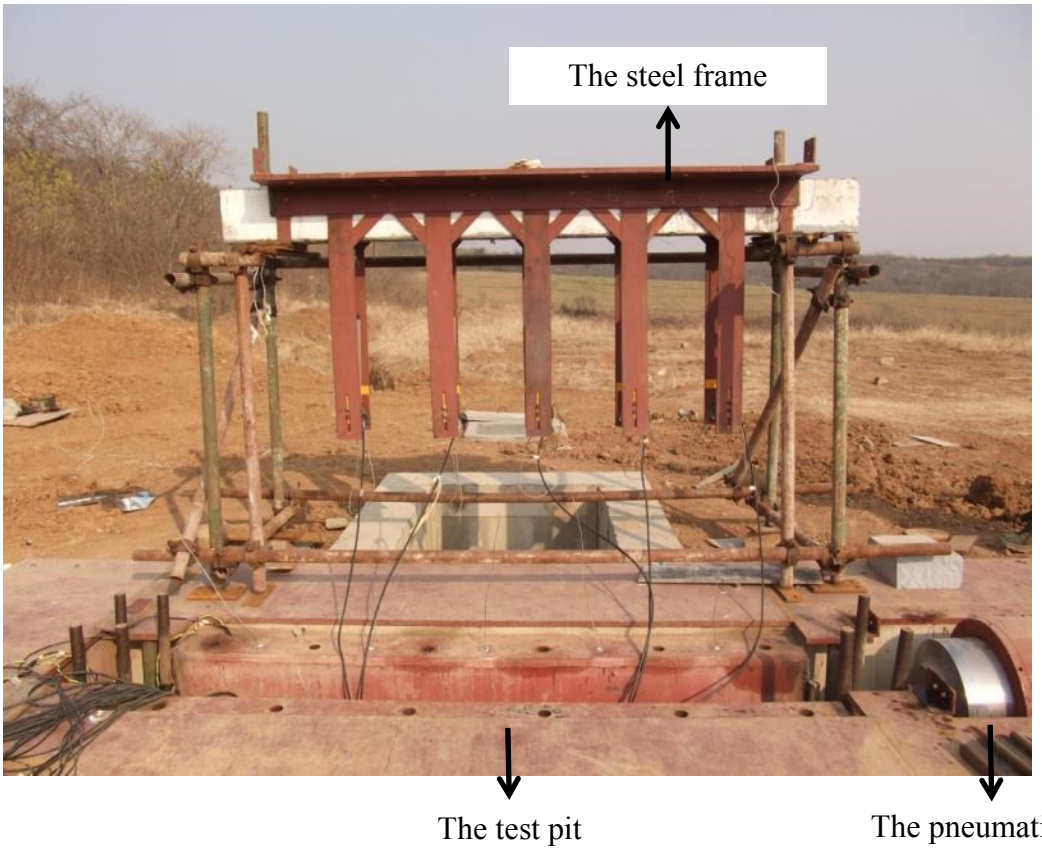

Fig. 4: The steel frame that holds the specimens in place

Fig. 5 shows the schematic view of the test setup: the test specimen was simply supported at both ends and bolts were also used to provide an upward restraint against column rebound, thus the effective span of the CFST specimen was around 2300 mm. Emulsion explosive was used in the experiment which has an average TNT-equivalent value of 0.7 in terms of the magnitude of blast impulse [34].

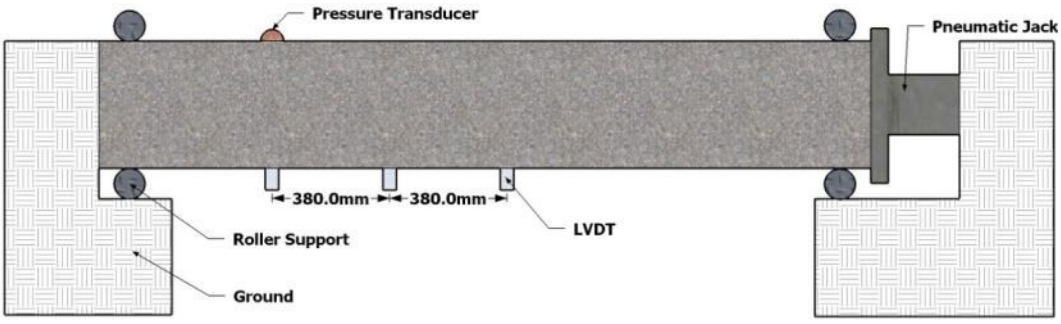

Fig. 5: The schematic view of the test setup

3.4.1 Data Acquisition and Measurement Devices

As shown in Figs. 5 and 6, three displacement gauges (LVDTs) spaced at 380 mm were attached to each test specimen to measure the displacement-time histories and each LVDT has a 120 mm measuring range for both upward and downward displacement.

Fig. 6: The installation of LVDTs

To capture the pressure-time history of each blast event acting on the specimens, a pressure transducer was also used. In order to minimise the risk of damaging the pressure transducer, it was positioned 760 mm away from, instead of right under, the centre of the specimen as shown in Figs. 7 and 8.

Fig. 7: The position of the pressure transducer

Fig. 8: Detailed view of the pressure transducer

All the data cables of the measurement devices were buried beneath the ground and the data-acquisition system as well as the command console was placed inside a protected concrete bunker.

3.4.2 Test results

During the blast test on specimen S3, the blast wave propagating into the test pit and several recording apparatus were destroyed. Consequently, the deflection–time histories of specimen S3 were not recorded successfully and only the residual deflection was measured manually afterwards. Table 6 summaries the results of the blast test.

Table 6: Results of the blast test

Column No.	Cross Section	Tube Thickness (mm)	TNT Equivalence (kg)	Maximum deflection (mm)		Residual deflection (mm)	
				Test	LS-DYNA	Test	LS-DYNA
C3	Circular	3.8	25	20	23	4	5
S3		2.8	17.5	/	17	5	3
S4*	Square	2.8	35	60	46	34	38
S5		3.8	35	37	32	8	12

*Note: For specimen S4, the recording of LVDT1 was missing thus the value of LVDT2, which is 380 mm from LVDT1, was used instead.

4. Finite element Model validation

4.1 Validation of Three Point Bending Tests

The corresponding LS-DYNA numerical model of the three point bending test shown in Fig. 3 is presented in Fig. 9. The cross section geometries and meshing for the

CFST members are shown in Fig. 10. In the current research, the average mesh size was 8 mm and a mesh size convergence study was also performed which suggested that further refining the mesh can only marginally improve the performance but greatly increase the computational burden. The interface between the steel tube and the concrete was merged to assume a perfect bonding between them since no research has mentioned noticeable debonding issue during their experiments. The model was simply supported at both ends and the axial load was applied on the rotatory hinge. It should be noted that the numerical model was analysed by using the implicit solver in LS-DYNA to simulate the static loading condition.

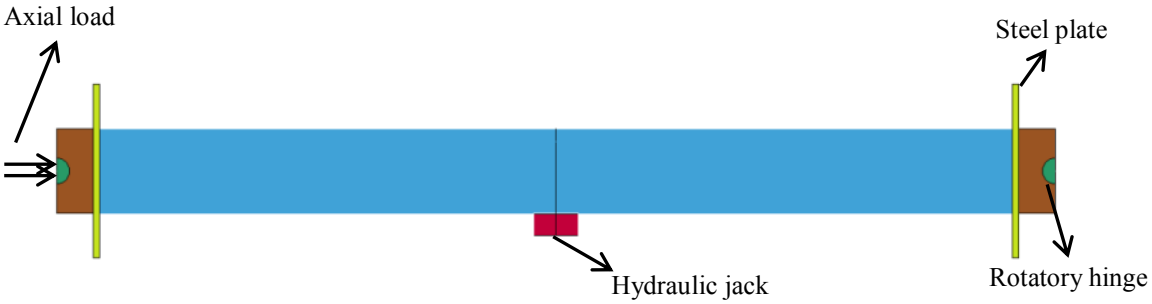

Fig. 9: The numerical model for three point bending test

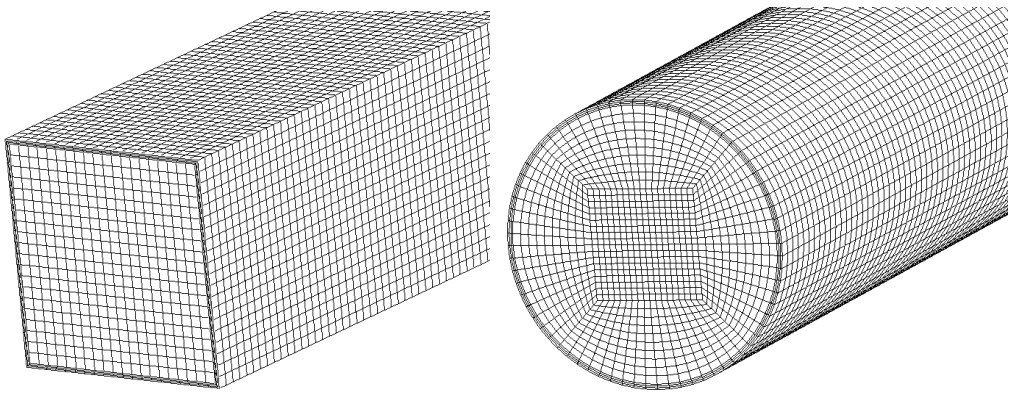

Fig. 10: Element division of the numerical model

Table 5 shows the comparisons of the maximum lateral forces between the laboratory tests and the numerical simulations and Figs. 11–13 compare the force–displacement histories obtained from the laboratory tests and the numerical simulations. It is evident that the proposed numerical model can not only provide accurate predictions of the maximum lateral load bearing capacities of the tested CFST specimens with no more than 10% error,

it can also correctly predict the lateral displacement at which the tested CFST columns reach their peaks along with the corresponding descending branches.

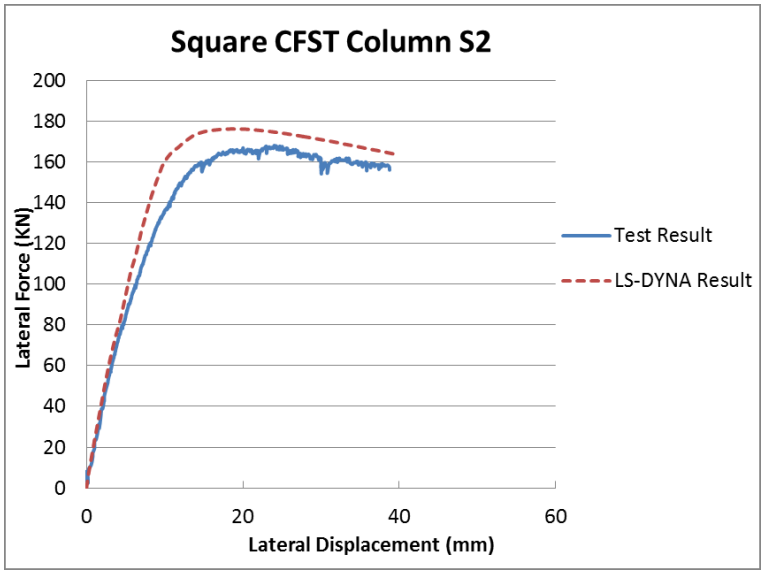

Fig. 11: Comparison between the numerical results and test results for column S2

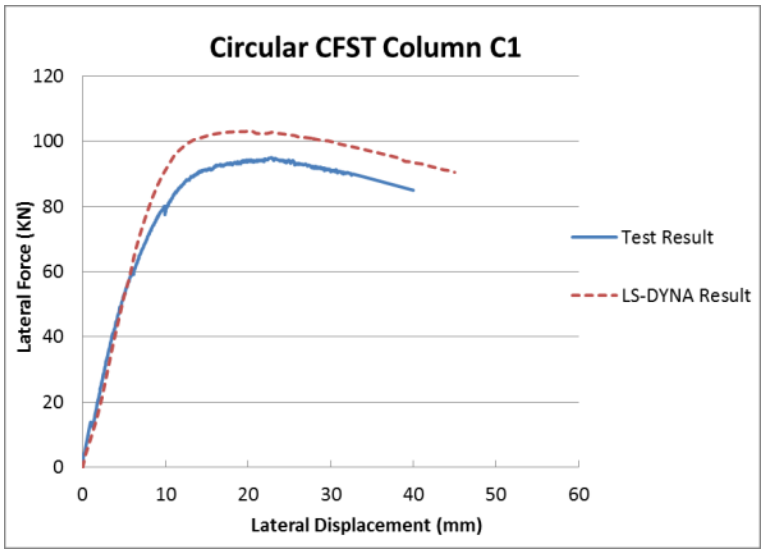

Fig. 12: Comparison between the numerical results and test results for column C1

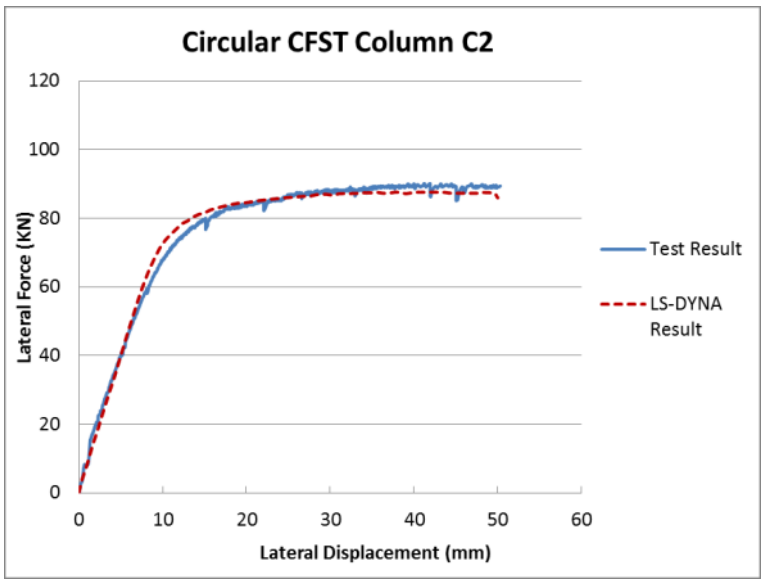

Fig. 13: Comparison between the numerical results and test results for column C2

By comparing specimen C1–C2, it is clear that the applied axial load increased the maximum flexural load capacity while sacrificing the specimen's ductility. To further demonstrate the influence of axial load on the flexural load capacity and the ductility, another numerical simulation was conducted on a circular CFST specimen with an axial load of 808 kN, around 40% of the ultimate axial load capacity. Fig. 14 compares the force–displacement histories of circular CFST specimens with 3 axial load levels, namely 0%, 20% and 40% of their ultimate capacity. It is evident that the ductility of a circular CFST specimen decreased significantly with the increase in the applied axial load; however, the flexural load capacity does not always increase with the increase in the applied axial load: the specimen with 404 kN axial load actually resulted in a greater flexural load capacity than the one with 808 kN axial load.

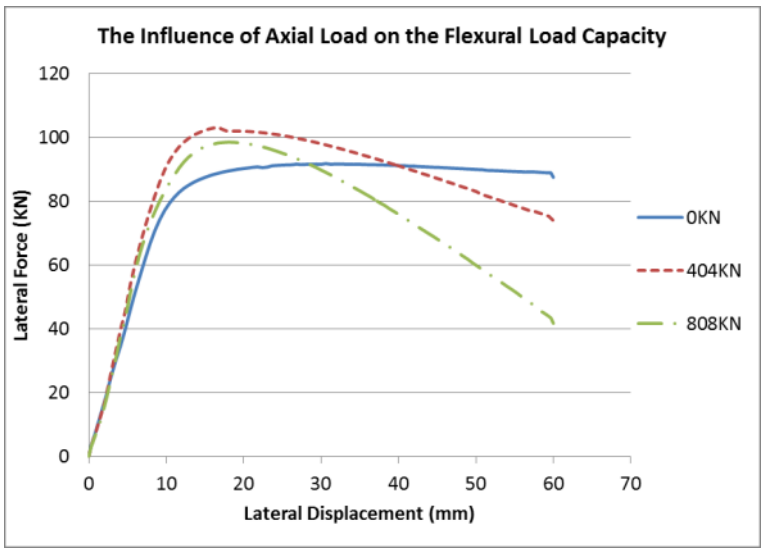

Fig. 14: The influence of axial load on the flexural load capacity

4.2 Validation of the Blast Tests

Fig. 15 shows the numerical model corresponding to the blast tests mentioned previously. The column was 2500 mm in length which was simply supported by 4 rollers – 2 at each ends and all rollers were fully fixed against motions in all directions. A thick steel plate was also placed in between the roller and the column to avoid stress concentration. A head and a footing were included in the numerical model for the purpose of applying axial load.

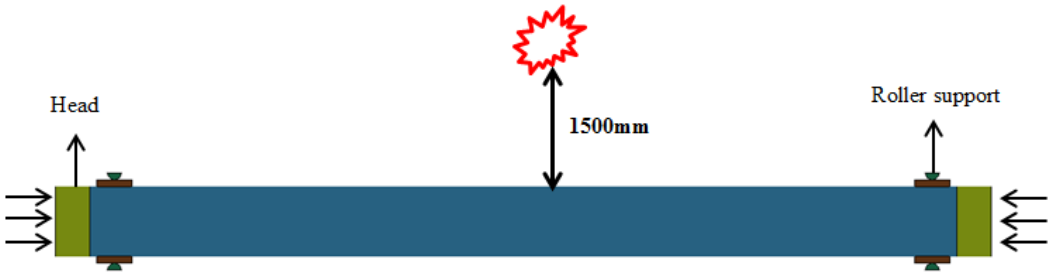

Fig. 15: The numerical model for the blast test

In blast effects analysis of columns, it is often necessary to use several phases to apply the loading to avoid undesired oscillation [24]. In this paper, two loading phases, as shown in Fig. 16, were used and these included: (1) to apply the axial load to the column prior to the detonation of the explosive. This was done by applying a gradually increased axial quasi-static load to the top of the column implicitly to avoid too much oscillation in

the way of wave propagation and (2) to apply the blast load while keeping the axial load unchanged and at this stage, the computational algorithm was switched from implicit to explicit in order to allow for dynamic analysis of the CFST specimens.

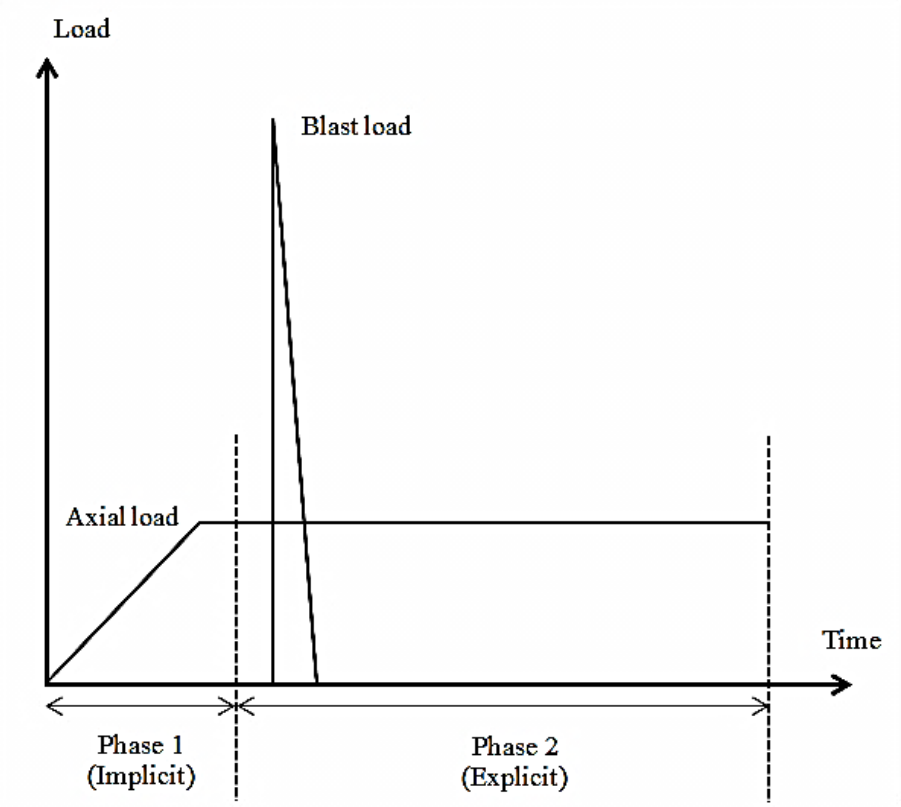

Fig. 16: Two loading phases (not to scale)

In LS-DYNA, one approach to simulate a blast event is to build an air domain which contains the explosive and target structure inside. However, in order to capture the realistic blast physics such as wave propagation within the air, a very high grid resolution is required which is too computationally expensive especially for a large standoff distance.

An alternative way is to use the ConWep air blast model [35] which was derived empirically from a large number of well-designed blast experiments. It is a built-in function, namely Load Blast Enhanced, in LS-DYNA which only requires simple inputs such as equivalent TNT charge weight and charge location [36]. The blast load acts on a set of user-predefined receptor segments (normally the area that faces the explosive) and the magnitude of pressure p that acts on each segment is calculated by:

$$\mathrm{p} = p_i \times (1 + \cos\theta - 2\cos^2\theta) + p_r \times \cos^2\theta \qquad (9)$$

where p_i and p_r are the incident pressure and reflected pressure respectively and θ is the angle of incidence of the pressure wave.

ConWep air blast model has been widely adopted to investigate the structural response under blast load and it has shown a high level of accuracy with a reasonable computational cost compared to other techniques [37-39]. However, it should be noted that ConWep is only applicable to situations where there is no offset or superposition of blast waves and the explosive must be either spherical or hemi-spherical. In the current research, ConWep air blast model was utilised due to the fact that (1) the method of building an air domain returned unrealistic computational time and (2) there was no obstacle between the explosive and the column so that ConWep was actually practicable.

4.2.1 Conversion between emulsion explosives and TNT explosives

Emulsion explosives were used in the current study during the blast test. Simoens [34] discovered that emulsion explosives generated blast wave that has peak pressures of the same magnitude as an identical mass of TNT and for impulse however, a mass of emulsion explosives equals about 70% of that mass in TNT. It should be noted that Simoens [34] only tested on a relatively small amount of emulsion explosives (i.e. up to 4.8kg), therefore if the conversion factors still holds once much larger charge weight is used needs to be examined. In addition, according to Wu et al. [40], the shape of the explosive also plays a significant role in the pressure-time history. In the current study, the applied charge weight is up to 50 kg which is too large to be made spherical; therefore the explosive is more cylindrical rather than spherical which could potential make a significant difference in the blast pressure–time histories.

To investigate the aforementioned matters, ConWep is used as a benchmark for the peak overpressure and the impulse for TNT [35, 41]. It should also be noted that in ConWep, the shape of the explosive is assumed to be spherical. Figs. 17–20 show the

comparison between the measured pressure-time histories and the ConWep predicted pressure-time histories of the corresponding TNT equivalences. Although the measured reflected pressures were slightly different to the predicted ones by equating 1.4 mass of emulsion explosive to 1 mass of TNT, the predicted blast impulses (i.e. the area enclosed by the curve) and loading duration agreed with the experiment data very well. Therefore, it is of reasonable accuracy to use ConWep to simulate the blast pressure in LS-DYNA and it also makes no significant difference by assuming the explosive charge weight to be spherical although it is closer to be cylindrical in the current study.

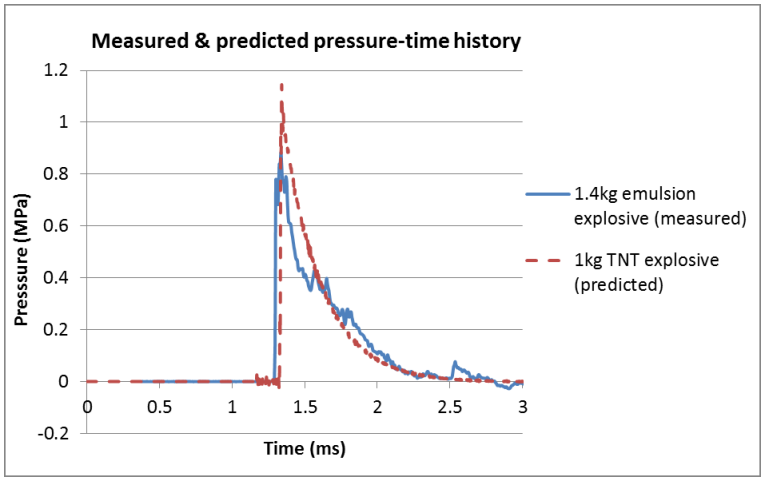

Fig. 17: Comparison between 1.4kg emulsion explosive and 1kg TNT explosive

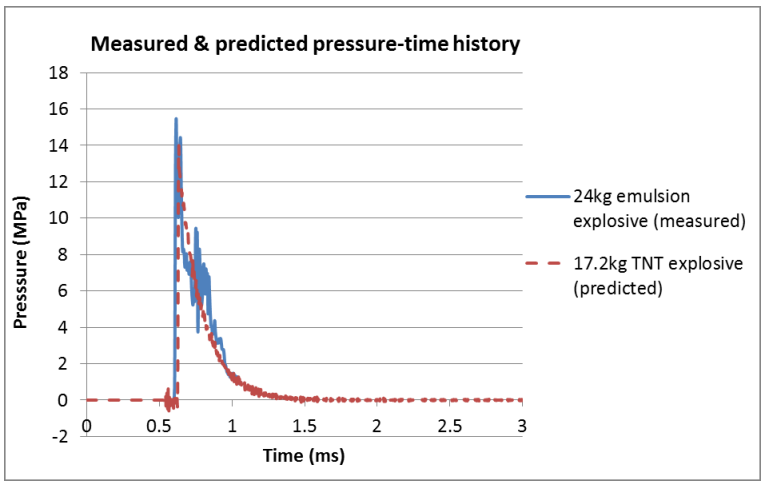

Fig. 18: Comparison between 24kg emulsion explosive and 17.2kg TNT

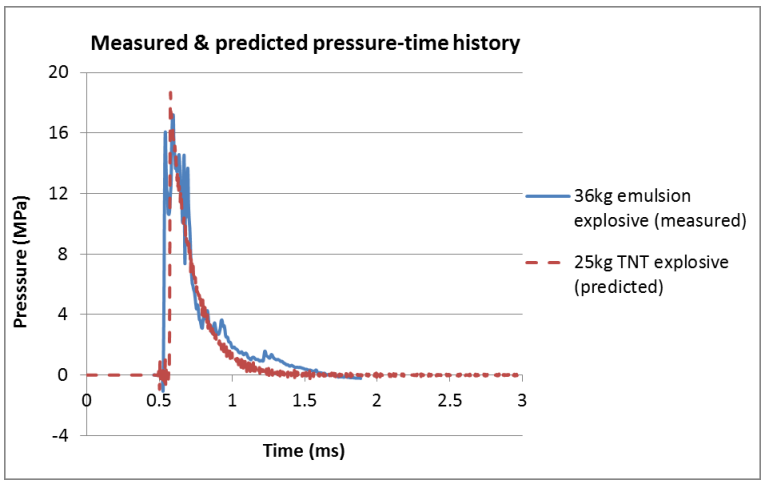

Fig. 19: Comparison between 36kg emulsion explosive and 25kg TNT

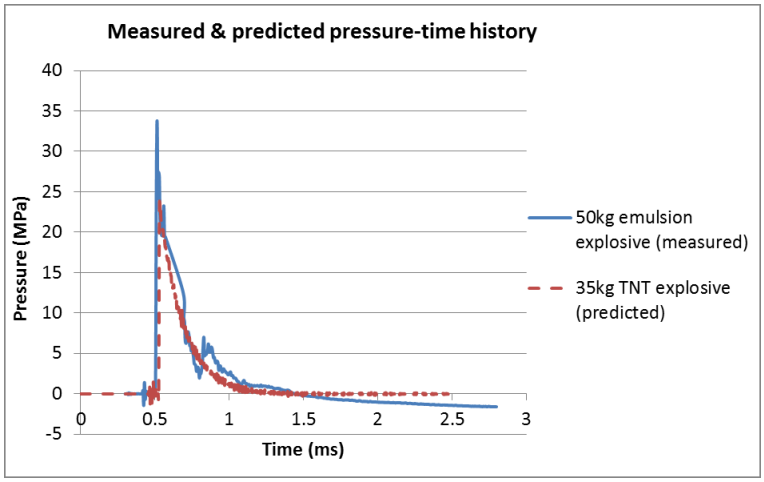

Fig. 20: Comparison between 50kg emulsion explosive and 35kg TNT

4.2.2 Validation results

Table 6 lists the numerical results of the blast tests against the experiment results and Figs. 21–23 compare the predicted and measured displacement-time histories. The comparisons indicate that the predicted maximum deflection and period of oscillation correspond with the measured curves very well. Although there are discrepancies in the residual deflections between the test results and the predictions, the difference is no more than 10 mm which was acceptable considering the complexity and uncertainty associated with blast experiments.

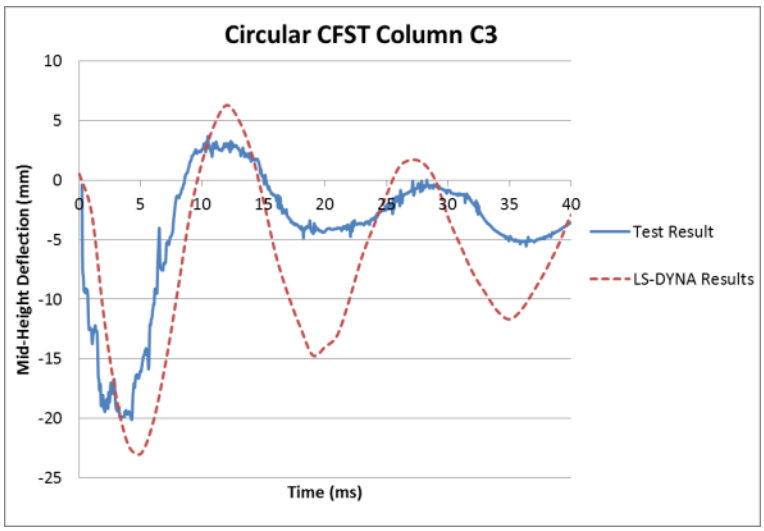

Fig. 21: Comparison between the numerical results and test results for column C3

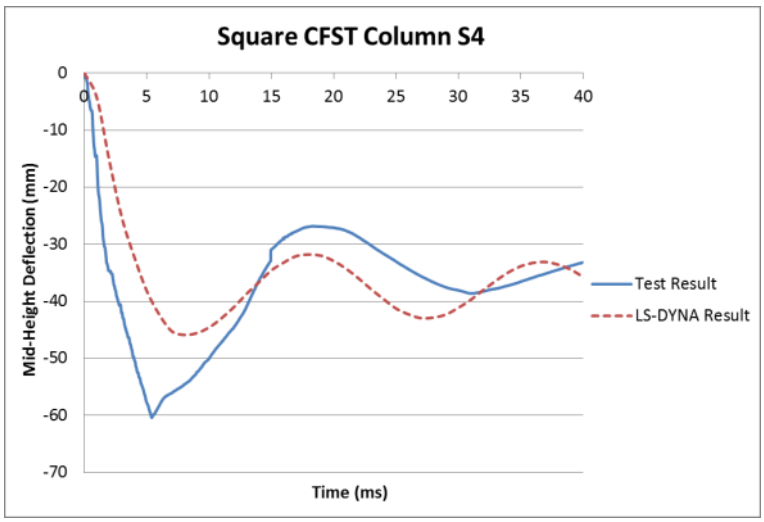

Fig. 22: Comparison between the numerical results and test results for column S4

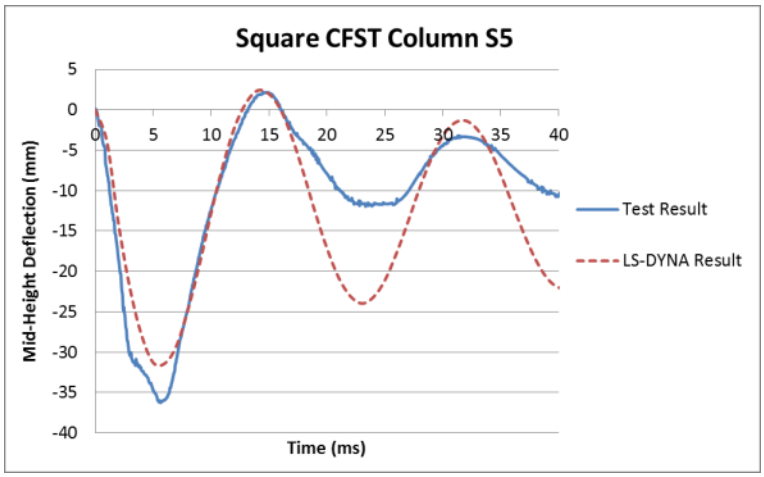

Fig. 23: Comparison between the numerical results and test results for column S5

It is well known that steel structure is prone to local buckling due to its thinness which can result in the reduction of load capacity. Although the concrete infill can delay the local buckling of the steel tube, it still cannot be prevented especially when subjected to large impact load [14, 42]. Fig. 24 compares the deformed shape along with the crack formations between the tested specimen S4 and the numerical simulation. Fig. 25 evidently demonstrates the ability of the proposed numerical model to accurately capture the localised structural responses (i.e. local buckling of steel) during the blast experiment which can be hardly achieved by other analytical methods.

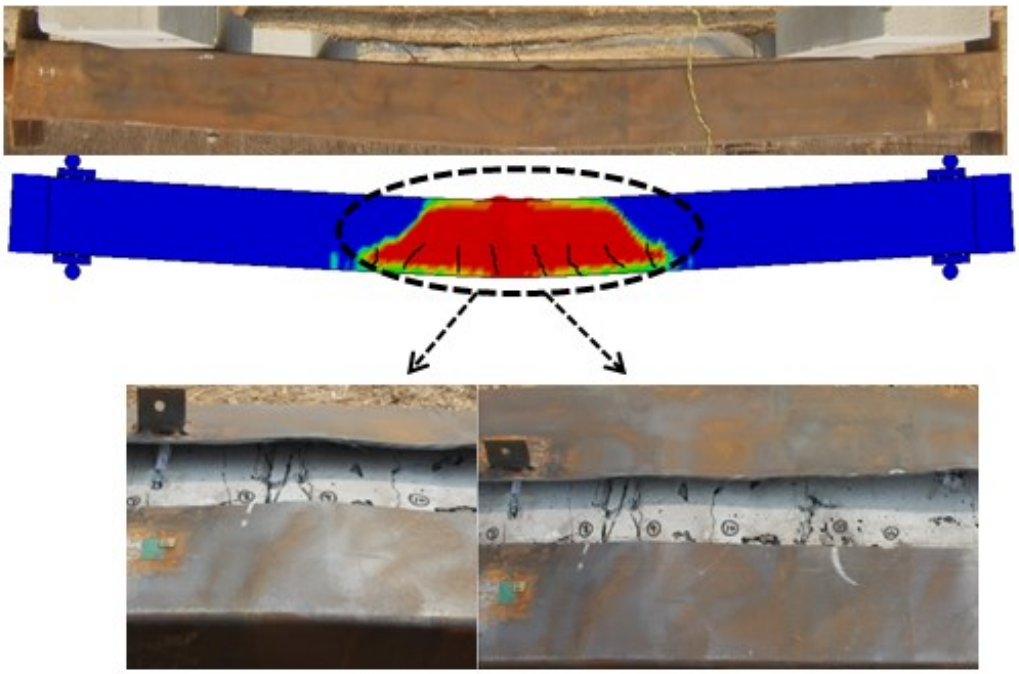

Fig. 24: Comparison of the deformed shape and cracks from numerical and experimental studies for specimen S4

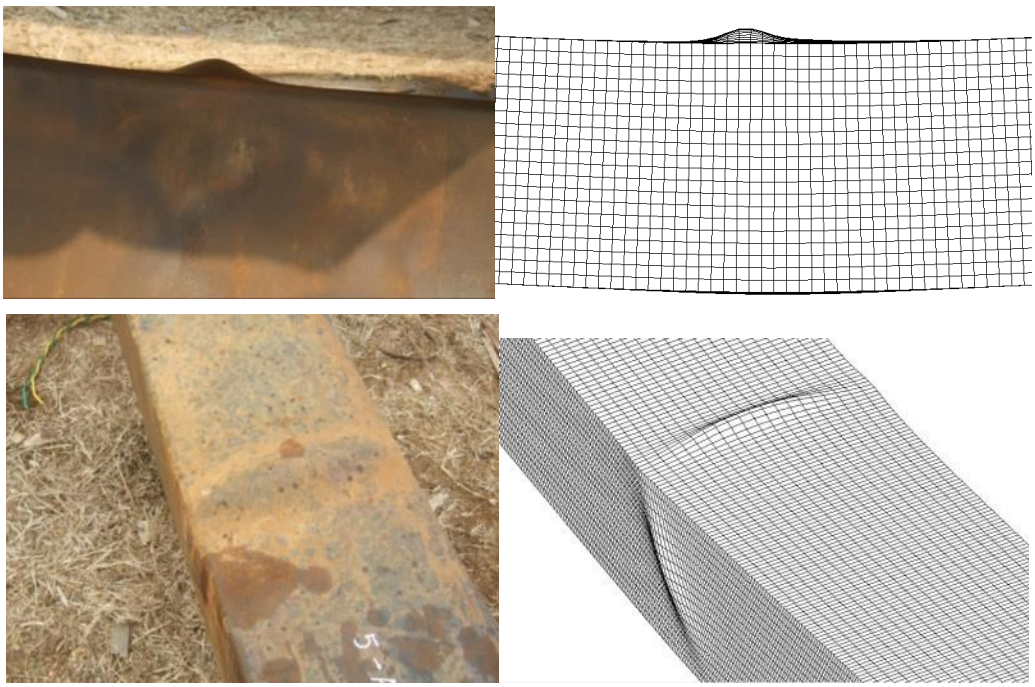

Fig. 25: The observed local buckling (right) and the predicted local buckling (left) on specimen S4

4.2.3 Energy absorbed by local and flexural deformation

The energy absorbed by local and flexural deformation was investigated based on the numerical simulation of specimen S4. The local deformation, as shown in Fig. 25, was only found at mid-span and its width was measured to be approximately 95 mm. According to Jama [21], the energy absorbed by local deformation can be up to 50% of the total energy absorbed for a steel square hollow section under transverse blast loads. Under blast loading, the work done by the external force is firstly turned into kinetic energy of the specimen and then the kinetic energy is further absorbed by local and global plastic deformation, which is also known as the internal energy. Fig. 26(a) shows the internal energy of the entirety of specimen S4 after blast loading and Fig. 26(b) shows only the internal energy of where the local deformation occurred. It should be noted that Jama [21] assumed that the local deformation preceded the global deformation; however, it is not the case for CFST specimens in the current research. It was observed from the numerical simulation that the specimen began to deform as soon as the blast wave reached (i.e. t=0 ms) whereas the sign of local deformation was only found 3 milliseconds later (i.e. t=3 ms).

The global and local deformation continued developing simultaneously until 6 milliseconds after the time of arrival (i.e. t=6 ms), at which the local deformation fully developed. The global deformation then continued developing and reached its peak at t= 13 ms. Significant changes in slope of Fig. 26(b) can be noticed at t= 3 ms and t= 6 ms which indicates that the local deformation does have a notable impact on the energy absorbing mechanism of CFST columns.

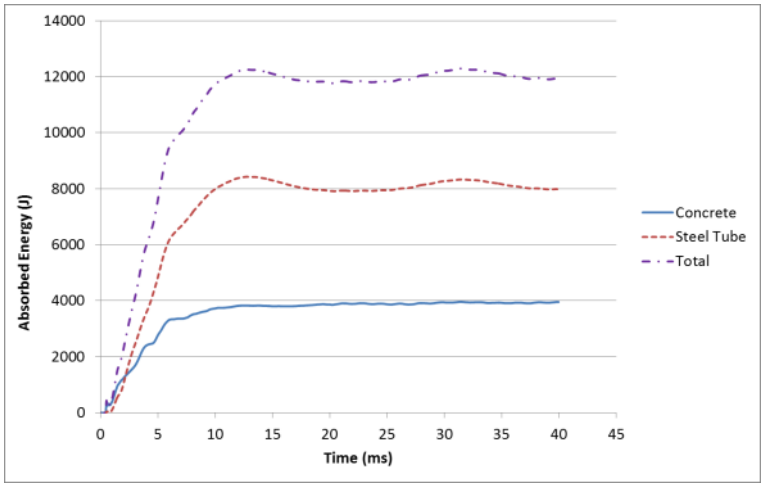

(a)

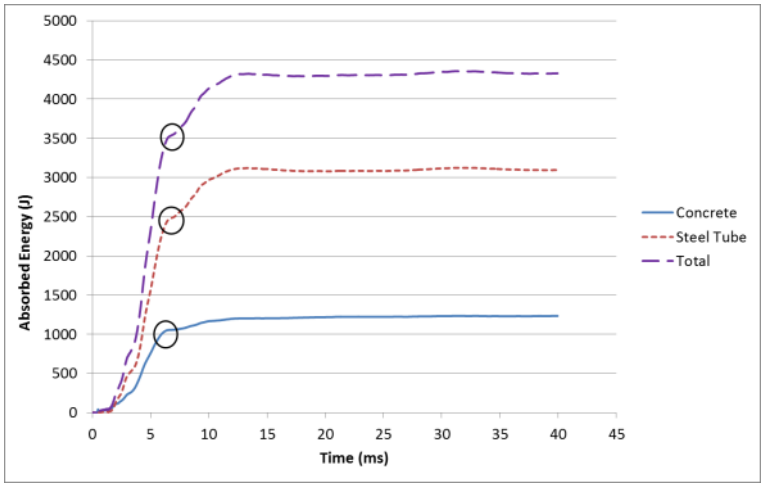

(b)

Fig. 26: The internal energy of (a) the entire specimen S4 and (b) the mid-span part of S4 where local deformation occurred

In order to compare the ratio between the energy absorbed by local and global deformation, it is assumed that between t=3 ms and t=6 ms, all of the energy absorbed in Fig. 26(b) was due to local deformation. It should be mentioned that this assumption overestimates the energy absorbed by local deformation because global deformation also

happens between t=3 ms and t= 6ms simultaneously. With the assumption made, the energy absorbed by local deformation of specimen S4 was 2600 J and the energy absorbed by local and global deformation combined was 12000 J which means local deformation accounts for 22% of the total energy absorbed.

5. Conclusions

This paper presented a numerical study of CFST members, with both circular and square cross sections, under both static and blast loads and the following conclusions can be drawn based on the numerical results presented in this paper:

1. The CFST member behaved in a very ductile manner under lateral static load. The applied axial load can slightly increase its flexural load capacity, however, at the cost of reducing the column's ductility at the same time.

2. The numerical model developed in this paper can deliver accurate predictions for CFST members under transverse static load. When validated against the blast test, the model still corresponded with test results quite well in terms of the maximum deflection and the period of oscillation. Discrepancies in the residual deflections were found, however considering the complexity and uncertainty associated with a blast experiment, the error is still within the acceptable range.

3. Based on the numerical results, for a CFST member under blast loading, the majority of the energy is absorbed by global deformation due to the fact that local deformation of steel can be effectively prevented by the infilled concrete.

More parametric studies can be made using the developed numerical models in the future to address the key parameters that affect the overall behaviours of CFST members under blast loading.

Acknowledgements

The authors gratefully acknowledge the National Natural Science Foundation of China under Grants 51108106 and the ARC Discovery Grants DP130100181 and DP140103025.

References

[1] Morino S., UMYI, *Concrete-Filled Steel Tube Column System - Its Advantages.* Steel Structures, 2001: p. 33-44.

[2] Morino, S and Tsuda, K, *Design and construction of concrete-filled steel tube column system in Japan.* Earthquake Engineering and Engineering Seismology, 2003. **4**(1): p. 51-73.

[3] Uy, B, Tao, Z, Han, L-H, and He, S-H, *Design of concrete-filled steel tubular members according to the Australian Standard AS 5100 model and calibration.* Australian Journal of Structural Engineering, 2008. **8**(3): p. 197.

[4] Clark, W, *Axial Load Capacity of Circular Steel Tube Columns Filled with High Strength Concrete*, in *Department of Civil and Building Engineering*1994, Victoria University of Technology: Australia. p. 175.

[5] Hu, H-T, Huang, C-S, Wu, M-H, and Wu, Y-M, *Nonlinear analysis of axially loaded concrete-filled tube columns with confinement effect*. Journal of Structural Engineering, 2003. **129**(10): p. 1322-1329.

[6] Han, LH, Tao, Z, Huang, H, and Zhao, XL, *Concrete-filled double skin (SHS outer and CHS inner) steel tubular beam-columns.* Thin-Walled Structures, 2004. **42**: p. 1329-1355.

[7] Inai, E, Mukai, A, Kai, M, Tokinoya, H, Fukumoto, T, and Mori, K, *Behavior of concrete-filled steel tube beam columns.* Journal of Structural Engineering, 2004. **130**(2): p. 189-202.

[8] Liang, QQ and Fragomeni, S, *Nonlinear analysis of circular concrete-filled steel tubular short columns under axial loading.* Journal of Constructional Steel Research, 2009. **65**(12): p. 2186-2196.

[9] Prichard, S and Perry, S, *The impact behaviour of sleeved concrete cylinders.* Structural Engineer, 2000. **78**(17): p. 23-7.

[10] Xiao, Y and Shen, Y, *Impact Behaviors of CFT and CFRP Confined CFT Stub Columns.* Journal of Composites for Construction, 2012. **16**(6): p. 662-670.

[11] Han, L-H, Hou, C-C, Zhao, X-L, and Rasmussen, KJ, *Behaviour of high-strength concrete filled steel tubes under transverse impact loading.* Journal of Constructional Steel Research, 2014. **92**: p. 25-39.

[12] Yousuf, M, Uy, B, Tao, Z, Remennikov, A, and Liew, J, *Transverse impact resistance of hollow and concrete filled stainless steel columns.* Journal of Constructional Steel Research, 2013. **82**: p. 177-189.

[13] Deng, Y, Tuan, CY, and Xiao, Y, *Flexural behavior of concrete-filled circular steel tubes under high-strain rate impact loading.* Journal of Structural

Engineering, 2011. **138**(3): p. 449-456.
[14] Wang, R, Han, L-H, and Hou, C-C, *Behavior of concrete filled steel tubular (CFST) members under lateral impact: Experiment and FEA model.* Journal of Constructional Steel Research, 2013. **80**: p. 188-201.
[15] Remennikov, AM, Kong, SY, and Uy, B, *Response of foam-and concrete-filled square steel tubes under low-velocity impact loading.* Journal of Performance of Constructed Facilities, 2010. **25**(5): p. 373-381.
[16] Deng, Y and Tuan, CY, *Design of Concrete-Filled Circular Steel Tubes under Lateral Impact.* ACI Structural Journal, 2013. **110**(4): p. 691.
[17] Qu, H, Li, G, Chen, S, Sun, J, and Sozen, MA, *Analysis of Circular Concrete-Filled Steel Tube Specimen under Lateral Impact.* Advances in Structural Engineering, 2011. **14**(5): p. 941-952.
[18] Langdon, G, Ozinsky, A, and Yuen, SCK, *The response of partially confined right circular stainless steel cylinders to internal air-blast loading.* International Journal of Impact Engineering, 2014. **73**: p. 1-14.
[19] Wu, C, Huang, L, and Oehlers, DJ, *Blast Testing of Aluminum Foam–Protected Reinforced Concrete Slabs.* Journal of Performance of Constructed Facilities, 2010. **25**(5): p. 464-474.
[20] Hanssen, A, Enstock, L, and Langseth, M, *Close-Range Blast Loading of Aluminium Foam Panels.* International Journal of Impact Engineering, 2002. **27**(6): p. 593-618.
[21] Jama, H, Nurick, G, Bambach, M, Grzebieta, R, and Zhao, X, *Steel square hollow sections subjected to transverse blast loads.* Thin-Walled Structures, 2012. **53**: p. 109-122.
[22] Beppu, M, Ohno, T, Ohkubo, K, Li, B, and Satoh, K, *Contact Explosion Resistance of Concrete Plates Externally Strengthened with FRP Laminates.* International Journal of Protective Structures, 2010. **1**(2): p. 257-270.
[23] Hallquist, JO, *LS-DYNA Keyword User's Manual.* Livermore Software Technology Corporation, 2007.
[24] Crawford, J, Wu, Y, Magallanes, J, and Lan, S, *Use and Validation of the Release II K&C Concrete Material Model in LS-DYNA.* Karagozian & Case, Glendale, 2012.
[25] Shi, Y, Hao, H, and Li, Z-X, *Numerical Derivation of Pressure–Impulse Diagrams for Prediction of RC Column Damage to Blast Loads.* International Journal of Impact Engineering, 2008. **35**(11): p. 1213-1227.
[26] Malvar, LJ and Ross, CA, *Review of Strain Rate Effects for Concrete in Tension.* ACI Materials Journal, 1998. **95**(6).
[27] Malvar, LJ, Crawford, JE, Wesevich, JW, and Simons, D, *A Plasticity Concrete Material Model for DYNA3D.* International Journal of Impact Engineering, 1997. **19**(9): p. 847-873.
[28] Wu, Y, Crawford, JE, and Magallanes, JM. *Performance of LS-DYNA concrete constitutive models*. in *12th International LS-DYNA Users Conference*. 2012.
[29] Wu, Y, Crawford, JE, Lan, S, and Magallanes, JM, *Validation Studies for Concrete Constitutive Models with Blast Test Data*, in *13th International LS-DYNA Users Conference*2013: Detroit.
[30] Béton, CE-Id, *CEB-FIP model code 1990: design code*. 1993: Telford.

[31] Malvar, LJ and Crawford, JE, *Dynamic Increase Factors for Concrete*, 1998, DTIC Document.

[32] Abramowicz, W and Jones, N, *Dynamic progressive buckling of circular and square tubes.* International Journal of Impact Engineering, 1986. **4**(4): p. 243-270.

[33] Zhong, S, *The Unified Theory for Concrete Filled Steel Tubes*. 2006, China: Tsinghua University.

[34] Simoens, B, Lefebvre, MH, and Minami, F, *Influence of Different Parameters on the TNT-Equivalent.* Central European Journal of Energetic Materials, 2011. **8**(1): p. 53-67.

[35] Kingery, CN and Bulmash, G, *Air blast parameters from TNT spherical air burst and hemispherical surface burst*. 1984: Ballistic Research Laboratories.

[36] Randers-Pehrson, G and Bannister, KA, *Airblast Loading Model for DYNA2D and DYNA3D*, 1997, DTIC Document.

[37] Bao, X and Li, B, *Residual Strength of Blast Damaged Reinforced Concrete Columns.* International journal of impact engineering, 2010. **37**(3): p. 295-308.

[38] Williams, K, McClennan, S, Durocher, R, St-Jean, B, and Tremblay, J. *Validation of a Loading Model for Simulating Blast Mine Effects on Armoured Vehicles*. in *Proceeding from the 7th International LS-DYNA Users Conference*. 2002.

[39] Tanapornraweekit, G, Haritos, N, Mendis, P, and Ngo, T, *Modelling of a Reinforced Concrete Panel Subjected to Blast Load by Explicit Non-linear FE Code.* The Australian Earthquake Engineering Society, 2007.

[40] Wu, C, Fattori, G, Whittaker, A, and Oehlers, DJ, *Investigation of air-blast effects from spherical-and cylindrical-shaped charges.* International Journal of Protective Structures, 2010. **1**(3): p. 345-362.

[41] Hyde, D, *ConWep, conventional weapons effects program.* US Army Engineer Waterways Experiment Station, USA, 1991.

[42] Han, L-H, *Flexural Behaviour of Concrete-filled Steel Tubes.* Journal of Constructional Steel Research, 2004. **60**(2): p. 313-337.

Statement of Authorship

Title of Paper	Numerical modelling of concrete-filled double-skin steel square tubular columns under blast loading
Publication Status	☑ Published ☐ Accepted for Publication ☐ Submitted for Publication ☐ Unpublished and Unsubmitted w ork w ritten in manuscript style
Publication Details	Zhang, F., Wu, C., Zhao, X.-L., Li, Z.-X., Heidarpour, A. & Wang, H. 2015. Numerical modeling of concrete-filled double-skin steel square tubular columns under blast loading. *Journal of Performance of Constructed Facilities,* 29, B4015002.

Principal Author

Name of Principal Author (Candidate)	Fangrui Zhang		
Contribution to the Paper	The author developed numerical model, undertook data analysis and prepared manuscript.		
Overall percentage (%)	60%		
Certification:	This paper reports on original research I conducted during the period of my Higher Degree by Research candidature and is not subject to any obligations or contractual agreements with a third party that would constrain its inclusion in this thesis. I am the primary author of this paper.		
Signature		Date	

Co-Author Contributions

By signing the Statement of Authorship, each author certifies that:

i. the candidate's stated contribution to the publication is accurate (as detailed above);

ii. permission is granted for the candidate in include the publication in the thesis; and

iii. the sum of all co-author contributions is equal to 100% less the candidate's stated contribution.

Name of Co-Author	Chengqing Wu		
Contribution to the Paper	This co-author supervised research, provided critical manuscript evaluation and acted as corresponding author.		
Signature		Date	6/6/2016

Name of Co-Author	Xiao-Ling Zhao		
Contribution to the Paper	This co-author provided critical manuscript evaluation		
Signature		Date	05/06/16

Name of Co-Author	Zhong-Xian Li		
Contribution to the Paper	This co-author provided manuscript evaluation		
Signature		Date	2016.6.6

Name of Co-Author	Amin Heidarpour		
Contribution to the Paper	This co-author provided manuscript evaluation		
Signature		Date	5. Jun. 2016

Name of Co-Author	Hongwei Wang		
Contribution to the Paper	This co-author provided manuscript evaluation		
Signature		Date	2016.6.3

NUMERICAL MODELING OF CONCRETE-FILLED DOUBLE-SKIN STEEL SQUARE TUBULAR COLUMNS UNDER BLAST LOADING

Fangrui Zhang, Chengqing Wu, Xiao-Ling Zhao, Zhong-Xian Li, Amin Heidarpour, Hongwei Wang

Abstract

Concrete-filled double-skin steel tubes (CFDST) have been widely used in constructing high-rise buildings, arch bridges, and factories over the past years. Although a number of researches have been conducted to study the behaviour of CFDST columns under a variety of loading conditions, their performance when subjected to lateral impact load is still lacking. In this paper, numerical models of CFDST columns with two different cross sections are developed: one is with a CHS (circular hollow section) outer and CHS (circular hollow section) inner, and the other one is with SHS (square hollow section) outer and SHS (square hollow section) inner. Conventional concrete is filled in double-skin steel tubes. Different blast loads are applied to the surface of these columns for dynamic analysis. In addition, different axial loads are also applied to simulate combined load conditions. The displacement-time history obtained from each simulation is recorded and then compared. The key parameters that affect the performance of CFDST columns under blast load are also investigated.

1. Introduction

Due to the increasing threat of terrorist activities over the world, much research has been done to protect important structures as well as to reduce human casualties from blast loads. Some literatures discussed the feasibility of using retrofitting techniques to protect existing structures [1-4] while others proposed the use of new materials with higher strengths to construct new buildings [5, 6]. In recent years, a new steel-concrete composite

structure developed based on the concept of the Concrete-filled tube, also known as CFT [7-9], has gained much popularity in the construction industry due to its attractive properties such as ease of construction, light weight, high strength, and good seismic resistance. This new composite structure is known as a Concrete-Filled Double-Skin Tube (CFDST), which is simply made from two concentrically placed steel skins filled with concrete in between.

A CFDST column utilizes the advantages of both steel and concrete. Its advantages over conventional reinforced-concrete structures or steel structures include:

- The presence of concrete can effectively restrain and delay the local buckling of steel tubes, and the presence of steel tubes, on the other hand, can prevent spalling damage of the core concrete;
- The interaction between steel tubes and concrete induces a confining pressure on the concrete that significantly increases its strength and ductility;
- A CFDST column requires a smaller cross section area, hence less self-weight, to achieve the same axial load capacity compared to a RC column;
- The steel tube can be used as a framework for concrete pouring and it can also provide a self-curing environment for the concrete afterwards;
- A CFDST column has good fire resistance as concrete has low thermal conductivity, which protects the inner steel tube;
- The core concrete requires less maintenance as the outer steel tube isolates it from the outer environment.

So far, not much research has been undertaken to directly evaluate the blast resistance of CFDST columns; however, a number of static tests have shown some promising results, suggesting that CFDST columns can effectively mitigate blast damage.

Under axial compression, due to the different expansion rates of the steel tube and concrete, the core concrete of a CFDST column is tri-axially confined by (1) the axial

pressure induced by dead and live loads, (2) the lateral pressure induced by steel tubes, and (3) the circumferential pressure induced by arching action. As a result, these confining pressures can effectively enhance the strength and the ductility of the core concrete, which is known as the confinement effect [8, 10]. The effect of confinement has been verified by several quasi-static tests. Wei et al. [11] firstly reported their investigation on 26 CFDST stub columns under axial compression. In their experiment, the overall axial load capacity of the CFDST stub columns was 10–30% larger than the combined ultimate capacity of the steel tubes and concrete when acting alone. In addition, the ultimate axial strain at failure was also much larger than these components acting alone. Subsequent to Wei [11], Uenaka et al. [12] investigated the influence of hollowness ratio (i.e. the ratio between the inner diameter D_i and the outer diameter D_o) on the confinement effect of CFDST columns under axial compression. The test results showed that the confinement effect developed in the CFDST columns enhanced the concrete's strength by 5% up to 30%, which was inversely proportional to the hollowness ratio. Han [9] introduced a constraining factor ξ, which is a function of steel ratio, steel yield strength and concrete cube strength, to describe the confinement effect between the steel tube and concrete. They reported that the higher the constraining factor ξ, the stronger and more ductile the CFDST columns are [13].

Han et al. [14] and Fan et al. [15] both investigated the influence of cross section geometry on the behavior of CFDST columns under axial and flexural loads, respectively. The columns with circular cross sections exhibited better ductility than those with square cross sections under either axial loads or flexural loads. Furthermore, CFDST columns behaved in a similar manner as CFT columns under flexural load, the latter of which can be accurately predicted by the analytical model developed by Han and Yang [16].

Several experiments conducted recently investigated the failure modes of CFDST columns under different load conditions [17-19]. Under axial compression, the failure

mode of CFDST columns was local bulking of both tubes associated with shear failure of the core concrete, however, the thickness of the inner tube did not significantly affect the structural response. Under a flexural load, the failure model of CFDST columns was local bulking and cracking of the outer steel tube while the deformability of CFDSTs with a small hollowness ratio obtained under flexural load was similar to that of CFTs.

Although a large number of experimental studies have been carried out, the numerical analysis of CFDST columns is still lacking; however, some numerical and analytical studies on CFT columns or steel elements [20, 21] or steel-concrete composite elements [22] have been conducted previously.

Fouché and Bruneau [23] studied the behavior of cylindrical CFT bridge piers under multihazard conditions including close-range explosions. LS-DYNA [24] was used in their research to build numerical models and then to conduct parametric studies. It was found that LS-DYNA models slightly overestimated blast impulses due to the roundness of the section. As a result, a correction factor was applied to the pressure history to account for the reduction in impulse, and the overall results then showed reasonably good correlation with the experiment data.

Qu et al. [25] simulated the drop hammer test conducted by Li [26] using LS-DYNA. The column was simply supported at one end while being fixed at the other. Since the model was fully symmetric along its length, only a half model was analyzed. The concrete material model used in their research was CONCRETE_ DAMAGE_REL3 [27] and the steel material model used was PLASTIC_KINEMATIC, which assumes a bilinear stress-strain relationship. The interface between the steel tube and the concrete was assumed to be bonded perfectly, thus excluding any considerations of debonding. Only small discrepancy was observed between the numerical simulation and the experimental results, showing that LS-DYNA is able to account for the increase in concrete strength due

to the confinement effect and strain rate effect, thus being a reliable tool to study CFDST columns.

In summary, most existing research as only investigated the behavior of CFDST columns under static loads; however, knowledge of the behavior of CFDST columns under impact loads, especially under blast loads, is lacking.

In the current research, the performance of CFDST columns under close-range blast loading is studied using LS-DYNA. The main objectives include: firstly, to study the structural response of CFDST columns under different blast loads ranging from 20 to 80 kg TNT charge weight, from a standoff distance of 1.5 m; secondly, to determine the influence of parameters such as the concrete strength, outer and inner tubes thicknesses, cross section type on blast response of CFDST columns; and finally, to determine the influence of axial load and support condition on CFDST columns under blast loads.

2. Finite Element Modelling

2.1 Elements and boundaries

In order to conduct a parametric study, different model set-ups are used. However, for comparison purposes, a control specimen is introduced. The circular CFDST control specimen has a 210 mm outer diameter and a 100 mm inner diameter as shown in Fig. 1, with a clear span of 2,500 mm. Both its inner and outer steel tubes are 5 mm thick. All elements are built using hexahedrons to achieve the best stability, and solid elements of around 6 mm cube with single point integration algorithm are used. Mesh size convergence study suggests that further refinement of the mesh only has a marginal effect on the numerical results but significantly increases the computational effort.

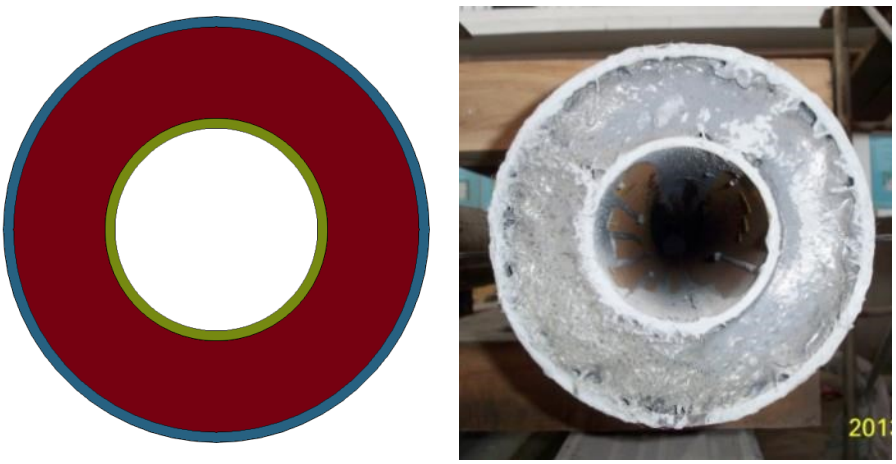

Fig. 1: Circular cross section of the numerical model (left) and the actual column (right)

Similarly, Fig. 2 depicted the square CFDST control specimen. It has a 210 mm outer side length and 100 mm inner side length. The rest of its parameters are the same as those of the circular column.

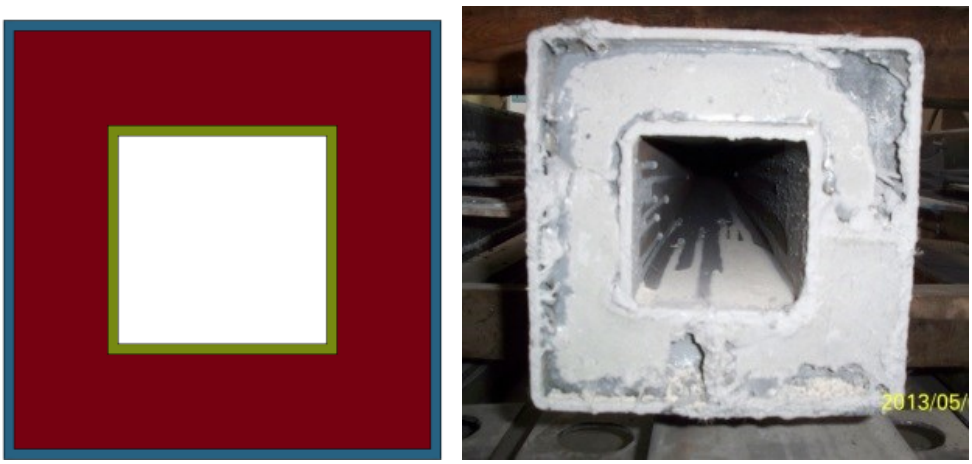

Fig. 2: Square cross section of the numerical model (left) and the actual column (right)

In order to provide higher fidelity for the column end constraints, a footing and a head are included in the numerical model as shown in Fig. 3. The outer face of head and footing are constrained against horizontal motions (i.e., in x and y directions)— both translational or rotational motions [28]. For a structural member with fully fixed support conditions on both ends, brittle shear failure near the supports could be the potential concern. In circumstances where CFDST or CFT columns are used, hardly any studies but Wang et al. [29], who reported an occurrence of shear failure: it only occurred on the column with an extremely thin outer steel tube (1.7 mm) and there were no signs of shear

failure on any other columns with a steel tube thicker than 1.7 mm. In the current research, outer and inner steel tubes are both 5 mm thick, thus shear failure near supports is not expected nor considered. Furthermore, almost no researchers except Yu et al. [30] discovered noticeable slip between the concrete and the tube. Therefore, in this paper, the nodes at the interface of concrete and steel tubes are merged to assume no debonding conditions.

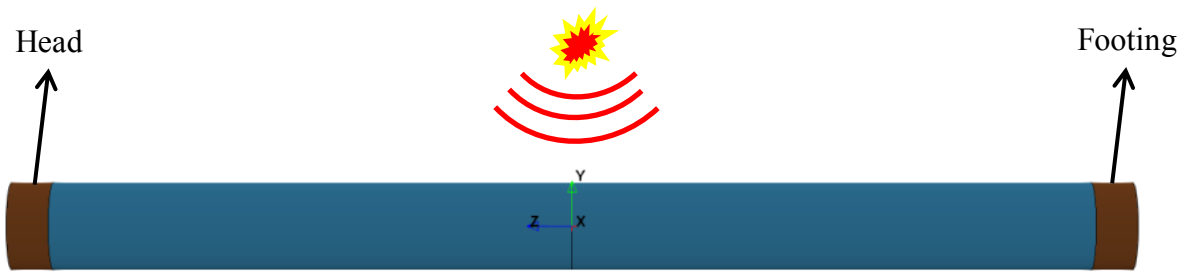

Fig. 3: Model set-up of circular column

2.2 Material properties

2.2.1 Concrete model

It is well known that under a high strain rate impact, the strength of concrete can significantly increase, by more than 100% for concrete in compression and by more than 600% for concrete in tension [31], thus the strain rate effect cannot be neglected in the numerical model.

The dynamic increase factor (DIF) is usually used to represent the increase of concrete's compressive and tensile strength under blast loading. For concrete in compression, the CEB Code [32], which has been widely used by most researchers as an accurate representation of actual behaviour, is adopted. The DIF of the concrete strength in compression is given by:

$$\frac{f_c}{f_{cs}} = \left(\frac{\dot{\varepsilon}}{\dot{\varepsilon}_s}\right)^{1.026\alpha_s} \quad for\ \dot{\varepsilon}_s \leq 30\ s^{-1} \tag{1a}$$

$$= \gamma_s \left(\frac{\dot{\varepsilon}}{\dot{\varepsilon}_s}\right)^{1/3} \quad for\ \dot{\varepsilon}_s > 30\ s^{-1} \tag{1b}$$

where f_c = dynamic compressive strength at $\dot{\varepsilon}$

f_{cs} = static compressive strength at $\dot{\varepsilon}_s$

$\dot{\varepsilon}$ = strain rate in the range of $30 \times 10^{-6}\ to\ 300\ s^{-1}$

$\dot{\varepsilon}_s$ = static strain rate which is 30×10^{-6}

$\log_{\gamma_s} = 6.156\alpha - 2$

$\alpha = 1/(5 + 9f_{cs}/f_{co})$

f_{co} =10MPa

The formulation used for concrete DIF in tension was developed by Malvar and Crawford [33] which essentially was a modification to the CEB Code [32] and it is given by:

$$\frac{f_t}{f_{ts}} = \left(\frac{\dot{\varepsilon}}{\dot{\varepsilon}_s}\right)^{\delta} \quad for\ \dot{\varepsilon}_s \leq 1\ s^{-1} \tag{2a}$$

$$= \beta \left(\frac{\dot{\varepsilon}}{\dot{\varepsilon}_s}\right)^{1/3} \quad for\ \dot{\varepsilon}_s > 1\ s^{-1} \tag{2b}$$

where f_t = dynamic tensile strength at $\dot{\varepsilon}$

f_{ts} = static tensile strength at $\dot{\varepsilon}_s$

$\dot{\varepsilon}$ = strain rate in the range of $10^{-6}\ to\ 160\ s^{-1}$

$\dot{\varepsilon}_s$ = static strain rate which is 10^{-6}

$\log_{\beta} = 6\delta - 2$

$\delta = 1/(1 + 8f_{cs}/f_{co})$

f_{co} =10MPa

The K&C concrete model (MAT_72_REL3) is used in the current research. The K&C concrete model is a plasticity-based model that can be used either with complete user-specified inputs or internal parameter generation. Internal parameter generation only requires the concrete's unconfined compressive strength. This model includes (1) a third, independent failure surface based on a Willam-Warnke three-invariant formulation, (2) introduction of a radial stress path for the strain rate enhancement algorithm, and (3) a

fracture-energy-dependent strain in tension [27]. Previous researches suggest that the K&C concrete model is able to provide a robust representation of the complex behaviours of concrete; thus it can be used to analyse the structure's response under a blast load [27, 28, 31, 34].

2.2.2 Steel model

The steel tube is modelled by PLASTIC_KINEMATIC (MAT_003) due to its simplicity of the input parameters as well as the ability to incorporate the strain-rate effect [24]. In the current research, a perfect elasto-plastic stress-strain relationship for steel is assumed. The DIF for steel is calculated by the Cowper and Symonds Model [24], which multiplies the yield stress by a factor given as:

$$DIF\ of\ steel = 1 + \left(\frac{\dot{\varepsilon}}{C}\right)^{\frac{1}{P}} \quad (3)$$

$\dot{\varepsilon}$ =strain rate of steel

C = 40.4 s^{-1} & P = 5 are used in the current research as this combination was used in other literatures and it has shown a reasonable accuracy [35]. The material properties of steel tube are listed in Table 1.

Table 1: Material properties of steel tube

Parameter	**Value**
Mass density (kg/m^3)	7830
Yield stress (MPa)	300
Young's modulus (GPa)	200
Poisson's ratio	0.28

2.3 Simulation of blast load

In LS-DYNA, one standard approach to simulate a blast event is to build an air domain that contains the explosive and target structure inside. However, in order to capture the realistic blast physics in which the wave propagates within the air, a very high grid resolution is required and this is too computationally expensive, especially for a large standoff distance.

An alternative way is to use the conventional weapons (ConWep) air blast model [36], which was derived empirically from a large number of blast experiments. It is a build-in function in LS-DYNA, which only requires simple inputs such as equivalent TNT charge weight and charge location. This model has been widely adopted to investigate the structural response under blast loads and it has shown a high level of accuracy with a reasonable computational cost compared to any other analytical techniques [37-39]. However, it should be noted that this model is only applicable to situations where there is no offset or superposition of blast waves and the explosive must be either spherical or hemispherical.

In the present research, the ConWep air blast model is utilized due to the fact that no obstacle is present between the explosive and the column.

2.4 Validation of the uniaxial compression test

As mentioned previously, confinement effects due to composite action are very important for CFDST members. Therefore, the proposed numerical model was validated against the uniaxial compression tests conducted by Fan [15] to demonstrate the capability of the proposed LS-DYNA numerical model to accurately account for the strength enhancement due to confinement.

Two specimens reported by Fan [15] were included in the validation study. They are both 720 mm in height, and one has a 240 mm outer diameter and 80 mm inner diameter and the other one has a 240 mm outer diameter and 120 mm inner diameter. The outer and inner steel tubes for both specimens are 4 mm thick. The elastic modulus of steel E_s is 200,000 MPa, and the modular of concrete E_c is 29,000 MPa. The average yield stress of steel is 280 MPa and the average cylinder strength of concrete is 29 MPa. The loading condition is axial compression applied by using the implicit solver in LS-DYNA to achieve force equilibrium at each time step. Fig. 4 shows the comparisons between the test results

and the numerical results. In general, the numerical results slightly overestimate the initial stiffness of the tested CFDST specimens; however, the predicted ultimate axial load capacities as well as the predicted post-yield behaviours are in close agreement with the experimentally measured values. By comparison to the ACI [40] design code as shown in Table 2, the numerical results only deviate from the experimental results by 8% while the design code underestimates the axial load capacity by 26% since it does not take into consideration the concrete confinement.

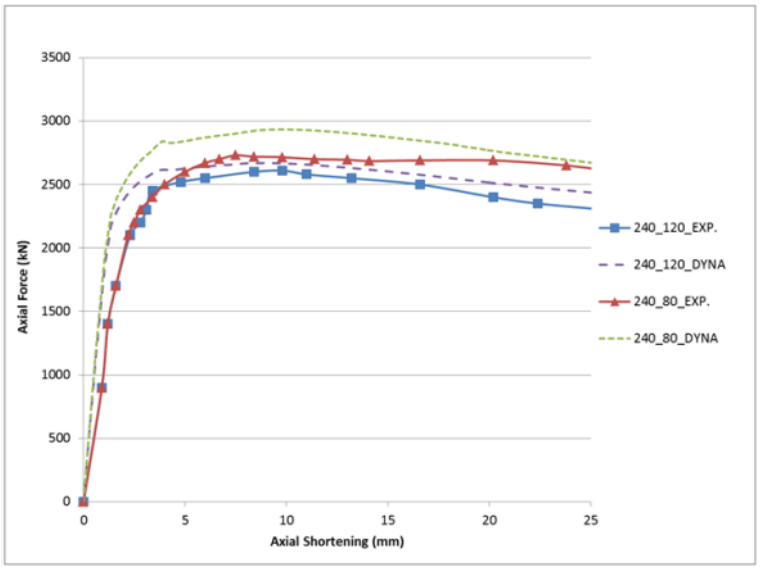

Fig. 4: Validation results against experiment data [15]

Table 2: Values given by numerical model, ACI code and test results

Column Dimension	Experiment Result	Numerical Result	Num./Exp.	ACI Prediction	ACI/Exp.
240x80	2735	2670	0.98	2072	0.76
240x120	2571	2930	1.14	1887	0.73

3. Parametric Studies and Discussions

The previously introduced numerically validated model is used to study the influence of different parameters on CFDST columns under blast loads. The parameters investigated in this research include concrete strength, outer and inner tube thicknesses, cross section geometry, hollowness ratio, support condition, and axial load. The concrete strength varies from 30 to 60 MPa; the outer and inner tube thicknesses vary from 2 to 5 mm; the cross section geometry is either circular or square; the hollowness

ratio varies from 0 to 0.75; the support is either fixed or pinned, and the axial load ratio varies from 0 to 50% of the ultimate axial load capacity. The gauge point is located on the centre of each column to measure the deflection-time history.

3.1 Concrete strength

To investigate the influence of the concrete strength on CFDST columns under blast loads, three different concrete strengths, namely 30, 45, and 60 MPa, are studied. The applied equivalent TNT charge varies from 20 to 80 kg and the standoff distance remains 1,500 mm for all cases thus making the scaled distance range from 0.35 m/kg$^{1/3}$ to 0.55 m/kg$^{1/3}$. Table 3 lists the maximum pressure and impulse values of a blast event at a variety of standoff distances. The column configuration in this section is the same as the circular CFDST control specimen as shown in Fig. 1.

Table 3: Pressure & impulse values at various scaled distances

TNT Equivalence (kg)	Standoff Distance (m)	Scaled Distance (m/kg$^{1/3}$)	Pressure (Mpa)	Impulse (MPa·ms)
20	1.5	0.55	24.6	3.2
40	1.5	0.44	43.7	6.04
60	1.5	0.38	50.5	8.83
80	1.5	0.35	63.2	10.6

Interestingly, Fig. 5 shows that varying the concrete strength between 30 and 60 MPa when the column is subjected to 60 kg charge weight has no significant influence on the maximum deflection. It is believed that the steel tubes of a CFDST specimen are the main contributor to the section moment, which makes the concrete strength become insignificant as normal strength concrete is knowingly very weak in tension. Similar results were also reported by other researches on CFT columns as well [41].

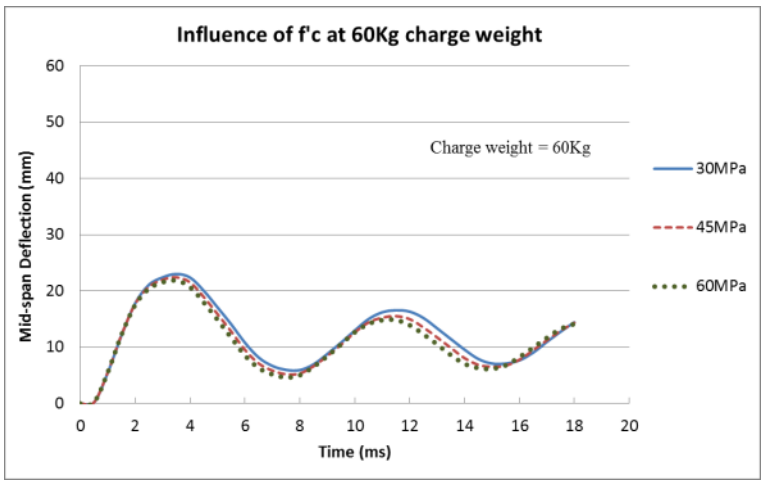

Fig. 5: Influence of f'c when charge weight = 60 kg

Similar trends are also found when subjecting the column to 20, 40, and 80 kg charge weights, which are not further discussed herein.

3.2 Outer tube thickness

To investigate the influence of outer tube thickness on the response of CFDST columns under blast loads, the outer tube thickness is varied between 2 and 5 mm, while keeping the other parameters the same as the circular CFDST control specimen.

Fig. 6 shows the deflection-time histories for CFDST columns under the blast load induced by 60 kg TNT. Generally, the column's maximum deflection decreases with increases in outer tube thickness. However, thicker the outer tube, the lower the reduction rate in the maximum deflection that can be achieved by further thickening. For example, by increasing the outer tube thickness from 2 to 3 mm, the maximum deflection can be reduced by 31%, whereas by increasing it from 4 to 5 mm, the reduction in the maximum deflection is only 17%.

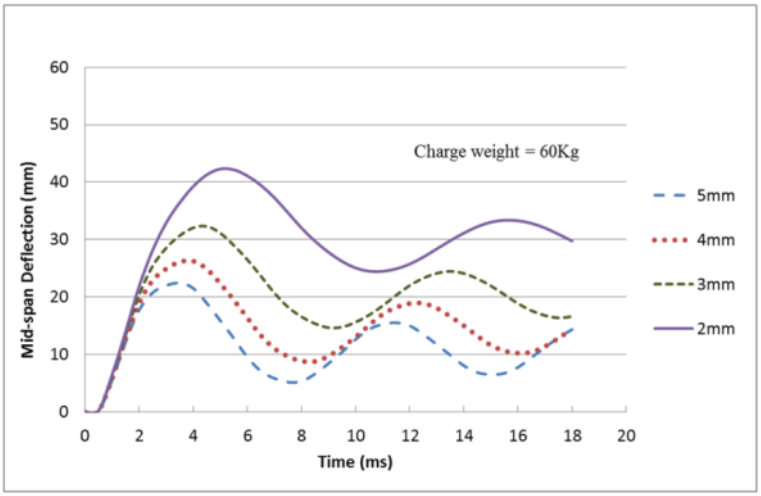

Fig. 6: Influence of outer tube thickness when charge weight = 60 kg

Fig. 7 shows the maximum deflection versus outer tube thickness of the column under various loading conditions. The slope of these curves becomes steeper as the TNT charge weight increases, suggesting that it is more cost-effective to increase the outer steel tube thickness only when a large blast load is expected.

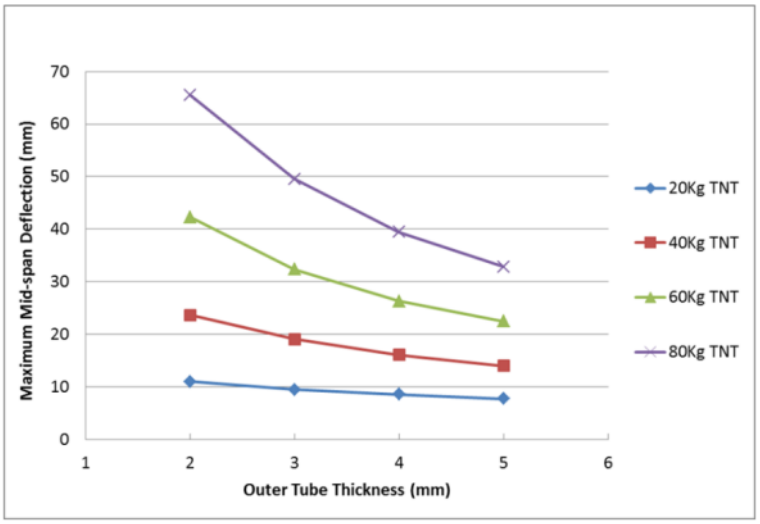

Fig. 7: Maximum deflection vs. outer tube thickness for various blast loads

Moreover, it is also observed that local buckling (bulge on the steel tube) is likely to occur near the fixed ends on a column with a thinner outer tube rather than on one with a thicker outer tube as shown in Fig. 8.

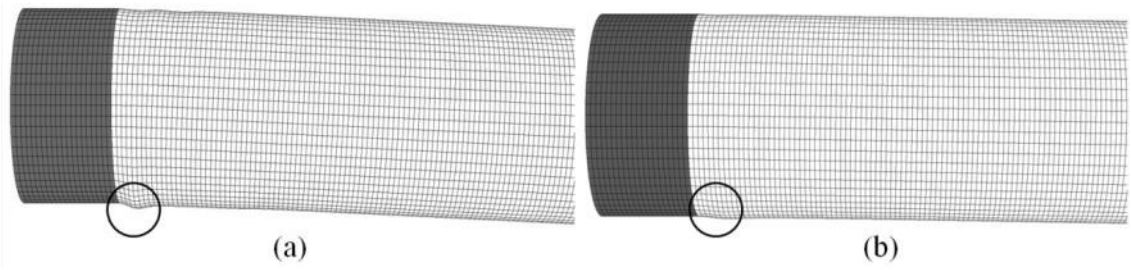

Fig. 8: Local buckling near column support for (a) 2-mm-thick outer tube; (b) 5-mm-thick outer tube

3.3 Inner tube thickness

Similar to the study of outer tube thickness, the influence of inner tube thickness is also investigated in a similar fashion by varying the inner tube thickness from 2 to 5 mm while keeping the remaining parameters the same as for the circular CFDST control specimen.

Figs. 9 and 10 indicate that increasing the inner tube thickness can also reduce the maximum deflection, but much less significantly compared to increasing the outer tube thickness. This may be due to the fact that since the outer diameter is considerably larger than the inner diameter, increasing the outer tube thickness by 1 mm can result in a greater increase in the steel ratio than increasing the inner tube thickness by the same amount (e.g., increasing the outer tube thickness from 4 to 5 mm increases the cross section area by 657 mm^2 while doing the same for the inner tube only increases the cross section area by 317 mm^2).

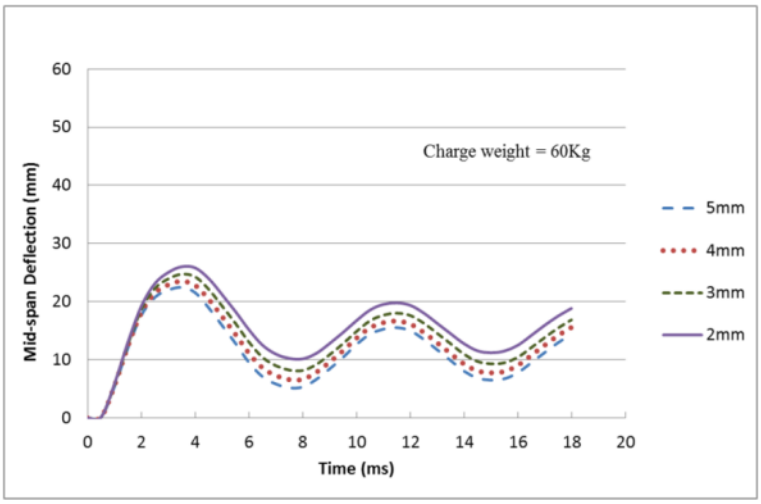

Fig. 9: Influence of inner tube thickness when charge weight = 60 kg

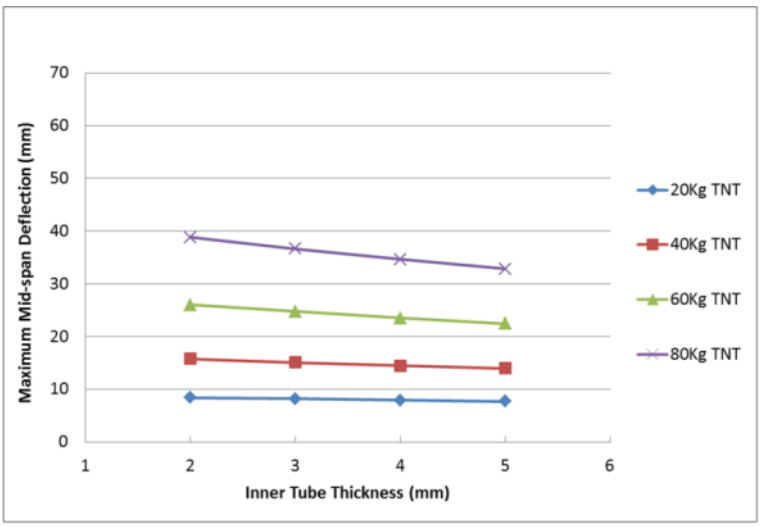

Fig. 10: Maximum deflection vs. inner tube thickness for various blast loads

3.4 Cross sectional geometry

Two commonly used cross section geometries, namely circular cross sections and square cross sections, are investigated in this section. Han [14] suggested that under lateral static loads (i.e., cyclic flexural load), the energy dissipation ability of the CFDST column with a circular cross section was much higher than those of the specimens with a square cross section. Similar trends (as shown in Fig. 11) are also observed when subjecting CFDST columns to blast loads, but it is only valid when the explosive charge weight is more than 60 kg. However, for a moderate blast load (i.e., less than 40 kg TNT), columns with circular and square cross sections both yield the similar maximum deflections.

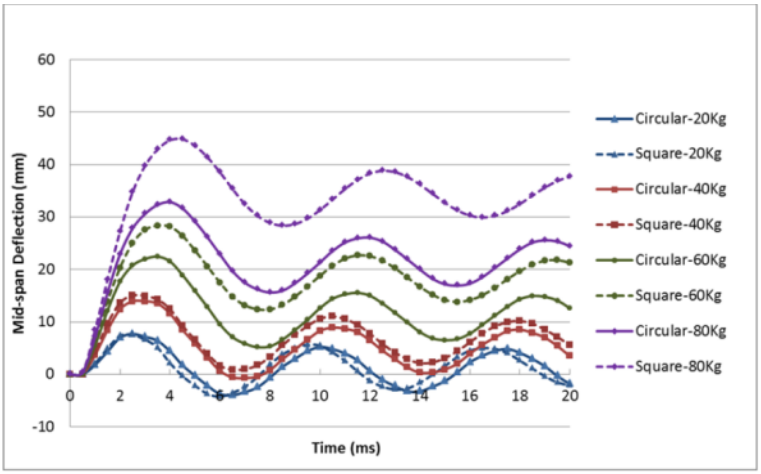

Fig. 11: Influence of cross section geometry

To compare the blast force experienced by both circular and square columns in the numerical analysis, pressure-time histories recorded from 80 kg TNT at three locations on the cross section of the mid-span are outputted as shown in Figs. 12–15. Sensor 1 is located right under the explosive, thus receiving the largest blast load. Sensor 3 is located at the edge, thus receiving the smallest blast load. Sensor 2 is located between Sensors 1 and 3. The pressure-time histories recorded at Sensor 1 are almost identical for both circular and square columns. Once looking at Sensors 2 and 3, the maximum pressure on the circular columns declines dramatically whereas no significant change in the maximum pressure is experienced by the square counterpart, consequently the impulse values for circular columns at Locations 2 (6.42 MPa • ms) and 3 (1.06 MPa • ms) are 40 and 90% smaller than those for square columns, respectively. The simulated results are somewhat in agreement with the experimental data of Allahverdi [42]. In his experiment, it was observed that the cross section geometry of a RC column could considerably affect the blast wave propagation pattern. The impulse experienced by a circular column was, on average, 20% less than that experienced by a square column.

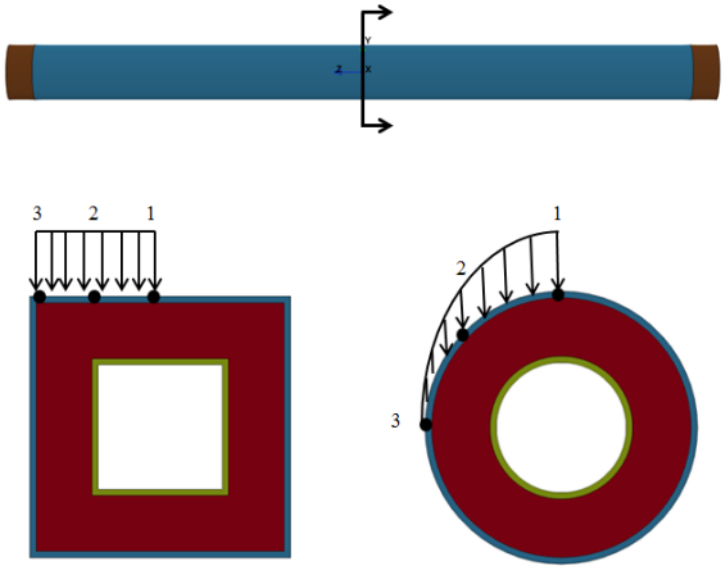

Fig. 12: Locations of the pressure sensors 1, 2 and 3 and the pressure distribution

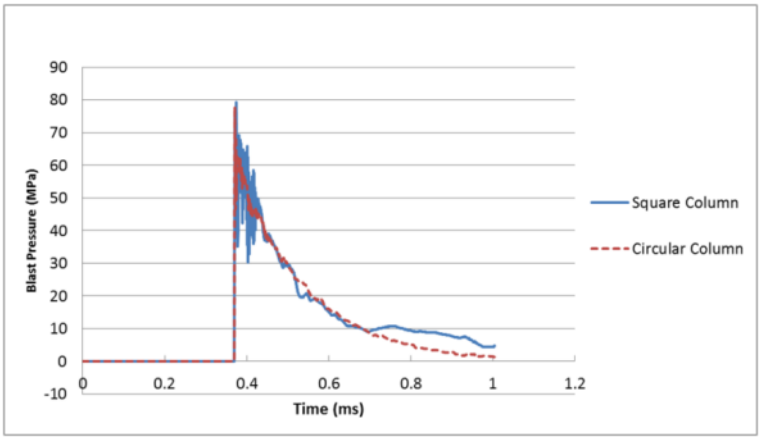

Fig. 13: Force vs. time history at sensor 1 for charge weight = 80 kg

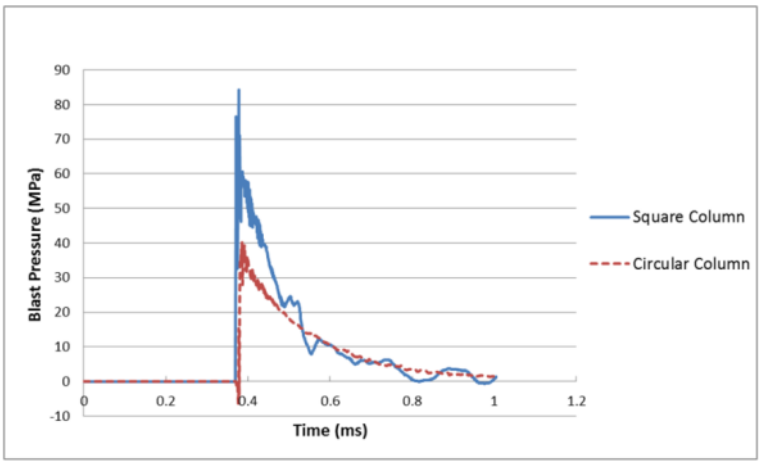

Fig. 14: Force vs. time history at sensor 2 for charge weight = 80 kg

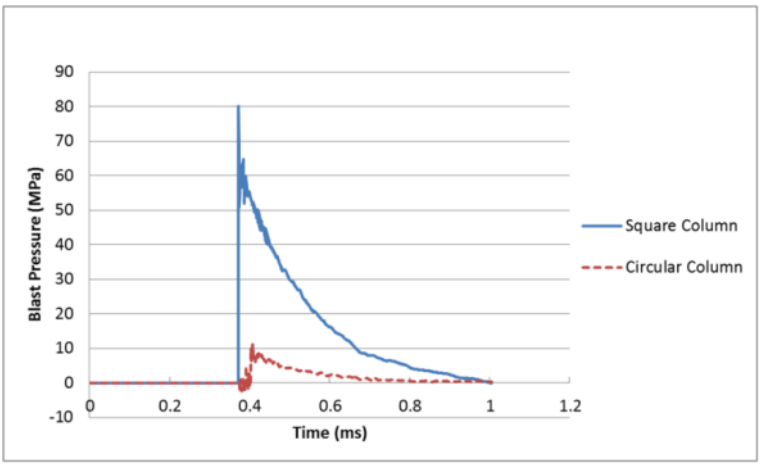

Fig. 15: Force vs. time history at sensor 3 for charge weight = 80 kg

Another possible reason for square CFDST columns having a larger mid-span deflection than circular CFDST columns might be because the effective confinement area obtained from a square cross section is much less than that from a circular cross section [43-45]. The boundaries that identify the effective confinement of a square cross section

are four parabolas intersecting the edges at 45°, while the entire concrete area of a circular cross section can be effectively confined as shown in Fig. 16.

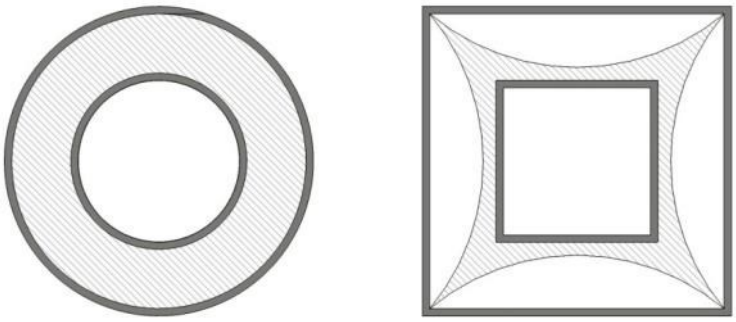

Fig. 16: Effective confinement area (shadowed) for both circular and square cross section (Mander [43])

3.5 Hollowness ratio

Hollowness ratio (χ) is defined as the ratio between the inner diameter D_i and the outer diameter D_o as shown in Fig. 17, and $\chi = 0$ indicates a Concrete Filled Tube (CFT).

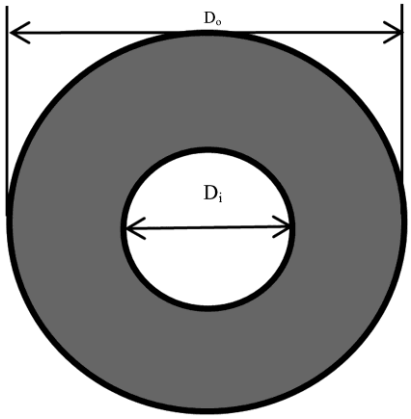

Fig. 17: Hollowness ratio $\chi = \frac{D_i}{D_o}$

Some research [12] suggested that when subjected to axial load, the effectiveness of confinement is inversely proportional to the hollowness ratio; however, the influence of hollowness ratio on CFDST columns under blast loads has not been yet investigated. Therefore, in the current study, four different hollowness ratios are studied and compared, namely χ = 0, 0.25, 0.35, 0.5 and 0.75 as shown in Fig. 18.

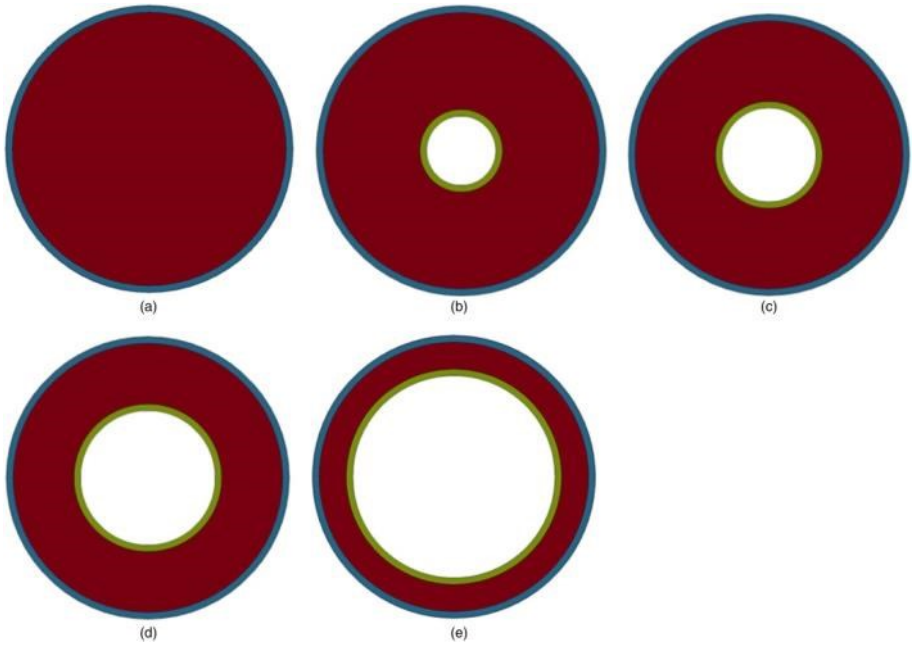

Fig. 18: Cross sections of columns with different hollowness ratios

Figs. 19 and 20 indicate that when χ is less than 0.5, columns with different hollowness ratios behave in a very similar manner, resulting in almost identical deflection-time histories. However, once χ is further increased beyond 0.5 (i.e., to 0.75), a noticeable difference can be observed in the maximum deflection and residual deflection as well as in the period of structural response. More interestingly, when χ is less than 0.5, the differences between a single-skinned column (i.e., CFT) and a double-skinned column (i.e., CFDST) seem insignificant, which again proves the fact that the core concrete contributes more to preventing steel tube buckling rather than to increasing the moment capacity.

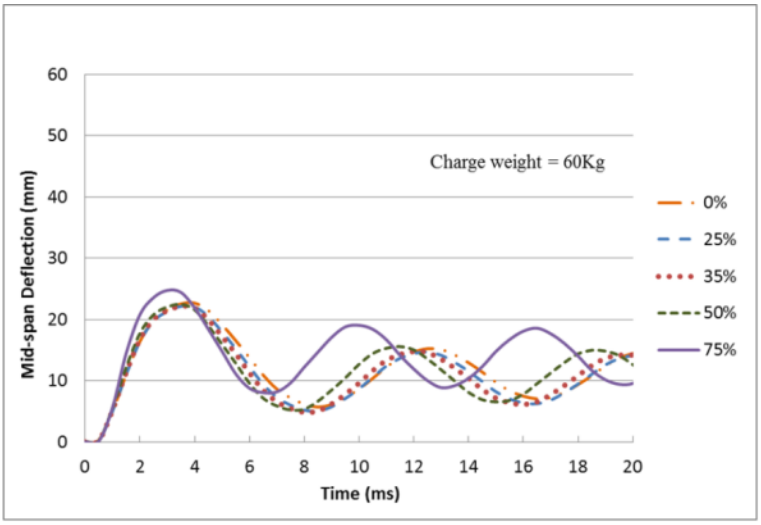

Fig. 19: Influence of hollowness ratio when charge weight = 60 kg

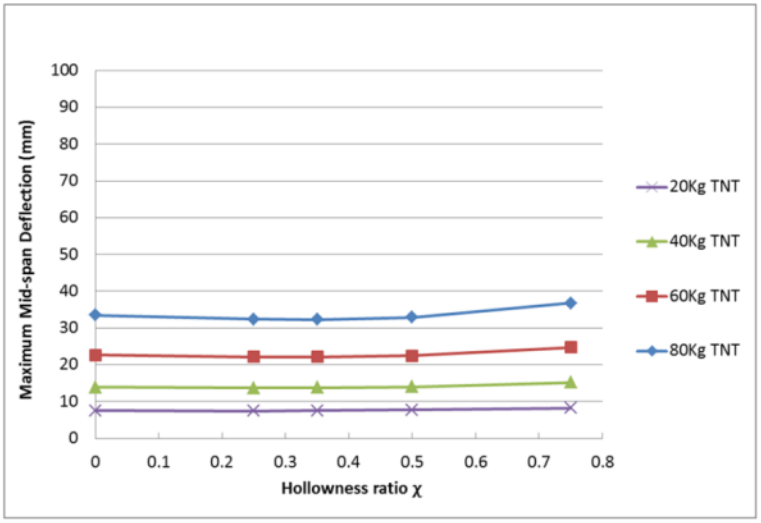

Fig. 20: Maximum deflection vs. hollowness ratio for various blast loads

3.6 Axial load

In reality, columns are always loaded by live and dead load prior to a blast incident. Several literatures [37, 46] reported that compared to unloaded RC columns, the maximum deflection of axially loaded RC columns under blast loads increases dramatically with increasing axial load. The amplification of deflection is caused by the "P-Δ" effect: when a column deflects due to blast loads, the applied axial load causes a moment at each end that can further increases the deflection; as the deflection increases, the column reaches its plastic limit, transitioning from a gradual strength degradation to a rapid loss of strength due to buckling.

In order to reflect the influence of axial load on CFDST columns under blast loads, three axial loads, namely 575, 862, and 1,150 kN, corresponding to 25, 37.5, and 50% of the ultimate axial load capacity respectively, are applied.

In the blast effects analysis of columns, it is often necessary to use several phases to apply the loading to avoid undesired oscillation [47]. In this paper, two loading phases, as shown in Fig. 21, are used. These include: (1) applying the axial load to the column prior to the detonation of the explosive. This is done by applying a gradually increased axial quasi-static load to the top of the column implicitly to avoid too much oscillation in the way of wave propagation; (2) applying the blast load while keeping the axial load

unchanged; at this stage, the computational algorithm is switched from implicit to explicit to allow for dynamic analysis of the column.

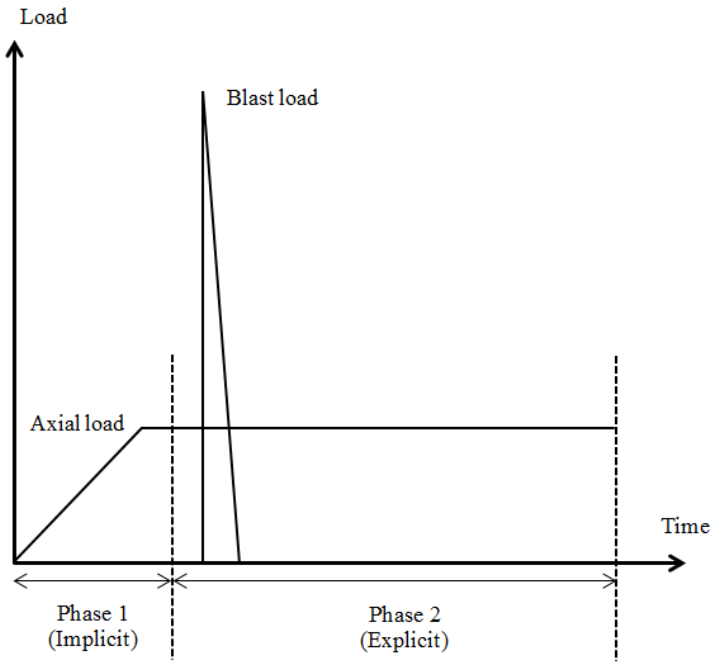

Fig. 21: Two loading phases (not to scale)

It can be seen from Figs. 22 and 23 that the magnitude of axial load ratio does not have a noticeable effect on the maximum deflection, especially when the charge weight is small. This is because the blast-induced deflection is relatively small for these analysed CFDST columns, thus the moment caused by the P-Δ effect is not large enough to have a significant increase in the maximum deflection.

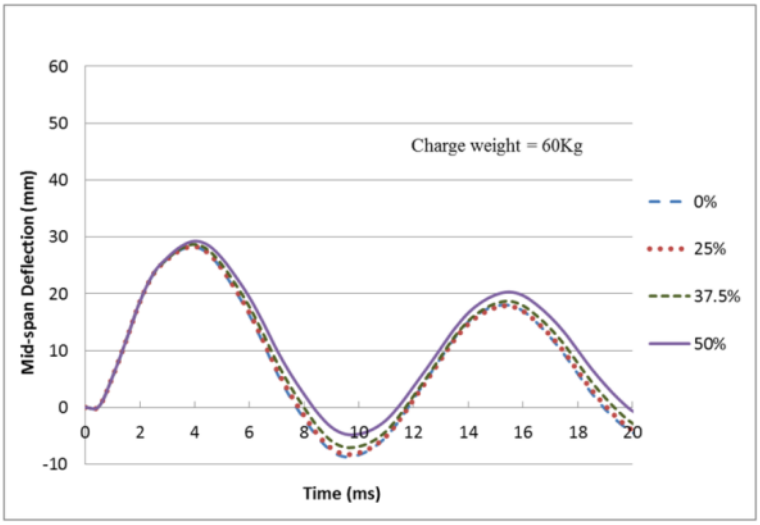

Fig. 22: Influence of axial load when charge weight = 60 kg

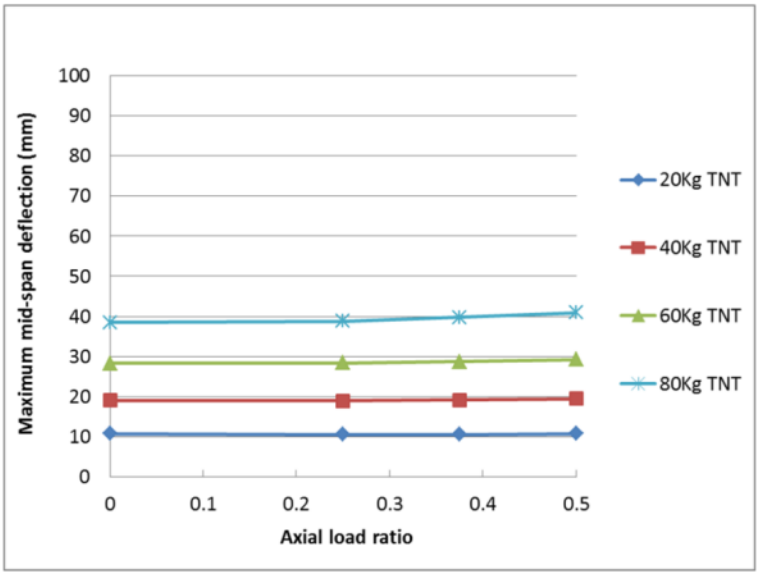

Fig. 23: Maximum deflection vs. axial load ratio of fixed column for various blast loads

3.7 Support condition

The support condition plays an important role when analysing structural response and determining structural damage. The numerical results discussed previously were all obtained from CFDST columns with fixed-support conditions. In this study, the influence of support condition is also investigated by changing the fixed-fixed support condition to the pin-pin support condition.

Necessary modifications to the LS-DYNA model are made to account for the change of support condition, and Fig. 24 shows the modified model setup. Different axial load ratios are also applied and all results are then compared to the CFDST columns discussed in the previous section.

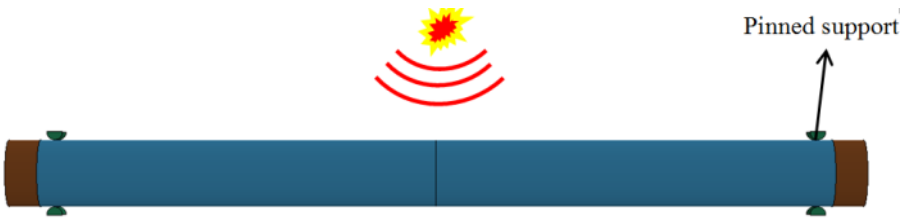

Fig. 24: Model set-up of circular column with pinned support

Figs. 25 and 26 indicate that under severe blast loads of more than 60 kg TNT charge weight, the maximum deflection of a CFDST column increases dramatically with axial

load ratio; however, for moderate blast loads (20 and 40 kg TNT), varying axial load ratio does not have a significant influence.

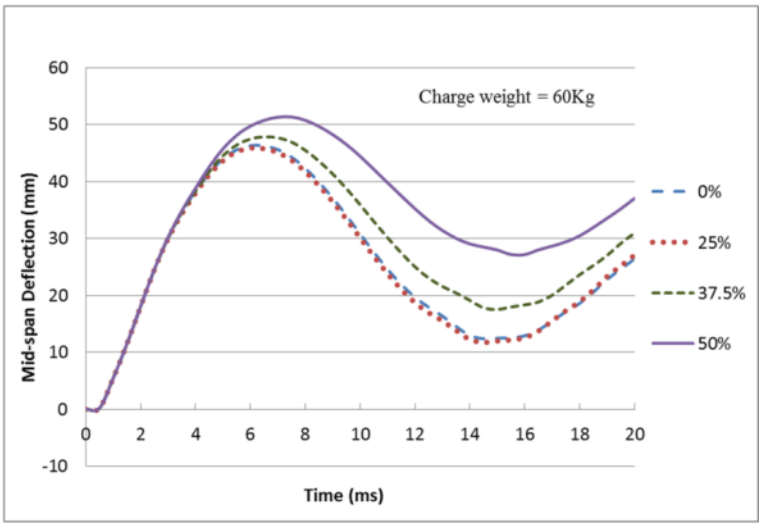

Fig. 25: Influence of axial load ratio on pinned column

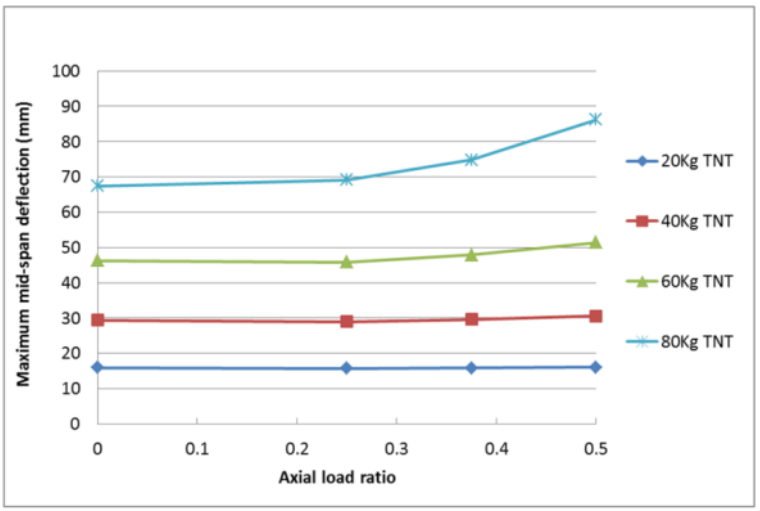

Fig. 26: Maximum deflection vs. axial load ratio of pinned column for various blast loads

Fig. 27 shows the comparison of deflection-time histories between CFDST columns with fixed ends and pinned ends. In general, under the same blast load, columns with pinned ends result in the maximum deflection more significantly than those with fixed ends. The difference in the maximum deflection also increases with the increase in TNT charge weight.

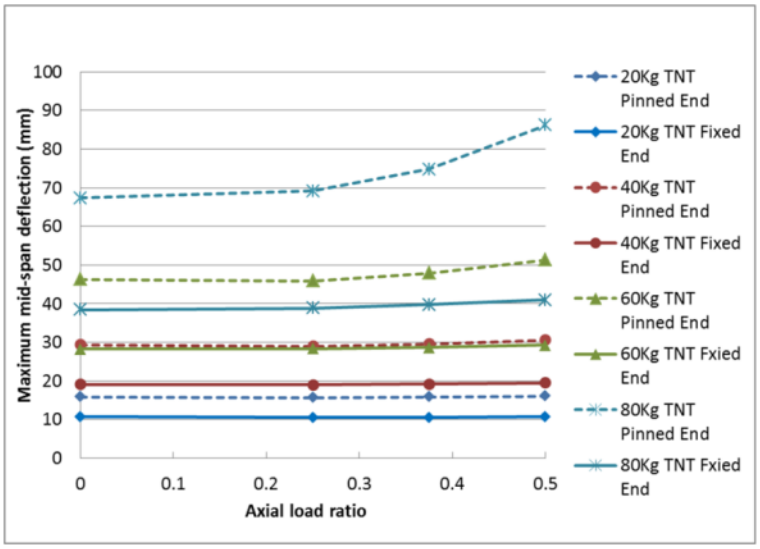

Fig. 27: Comparison between pinned support and fixed support for various blast loads

4. Conclusion

This paper numerically evaluates the influence of the concrete strength, outer and inner tube thickness, cross section geometry, hollowness ratio, axial load level, and support condition on the blast load resistance of CFDST columns. The main findings are as follows:

1. Steel tubes are the main contributor to the blast resistance of a CFDST column subjected to blast load while concrete strength has no significant influence on the mid-span deflection.

2. The outer tube thickness has a significant influence on the mid-span deflection while the influence of inner tube thickness is much less significant.

3. Under a severe blast event (e.g., greater than 40 kg charge weight), columns with a square cross section undergo much larger mid-span deflection compared to those with a circular cross section due to the fact that the roundness of a circular column can effectively reduce the peak pressure and impulse.

4. No significant change in the mid-span deflection can be seen by varying the hollowness ratio between 0 and 0.5. However, once it is increased beyond 0.5, a noticeable increase in the maximum deflection can be observed.

5. The influence of axial load ratio is not noticeable on CFDST columns with fixed supports; however for CFDST columns with pinned supports, the maximum deflection increases dramatically with axial load ratio.

6. On average, columns with pinned supports yield the maximum deflection more significantly than those with fixed supports under the same blast load.

Acknowledgements

The financial support of the Australian research Council under ARC Discovery Projects DP130100181 and DP140103025, and the Natural National Science Foundation of China under Grants 51238007 and 51108106, is gratefully acknowledged.

References

[1] Wu, C, Huang, L, and Oehlers, DJ, *Blast Testing of Aluminum Foam–Protected Reinforced Concrete Slabs.* Journal of Performance of Constructed Facilities, 2010. **25**(5): p. 464-474.

[2] Ye, Z and Ma, G, *Effects of Foam Claddings for Structure Protection against Blast Loads.* Journal of Engineering Mechanics, 2007. **133**(1): p. 41-47.

[3] Ma, G and Ye, Z, *Analysis of Foam Claddings for Blast Alleviation.* International Journal of Impact Engineering, 2007. **34**(1): p. 60-70.

[4] Hanssen, A, Enstock, L, and Langseth, M, *Close-Range Blast Loading of Aluminium Foam Panels.* International Journal of Impact Engineering, 2002. **27**(6): p. 593-618.

[5] Wu, C, Oehlers, DJ, Rebentrost, M, Leach, J, and Whittaker, AS, *Blast Testing of Ultra-High Performance Fibre and FRP-Retrofitted Concrete Slabs.* Engineering Structures, 2009. **31**(9): p. 2060-2069.

[6] Dragos, J, Wu, C, Haskett, M, and Oehlers, D, *Derivation of Normalized Pressure Impulse Curves for Flexural Ultra High Performance Concrete Slabs.* Journal of Structural Engineering, 2012. **139**(6): p. 875-885.

[7] Morino S., UMYI, *Concrete-Filled Steel Tube Column System - Its Advantages.* Steel Structures, 2001: p. 33-44.

[8] Clark, W, *Axial Load Capacity of Circular Steel Tube Columns Filled with High Strength Concrete*, in *Department of Civil and Building Engineering*1994, Victoria University of Technology: Australia. p. 175.

[9] Han, L-H, Yang, Y-F, and Tao, Z, *Concrete-filled Thin-walled Steel SHS and RHS Beam-columns Subjected to Cyclic Loading.* Thin-Walled Structures, 2003. **41**(9): p. 801-833.

[10] Han, T-H, Michael Stallings, J, and Kang, YJ, *Nonlinear Concrete Model for*

Double-Skinned Composite Tubular Columns. Construction and Building Materials, 2010. **24**(12): p. 2542-2553.

[11] Wei, S, Mau, S, Vipulanandan, C, and Mantrala, S, *Performance of New Sandwich Tube under Axial Loading: Experiment.* Journal of Structural Engineering, 1995. **121**(12): p. 1806-1814.

[12] Uenaka, K, Kitoh, H, and Sonoda, K, *Concrete Filled Double Skin Circular Stub Columns under Compression.* Thin-Walled Structures, 2010. **48**(1): p. 19-24.

[13] Han, L-H, *Flexural Behaviour of Concrete-filled Steel Tubes.* Journal of Constructional Steel Research, 2004. **60**(2): p. 313-337.

[14] Han, L-H, Huang, H, Tao, Z, and Zhao, X-L, *Concrete-filled Double Skin Steel Tubular (CFDST) Beam–columns Subjected to Cyclic Bending.* Engineering Structures, 2006. **28**(12): p. 1698-1714.

[15] Fan, J, Baig, M, and Nie, J, *Test and Analysis on Double-Skin Concrete Filled Tubular Columns.* Tubular Structures XII: Proceedings of Tubular Structures XII, Shanghai, China, 8-10 October 2008, 2010: p. 407.

[16] Han, L-H and Yang, Y-F, *Cyclic Performance of Concrete-filled Steel CHS Columns under Flexural Loading.* Journal of Constructional Steel Research, 2005. **61**(4): p. 423-452.

[17] Yuan, W-b and Yang, J-j, *Experimental and Numerical Studies of Short Concrete-Filled Double Skin Composite Tube Columns under Axially Compressive Loads.* Journal of Constructional Steel Research, 2013. **80**: p. 23-31.

[18] Uenaka, K and Kitoh, H, *Concrete Filled Double Skin Circular Tubular Members Subjected to Pure Bending and Centric Compressive Loading.* Tubular Structures 14, 2012: p. 81.

[19] Dong, CX and Ho, JCM, *Uni-axial Behaviour of Normal - Strength CFDST Columns with External Steel Rings.* Steel and Composite Structures, 2012. **13**(6): p. 587-606.

[20] Heidarpour, A and Bradford, MA, *Nonlinear Elasto-Dynamic Analysis of Bi-material Composite Members Subjected to Explosion.* Journal of Constructional Steel Research, 2012. **68**(1): p. 97-106.

[21] Heidarpour, A, Bradford, MA, and Liu, J, *Steel Arches Subjected to Blast Loading: A Non-discretisation Analysis Approach.* Applied Mathematical Modelling, 2012. **36**(9): p. 3971-3984.

[22] Heidarpour, A and Bradford, MA, *Beam–Column Element for Non-linear Dynamic Analysis of Steel Members Subjected to Blast Loading.* Engineering Structures, 2011. **33**(4): p. 1259-1266.

[23] Fouché, P and Bruneau, M. *Non-Linear Analysis of Multi-Hazard Performance of Cylindrical Concrete Filled Steel Tubes Bridge Piers*. in *Proceedings of 8th International Conference on Short and Medium Span Bridges*. 2010. Niagara Falls, Canada.

[24] Hallquist, JO, *LS-DYNA Keyword User's Manual.* Livermore Software Technology Corporation, 2007.

[25] Qu, H, Li, G, Chen, S, Sun, J, and Sozen, MA, *Analysis of Circular Concrete-Filled Steel Tube Specimen under Lateral Impact.* Advances in Structural Engineering, 2011. **14**(5): p. 941-952.

[26] Li, WL, *Experimental Study and Numerical Simulation Analysis of the Concrete Filled in Steel Tube Specimens under Lateral Impact*, 2007, Taiyuan University of Technology: Taiyuan, China.

[27] Malvar, LJ, Crawford, JE, Wesevich, JW, and Simons, D, *A Plasticity Concrete Material Model for DYNA3D.* International Journal of Impact Engineering, 1997. **19**(9): p. 847-873.

[28] Shi, Y, Hao, H, and Li, Z-X, *Numerical Derivation of Pressure–Impulse Diagrams for Prediction of RC Column Damage to Blast Loads.* International Journal of Impact Engineering, 2008. **35**(11): p. 1213-1227.

[29] Wang, R, Han, L-H, and Hou, C-C, *Behavior of concrete filled steel tubular (CFST) members under lateral impact: Experiment and FEA model.* Journal of Constructional Steel Research, 2013. **80**: p. 188-201.

[30] Yu, T, Wong, Y, Teng, J, Dong, S, and Lam, E, *Flexural Behavior of Hybrid FRP-Concrete-Steel Double-Skin Tubular Members.* Journal of Composites for Construction, 2006. **10**(5): p. 443-452.

[31] Malvar, LJ and Ross, CA, *Review of Strain Rate Effects for Concrete in Tension.* ACI Materials Journal, 1998. **95**(6).

[32] Béton, CE-Id, *CEB-FIP model code 1990: design code*. 1993: Telford.

[33] Malvar, LJ and Crawford, JE, *Dynamic Increase Factors for Concrete*, 1998, DTIC Document.

[34] Wu, Y, Crawford, JE, and Magallanes, JM. *Performance of LS-DYNA concrete constitutive models*. in *12th International LS-DYNA Users Conference*. 2012.

[35] Deng, Y and Tuan, CY, *Design of Concrete-Filled Circular Steel Tubes under Lateral Impact.* ACI Structural Journal, 2013. **110**(4): p. 691.

[36] Kingery, CN and Bulmash, G, *Air blast parameters from TNT spherical air burst and hemispherical surface burst*. 1984: Ballistic Research Laboratories.

[37] Bao, X and Li, B, *Residual Strength of Blast Damaged Reinforced Concrete Columns.* International journal of impact engineering, 2010. **37**(3): p. 295-308.

[38] Williams, K, McClennan, S, Durocher, R, St-Jean, B, and Tremblay, J. *Validation of a Loading Model for Simulating Blast Mine Effects on Armoured Vehicles*. in *Proceeding from the 7th International LS-DYNA Users Conference*. 2002.

[39] Tanapornraweekit, G, Haritos, N, Mendis, P, and Ngo, T, *Modelling of a Reinforced Concrete Panel Subjected to Blast Load by Explicit Non-linear FE Code.* The Australian Earthquake Engineering Society, 2007.

[40] ACI, C. *Building code requirements for structural concrete (ACI 318-05) and commentary (ACI 318R-05)*. 2005. American Concrete Institute.

[41] Han, L-H, Hou, C-C, Zhao, X-L, and Rasmussen, KJ, *Behaviour of high-strength concrete filled steel tubes under transverse impact loading.* Journal of Constructional Steel Research, 2014. **92**: p. 25-39.

[42] Allahverdi, NH, *Coupled Simulation of Loading and Response of Columns under Extreme Events*, in *Department of Civil and Environmental Engineering*2010, New Jersey Institute of Technology: New Jersey. p. 156.

[43] Mander, JB, Priestley, MJ, and Park, R, *Theoretical Stress-Strain Model for Confined Concrete.* Journal of Structural Engineering, 1988. **114**(8): p. 1804-1826.

[44] Idris, Y and Ozbakkaloglu, T, *Seismic behavior of high-strength concrete-filled FRP tube columns.* Journal of Composites for Construction, 2013. **17**(6).

[45] Ozbakkaloglu, T and Saatcioglu, M, *Seismic Performance of Square High-Strength Concrete Columns in FRP Stay-in-Place Formwork.* Journal of Structural Engineering, 2007. **133**(1): p. 44-56.

[46] Godinho, J, Montalva, A, and Gallant, S, *Analysis of Steel Columns for Air-Blast Loads*, in *Structure Magazine*2007.

[47] Crawford, J, Wu, Y, Magallanes, J, and Lan, S, *Use and Validation of the Release II K&C Concrete Material Model in LS-DYNA*. Karagozian & Case, Glendale, 2012.

Statement of Authorship

Title of Paper	Experimental and numerical study of blast resistance of square CFDST columns with steel-fibre reinforced concrete
Publication Status	☑ Published ☐ Accepted for Publication ☐ Submitted for Publication ☐ Unpublished and Unsubmitted w ork w ritten in manuscript style
Publication Details	Zhang, F., Wu, C., Zhao, X.L., Heidarpour, A. and Li, Z., 2016. Experimental and numerical study of blast resistance of square CFDST columns with steel-fibre reinforced concrete. *Engineering Structures*.

Principal Author

Name of Principal Author (Candidate)	Fangrui Zhang		
Contribution to the Paper	The author developed numerical model, undertook data analysis and prepared manuscript.		
Overall percentage (%)	60%		
Certification:	This paper reports on original research I conducted during the period of my Higher Degree by Research candidature and is not subject to any obligations or contractual agreements with a third party that would constrain its inclusion in this thesis. I am the primary author of this paper.		
Signature		Date	

Co-Author Contributions

By signing the Statement of Authorship, each author certifies that:

i. the candidate's stated contribution to the publication is accurate (as detailed above);

ii. permission is granted for the candidate in include the publication in the thesis; and

iii. the sum of all co-author contributions is equal to 100% less the candidate's stated contribution.

Name of Co-Author	Chengqing Wu		
Contribution to the Paper	This co-author supervised research, provided critical manuscript evaluation and acted as corresponding author.		
Signature		Date	6/6/2016

Name of Co-Author	Xiao-Ling Zhao		
Contribution to the Paper	This co-author provided critical manuscript evaluation		
Signature		Date	05/06/16

Name of Co-Author	Amin Heidarpour		
Contribution to the Paper	This co-author provided manuscript evaluation		
Signature		Date	5. Jun. 2016

Name of Co-Author	Zhong-Xian Li		
Contribution to the Paper	This co-author provided manuscript evaluation		
Signature		Date	2016.6.6

EXPERIMENTAL AND NUMERICAL STUDY OF BLAST RESISTANCE OF SQUARE CFDST COLUMNS WITH STEEL-FIBRE REINFORCED CONCRETE

Fangrui Zhang, Chengqing Wu, Xiao-Ling Zhao, Amin Heidarpour, Zhongxian Li

Abstract

In recent years, a large number of studies have been carried out to investigate behaviours of concrete filled double skin steel tube (CFDST) members due to its increasing popularity in the construction industry. This paper firstly presents an experimental study on ultra-high performance concrete filled double-skin tubes subjected to close-range blast loading with cross section being square for both inner and outer steel tubes. It is evident that the proposed CFDST column was able to withstand a large blast load without failure so that it has the potential to be used in high-value buildings as well as critical infrastructures. Then, to further investigate the behaviours of the proposed CFDST column, a number of parametric studies were carried out by using a numerical model which was developed and calibrated based on the data acquired from the blast test along with some laboratory tests. Parameters that affect the behaviours of concrete filled double skin steel tube (CFDST) members against blasts are characterised.

Keywords: Steel-fibre reinforced concrete; CFDST members; Blast loading; Numerical model

1. Introduction

As a result of the ever increasing threat of terrorist activity, countless effort has been made to mitigate blast effect on structures so that they can withstand more severe explosion accidents without catastrophic failure, thus to reduce the number of human casualties. Indirect means such as using blast barrier to protect vulnerable infrastructures

and people inside them are widely used. However, several recent terrorist attacks suggested that such indirect methods cannot effectively prevent attacks initiated by suicide bombers or suitcase bombs. Therefore, there is an urgent need to directly enhance the blast-resistance of important structures through using new structural types or new materials.

Recently, concrete-filled steel tubes, as a relatively new steel-concrete composite structure, have attracted tremendous amount of attention in the civil engineering field due to their high strength and excellent durability. A concrete filled double-skin steel tube (CFDST) is normally constructed by filling concrete in-between two concentrically placed steel tubes. The main advantage of this structural type is its passive confining pressure on the concrete filler resulted from the steel tubes. Due to the confining pressure, the strength and ductility of the concrete filler can be significantly enhanced whilst the buckling of steel tubes can be delayed, if not completely prevented, by the concrete filler. It was found that under axial compression, axial load-carrying capacity of a CFDST column was usually 10%-30% larger than the simply superposed axial load-carrying capacity of the steel tubes and the concrete filler when acting alone [1]. The predominant failure mode of CFDST columns under axial compression was found to be buckling of the outer steel tube associated with shear and spalling damage of the concrete filler at the same location [2]. Based on test results, analytical models were derived to predict the behaviour of CFDST members under axial compression which showed good agreement with the experimental data [3, 4]. A tremendous amount of effort were also made to study the flexural behaviour [5, 6], tensile behaviour [7], torsional behaviour [8] and fire resistance of CFDST columns [9] and all of the research indicated that CFDST columns are able to well adapt to a variety of loading conditions. Despite all the previously mentioned studies on CFDST columns, there is only limited knowledge with regard to the behaviours of CFDST columns under dynamic impact loading. Experiments were conducted to study concrete filled steel tubes

under transverse impact/blast loading and then compare them to hollow steel tubes with the same dimensions [10-13]. In general, hollow steel tubes under transverse impact/blast loading fail prematurely due to severe local buckling or even rapture before the material can develop its peak strength; on the other hand, for concrete filled steel tubes, the concrete filler can effectively prevent steel buckling, thus enabling the steel tube to develop its full strength and resulting in less deflection or structural damage. Also, compared to conventional RC columns, breaching and spalling damage of concrete are less likely to occur in concrete filled steel tubes when subjected to blast loading.

The majority of the existing studies on CFDST columns only use normal strength concrete filler. However, the recent trends of constructing high-rises and long-span bridges mandate the use of ultra-high performance concrete (UHPC) more and more due to the outstanding safety, serviceability, durability, and economical advantages. UHPC is known for its superior strength which can reach up to 200 MPa in compression and up to 40 MPa in tension. Also, owing to the inclusion of steel fibres, the crack propagation can be well controlled, leading to an outstanding ductility and energy absorbing capacity so as to make it an ideal material for structural members that are under the constant threat of blast attacks. There is a large number of studies that discuss the blast-resistance of UHPC structures and it was reported that UHPC materials with nano addition provide sufficient strength, ductility, and confer outstanding energy absorption and crack controlling capacities when compared to conventional normal strength concrete [14-18]. Therefore, advantages can be achieved by filling CFDST columns with UHPC: first of all, the cross-section area and self-weight of the column can be significantly reduced which allows for more slim and aesthetic design; moreover, the UHPC filler is less likely to suffer from spalling and breach damage, resulting in the steel tubes being less likely to undergo local buckling.

This paper firstly presents an experimental investigation on UHPC filled double-skin tubes subjected to close-range blast loading. In total, six CFDST column specimens, with

SHS (square hollow section) outer and SHS inner were investigated. All specimens were filled with UHPC of compressive and flexural tensile strength averaging 170 MPa and 33.8 MPa, respectively. In addition, numerical models were also developed by using the finite element tool LS-DYNA. Those models were calibrated based on a series of laboratory test data and then validated against the field blast test data. Good agreement was achieved between the numerical results and the experimental results. By using the numerical model, an extensive parametric study was carried out, where the parameters investigated were the axial load ratio, the hollow section area ratio, the inner & outer steel tube thickness, the concrete filler strength and the inner & outer cross section geometry.

2. Experiment

2.1 Specimen fabrication

All specimens were 2500 mm in length and their outer and inner widths were 210 mm and 100 mm, respectively with both outer/inner steel tubes being 5 mm thick. For ease of concrete pouring, a steel plate was welded to one end of the empty steel tube first. The inner and outer steel tubes were then put up straight and the concrete filler was poured from the top with concrete vibrators being used for consolidation. All specimens were then maintained at room temperature for 28 days and then they were levelled and polished before commencing tests. Fig. 1 depicts the cross section of the square CFDST specimen and Table 1 lists the characteristics of each specimen used in the blast test.

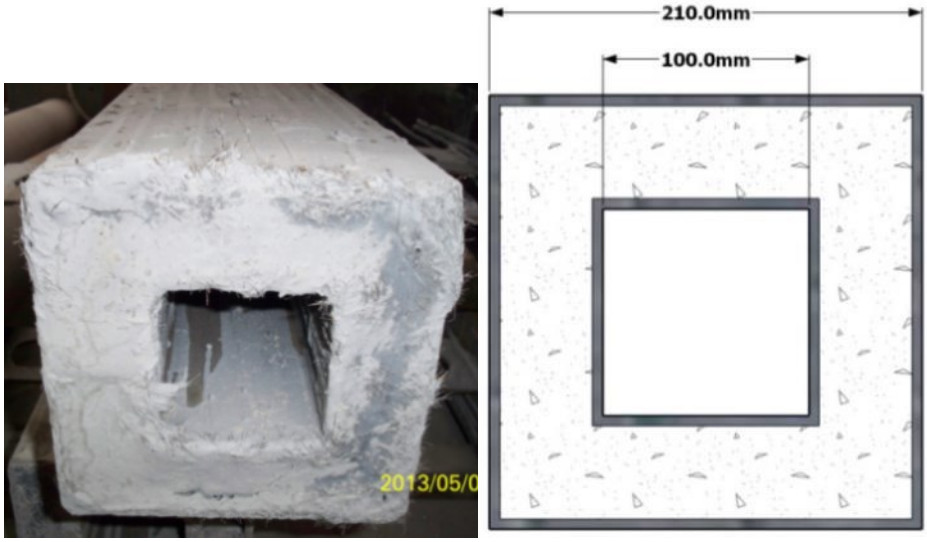

Fig. 1: Cross sections of a square CFDST specimen [19]

Table 1: Detailed information for each test specimen [19]

Specimen	L (mm)	Nominal outer dimensions (D x t_{so} mm)	Nominal inner dimensions (D x t_{io} mm)	Standoff distance (mm)	TNT (kg)*	Axial load (kN)	Maximum Δ (mm)	Residual Δ (mm)
S1A	2500	210 x 5	110 x 5	1500	35	0	41	16
S1B	2500	210 x 5	110 x 5	1500	50	0	49	22
S2A	2500	210 x 5	110 x 5	1500	35	1000	36	8
S2B	2500	210 x 5	110 x 5	1500	50	1000	/	/
S3A	2500	210 x 5	110 x 5	1500	50	1000	41	8
S3B	2500	210 x 5	-**	1500	50	1000	50	10

Note: *TNT-equivalent charge based on impulse
**S3B is a CFST specimen thus without hollow area inside

2.2 Material properties

The mechanical properties of the steel tubes were determined from tensile coupons. The average yield and ultimate strength of the steel were 360 MPa and 515 MPa, respectively with an average elongation of 22%.

Steel-fibre reinforced self-consolidating concrete with nanoparticles was used as the concrete in all CFDST specimens. The nanoparticle, i.e. $CaCO_3$, was used as a nano-scale additive to fill up the void existing in concrete as well as to enhance the hydration process.

Twenty-nine $100\text{mm} \times 100\text{mm} \times 100\text{mm}$ specimens were made for compressive tests and another twenty-nine$100\text{mm} \times 100\text{mm} \times 400\text{mm}$ specimens for flexural tensile tests. Each specimen was properly levelled, sanded, polished, cleaned and dried to attain smooth surfaces. The average compressive strength and the flexural tensile strength of the

concrete at 28 days were 170 MPa and 33.8 MPa, respectively, which are much higher than normal strength concrete.

2.3 Experiment setup

A 3 m × 0.4 m × 1.5 m test pit, as shown in Fig. 2, was excavated for the placement of recording devices and data cables. Thick steel plates were used to cover the test pit to prevent the blast wave from traveling into the pit and damaging the apparatus consequently. A pneumatic jack was installed and buried beneath the ground at one side of the test pit to apply an axial load to the test specimen. Roller supports were used near both ends to simulate simply supported conditions. Steel bolts were also used to provide an upward restraint against column rebound, thus making the effective span of the CFDST specimen 2300 mm. It should be mentioned that the test pit was designed to be as wide as the test specimen, therefore when the square specimen was placed into it, its front side (the side which received the blast load) was levelled with the ground surface so that there would be no clearing effect nor would the incident wave damage the recording apparatus at the bottom of the pit.

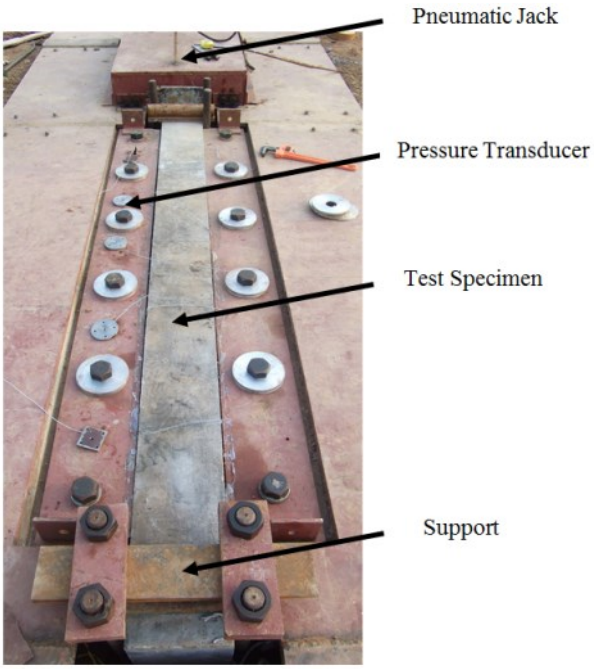

Fig. 2: Test pit

As shown in Fig. 3, three displacement gauges (LVDTs) spaced at 380 mm were attached to the test specimen to measure the displacement-time histories. The maximum measuring range of the LVDT was 120 mm for both upward and downward motions. A pressure transducer was also used in order to capture the pressure-time history. However, if directly placed under the explosive, there was a high chance of damaging the pressure transducer. Therefore, it was positioned 760 mm away from the centre of the specimen.

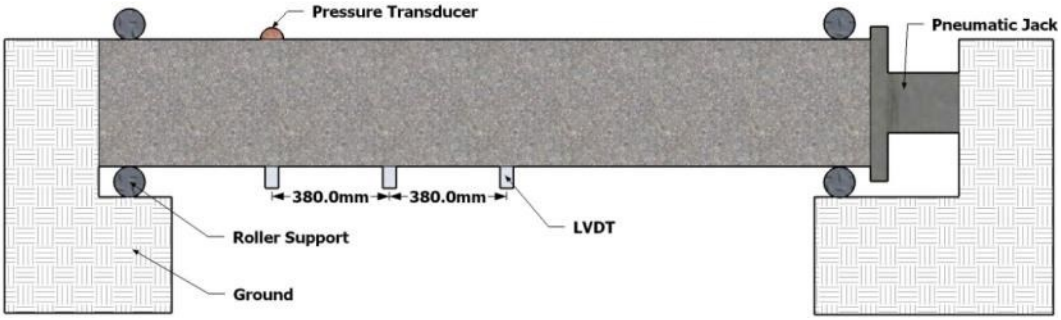

(a) Side view

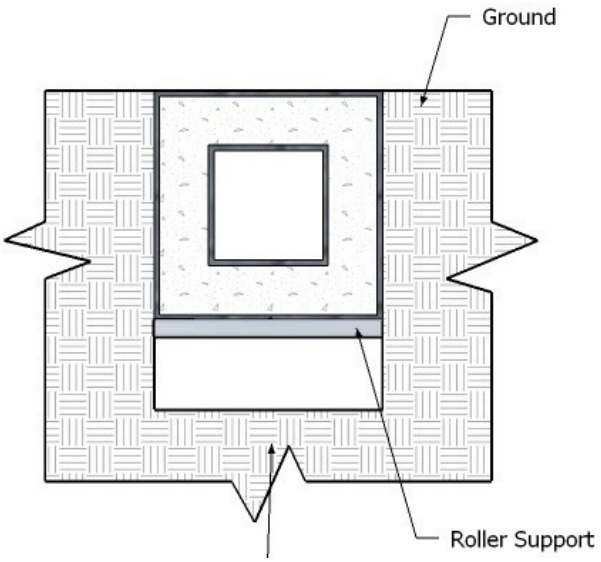

(b) Cross-sectional view

Fig. 3: Schematic view of the test setup [19]

3. Test Results

The results of this experiment has been reported in the authors' previous work [19], hence it is not discussed in great detail herein, only important results are iterated in the following sections.

3.1 Pressure-time histories

Emulsion explosive was used in the current blast test program. Simoens et al. [20] reported that the emulsion explosive generates a blast wave that has peak pressures of the same magnitude as an identical mass of TNT explosive but for impulse, a mass of emulsion explosives equals only about 70% of that mass in TNT. Since the blast impulse predominantly determines the structural response under high strain rate impact, therefore 1.4 kg of emulsion explosive was equated to 1 kg of TNT in the current study. It should be mentioned that Simoens [20] only tested small amounts of emulsion explosive (e.g. 4.8 kg), therefore the conversion factor may vary with charge weights.

In this study, CONWEP predictions of spherical explosive was used as benchmarks for the peak reflected pressure and impulse [21, 22]. Fig. 4 shows some typical pressure-time histories recorded during the experiment along with the comparisons to CONWEP predictions. It is evident that the measured blast loads agrees with the CONWEP-predictions reasonably. The discrepancies were mainly resulted from the following reasons: 1) when the blast wave travels toward a test specimen, sand and soil particles are raised and then inevitably fell on the pressure transducer. As the pressure transducer is highly sensitive, the pressure resulted from the particle collision is therefore also regarded as part of the blast load; 2) the explosive charge weights used in the blast tests are relatively large, therefore the accuracy and sensitivity of the pressure transducer can deteriorate over time; 3) the size of the explosive can be too large that the chemical reactions within the explosive compound were unthorough and incomplete at the initial detonation.

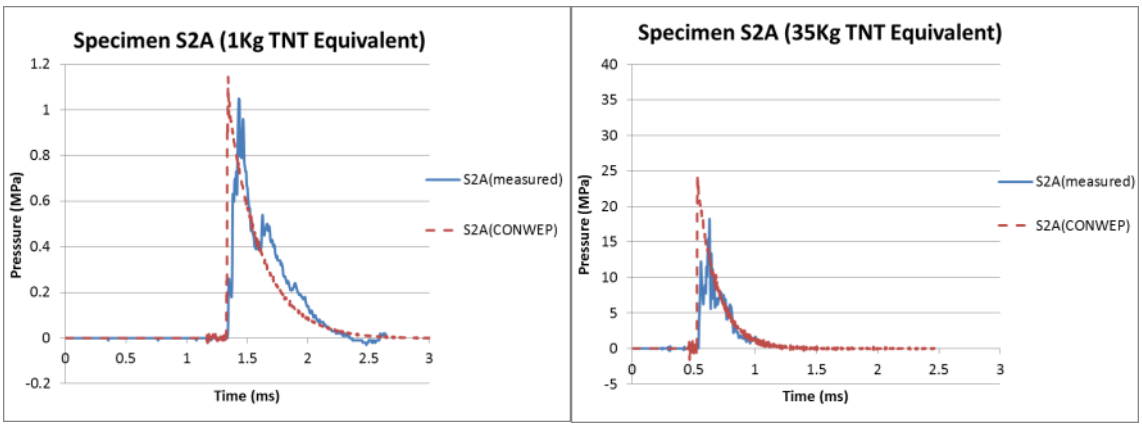

(a) (b)

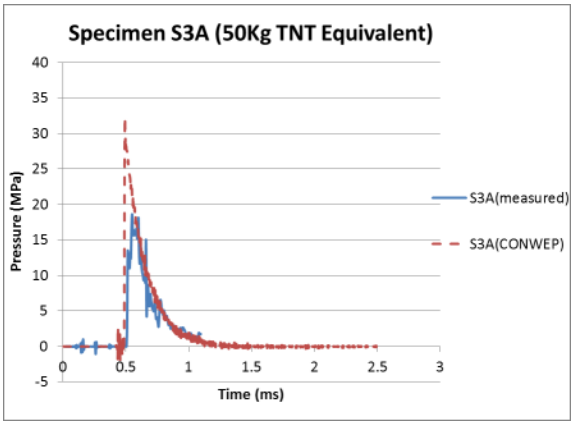

(c)

Fig. 4: Typical pressure-time histories for tested specimens

3.2 Displacement-time histories

Fig. 5 reports a typical displacement-time history of the test specimens. All three LVDTs were aligned along the centreline of the member. None of the displacement measurements went beyond the LVDT's measuring range (120 mm). The mid-span residual displacements of the tested specimens were measured manually post-testing and they were found to be in good agreement with the LVDT readings.

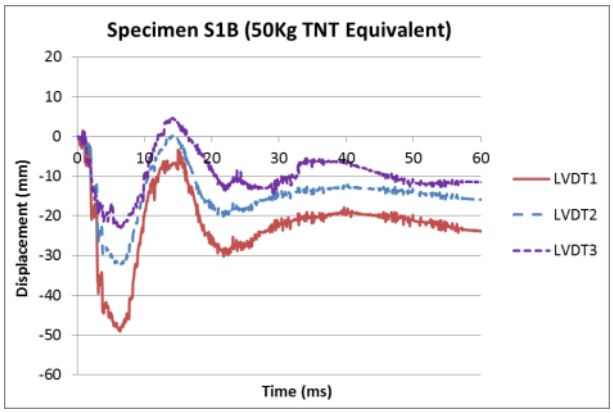

Fig. 5: Typical displacement-time histories for tested specimens

3.3 Failure mode

Since the CFDST specimen is filled with steel-fibre reinforced UHPC in this paper; therefore its structural response is very different from those filled with normal strength concrete. It is evident from Fig. 6 that neither steel buckling nor localised damage can be observed on the specimen which was subjected to 35 kg TNT equivalent. Moreover, once the outer steel tube was removed, there was also no obvious sign of concrete crushing neither, and only minor flexural cracks of no more than 0.5 mm width were seen on the tensile face of the specimen. Therefore, it is evident that the CFDST specimens are able to remain overall of global flexural response as opposed to localised structural failure.

(a) Overall deformation

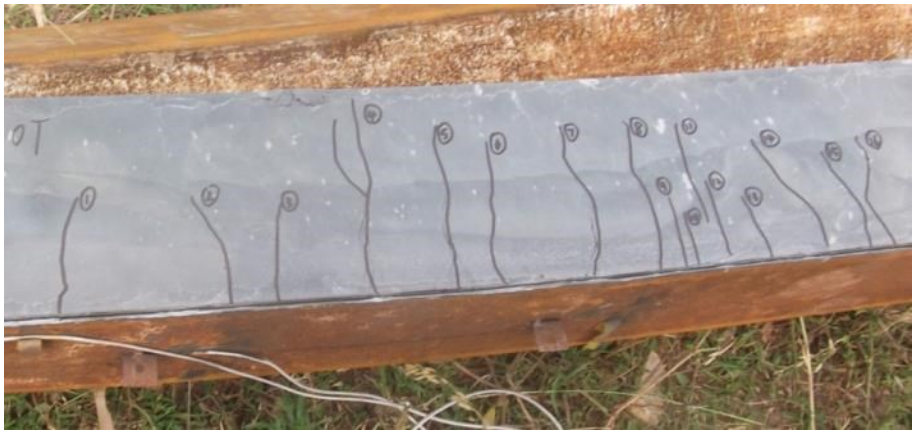

(b) Crack propagation in concrete

Fig. 6: Deformed shape and crack propagation in specimens S1A [19]

4. Numerical Simulation

In this paper, finite element models were developed with 8-node solid elements with single point integration algorithm in LS-DYNA [23]. LS-DYNA/Implicit Solver was used for the static test and LS-DYNA/Explicit Solver was used for the blast test. Viscos-type

hourglass control was activated during the blast test simulation to prevent element distortion and zero energy modes.

4.1 Model Calibration

Material model 24, namely MAT_PIECEWISE_LINEAR_PLASTICITY, is used to model the behaviours of the steel tube. The actual stress-strain relationship obtained from tensile coupon test was used which is shown in Fig. 7.

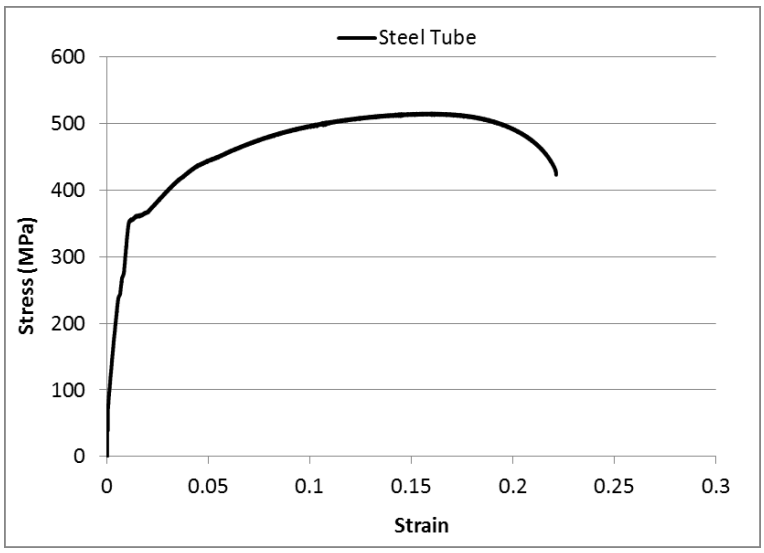

Fig. 7: Stress-strain relationship for the steel tube

As for concrete filler, there are several material models in LS-DYNA that can be used [24, 25] and among which, the K&C concrete model (also known as "MAT CONCRETE DAMAGE REL3") is most widely used for its ability to model the behaviours of concrete members under complex loading conditions, including situations involving active/passive confining stress and/or high strain rate effect, with efficiency and accuracy [26-29]. The K&C concrete model is defined by a number of material parameters, and users can either manually input the values obtained from actual material tests or directly use the default values generated by the program itself. The mechanism behind this constitutive model along with each material input has been thoroughly explained by [30], thus are not further discussed hereafter. However, it should be mentioned that the K&C model was primarily developed based on normal strength concrete, whereas the behaviours

of UHPC are significantly different. Therefore, the default K&C concrete model, or any other existing models for this matter, should not be directly applied to model the behaviours of UHPC structures without modifications.

In order to extend the K&C model to accommodate the behaviour of the proposed UHPC material, a number of laboratory tests were conducted for model calibration purpose, the material properties require calibration were: f_t, which is the uniaxial tensile strength; B_1, which governs the compressive damage and softening behaviour; w_{lz}, which governs the fracture energy of each element; ω, which governs the volume expansion; λ and η, which governs the damage function and scale factor respectively. The key parameters for UHPC material used in this paper are listed in Table 2 and Fig. 8.

Table 2: Key parameters for K&C concrete model

Model parameter	Value
f'_c	170 MPa
f_t	18 MPa*
Poisson's ratio	0.19
B1	0.8
w_{lz}	6.00 mm
ω	0.10

*note: f_t is the direct tensile strength, not the flexural tensile strength

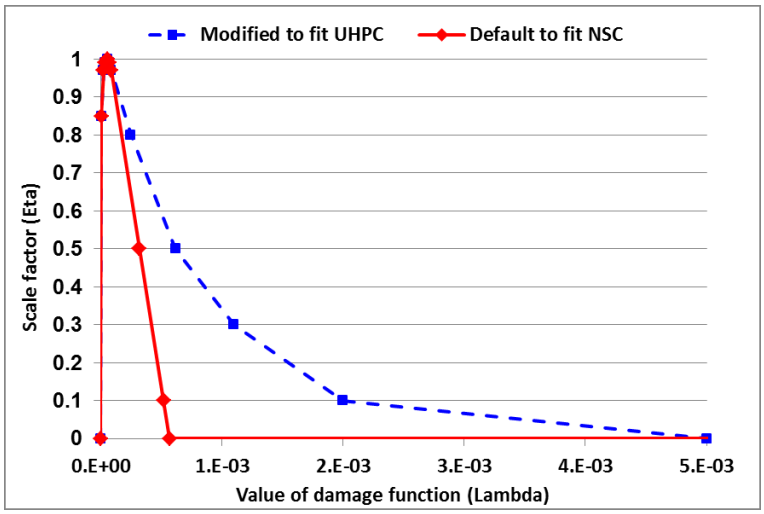

Fig. 8: λ and η for UHPC and normal strength concrete

4.1.1 Uniaxial compression test

As depicted in Fig. 9 that a numerical model was developed to calibrate material inputs such as B_1, w_{lz}, λ and η by using the laboratory results of the uniaxial test on 100

mm x 100 mm x 100 mm UHPC specimens. Fig. 10 indicated that reasonable agreement was achieved between the numerical and experimental stress-strain curves, demonstrating the modified material model was able to simulate the ductile post-peak softening phase of UHPC, which was very different from normal strength concrete.

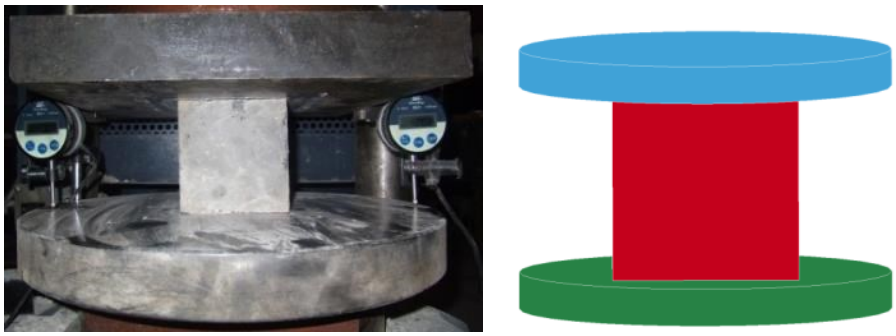

Fig. 9: Test setup of uniaxial compression test

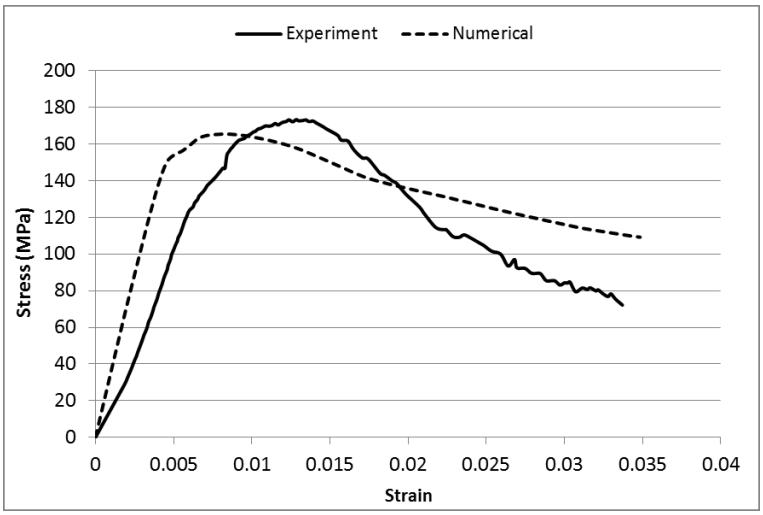

Fig. 10: Uniaxial compression test results

4.1.2 Four points bending test

Fig. 11 demonstrates the numerical model of the four points bending test which was used to calibrate material inputs such as f_t and w_{lz}. It is evident from Figs. 12 and 13 that not only did the numerical model using modified K&C accurately predicted the load-displacement curve, it also can correctly simulate the crack formation in the specimen. In the current numerical model, the concrete element eroded when the maximum shear strain reached 0.045.

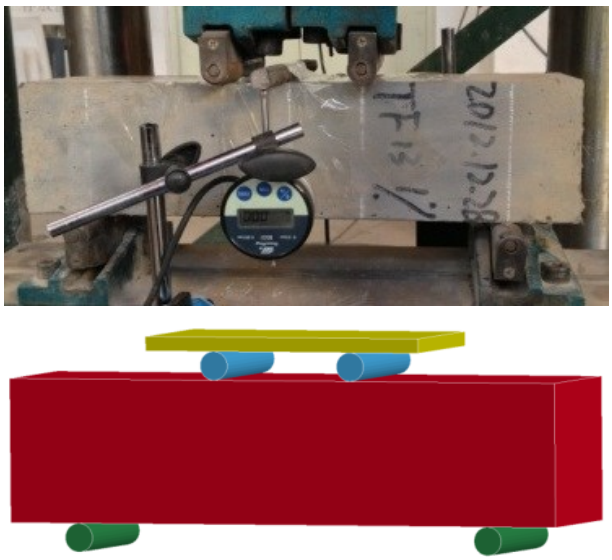

Fig. 11: Test setup for four points bending test

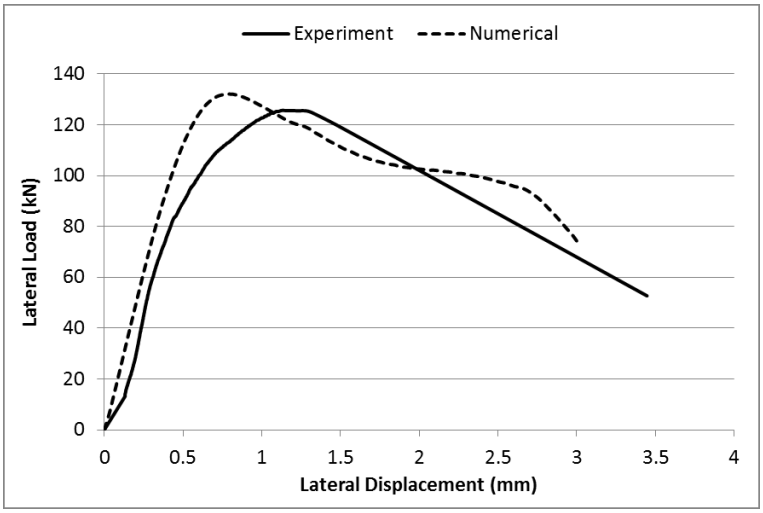

Fig. 12: Four points bending test results

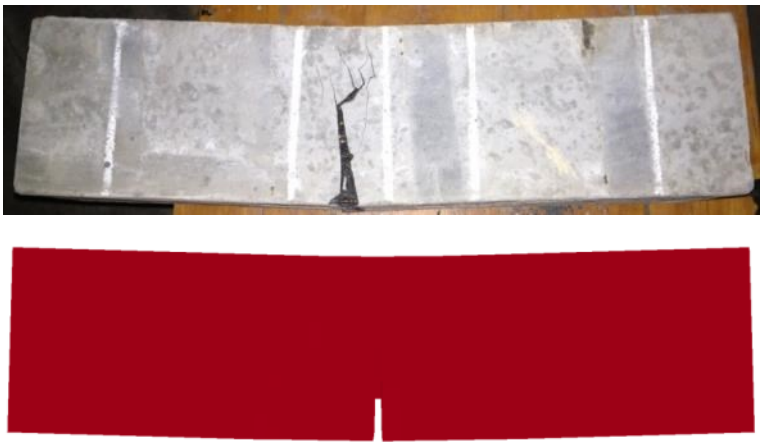

Fig. 13: Crack formation on UHPC specimen

4.2 Model Validation

4.2.1 Static Test

Static test was carried out to study the behaviours of UHPC filled CFDST specimens when subjected to quasi-static lateral load combined with constant axial load. As shown in Fig. 14 that the test equipment consisted of two hydraulic jacks: the vertical hydraulic jack, which was used to apply lateral load, was displacement-controlled and the horizontal hydraulic jack, which was used to apply axial load, was force-controlled. The specimen was simply supported near both ends by rollers and the axial load was applied by the horizontal hydraulic jack to only one end of the specimen.

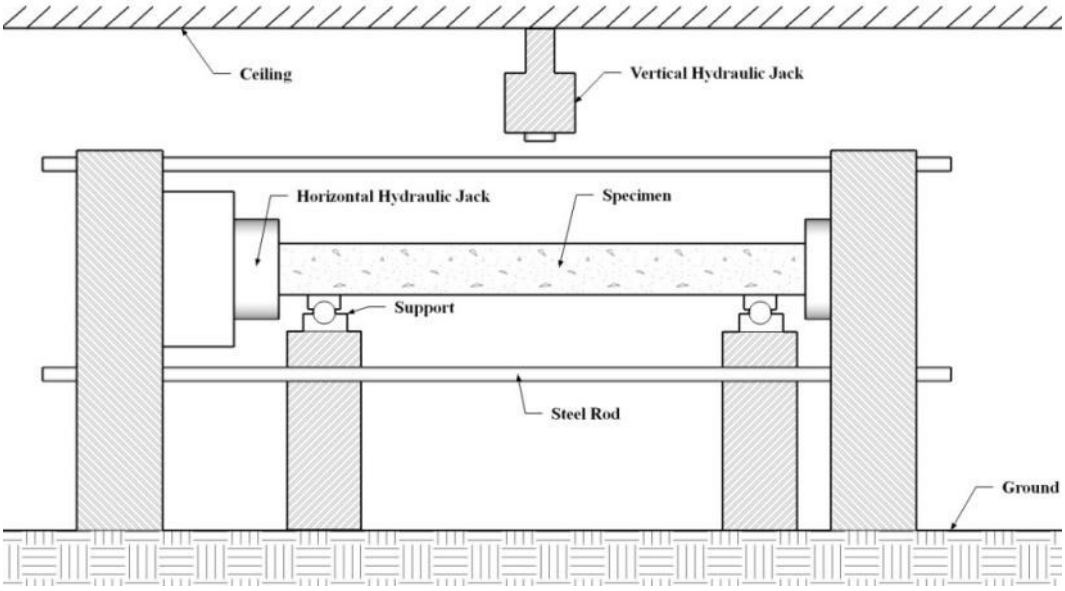

Fig. 14: Three points bending test setup

Fig. 15 illustrates the meshing of the numerical model: the characteristic length of each element ranged from 6.3 mm to 7.5 mm approximately. Mesh convergence study suggested that by further refining the mesh, only minor improvement can be made, however, with a great increase in the computation time.

Table 3 and Fig. 16 compare the numerical result to the experimental result of the static test. It can be seen that the initial stiffness of the numerical curve was slightly larger than that of the experimental curve which was similar to what was found in Fig. 10 and 12.

Apart from that, the numerical model showed excellent agreement with the experimental observations, yielding only 1.2% error in the maximum loads.

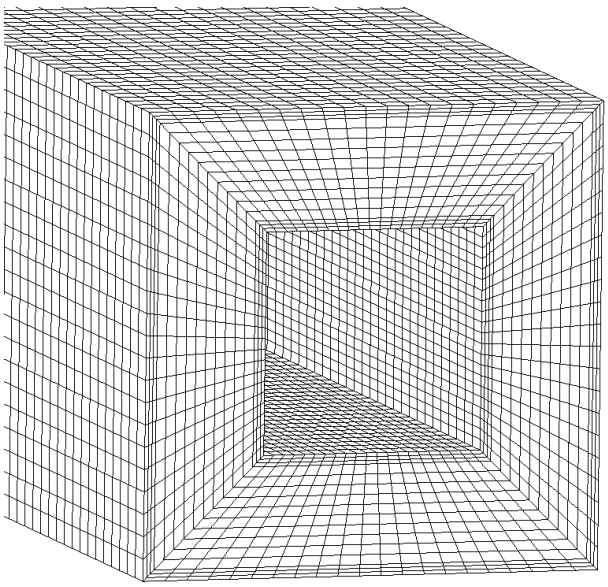

Fig. 15: Meshing of the numerical model

Table 3: Summary of three points bending tests

Outer dimensions (mm)	Inner dimensions (mm)	Tube thickness (mm)	Axial Load (kN)	Exp. Peak Load (kN)	LS-DYNA Peak Load (kN)	Error
210	100	5	1000	660	652	-1.2%

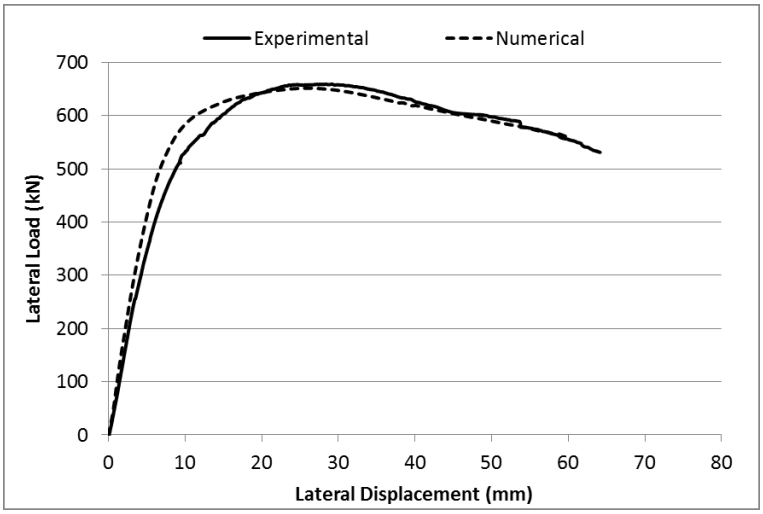

Fig. 16: Force-displacement histories of three points bending tests

These aforementioned results evidently confirmed the practicability and fidelity of numerically modelling UHPC filled CFDST specimens under static loads. Therefore, in the following section, the behaviours of UHPC filled CFDST specimens under blast loads were also numerically investigated in a similar manner.

4.2.2 Blast Test

It is well known that under high strain rate impact, the strength of normal concrete increases significantly, by more than 100% for concrete in compression and by more than 600% for concrete in tension and the dynamic increase factor (DIF) for normal strength concrete can be calculated by the CEB Code [31, 32]. However, there is very little knowledge on the strain rate behaviour of UHPC. Ngo et al. [33] developed DIF model for UHPC with compressive strength up to 160 MPa, it was reported that the strain rate effect on UHPC was significantly smaller than the CEB Code prediction [31, 32]. In the current research, the dynamic properties of UHPC were studied through Split Hopkinson's Pressure Bar (SHPB) test and the results are depicted in Fig. 17 [34]. In comparison to the normal strength concrete, the strain rate of UHPC did not have a significant effect until it reached 200/s for tension and 50/s for compression. The DIF of UHPC at the same strain rate was also much smaller compared to that of the normal strength concrete.

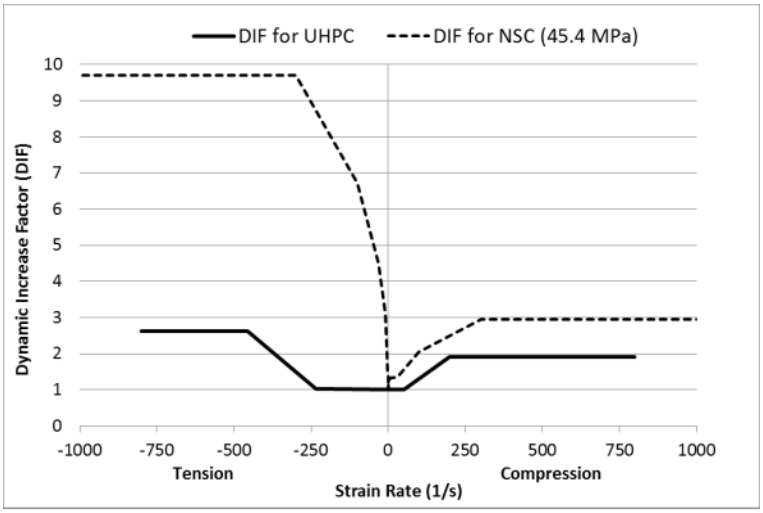

Fig. 17: DIF for UHPC & NSC

The strain rate effect on the steel tube was incorporated by the Cowper and Symonds law which multiplies the yield stress by a factor given as:

$$DIF\ of\ steel = 1 + \left(\frac{\dot{\varepsilon}}{C}\right)^{\frac{1}{P}} \quad (1)$$

where $\dot{\varepsilon}$ = strain rate of steel ; C and P are two constants.

In the current research, C = 6488 s^{-1} and P = 3.91 were used according to the dynamic axial crushing test on square tubes carried out by [35].

It can be concluded from Table 4 and Fig. 18 that, the proposed numerical model not only accurately predicted the maximum mid-span deflection, with or without axil load, the predicted period of oscillation also corresponded with the experimental curve very well. Although some insignificant discrepancies were seen in the residual deflection, the difference was within the acceptable range, considering the complexity and uncertainty associated with blast experiments.

Table 4: Summary of blast tests

Specimen No.	TNT Equivalent (Kg)	Axial Load (kN)	Standoff Distance (mm)	Mid-span Deflection (mm)		
				Measured	LS-DYNA	Error (%)
S1B	50	0	1500	49	42.1	-14%
S3A	50	1000	1500	41	37.9	-7.5%

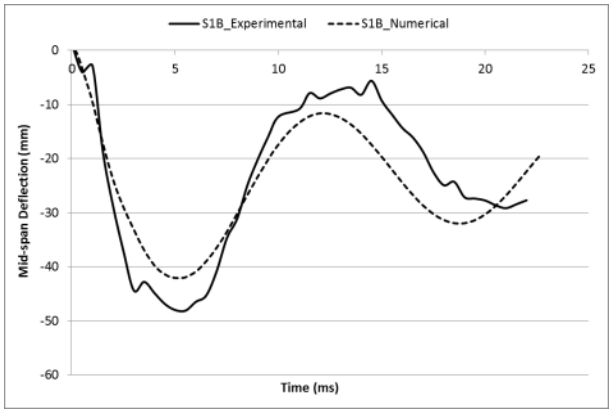

(a)

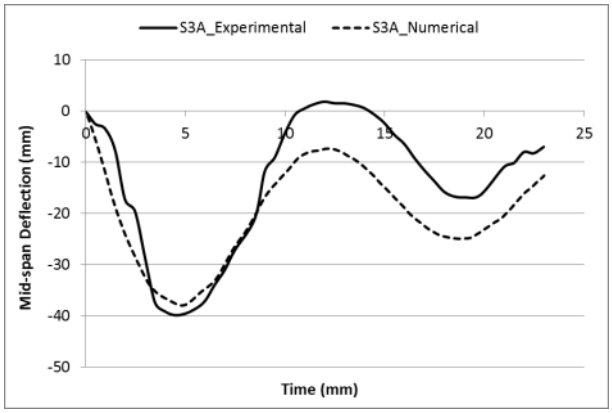

(b)

Fig. 18: Displacement-time histories of blast tests

5. Parametric Studies

A total of 33 numerical specimens were designed to investigate the effect of the cross-sectional dimensions and material properties on the behaviours of CFDST columns. Table 5 lists the characteristics of the specimens and Fig. 19 depicts the specimen setup in the numerical model: both ends of the column used for parametric study were embedded in concrete slabs and the outer faces of both slabs were restrained so that it can only move along the axial direction. The nominal length of all the specimens used in the parametric study was 3500 mm and the nominal yield strength of all steel tubes was 346 MPa.

The specimens were divided into six groups and each group represents one parameter. The first group, namely AR, investigated the effect of axial load ratio under blast loads of three different magnitudes. The second group, namely HR, consisted of five specimens having inner diameter ranging from 0 mm to 120 mm and a unit outer diameter of 210 mm. The next group, namely CS, focused the influence of concrete strength and the differences between normal strength concrete and UHPC. Groups 4 and 5 examined the impact of inner and outer tube thickness and as a result, all specimens under this category had different inner/outer tube thickness ranging from 3 mm to 6 mm. The last group compared the behaviours of CFDST specimens having different cross section geometries under the same blast loads. Four cross-sectional combinations were chosen under this category, including CHS (circular hollow section) inner + CHS outer, CHS inner + SHS (square hollow section) outer, SHS outer + CHS inner and SHS outer + SHS inner.

5.1 The effect of axial load ratio

Structural columns are under constantly changing live load therefore it is of great interest to see their behaviours under blast loading with different axial load ratios. Axial load ratio is the ratio between the actual applied axial load and the axial load-carrying capacity of the column. In the current research, three blast load levels were used in

conjunction with four axial load ratios ranging from 0.016 up to 0.5. It is evident from Figs. 20 and 21 that, within a certain limit (e.g. less than 0.16 in this paper), the increase in axial load ratio can result in a smaller deflection regardless of the magnitude of the blast loading. However, if the axial load ratio continued increasing beyond the critical value, a noticeable increase in the deflection or even structural instability can be seen with this effect being more significant when the specimen was subjected to a larger charge weight. This is due to the fact that with an increase in the applied axial load on columns, it resulted in an increase in the moment capacity and the nominal shear strength. However, once this critical axial load ratio was exceeded, the mid-span deflection increased greatly with increasing axial load. When a column undergoes large deflection and plastic hinges formation occurs near mid-span and fixed ends, axial loads will amplify the lateral deflection and internal moment due to the $P-\Delta$ effect. A number of studies also reported similar findings on other column tests [29, 36-38].

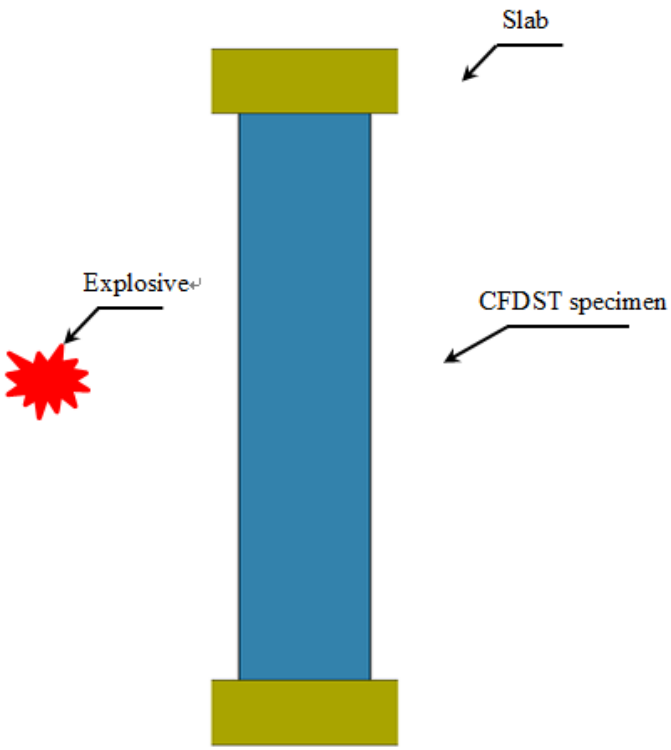

Fig. 19: Test setup for parametric study

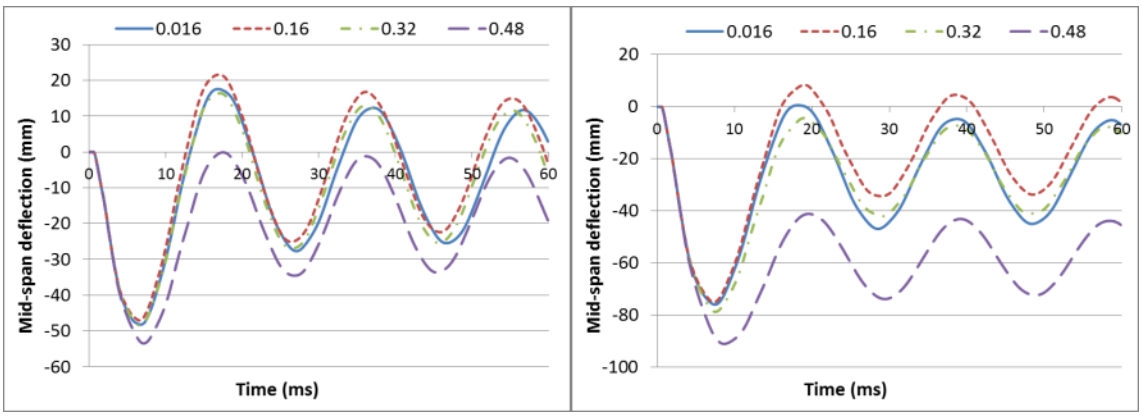

(a) 80 kg TNT (b) 120 kg TNT

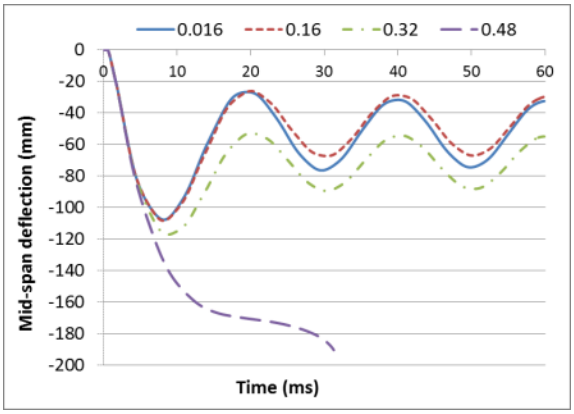

(c) 160 kg TNT

Fig. 20: Displacement-time histories for different axial load ratios

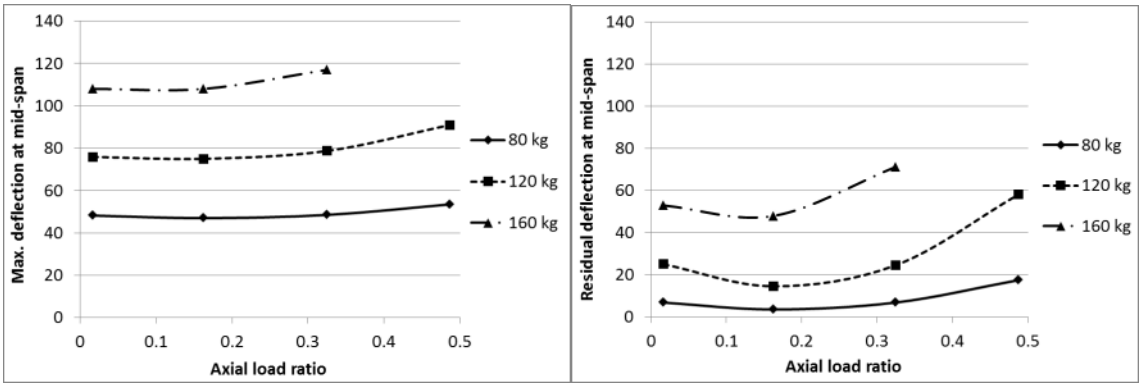

Fig. 21: The maximum and residual deflections for different axial load ratios

5.2 The effect of hollow section ratio

In this section, five hollow section ratios ($\chi = \frac{W_i}{W_o - 2t_{so}}$) were examined as shown in Figs. 22 and 23. It was concluded that the enlargement of inner width did not demonstrate a significant change in the behaviours of CFDST specimens until the hollow section ratio reached 0.5. From this point onward, the deflection started to increase notably along with a

shortening in the period of oscillation. The results also indicated that, CFDST specimens can achieve equal blast resistance, however with much less self-weight, when compared to CFST specimens (i.e. when $\chi = 0$).

Table 5: Characteristics for specimens used for parametric study

Group	Specimen	Dimensions				Axial load ratio	Charge weight (kg)	Concrete strength	
		Wo (mm)	to (mm)	Wi (mm)	ti (mm)			f'c (MPa)	f't (MPa)
1 (axial load ratio)	AR1	210	5	100	5	0.016	80	170	18
	AR2	210	5	100	5	0.162	80	170	18
	AR3	210	5	100	5	0.325	80	170	18
	AR4	210	5	100	5	0.487	80	170	18
	AR5	210	5	100	5	0.016	120	170	18
	AR6	210	5	100	5	0.162	120	170	18
	AR7	210	5	100	5	0.325	120	170	18
	AR8	210	5	100	5	0.487	120	170	18
	AR9	210	5	100	5	0.016	160	170	18
	AR10	210	5	100	5	0.162	160	170	18
	AR11	210	5	100	5	0.325	160	170	18
	AR12	210	5	100	5	0.487	160	170	18
2 (hollow section ratio)	HR1	210	5	-	-	0.325	120	170	18
	HR2	210	5	40	5	0.325	120	170	18
	HR3	210	5	80	5	0.325	120	170	18
	HR4	210	5	100	5	0.325	120	170	18
	HR5	210	5	120	5	0.325	120	170	18
3 (concrete strength)	CS1	210	5	100	5	0.325	120	30	2.9
	CS2	210	5	100	5	0.325	120	45	3.8
	CS3	210	5	100	5	0.325	120	60	4.6
	CS4	210	5	100	5	0.325	120	170	18
4 (inner tube thickness)	IT1	210	5	100	3	0.325	120	170	18
	IT2	210	5	100	4	0.325	120	170	18
	IT3	210	5	100	5	0.325	120	170	18
	IT4	210	5	100	6	0.325	120	170	18
5 (outer tube thickness)	OT1	210	3	100	5	0.325	120	170	18
	OT2	210	4	100	5	0.325	120	170	18
	OT3	210	5	100	5	0.325	120	170	18
	OT4	210	6	100	5	0.325	120	170	18
6 (cross section geometry)	CHS+CHS	210	5	100	5	0.325	120	170	18
	CHS+SHS	210	5	100	5	0.325	120	170	18
	SHS+CHS	210	5	100	5	0.325	120	170	18
	SHS+SHS	210	5	100	5	0.325	120	170	18

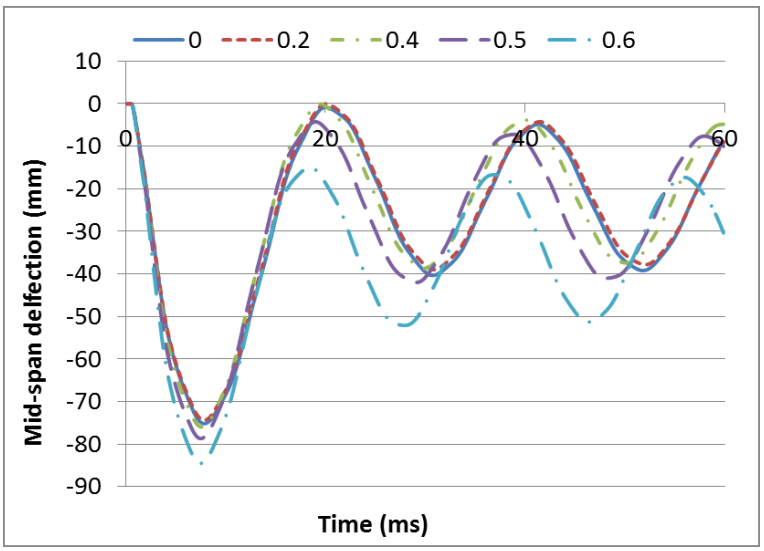

Fig. 22: Displacement-time histories for different hollow section ratios

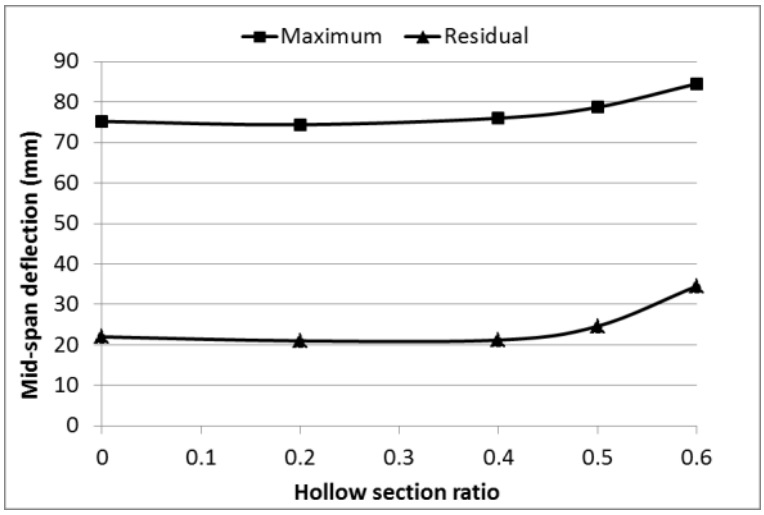

Fig. 23: The maximum and residual deflections for different hollow section ratios

5.3 The effect of concrete strength

Figs. 24 and 25 demonstrated the differences between CFDST specimens filled with UHPC and those filled with normal strength concrete. It can be concluded that, when only using normal strength concrete, the compressive strength of concrete did not have a significant impact on the structural behaviour. However, when UHPC was introduced into the comparison, a remarkable reduction in the residual deflection (up to 62.8%) was achieved whereas the decrement of the maximum deflection was much smaller in percentage (up to 12.8%). The reason for this is because: 1) the tensile strength of the concrete filler was very small compared to that of the steel tubes, therefore the steel tubes,

which were all of the same strength herein, provided a vital contribution in resisting the flexural loads whilst the concrete filler mainly contributed to the axial load capacity. As a result, there was little difference in the maximum deflection although UHPC was much stronger in strength than the normal strength concrete. 2) As for residual deflection, it can be seen in Fig. 26 that the CFDST specimen with normal strength concrete filler exhibited clear signs of steel buckling near the end slabs whereas none was observed on the specimen with UHPC filler. Therefore, the CFDST specimen with UHPC filler experienced less plastic deformation than that with normal concrete filler.

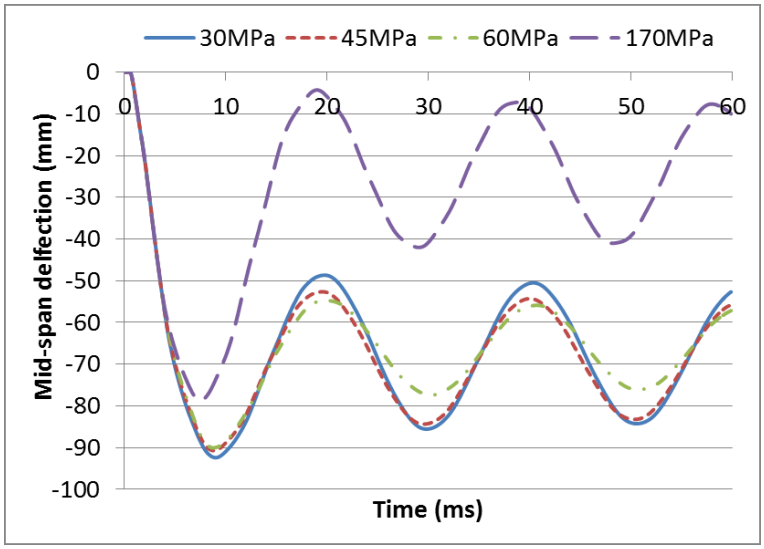

Fig. 24: Displacement-time histories for different concrete strengths

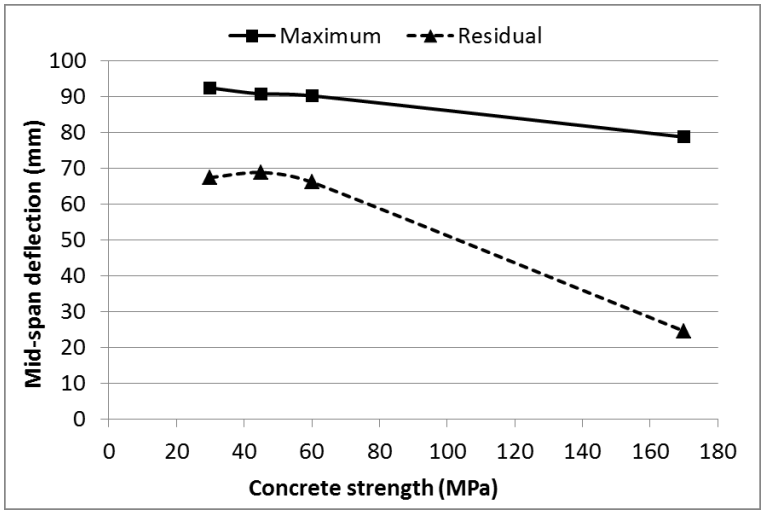

Fig. 25: Maximum and residual deflections for different concrete strengths

(a) Deformed shape of CFDST specimen with normal strength concrete filler

(b) Deformed shape of CFDST specimen with UHPC filler

Fig. 26: Failure mode of the CFDST specimens

5.4 The effect of inner & outer tube thickness

It can be seen in Figs. 27 and 28 that the increment in the thickness of the inner and outer steel tubes benefited the flexural load capacity, therefore resulting in smaller mid-span deflections. Both the maximum and residual mid-span deflections exhibited linear relationships with steel tube thickness. Nevertheless, the increase in the outer steel tube thickness resulted in a more significant reduction in the mid-span deflection than that in the inner steel tube thickness.

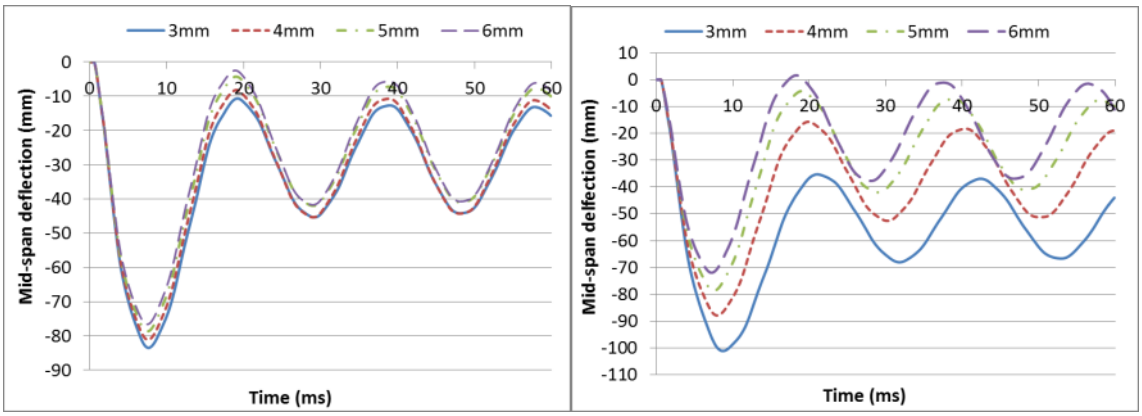

(a) inner steel tube (b) outer steel tube

Fig. 27: Displacement-time histories for different steel tube thickness

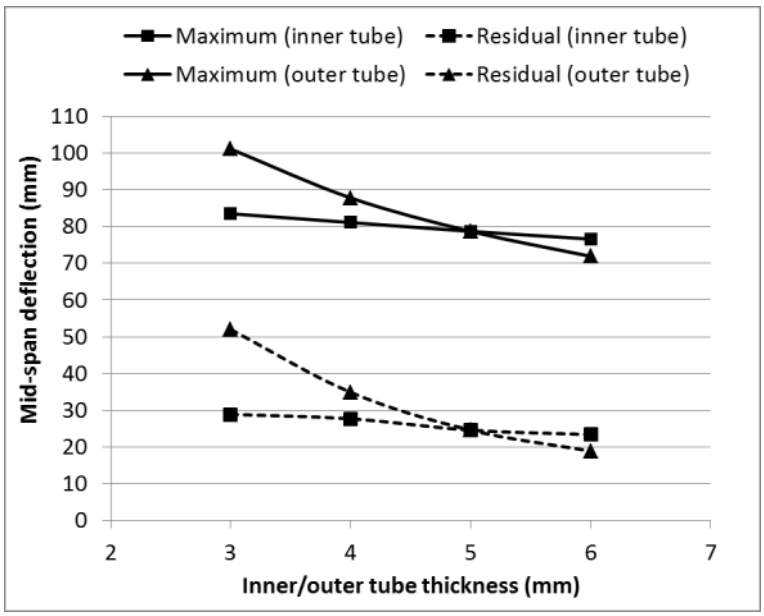

Fig. 28: Maximum and residual deflections for different steel tube thickness

5.5 The effect of cross-section geometry

In this section, four different cross-section combinations were examined. It is evident from Figs. 29 and 30 that the behaviours of CFDST specimens under blast loading were mainly dominated by the shape of the outer steel tube whereas the inner steel tube geometry did not have a significant impact.

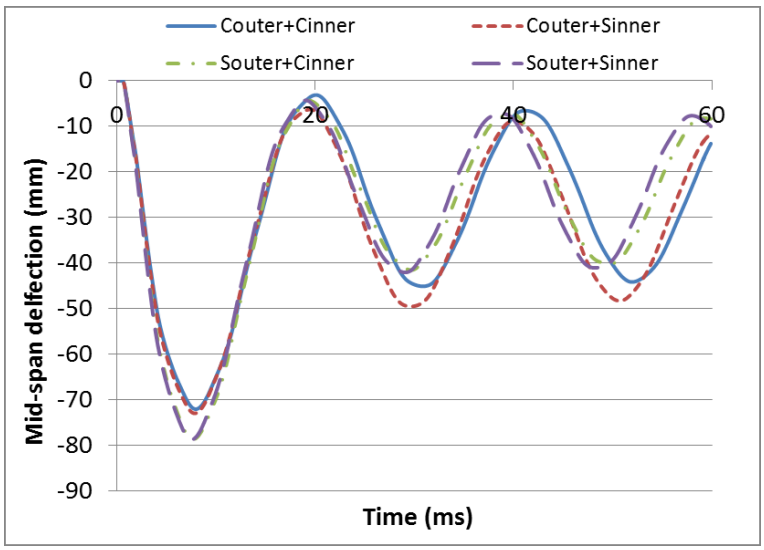

Fig. 29: Displacement-time histories for different cross section combinations

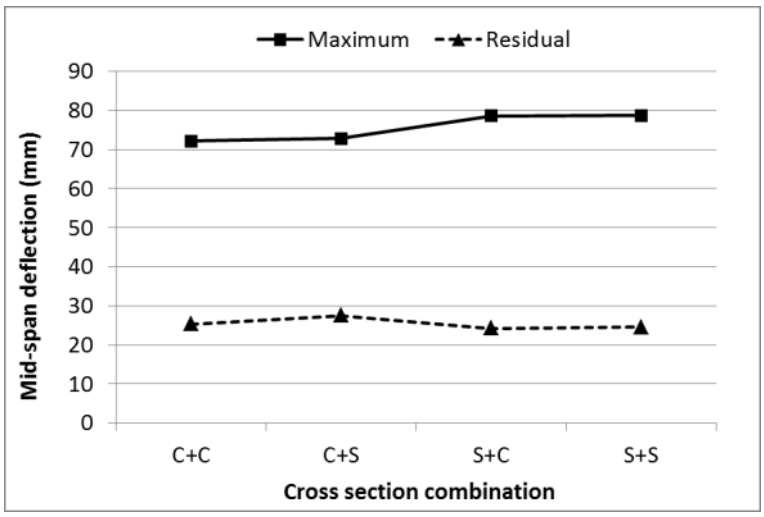

Fig. 30: The maximum and residual deflections for different cross section combinations

6. Conclusions

This paper has presented an experimental as well as a numerical study on the behaviours of concrete-filled double-skin steel tube columns under blast loading.

The experimental results indicated that the proposed CFDST columns can withstand severe blast load without failure, whilst no signs of steel buckling or concrete crushing were found on the test specimens after the tests. The increase in explosive charge weight caused a larger mid-span deflection, with this effect being more noticeable on axial-load-free specimens rather than axially-loaded specimens. The presence of an axial compressive load, corresponding to 25% of the squash load, led to a slight reduction in the maximum mid-span deflection in two comparative cases.

The numerical model of the proposed CFDST column was carefully calibrated by a series of laboratory test and when validated against the blast tests, good agreement was achieved. A number of parametric studies were then carried out numerically to further investigate the behaviours of the CFDST column under blast loading. The following conclusions can be drawn based on the results obtained from this paper:

1. Within a certain limit, the increase in the axial load ratio can slightly reduce the mid-span deflection. However, if it increases beyond the limit, a significant increase in the mid-span deflection or even structural instability can be caused.

2. For hollow section ratio up to 0.5, there were no notable differences in the behaviours of the CFDST specimens. Nevertheless, for hollow section ratio greater than 0.5, a significant increase in the deflection was observed along with a notable change in the period of oscillation.

3. Compared to normal strength concrete filler, the use of UHPC filler in the CFDST specimen remarkably reduced the residual deflection whereas the reduction in the maximum deflection was much less in percentage.

4. The increment in the inner and outer steel tube thickness both resulted in smaller mid-span deflections, however, with this effect being more noticeable on outer steel tube than inner.

5. The behaviours of CFDST specimens under blast loading were mainly dominated by the shape of the outer steel tube whereas the inner steel tube geometry did not have a notable impact

Acknowledgements

The financial support of the Australian research Council under ARC Discovery Project DP160104661, the Key Project of Tianjin Municipal Science and Technology Support Program 14ZCZDSF00016, and the National Basic Research Programme 2015CB058002 is gratefully acknowledged.

References

[1] Wei, S, Mau, S, Vipulanandan, C, and Mantrala, S, *Performance of New Sandwich Tube under Axial Loading: Experiment.* Journal of Structural Engineering, 1995. **121**(12): p. 1806-1814.

[2] Zhao, X-L, Tong, L-W, and Wang, X-Y, *CFDST stub columns subjected to large deformation axial loading.* Engineering Structures, 2010. **32**(3): p. 692-703.

[3] Huang, H, Han, L-H, Tao, Z, and Zhao, X-L, *Analytical behaviour of concrete-filled double skin steel tubular (CFDST) stub columns.* Journal of Constructional Steel Research, 2010. **66**(4): p. 542-555.

[4] Han, LH, Tao, Z, Huang, H, and Zhao, XL, *Concrete-filled double skin (SHS outer and CHS inner) steel tubular beam-columns.* Thin-Walled Structures, 2004. **42**: p. 1329-1355.

[5] Han, L-H, Huang, H, Tao, Z, and Zhao, X-L, *Concrete-filled Double Skin Steel Tubular (CFDST) Beam–columns Subjected to Cyclic Bending.* Engineering Structures, 2006. **28**(12): p. 1698-1714.

[6] Han, L-H, Huang, H, and Zhao, X-L, *Analytical behaviour of concrete-filled double skin steel tubular (CFDST) beam-columns under cyclic loading.* Thin-Walled Structures, 2009. **47**(6): p. 668-680.

[7] Li, W, Han, L-H, and Chan, T-M, *Tensile behaviour of concrete-filled double-skin steel tubular members.* Journal of Constructional Steel Research, 2014. **99**: p. 35-46.

[8] Huang, H, Han, L-H, and Zhao, X-L, *Investigation on concrete filled double skin steel tubes (CFDSTs) under pure torsion.* Journal of Constructional Steel Research, 2013. **90**: p. 221-234.

[9] Lu, H, Zhao, X-L, and Han, L-H, *Testing of self-consolidating concrete-filled double skin tubular stub columns exposed to fire.* Journal of Constructional Steel Research, 2010. **66**(8): p. 1069-1080.

[10] Bambach, M, Jama, H, Zhao, X, and Grzebieta, R, *Hollow and concrete filled steel hollow sections under transverse impact loads.* Engineering Structures, 2008. **30**(10): p. 2859-2870.

[11] Yousuf, M, Uy, B, Tao, Z, Remennikov, A, and Liew, J, *Transverse impact resistance of hollow and concrete filled stainless steel columns.* Journal of Constructional Steel Research, 2013. **82**: p. 177-189.

[12] Ngo, T, Mohotti, D, Remennikov, A, and Uy, B, *Numerical simulations of response of tubular steel beams to close-range explosions.* Journal of Constructional Steel Research, 2015. **105**: p. 151-163.

[13] Zhang, H, Li, Z, and Wu, C, *Investigation of Blast Effects on Double-Skinned Composite Steel Tubular Columns.* International Journal of Protective Structures, 2015. **6**(3): p. 403-418.

[14] Wu, C, Oehlers, DJ, Rebentrost, M, Leach, J, and Whittaker, AS, *Blast Testing of Ultra-High Performance Fibre and FRP-Retrofitted Concrete Slabs.* Engineering Structures, 2009. **31**(9): p. 2060-2069.

[15] Li, J, Wu, C, and Hao, H, *Investigation of ultra-high performance concrete slab and normal strength concrete slab under contact explosion.* Engineering Structures, 2015. **102**: p. 395-408.

[16] Yi, N-H, Kim, J-HJ, Han, T-S, Cho, Y-G, and Lee, JH, *Blast-resistant characteristics of ultra-high strength concrete and reactive powder concrete.* Construction and Building Materials, 2012. **28**(1): p. 694-707.

[17] Aoude, H, Dagenais, FP, Burrell, RP, and Saatcioglu, M, *Behavior of ultra-high performance fiber reinforced concrete columns under blast loading.* International Journal of Impact Engineering, 2015. **80**: p. 185-202.

[18] Xu, J, Wu, C, Xiang, H, Su, Y, Li, Z-X, Fang, Q, Hao, H, Liu, Z, Zhang, Y, and Li, J, *Behaviour of ultra high performance fibre reinforced concrete columns subjected to blast loading.* Engineering Structures, 2016. **118**: p. 97-107.

[19] Zhang, F, Wu, C, Zhao, X-L, Xiang, H, Li, Z-X, Fang, Q, Liu, Z, Zhang, Y,

Heidarpour, A, and Packer, JA, *Experimental study of CFDST columns infilled with UHPC under close-range blast loading.* International Journal of Impact Engineering, 2016.

[20] Simoens, B, Lefebvre, MH, and Minami, F, *Influence of Different Parameters on the TNT-Equivalent.* Central European Journal of Energetic Materials, 2011. **8**(1): p. 53-67.

[21] Kingery, CN and Bulmash, G, *Air blast parameters from TNT spherical air burst and hemispherical surface burst*. 1984: Ballistic Research Laboratories.

[22] Hyde, D, *ConWep, conventional weapons effects program.* US Army Engineer Waterways Experiment Station, USA, 1991.

[23] Hallquist, JO, *LS-DYNA Keyword User's Manual.* Livermore Software Technology Corporation, 2007.

[24] Wu, Y, Crawford, JE, Lan, S, and Magallanes, JM, *Validation Studies for Concrete Constitutive Models with Blast Test Data*, in *13th International LS-DYNA Users Conference*2013: Detroit.

[25] Wu, Y, Crawford, JE, and Magallanes, JM. *Performance of LS-DYNA concrete constitutive models*. in *12th International LS-DYNA Users Conference*. 2012.

[26] Crawford, J, Wu, Y, Magallanes, J, and Lan, S, *Use and Validation of the Release II K&C Concrete Material Model in LS-DYNA.* Karagozian & Case, Glendale, 2012.

[27] Shi, Y, Hao, H, and Li, Z-X, *Numerical Derivation of Pressure–Impulse Diagrams for Prediction of RC Column Damage to Blast Loads.* International Journal of Impact Engineering, 2008. **35**(11): p. 1213-1227.

[28] Zhang, F, Wu, C, Zhao, X-L, Li, Z-X, Heidarpour, A, and Wang, H, *Numerical Modeling of Concrete-Filled Double-Skin Steel Square Tubular Columns under Blast Loading.* Journal of Performance of Constructed Facilities, 2015.

[29] Zhang, F, Wu, C, Wang, H, and Zhou, Y, *Numerical simulation of concrete filled steel tube columns against BLAST loads.* Thin-Walled Structures, 2015. **92**: p. 82-92.

[30] Mao, L, Barnett, S, Begg, D, Schleyer, G, and Wight, G, *Numerical simulation of ultra high performance fibre reinforced concrete panel subjected to blast loading.* International Journal of Impact Engineering, 2014. **64**: p. 91-100.

[31] Béton, CE-Id, *CEB-FIP model code 1990: design code*. 1993: Telford.

[32] Malvar, LJ and Crawford, JE, *Dynamic Increase Factors for Concrete*, 1998, DTIC Document.

[33] Ngo, T, Mendis, P, and Krauthammer, T, *Behavior of ultrahigh-strength prestressed concrete panels subjected to blast loading.* Journal of Structural Engineering, 2007. **133**(11): p. 1582-1590.

[34] Su, Y, Li, J, Wu, C, Wu, P, and Li, Z-X, *Effects of steel fibres on dynamic strength of UHPC.* Construction and Building Materials, 2016. **114**: p. 708-718.

[35] Jones, N, *Structural impact*. 2011: Cambridge university press.

[36] Wang, R, Han, L-H, and Hou, C-C, *Behavior of concrete filled steel tubular (CFST) members under lateral impact: Experiment and FEA model.* Journal of Constructional Steel Research, 2013. **80**: p. 188-201.

[37] Zhao, X-L, Han, L-H, and Lu, H, *Concrete-filled tubular members and connections*. 2010: Spon Press London.

[38] Bao, X and Li, B, *Residual Strength of Blast Damaged Reinforced Concrete Columns.* International Journal of Impact Engineering, 2010. **37**(3): p. 295-308.

Chapter 3 – Numerical Derivation of Pressure-Impulse Diagrams

Introduction

The third chapter only contains one paper which is entitled "Numerical derivation of pressure-impulse diagrams for square UHPCFDST columns". It presents a numerical approach, which is based on the proposed numerical model discussed in chapter 2, to generate pressure-impulse diagrams for UHPCFDST columns with different dimensions. Extensive parametric studies are undertaken by using the numerical model described in the third paper. Based on the results, analytical formulae, as functions of column dimension and material properties, are developed through regression analysis which can be easily and quickly used to construct pressure-impulse diagrams for UHPCFDST columns.

Statement of Authorship

Title of Paper	Numerical derivation of pressure-impulse diagrams for square UHPCFDST columns
Publication Status	☐ Published ☐ Accepted for Publication ☑ Submitted for Publication ☐ Unpublished and Unsubmitted w ork w ritten in manuscript style
Publication Details	

Principal Author

Name of Principal Author (Candidate)	Fangrui Zhang		
Contribution to the Paper	The author developed numerical model, undertook data analysis and prepared manuscript.		
Overall percentage (%)	70%		
Certification:	This paper reports on original research I conducted during the period of my Higher Degree by Research candidature and is not subject to any obligations or contractual agreements with a third party that would constrain its inclusion in this thesis. I am the primary author of this paper.		
Signature		Date	

Co-Author Contributions

By signing the Statement of Authorship, each author certifies that:

i. the candidate's stated contribution to the publication is accurate (as detailed above);

ii. permission is granted for the candidate in include the publication in the thesis; and

iii. the sum of all co-author contributions is equal to 100% less the candidate's stated contribution.

Name of Co-Author	Chengqing Wu		
Contribution to the Paper	This co-author supervised research, provided critical manuscript evaluation and acted as corresponding author.		
Signature		Date	6/6/2016

Name of Co-Author	Xiao-Ling Zhao		
Contribution to the Paper	This co-author provided critical manuscript evaluation		
Signature		Date	05/06/16

Name of Co-Author	Zhong-Xian Li		
Contribution to the Paper	This co-author provided manuscript evaluation		
Signature		Date	2016.6.6

NUMERICAL DERIVATION OF PRESSURE-IMPULSE DIAGRAMS FOR SQUARE UHPCFDST COLUMNS

Fangrui Zhang, Chengqing Wu, Xiao-Ling Zhao Zhong-Xian Li

ABSTRACT

Terrorist activities, especially bomb attacks, have become more and more frequent in the past decades which put thousands of innocent lives in danger. The most common failure mode of structures subjected to blast loading is progressive collapse which is mainly resulted from the failure of load bearing columns. In this paper, finite element analysis tool, LS-DYNA is utilized to study the behaviours of ultra-high performance concrete filled double-skin steel tube (UHPCFDST) columns under blast loading. The numerical model is firstly validated against a series of laboratory and field tests and then used to derive pressure-impulse diagrams for UHPCFDST columns in terms of their residual axial load-carrying capacity after being subjected to blast loading. Different parameters are studied to investigate the effects of axial load ratio, steel tube thickness, column dimension and concrete strength on the pressure-impulse diagrams.

Keywords: CFDST; UHPC; blast loading; pressure-impulse diagram.

1. Introduction

Concrete filled double skin tubular (CFDST) columns have the potential to be widely used in the construction industry owing to properties such as high strength and excellent ductility.

A large number of experimental studies have been carried out to investigate the behaviours of CFDST columns under a variety of loading conditions, including: axial compressive loading [1-3], cyclic lateral loading [4], tensile loading [5], pure torsion [6]

and fire [7]. Their results indicate that CFDST columns are able to provide robust performance under multi-hazardous environment.

Recently, the authors have carried out a series of laboratory and field blast tests on ultra-high performance concrete filled double-skin steel tube (UHPCFDST) columns [8, 9]. In comparison to normal strength concrete, UHPC is known for its superior strength which can reach up to 200 MPa in compression and 40 MPa in tension, resulting in a significantly smaller cross-sectional area for the same axial load-carrying capacity. Due to the inclusion of steel fibres, the formation of large cracks can be effectively delayed, leading to an outstanding ductility and energy absorbing capacity so as to make it an ideal material for blast resistant structural components. Recent blast experiments indicated that steel-fibre reinforced UHPC slabs and columns are able to withstand severe blast loading without catastrophic failure [10-13].

In this paper, the pressure-impulse diagram is introduced to develop a systematic method of assessing structural damage in UHPCFDST columns after being subjected to blast loading. A pressure-impulse (P-I) diagram represents a group of loading histories (e.g. blast load) that cause the same level of damage to a structural component. It is widely used as the basis to assess the damage in a structural component or even the blast-induced human injury [14, 15].

Fig. 1 depicts a typical pressure-impulse diagram. In terms of loading types, a Pressure-impulse diagram can be categorised into three zones: 1) the impulsive loading zone where loads are large in magnitude but with very short duration; 2) the quasi-static loading zone where loads are small in magnitude but with very long duration; 3) the dynamic loading zone which lies in between the impulsive and quasi-static loading zone. The impulsive zone and the quasi-static zone are differentiated by two vertical asymptotes, namely, the pressure asymptote and the impulse asymptote. In addition, in terms of damage

levels, a pressure-impulse diagram can be divided into two zones, namely the safe zone (i.e. to the left and below the curve) and the damage zone (i.e. to the right and above the curve).

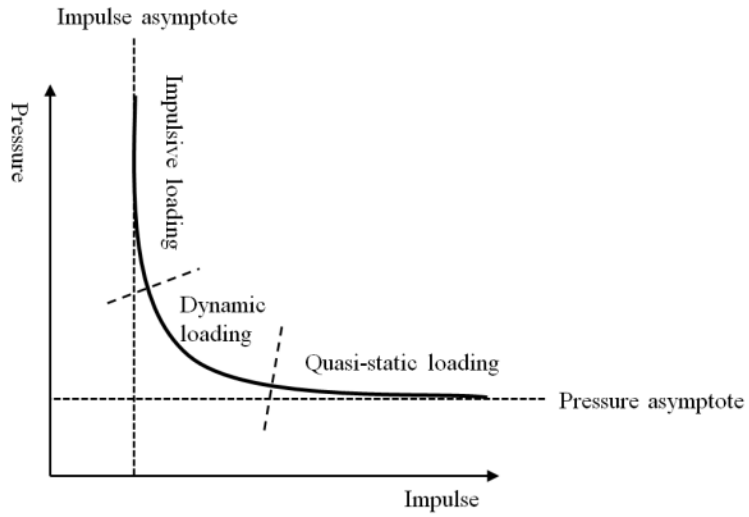

Fig. 1: A typical pressure-impulse diagram

There are a number of methods to obtain the Pressure-impulse diagram for a particular structural component, both analytically and numerically. Fallah and Louca [16] proposed a SDOF model based on a bi-linear resistance-deflection function which can be used to derive Pressure-impulse diagrams. This method provides an easy means to assess the structural damage under blast loading; however, it cannot incorporate strain rate effect therefore is likely to underestimate damage under impulsive loading, and is incapable of considering different failure modes – its damage criterion is either based on the maximum column deflection or end rotation. Most analytical analysis are limited to simple structural types and loading conditions, therefore numerical approaches are required when more complex problems are involved.

This paper presents a numerical method to evaluate the damage caused by blast loading in a UHPCFDST column. High-fidelity physics based finite element tool, LS-DYNA, is utilized in the current study to numerically simulate the dynamic response of UHPCFDST columns subjected to blast loads. LS-DYNA is widely adopted within the engineering society as a more efficient and economical alternative to field experiments. There are a large number of open literatures with regards to using LS-DYNA to study

structural columns [17-23]. The results indicate that, with a properly calibrated model, LS-DYNA is able to accurately predict the structural response of a column under blast loading.

2. Numerical Modelling

In this paper, the commercial software package LS-DYNA was used to investigate the behaviours of UHPCFDST columns under blast loading [24]. In the numerical model, both steel tubes and concrete filler were modelled by hexahedral solid elements with single point integration algorithm.

2.1 Concrete constitutive model

Various concrete constitutive models in LS-DYNA can be used to model concrete structures under dynamic loading, including material type 72 (K&C concrete), material type 84(Winfrith Concrete), material type 111 (JHC) and material type 159 (CSCM) [25, 26]. Among those different material models, the K&C model is most widely used nowadays to investigate the dynamic behaviours of concrete structures under complex loading conditions, including situations involving active/passive confining stress and/or high strain rate impact [18, 27].

The K&C concrete model is a plasticity-based model which uses three shear failure surfaces, includes damage and strain-rate effect. This model allows automatic generation of material properties based on a single user-input which is the unconfined compressive strength of concrete. The mechanism behind this constitutive model along with the material inputs have been introduced by Crawford [27], thus are not discussed in great detail herein. It should be mentioned that the K&C model, or any other concrete material models in LS-DYNA for this matter, was primarily developed based on test results of normal strength concrete only. Therefore any attempts to extend the use of its default material properties to

UHPC should be dealt with great caution since the significant differences in the structural behaviours of normal strength concrete and UHPC cannot be accounted for just by changing the maximum compressive or tensile strength.

It is well known that under high strain rate impact, the concrete strength can be enhanced significantly and the dynamic increase factor (DIF) for normal strength concrete under both compression and tension can be calculated by CEB Code [28, 29]. However, this formula is only applicable for concrete strength up to 60 MPa thus is not suitable for UHPC. Ngo et al. [30] studied the DIF for UHPC with compressive strength up to 160 MPa, it was reported that the strain rate effect on UHPC was notably smaller than CEB Code predictions. In this paper, the dynamic properties of UHPC were derived through Hopkinson's pressure bar test and the results are depicted in Fig. 2 [31]. It is evident that in comparison to normal strength concrete [28], the strain rate effect on UHPC is not noticeable until the strain rate reached 200/s for tension and 50/s for compression.

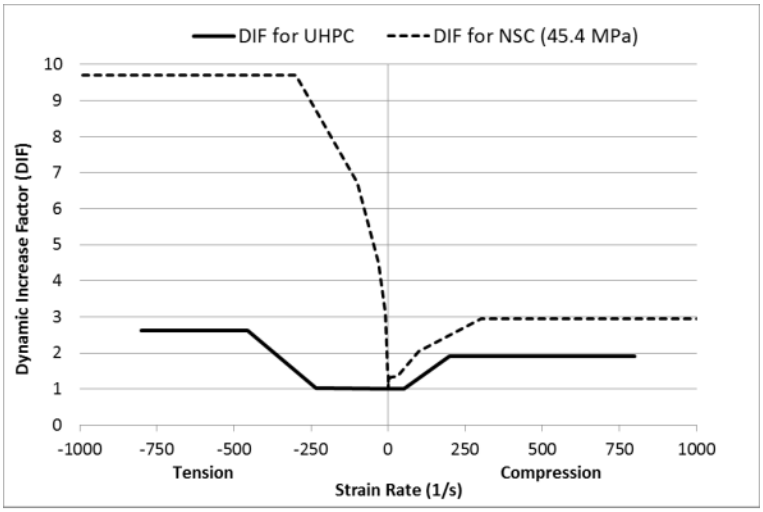

Fig. 2: DIF for UHPC & normal strength concrete

In the current research, the authors firstly used the automatically-generated default material properties as a basis and then calibrated & validated the material model by a number of test results. These key material parameters include: f_t, which is the uniaxial tensile strength; B1, which governs the compressive damage and softening behaviour; B2 and w_{lz}, which govern the fracture energy of each element; ω, which governs the volume

expansion; λ and η, which govern the damage function and scale factor respectively. Table 1 and Fig. 3 summarise the key material inputs.

Table 1: Key parameters for K&C concrete model

Model parameter	Value
f_c'	170 MPa
f_t	18 MPa
Poisson's ratio	0.19
B1	0.8
B2	1.35
w_{lz}	6.00 mm
ω	0.10

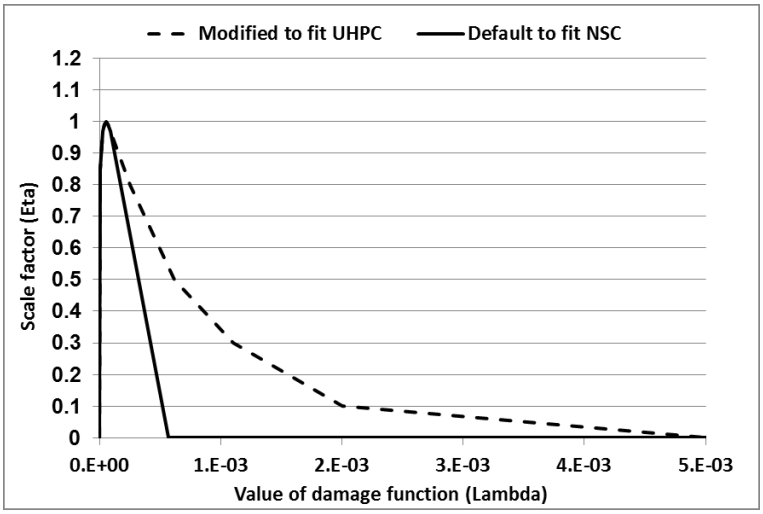

Fig. 3: λ and η for UHPC and normal strength concrete

2.2 Steel constitutive model

Material model 24, namely PIECEWISE LINEAR PLASTICITY model, was used to represent the steel tubes in this paper. The user can either assume an elastic-perfectly-plastic stress-strain relationship or, if available, use the actual non-linear stress-strain relationship. For validation purpose, the average stress-strain relationship obtained from tensile coupon tests was directly used as material input as shown in Fig. 4. The average yield strength was 346 MPa with an elongation of 22%.

The strain rate effect in this material model was incorporated by the Cowper and Symonds law which multiplies the yield stress by a factor given as:

$$DIF\ of\ steel = 1 + \left(\frac{\dot{\varepsilon}}{C}\right)^{\frac{1}{P}} \quad (1)$$

where $\dot{\varepsilon}$ = strain rate of steel ; C and P are two constants.

In this paper, C = 6488 s^{-1} and P = 3.91 were used according to the dynamic axial crushing test on square tubes carried out by Jones [32].

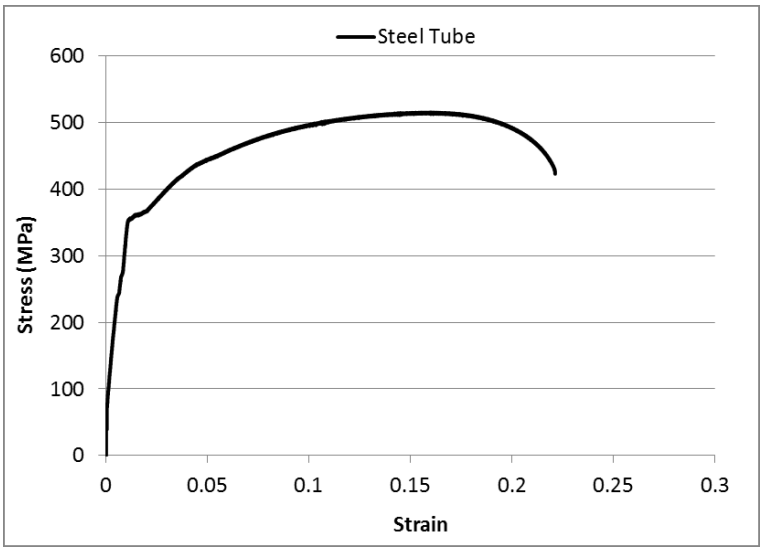

Fig. 4: Stress-strain relationship for the steel tube

2.3 Meshing and boundaries

The UHPCFDST specimen studied herein is shown in Fig. 5. It can be seen from Fig. 5(a) that both ends of the UHPCFDST specimen were fully embedded in concrete slabs and the outer face of both end slabs were restrained against x and z directions so that it can only move along the axial direction. The meshing and element division are shown in Fig. 5(b). The average characteristic size of the concrete element was 7 mm and the mesh size convergence study shows that further refinement of the numerical model has little effect on the results but significantly increases the computational burden.

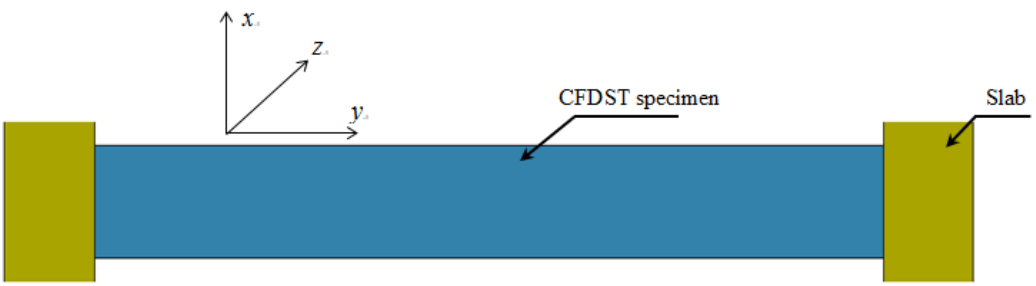

(a)

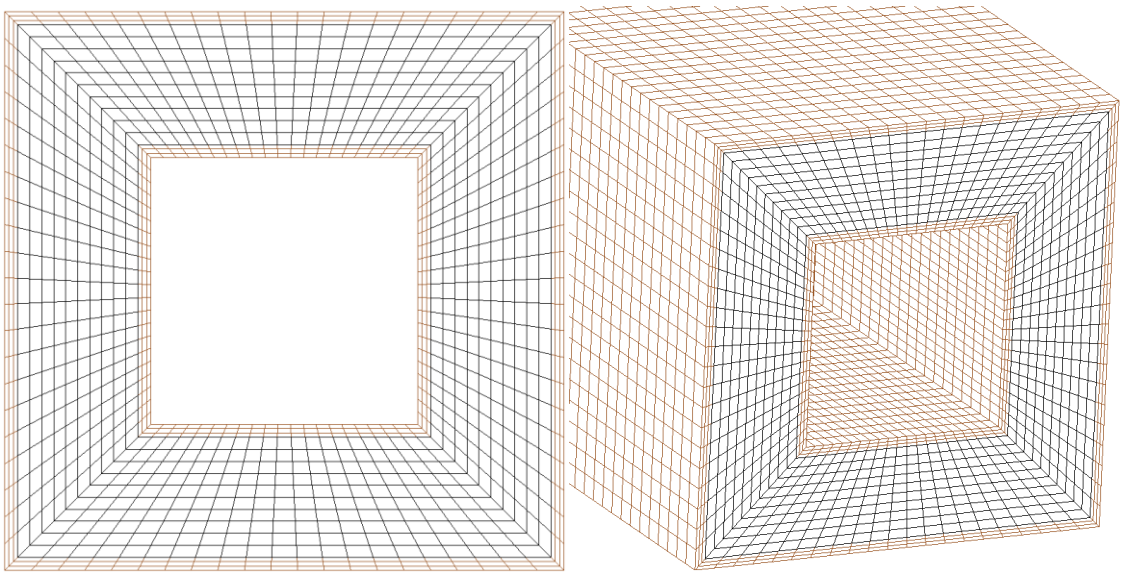

(b)

Fig. 5: Model setup and mesh size

2.4 Application of blast loading

In this paper, the validation of the proposed numerical model against the field blast tests was done by using the CONWEP model in LS-DYNA [33]. As for the parametric studies to obtain the pressure-impulse diagram, the idealised triangular-shape pressure-time history was used to simulate the blast loading in the analysis. In addition, the blast wave was also assumed to be plane wave, therefore the blast load was uniformly distributed on the front face of the UHPCFDST specimen. It should be mentioned that, under circumstances where the explosive is placed in close vicinity of the target structure, this assumption could overestimate the blast load and as a result, i.e., overestimate the column damage.

2.5 Validation of the numerical model

Five tests, including three laboratory tests and two field blast tests, were used to demonstrate the ability of the proposed numerical model to accurately predict the behaviour of UHPCFDST structures. The test setups and results of all tests have been discussed in the authors' previous works, therefore only the validation results are given

hereafter [8, 9]. Fig. 6 shows the validation of the uniaxial compressive test on 100 mm x 100 mm x 100 mm UHPC specimens; Fig. 7 shows the validation of the four point bending test on 100 mm x 100 mm x 400 mm UHPC specimens; Fig. 8 shows the validation of the three point bending test on 2500 mm long square UHPCFDST specimen; Fig. 9 shows the validation results of the blast tests of two square UHPCFDST subjected to 50 kg TNT equivalence at 1.5 meters. The validation results are in good agreement with the test results which shows the ability and fidelity of the proposed numerical model to accurately predict the behaviours of UHPCFDST columns under different loading conditions.

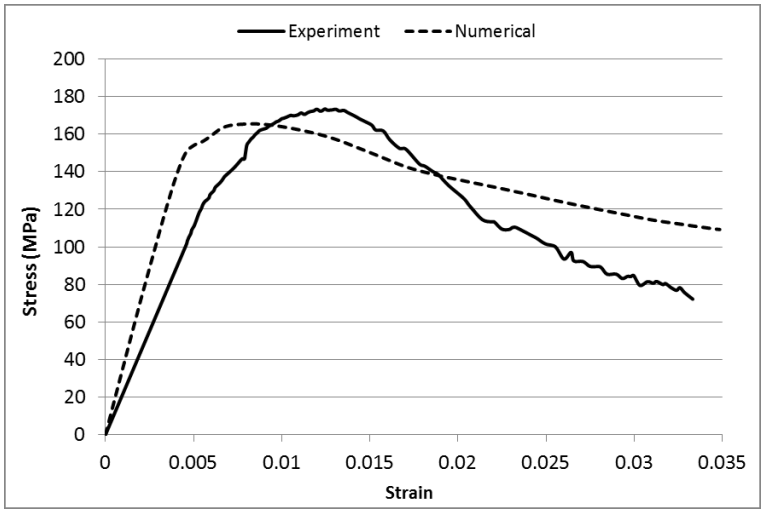

Fig. 6: Validation of the uniaxial compression test on the UHPC specimen

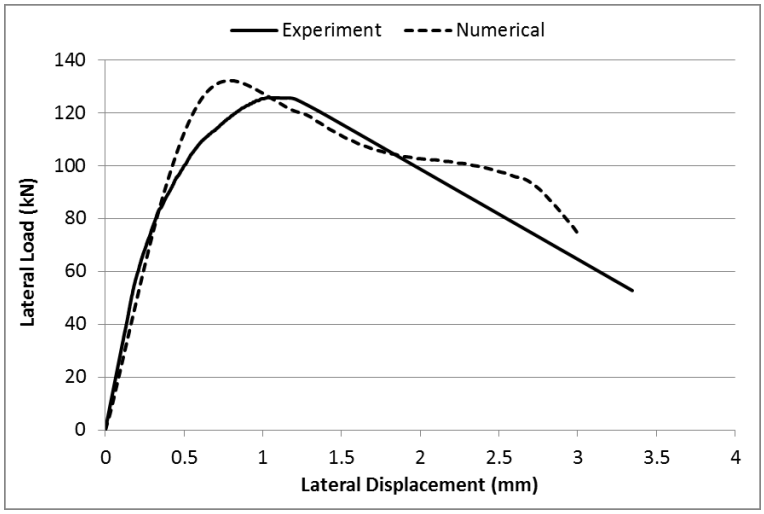

Fig. 7: Validation of the four points bending test on the UHPC specimen

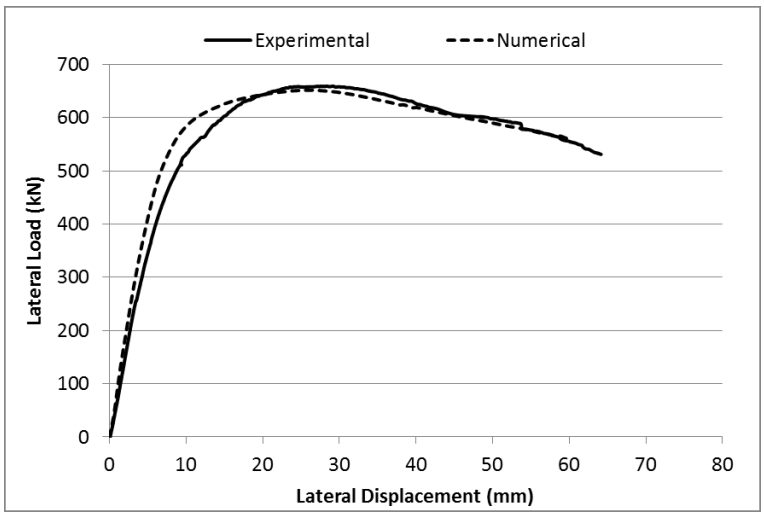

Fig. 8: Validation of the three points bending test on the UHPCFDST specimen

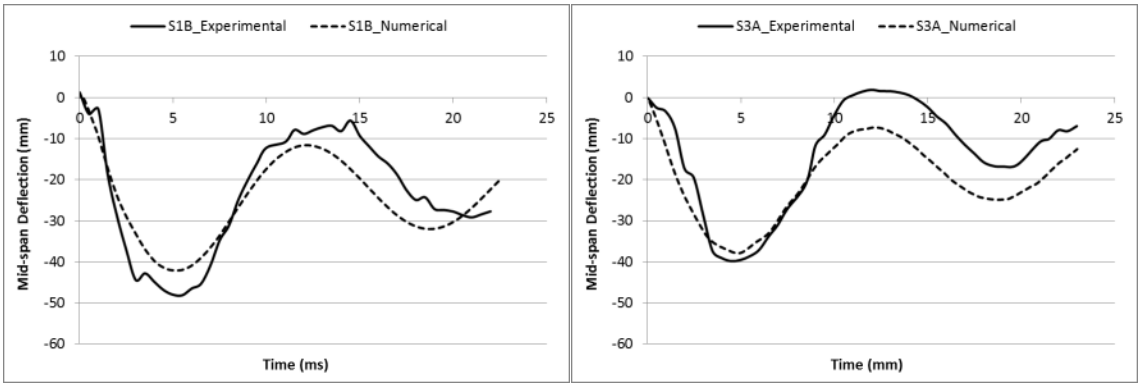

(a) (b)

Fig. 9: Validation of the blast tests on the UHPCFDST specimen

3. Numerical Derivation of Pressure-Impulse Diagram

A pressure-impulse diagram can be numerically generated by having a set of data points that represent the same level of structural damage, however resulted from different pressure and impulse combinations. Although the numerical method can accurately describe the dynamic behaviour of a structure, it is very computationally expensive since it normally requires multiple trials to get one satisfactory point. In this paper, the standard procedure of generating a pressure-impulse diagram is shown in Fig. 10: 1) choose one pressure and impulse value as the starting point; 2) keep the pressure constant and gradually modify the impulse (by increasing/decreasing the loading duration) until the structural damage has reached the pre-determined level; 3) reduce the pressure and re-adjust the impulse value until the structural damage has also reached the damage level

defined in step 2; 4) repeat step 1 – 3 for the rest of the data points until a smooth curve can be drawn.

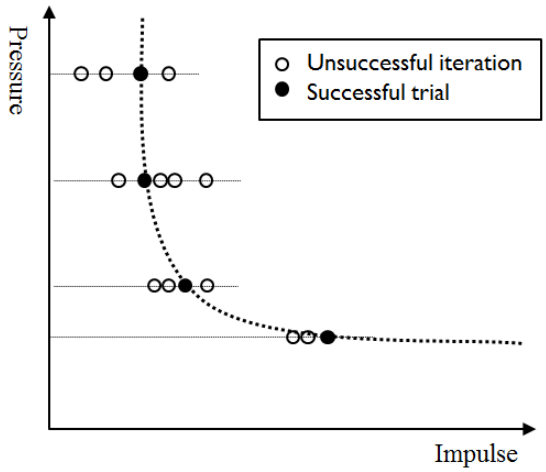

Fig. 10: The method to generate a pressure-impulse diagram

3.1 Damage criterion

There are a number of criteria that are commonly used to quantify the damage accumulated in a column. In the current research, the damage in a UHPCFDST column caused by the blast loading is quantified by the residual axial load-carrying capacity: the more residual axial load-carrying capacity, the less accumulated blast damage and vice versa. Shi [20] firstly introduced this method to evaluate the damage on RC columns, the advantage of this criterion includes: it can be used to evaluate damage accumulated in structural columns from different damage modes; it is straightforward to tell whether a column is severely damaged or not; it is easily obtainable either through numerical simulations or field tests. The damage index D is defined as:

$$D = 1 - \frac{P_{residual}}{P_{design}} \tag{2}$$

where $P_{residual}$ and P_{design} are the axial load-carrying capacity of the damaged and undamaged UHPCFDST columns, respectively. Both values can be obtained numerically by gradually applying axial load to a damaged/undamaged UHPCFDST specimen until collapse.

In the current study, the column is considered failed once its axial load-carrying capacity is halved, in other words when $D = 0.5$, after the explosion. It should be noted that the definition of column failure varies from person to person and case to case. The authors adopted $D = 0.5$ specifically for UHPCFDST columns in this paper based on their engineering judgment and experience which may not be valid for other column types. However, this method should be applicable for assessing most structural columns although the definition of the damage degree at failure varies from column to column.

3.2 Numerical derivation of damage index D

In the numerical simulation, the UHPCFDST column was mainly subjected to two loads, namely the axial load and the transverse blast load. The undamaged axial load-carrying capacity P_{design} was derived straightforwardly by applying a displacement-controlled axial loading until the column fails. However, the residual axial load-carrying capacity, on the other hand, was much more complicated.

The method of obtaining damage index D consists of 4 phases of loading as shown in Fig. 11: 1) The first phase is the pre-loading phase, an axial load, which is roughly 30% of the column axial load-carrying capacity, is applied to the UHPCFDST column to simulate the live load and the self-weight present in the column prior to the explosion. It should be mentioned that the axial load in this phase was applied by using the implicit solver in LS-DYNA to avoid oscillation in the way of wave propagation [27]. This is the ideal method for applying quasi-static load since the stress equilibrium is achieved at the end of every time step. If the explicit solver is used, even if a very long ramping time is set, the sudden introduction of axial load is still highly-likely to cause localised damage near where the axial load is applied; 2) during the second phase, the axial load applied during the first phase is kept constant. The computational algorithm is switched from implicit to explicit right before the blast load is applied in order to allow for the dynamic analysis; 3)

the third phase starts when the free vibration of the column almost stops. The computational algorithm is switched from explicit back to implicit and during which, the velocities of all nodes are set to zero. The axial load applied throughout phase 1 and 2 is slowly unloaded during this phase and the column is kept load-free afterwards; 4) the evaluation of the residual axial load-carrying capacity $P_{residual}$ is carried out in the final phase by gradually applying a displacement-controlled axial loading until failure. $P_{residual}$ and P_{design} can be then used to determine the damage index D of the column.

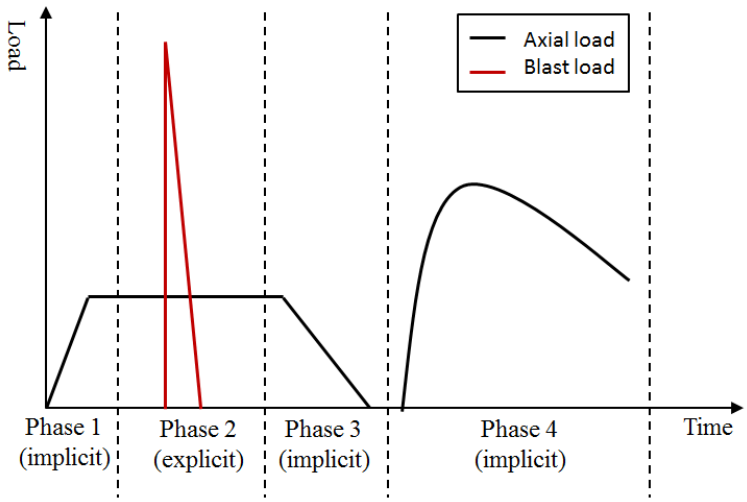

Fig. 11: Loading schematic (not to scale)

4. Parametric Studies and Results

Systematic parametric studies are carried out by using the proposed numerical model to investigate the effect of different parameters on the pressure-impulse diagram of UHPCFDST columns. Analytical formulae for constructing pressure-impulse diagrams for UHPCFDST columns of different configurations are also derived from the results of the parametric study. In total, eight parameters are investigated, namely cross-sectional area, column height, axial load ratio, hollow section ratio, inner and outer tube steel ratio, compressive strength of the concrete and yield strength of the steel tube. Table 2 lists the range of each parameter that is investigated in this paper. For easy analysis purpose, a control column is introduced; all specimens have the same dimensions as the control

specimen during the parametric study unless otherwise specified. The control column is 3500 mm in height, 200 mm in cross section side length with its axial load ratio being 0.3, hollow section ratio being 0.25, inner tube steel ratio being 0.070, outer tube steel ratio being 0.128, compressive strength of the concrete filler being 170 MPa and steel yield strength being 350 MPa.

Table 2: Parameters used in the parametric studies

Side length (mm)	Height (mm)	Axial load ratio	Hollow section ratio	Inner tube steel ratio	Outer tube steel ratio	Concrete strength (MPa)	Steel Strength (MPa)
200*	2500	0.1	0.04	0.041	0.080	140	280
250	3500*	0.2	0.16	0.056	0.105	170*	350*
300	4500	0.3*	0.25*	0.070*	0.128*	200	420
400	5500	0.4	0.36	0.085	0.151	/	525

Note: the superscript * indicates this particular value is used for the control specimen during the parametric study.

4.1 Side length, b

To investigate the effect of cross section side length, the pressure-impulse diagrams of 4 CFDST columns with different cross section side lengths, i.e. 200, 250, 300 and 400 mm, are generated using the numerical method introduced in the previous section. For easy comparison, Table 3 lists the pressure and impulse asymptotes of each pressure-impulse diagram and Fig. 12 shows all the numerical points that are used to derive each pressure-impulse diagram along with the fitted curve. It can be seen that both the pressure and impulse asymptotes are increased significantly with the increase in side length. This is because a larger cross section results in a larger cross-section modulus which increases the flexural and shear resistance of the column.

Table 3: Effect of cross section side length on pressure and impulse asymptotes when D=0.5

Side (mm)	P_0(numerical) (MPa)	P_0(Eq. 5) (MPa)	***Error***	I_0(numerical) (MPa·ms)	I_0(Eq. 6) (MPa·ms)	***Error***
200	1.40	1.37	***-2.0%***	10.80	10.67	***-1.2%***
250	2.20	2.35	***7.0%***	14.30	14.31	***0.0%***
300	3.60	3.66	***1.7%***	19.00	18.16	***-4.4%***
400	7.40	7.35	***-0.6%***	26.00	26.40	***1.5%***

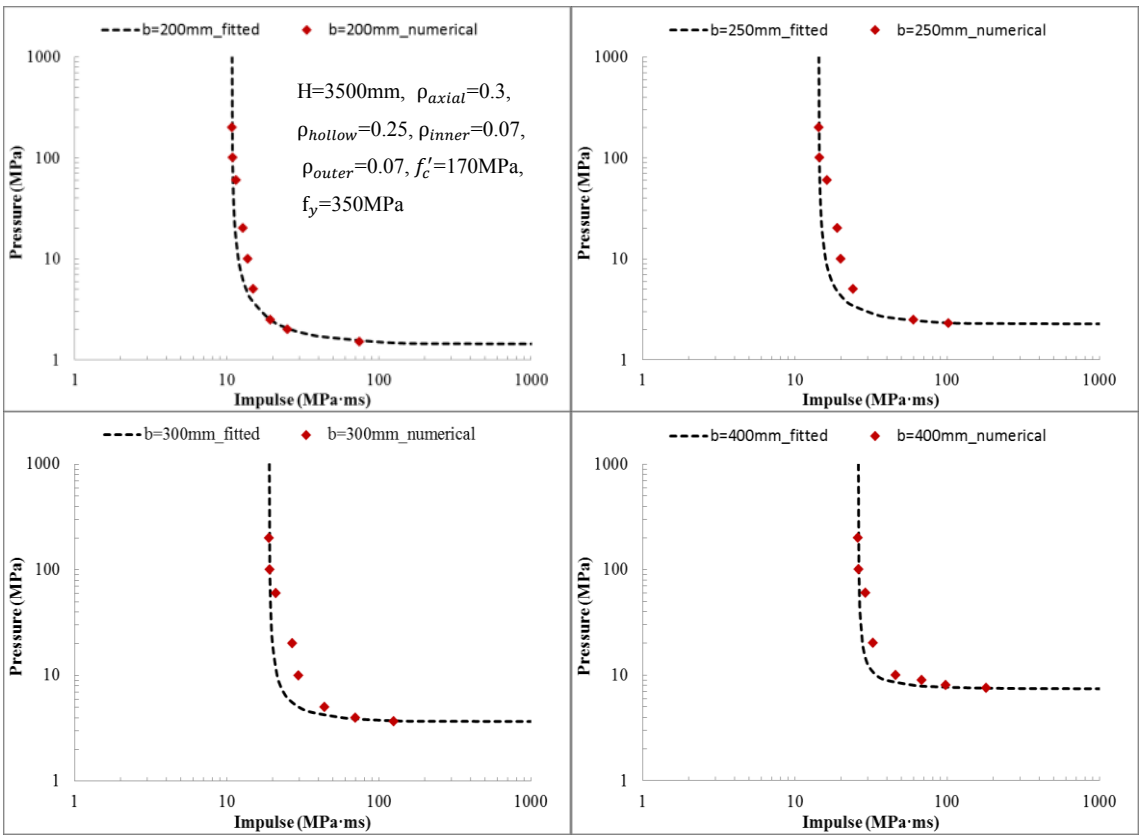

Fig. 12: Numerically derived pressure and impulse data points for different side length

4.2 Column height, H

Four different column heights are studied to investigate the effect on the pressure-impulse diagrams. The numerically derived pressure and impulse asymptotes are summarised in Table 4 and all data points used to derive the pressure-impulse diagrams are depicted in Fig. 13. In general, with all other parameters being constant, the maximum bending moment acting on a longer column is larger than that on a shorter column under the same uniformly distributed load. Therefore, it is evident that a higher CFDST column would result in smaller pressure and impulse asymptotes, with this effect being more notable on pressure asymptote than impulse asymptote

Table 4: Effect of column height on pressure and impulse asymptotes when D=0.5

Height (mm)	P_0(numerical) (MPa)	P_0(Eq. 5) (MPa)	*Error*	I_0(numerical) (MPa·ms)	I_0(Eq. 6) (MPa·ms)	*Error*
2500	3.50	3.49	***-0.4%***	13.60	14.41	***5.9%***
3500	1.40	1.37	***-2.0%***	10.80	10.67	***-1.2%***
4500	0.70	0.68	***-3.0%***	8.25	8.55	***3.6%***
5500	0.40	0.38	***-4.0%***	6.50	7.18	***10.5%***

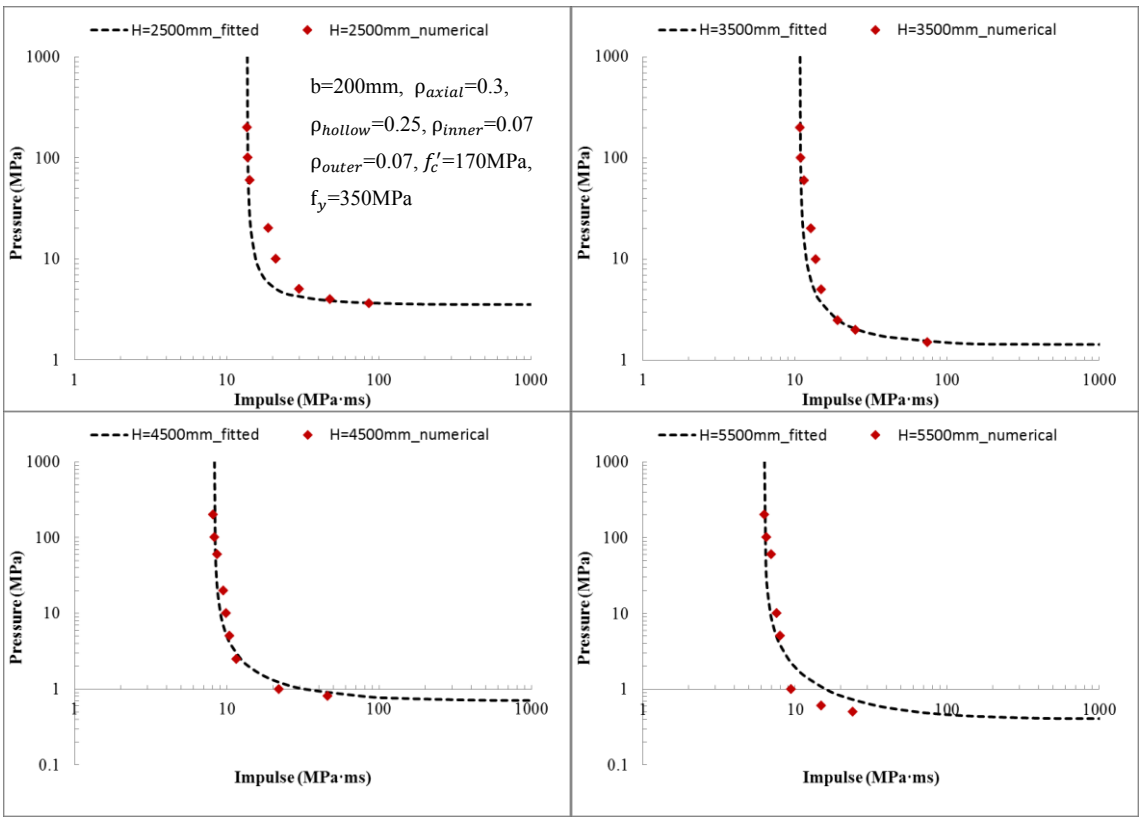

Fig. 13: Numerically derived pressure and impulse data points for different column height

4.3 Axial load ratio, ρ_{axial}

The axial load ratio, ρ_{axial}, is defined as the applied axial load over the design axial load-carrying capacity of the column, $\rho_{axial} = \frac{P_{applied}}{P_{design}}$. In this paper, four different axial load ratios ranging from 0.1 to 0.4 are investigated. From Table 5 and Fig. 14, one can see that the values for the pressure and impulse asymptotes peak at $\rho_{axial} = 0.2$ then gradually decreases as the axial load ratio further increases. This is because when an axial load is applied to a column, it induces two effects: one is the compressive membrane effect which reduces the column deflection and the other one is the P-Δ effect which amplifies the column deflection. In general, when the axial load ratio is small, the compressive membrane effect is more dominant and vice versa [34]. Therefore, for CFDST columns studied in the current research, when ρaxial is less than 0.2, the compressive membrane effect is more dominant than the P-Δ effect; however, once ρ_{axial} goes beyond 0.2, the

P-Δ effect starts to have a larger impact, the pressure and impulse asymptotes therefore become smaller.

Table 5: Effect of axial load ratio on pressure and impulse asymptotes when D=0.5

ρ_{axial}	P_0(numerical) (MPa)	P_0(Eq. 5) (MPa)	***Error***	I_0(numerical) (MPa·ms)	I_0(Eq. 6) (MPa·ms)	***Error***
0.1	1.50	1.51	***0.5%***	10.60	10.65	***0.5%***
0.2	1.50	1.48	***-1.5%***	11.00	10.84	***-1.5%***
0.3	1.40	1.37	***-2.0%***	10.80	10.67	***-1.2%***
0.4	1.20	1.19	***-0.6%***	10.20	10.15	***-0.5%***

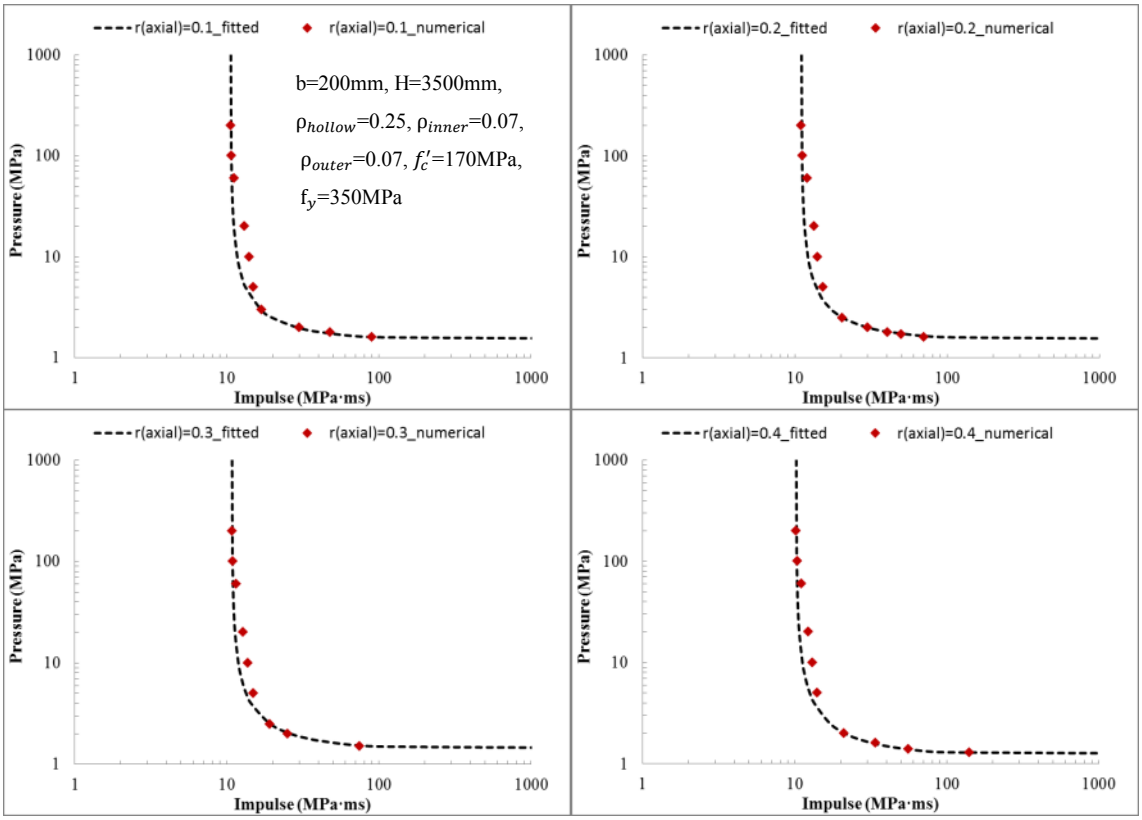

Fig. 14: Numerically derived pressure and impulse data points for different axial load ratio

4.4 Hollow section ratio, ρ_{hollow}

The hollow section ratio, ρ_{hollow}, is defined as $\frac{b_{inner}}{b_{outer}-2t_{outer}}$, where b_{outer} and b_{inner} are the outer and inner side length, respectively and t_{outer} is the thickness of the outer steel tube. In this paper, four hollow section area ratios, which are obtained by changing the inner side length while keeping the rest parameters constant, are discussed as shown in Table 6 and Fig. 15. It is evident that the pressure asymptote P_0 is not sensitive with the area of the hollow section. However, the impulse asymptote I_0 is stable until

ρ_{hollow} reaches 0.36 which indicates there is a change in the dynamic behaviour of the CFDST column. By examining the failure mode of the numerical model at different ρ_{hollow} values, it can be seen from Fig. 16 that when ρ_{hollow} is less than 0.36, flexural failure is the main failure model whereas signs of both shear and flexural failure are observed when ρ_{hollow} is greater than 0.36. It is well known that for the same structural component, the impulse asymptote is normally smaller for shear failure than flexural failure [35, 36].

Table 6: Effect of hollow section ratio on pressure and impulse asymptotes when D=0.5

ρ_{hollow}	P_0(numerical) (MPa)	P_0(Eq. 5) (MPa)	***Error***	I_0(numerical) (MPa·ms)	I_0(Eq. 6) (MPa·ms)	***Error***
0.04	1.20	1.20	***0.3%***	10.60	10.57	***-0.2%***
0.16	1.30	1.31	***1.1%***	10.90	10.99	***0.9%***
0.25	1.40	1.37	***-2.0%***	10.80	10.67	***-1.2%***
0.36	1.40	1.40	***0.3%***	9.50	9.53	***0.3%***

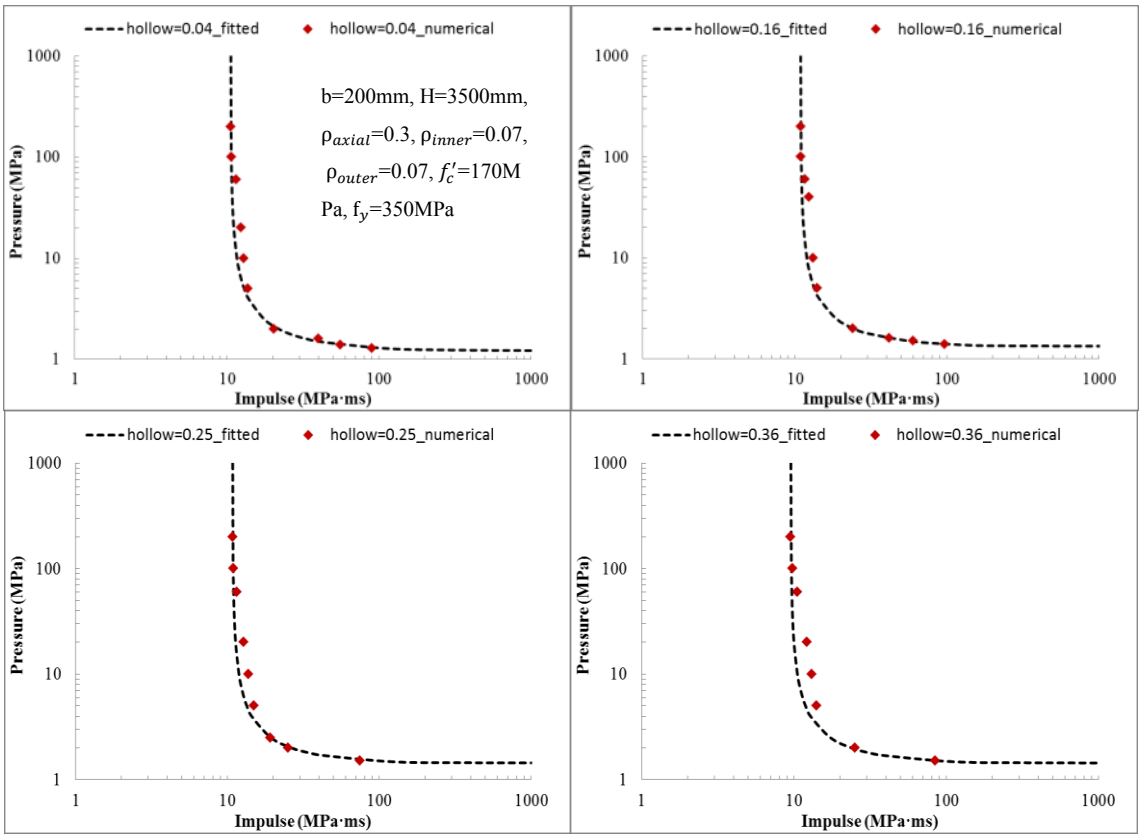

Fig. 15: Numerically derived pressure and impulse data points for different hollow section ratio

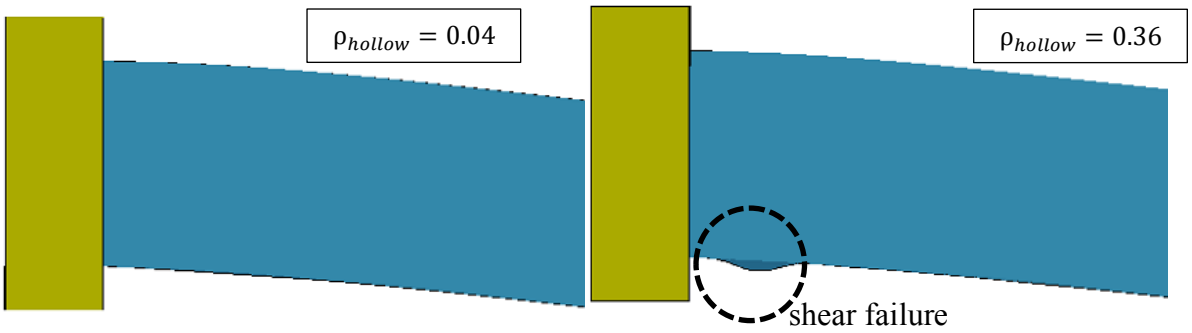

Fig. 16: Failure modes for different hollow section ratios

4.5 Inner tube steel ratio, ρ_{inner}

The inner tube steel ratio is defined as the cross-section area of the inner steel tube over that of the concrete filler, $\rho_{inner} = \frac{A_{inner\ steel}}{A_{Concrete}}$. The numerical results from Table 7 and Fig. 17 suggest that increasing the inner steel tube thickness alone does not exhibit a significant improvement on the pressure nor impulse asymptotes. This is because, first of all, the inner steel tube is not directly in contact with the blast load; also, the inner steel tube is the innermost part of the UHPCFDST column, the compressive/tensile stress distributed on which is therefore the smallest.

Table 7: Effect of inner tube steel ratio on pressure and impulse asymptotes when D=0.5

ρ_{inner}	P_0(numerical) (MPa)	P_0(Eq. 5) (MPa)	***Error***	I_0(numerical) (MPa·ms)	I_0(Eq. 6) (MPa·ms)	***Error***
0.041	1.30	1.29	***-0.5%***	10.10	10.03	***-0.7%***
0.055	1.36	1.33	***-2.0%***	10.40	10.34	***-0.5%***
0.070	1.40	1.37	***-2.0%***	10.80	10.67	***-1.2%***
0.085	1.45	1.41	***-2.7%***	11.20	11.00	***-1.8%***

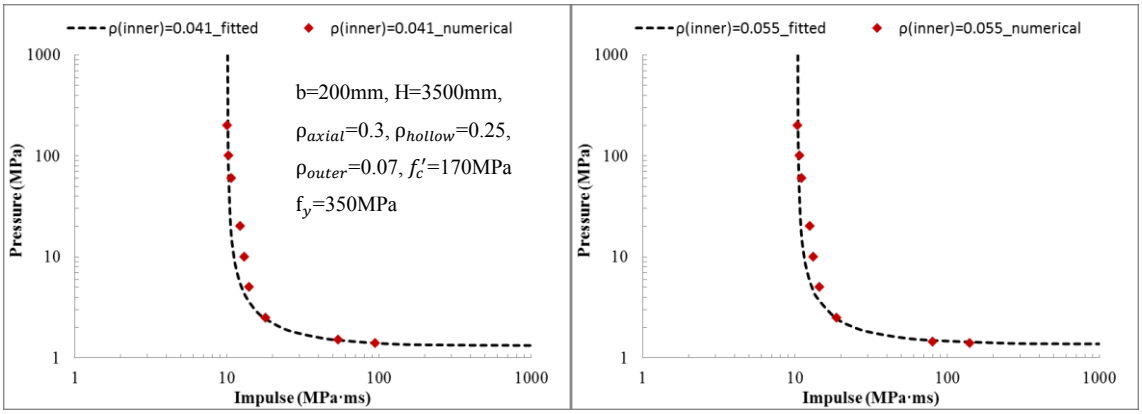

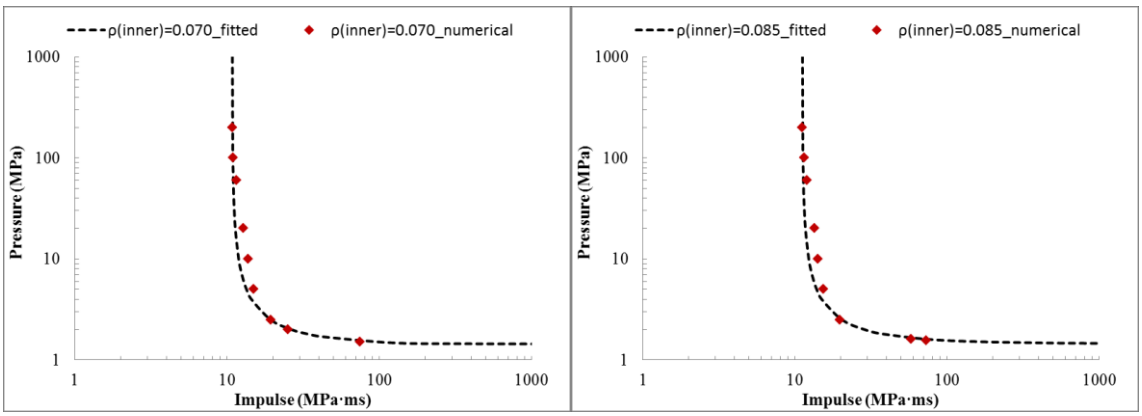

Fig. 17: Numerically derived pressure and impulse data points for different inner steel ratio

4.6 Outer tube steel ratio, ρ_{outer}

Similar to the inner tube, the outer tube steel ratio is defined as $\rho_{outer} = \frac{A_{outer\ steel}}{A_{Concrete}}$. One can see from Table 8 and Fig. 18 that, unlike the inner tube, the outer tube is in direct contact with the blast load; therefore it has a more noticeable impact on the pressure and impulse asymptotes, especially on the impulse asymptote. This indicates that increasing the outer tube steel ratio improves the flexural and shear resistance of a UHPCFDST column.

Table 8: Effect of outer tube steel ratio on pressure and impulse asymptotes when D=0.5

ρ_{outer}	P_0(numerical) (MPa)	P_0(Eq. 5) (MPa)	***Error***	I_0(numerical) (MPa·ms)	I_0(Eq. 6) (MPa·ms)	***Error***
0.080	1.10	1.09	***-1.2%***	8.30	8.26	***-0.5%***
0.105	1.20	1.23	***2.7%***	9.60	9.49	***-1.1%***
0.128	1.40	1.37	***-2.0%***	10.80	10.67	***-1.2%***
0.151	1.50	1.51	***0.3%***	12.00	11.80	***-1.7%***

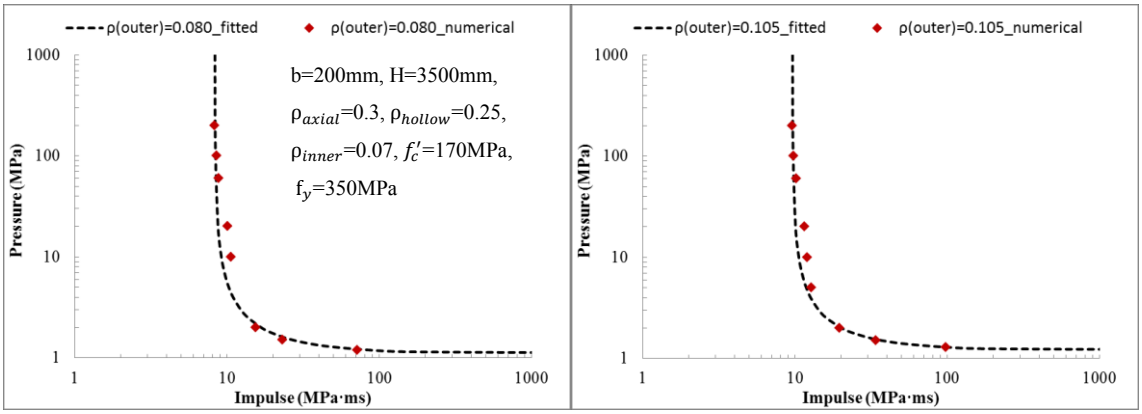

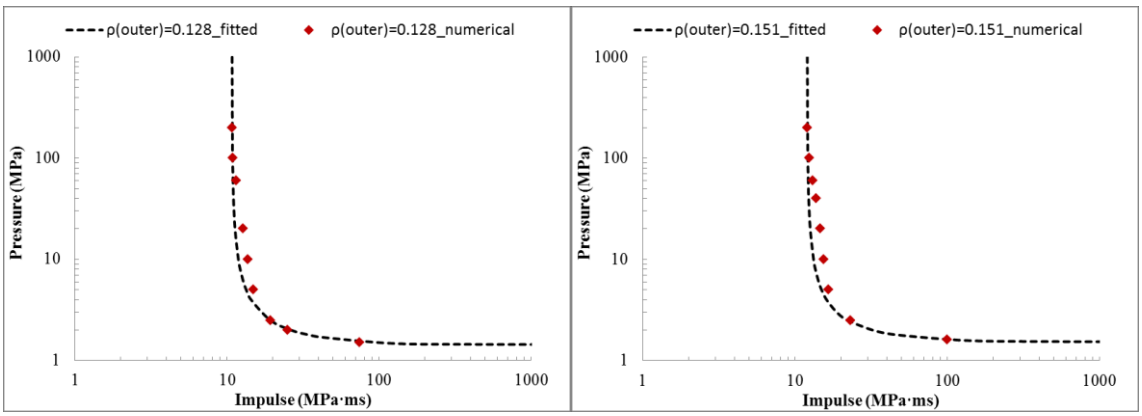

Fig. 18: Numerically derived pressure and impulse data points for different outer steel ratios

4.7 Concrete compressive strength, f'_c

CFDST columns with concrete strength of 140 MPa, 170 MPa and 200 MPa are considered. The numerical results are presented in Table 9 and Fig. 19. It is clear that increasing the concrete strength does not greatly increase the pressure or impulse asymptotes. This is owing to the fact that the concrete filler in a UHPCFDST column mainly contributes to the axial load-carrying capacity whereas its effect on the flexural or shear capacity is very limited. Similar results were also reported in other literatures [37, 38].

Table 9: Effect of concrete strength on pressure and impulse asymptotes when D=0.5

f'_c	P_0(numerical) (MPa)	P_0(Eq. 5) (MPa)	***Error***	I_0(numerical) (MPa·ms)	I_0(Eq. 6) (MPa·ms)	***Error***
140	1.30	1.27	***-2.2%***	10.40	10.40	***0.3%***
170	1.40	1.37	***-2.0%***	10.80	10.67	***-1.2%***
200	1.50	1.47	***-1.9%***	11.00	11.00	***0.3%***

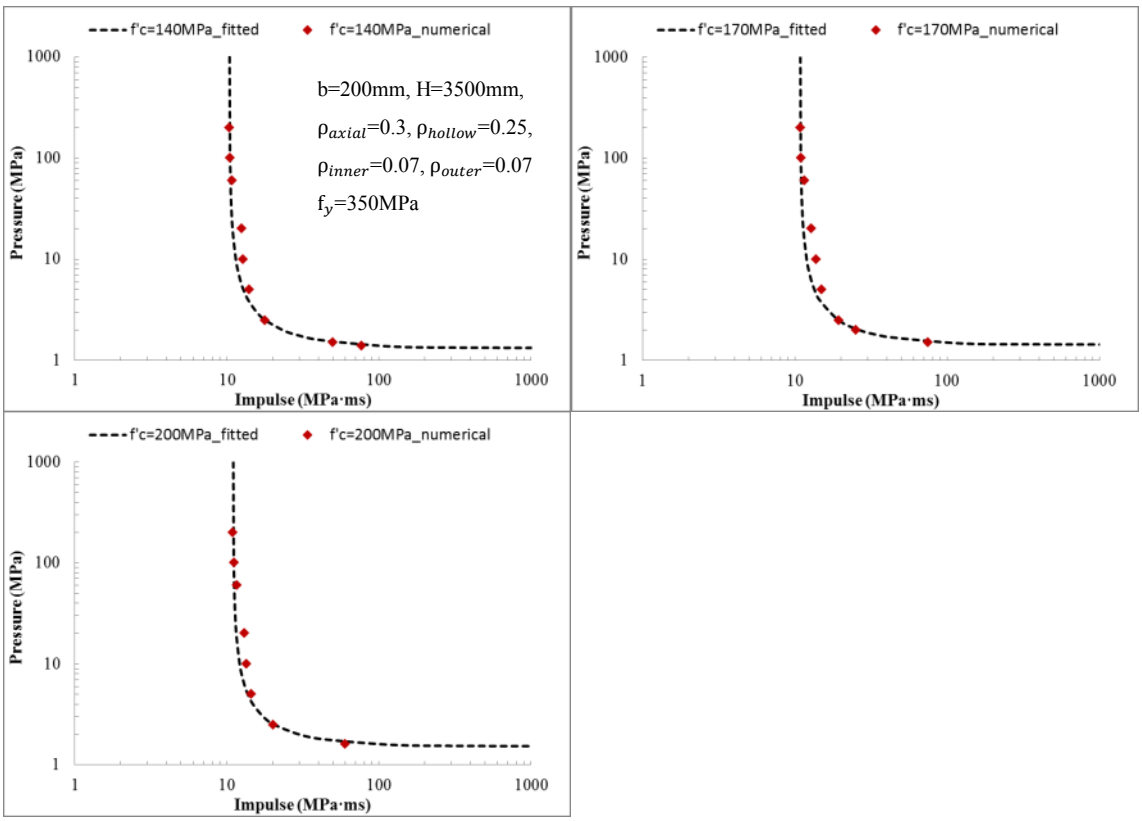

Fig. 19: Numerically derived pressure and impulse data points for different concrete strengths

4.8 Steel yield strength, f_y

In contrast to the concrete strength, the steel yield strength plays a more notable role in the pressure-impulse diagram of a UHPCFDST column as shown in Fig. 20. As expected, higher steel yield strength enhances both the flexural and shear resistance of a UHPCFDST column, therefore resulting in larger pressure and impulse asymptotes.

Table 10: Effect of steel yield strength on pressure and impulse asymptotes when D=0.5

f_y	P_0(numerical) (MPa)	P_0(Eq. 5) (MPa)	***Error***	I_0(numerical) (MPa·ms)	I_0(Eq. 6) (MPa·ms)	***Error***
280	1.20	1.21	***0.4%***	10.20	9.96	***-2.4%***
350	1.40	1.37	***-2.0%***	10.80	10.67	***-1.2%***
420	1.50	1.54	***2.5%***	11.50	11.38	***-1.0%***
525	1.80	1.79	***-0.7%***	12.50	12.45	***-0.4%***

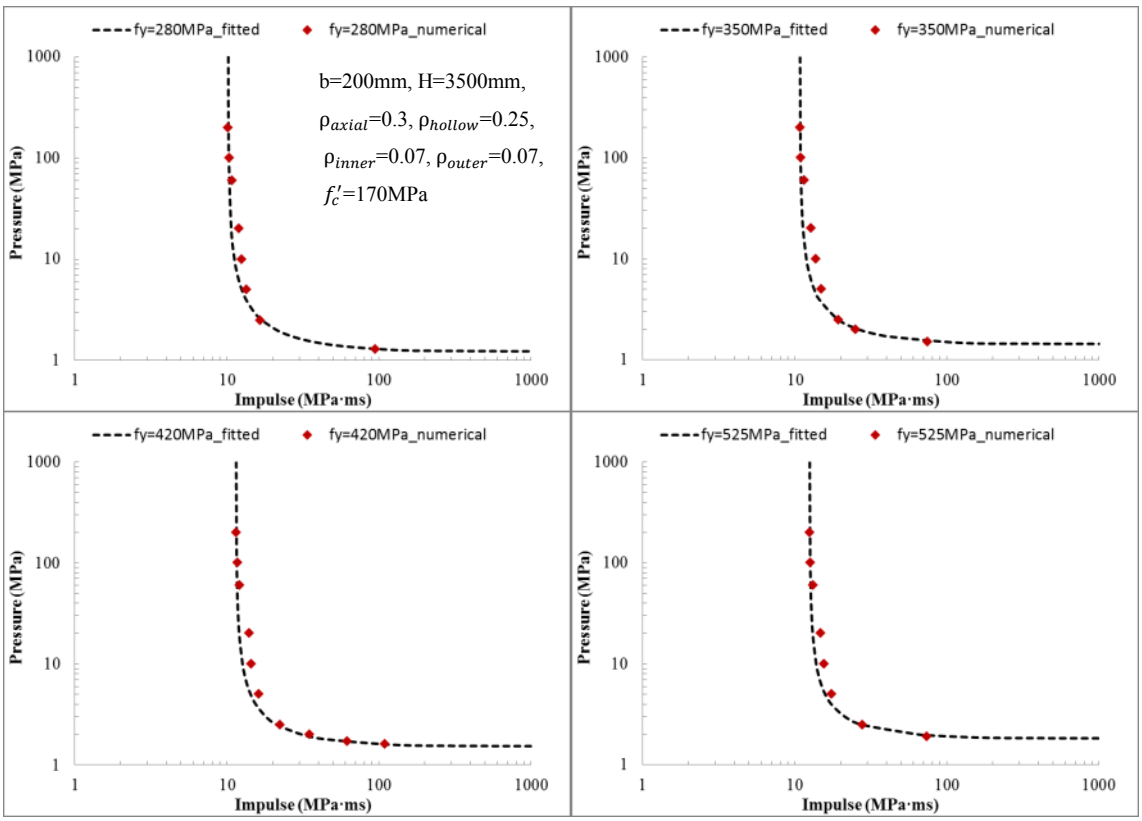

Fig. 20: Numerically derived pressure and impulse data points for different steel strengths

5. Normalisation of Pressure-Impulse Diagram

To normalise the pressure-impulse diagram of UHPCFDST columns, the simple hyperbolic function recommended by Oswald and Sherkut [39] are used. This method were adopted by [20] for RC columns and [21] for FRP strengthened RC columns, good results were achieved in both cases. The general form of this function can be written as:

$$(P - P_0)(I - I_0) = A(\frac{P_0}{2} + \frac{I_0}{2})^{\beta} \quad (3)$$

Where P_0 and I_0 are the pressure and impulse asymptotes of the UHPCFDST column, respectively; Coefficient A and β determines the shape of the hyperbola which can be obtained by fitting the numerically derived pressure-impulse points. Based on the numerical results of this paper, when A and β equate to 2.2 and 0.8 respectively, the constructed curve can fit through most data points. Therefore, equation (3) can be expressed as:

$$(P - P_0)(I - I_0) = 2.2(\frac{P_0}{2} + \frac{I_0}{2})^{0.8} \quad (4)$$

By using equation (4), a pressure-impulse diagram can be easily constructed if the pressure and asymptotes of a UHPCFDST column is given. The analytical formulae to predict the pressure and impulse asymptotes of a UHPCFDST column when the damage index D=0.5 can be derived by using the non-linear regression analysis in MATLAB. The pressure asymptote P_0 and impulse asymptote I_0 are derived as functions of square side length b, column height H, axial load ratio ρ_{axial}, hollow section ratio ρ_{hollow}, inner tube steel ratio ρ_{inner}, outer tube steel ratio ρ_{outer}, concrete compressive strength f_c', steel yield strength f_y. The functions are:

$$P_0 = 1.364\left(\frac{b}{200}\right)^{2.429} + 1.388\left(\frac{H}{3500}\right)^{-2.75} - 0.333\left(\frac{\rho_{axial}}{0.30}\right)^2 + 0.240\left(\frac{\rho_{axial}}{0.30}\right) - 0.105\left(\frac{\rho_{hollow}}{0.25}\right)^2 + 0.330\left(\frac{\rho_{hollow}}{0.25}\right) + 0.188\left(\frac{\rho_{inner}}{0.070}\right) + 0.763\left(\frac{\rho_{outer}}{0.128}\right) + 0.567\left(\frac{f_c'}{170}\right) + 0.831\left(\frac{f_y}{350}\right) - 3.863 \quad (5)$$

$$I_0 = 10.972\left(\frac{b}{200}\right)^{1.283} + 10.113\left(\frac{H}{3500}\right)^{-0.935} - 1.591\left(\frac{\rho_{axial}}{0.30}\right)^2 + 2.143\left(\frac{\rho_{axial}}{0.30}\right) - 2.112\left(\frac{\rho_{hollow}}{0.25}\right)^2 + 2.561\left(\frac{\rho_{hollow}}{0.25}\right) + 1.564\left(\frac{\rho_{inner}}{0.070}\right) + 6.456\left(\frac{\rho_{outer}}{0.128}\right) + 1.700\left(\frac{f_c'}{170}\right) + 3.562\left(\frac{f_y}{350}\right) - 24.700 \quad (6)$$

As listed in Tables 3-10, the error between the P_0 derived numerically and the P_0 predicted by equation (5) is 2% on average and 7% maximum; the error between the I_0 derived numerically and the I_0 predicted by equation (6) is also 2% on average but with the maximum error being 10.5%.

For easy comparison, the pressure-impulse curves constructed by using equation (4) are plotted in Figs. 12-15 and 17-20 alongside the numerically calculated data points. It is evident that the majority of the numerically derived data points closely follow the fitted curve calculated by the proposed analytical formulae developed in this paper.

6. Conclusion

This paper presents a numerical method of investigating UHPCFDST columns under blast loading. The numerical model is calibrated and validated against a series of blast tests

carried out by the authors previously and reasonably good agreement was achieved between the experimental and the numerical results.

To quantify the damage accumulated in the UHPCFDST column during blast loading, a damage criterion involving the residual axial load-carrying capacity is used and based on which, pressure-impulse diagrams are derived numerically. Parametric studies are also carried out to investigate the influence of key parameters such as cross-section dimension, column height, axial load ratio, hollow section ratio, inner and outer tube steel ratio, compressive strength of concrete and yield strength of steel tube. The cross-section dimension and column height have the most significant influence on both pressure and impulse asymptotes of the pressure-impulse diagram; the values for the pressure and impulse asymptotes peak at axial load ratio=0.2 and then gradually decreases as it further increases; The hollow section ratio does not exhibit notable impact until it reaches the critical level (i.e. 0.36); the increase in inner and outer tube steel ratios both slightly enhances the pressure and impulse asymptotes with this effect being more noticeable for outer tube; the increase in concrete and steel strength also both limitedly increases the pressure and impulse asymptotes.

Analytical formulae, as functions of column dimension and material properties, are developed which can be used to construct the pressure-impulse diagrams of UHPCFDST columns. The pressure–impulse curves calculated from the proposed analytical formulae are in good agreement with those derived from numerical simulations.

Acknowledgements

The research presented in this paper was jointly supported by the ARC Discovery Grant DP160104661, The National Basic Research Programme 2015CB058002 and Tsinghua Initiative Scientific Research Program (No.20131089347).

References

[1] Wei, S, Mau, S, Vipulanandan, C, and Mantrala, S, *Performance of New Sandwich Tube under Axial Loading: Experiment.* Journal of Structural Engineering, 1995. **121**(12): p. 1806-1814.

[2] Zhao, X-L, Tong, L-W, and Wang, X-Y, *CFDST stub columns subjected to large deformation axial loading.* Engineering Structures, 2010. **32**(3): p. 692-703.

[3] Uenaka, K, Kitoh, H, and Sonoda, K, *Concrete Filled Double Skin Circular Stub Columns under Compression.* Thin-Walled Structures, 2010. **48**(1): p. 19-24.

[4] Han, L-H, Huang, H, Tao, Z, and Zhao, X-L, *Concrete-filled Double Skin Steel Tubular (CFDST) Beam–columns Subjected to Cyclic Bending.* Engineering Structures, 2006. **28**(12): p. 1698-1714.

[5] Li, W, Han, L-H, and Chan, T-M, *Tensile behaviour of concrete-filled double-skin steel tubular members.* Journal of Constructional Steel Research, 2014. **99**: p. 35-46.

[6] Huang, H, Han, L-H, and Zhao, X-L, *Investigation on concrete filled double skin steel tubes (CFDSTs) under pure torsion.* Journal of Constructional Steel Research, 2013. **90**: p. 221-234.

[7] Lu, H, Zhao, X-L, and Han, L-H, *Testing of self-consolidating concrete-filled double skin tubular stub columns exposed to fire.* Journal of Constructional Steel Research, 2010. **66**(8): p. 1069-1080.

[8] Zhang, F, Wu, C, Li, Z-X, and Zhao, X-L, *Residual axial capacity of CFDST columns infilled with UHPFRC after close-range blast loading.* Thin-Walled Structures, 2015. **96**: p. 314-327.

[9] Zhang, F, Wu, C, Zhao, X-L, Xiang, H, Li, Z-X, Fang, Q, Liu, Z, Zhang, Y, Heidarpour, A, and Packer, JA, *Experimental study of CFDST columns infilled with UHPC under close-range blast loading.* International Journal of Impact Engineering, 2016.

[10] Wu, C, Oehlers, DJ, Rebentrost, M, Leach, J, and Whittaker, AS, *Blast Testing of Ultra-High Performance Fibre and FRP-Retrofitted Concrete Slabs.* Engineering Structures, 2009. **31**(9): p. 2060-2069.

[11] Li, J, Wu, C, and Hao, H, *Residual Loading Capacity of Ultra-High Performance Concrete Columns After Blast Loads.* International Journal of Protective Structures, 2015. **6**(4): p. 649-670.

[12] Xu, J, Wu, C, Xiang, H, Su, Y, Li, Z-X, Fang, Q, Hao, H, Liu, Z, Zhang, Y, and Li, J, *Behaviour of ultra high performance fibre reinforced concrete columns subjected to blast loading.* Engineering Structures, 2016. **118**: p. 97-107.

[13] Li, J, Wu, C, and Hao, H, *An experimental and numerical study of reinforced ultra-high performance concrete slabs under blast loads.* Materials & Design, 2015. **82**: p. 64-76.

[14] Baker, WE, Cox, P, Kulesz, J, Strehlow, R, and Westine, P, *Explosion hazards and evaluation*. 2012: Elsevier.

[15] Mays, G, *Blast effects on buildings: design of buildings to optimize resistance to blast loading*. 1995: Thomas Telford.

[16] Fallah, AS and Louca, L, *Pressure–impulse diagrams for*

elastic-plastic-hardening and softening single-degree-of-freedom models subjected to blast loading. International Journal of Impact Engineering, 2007. **34**(4): p. 823-842.

[17] Bao, X and Li, B, *Residual Strength of Blast Damaged Reinforced Concrete Columns.* International journal of impact engineering, 2010. **37**(3): p. 295-308.

[18] Zhang, F, Wu, C, Wang, H, and Zhou, Y, *Numerical simulation of concrete filled steel tube columns against BLAST loads.* Thin-Walled Structures, 2015. **92**: p. 82-92.

[19] Xiao, Y and Shen, Y, *Impact Behaviors of CFT and CFRP Confined CFT Stub Columns.* Journal of Composites for Construction, 2012. **16**(6): p. 662-670.

[20] Shi, Y, Hao, H, and Li, Z-X, *Numerical Derivation of Pressure–Impulse Diagrams for Prediction of RC Column Damage to Blast Loads.* International Journal of Impact Engineering, 2008. **35**(11): p. 1213-1227.

[21] Mutalib, AA and Hao, H, *Development of PI diagrams for FRP strengthened RC columns.* International Journal of Impact Engineering, 2011. **38**(5): p. 290-304.

[22] Yuan, W-b and Yang, J-j, *Experimental and Numerical Studies of Short Concrete-Filled Double Skin Composite Tube Columns under Axially Compressive Loads.* Journal of Constructional Steel Research, 2013. **80**: p. 23-31.

[23] Li, J and Hao, H, *Numerical study of concrete spall damage to blast loads.* International Journal of Impact Engineering, 2014. **68**: p. 41-55.

[24] Hallquist, JO, *LS-DYNA Keyword User's Manual.* Livermore Software Technology Corporation, 2007.

[25] Wu, Y, Crawford, JE, Lan, S, and Magallanes, JM, *Validation Studies for Concrete Constitutive Models with Blast Test Data*, in *13th International LS-DYNA Users Conference*2013: Detroit.

[26] Wu, Y, Crawford, JE, and Magallanes, JM. *Performance of LS-DYNA concrete constitutive models*. in *12th International LS-DYNA Users Conference*. 2012.

[27] Crawford, J, Wu, Y, Magallanes, J, and Lan, S, *Use and Validation of the Release II K&C Concrete Material Model in LS-DYNA*. Karagozian & Case, Glendale, 2012.

[28] Béton, CE-Id, *CEB-FIP model code 1990: design code*. 1993: Telford.

[29] Malvar, LJ and Crawford, JE, *Dynamic Increase Factors for Concrete*, 1998, DTIC Document.

[30] Ngo, T, Mendis, P, and Krauthammer, T, *Behavior of ultrahigh-strength prestressed concrete panels subjected to blast loading.* Journal of Structural Engineering, 2007. **133**(11): p. 1582-1590.

[31] Su, Y, Li, J, Wu, C, Wu, P, and Li, Z-X, *Effects of steel fibres on dynamic strength of UHPC.* Construction and Building Materials, 2016. **114**: p. 708-718.

[32] Jones, N, *Structural impact*. 2011: Cambridge university press.

[33] Kingery, CN, Bulmash, G, and Laboratory, USABR, *Air Blast Parameters from TNT Spherical Air Burst and Hemispherical Surface Burst*. 1984: Ballistic Research Laboratories.

[34] Zhao, X-L, Han, L-H, and Lu, H, *Concrete-filled tubular members and connections*. 2010: Spon Press London.

[35] Xu, J, Wu, C, and Li, Z-X, *Analysis of direct shear failure mode for RC slabs*

under external explosive loading. International Journal of Impact Engineering, 2014. **69**: p. 136-148.

[36] Krauthammer, T, Astarlioglu, S, Blasko, J, Soh, T, and Ng, P, *Pressure–impulse diagrams for the behavior assessment of structural components.* International Journal of Impact Engineering, 2008. **35**(8): p. 771-783.

[37] Han, L-H, Hou, C-C, Zhao, X-L, and Rasmussen, KJ, *Behaviour of high-strength concrete filled steel tubes under transverse impact loading.* Journal of Constructional Steel Research, 2014. **92**: p. 25-39.

[38] Zhang, F, Wu, C, Zhao, X-L, Li, Z-X, Heidarpour, A, and Wang, H, *Numerical modeling of concrete-filled double-skin steel square tubular columns under blast loading.* Journal of Performance of Constructed Facilities, 2015. **29**(5): p. B4015002.

[39] Oswald, C and Sherkut, D, *FACEDAP theory manual Version 1.2.* Omaha. Nebraska: US Army Corps of Engineers Omaha District, 1994.

Chapter 4 – Concluding Remarks and Recommendation for Future Work

Conclusion

This thesis mainly presented two approaches, namely experimental investigation and numerical analysis, to investigate the dynamic behaviours of concrete-filled tubular columns under blast loading.

For the experimental program, a close-range blast experiment was firstly carried out to investigate the behaviours of ten UHPCFDST specimens with both square and circular cross-sections when subjected to blast loading. Some of the test specimens were then taken back to the laboratory for the residual axial load-carrying capacity test.

As for the numerical analysis, numerical models were developed for normal-strength concrete filled CFST and CFDST columns as well as for ultra-high performance concrete filled CFDST columns. These numerical models were validated against the test data from the previously mentioned blast experiment and showed reasonable agreement. In addition, the proposed numerical models were then used to conduct a series of parametric studies to determine the influence of column dimensions to its blast-resistance. Finally, based on the results from the parametric studies, analytical formulae to construct pressure-impulse diagrams for UHPCFDST columns were also derived which can be used to quickly assess the survivability of a UHPCFDST column under a given blast load.

The major findings and contributions arise from this research are shown below:

1. UHPCFDST columns demonstrate the ability to withstand close-range blast loading without showing signs of catastrophic failure. After the blast tests, there was no obvious sign of spalling damage on the concrete filler after the blast tests and only minor flexural cracks of no more than 0.5 mm width can be seen on the tensile zone. The steel tubes also showed no sign of local buckling, thus suggesting UHPCFDST columns were able to remain overall of global flexural response under blast loading as opposed to localised failure which can be often observed on conventional reinforced concrete structures or steel structures.

2. UHPCFDST columns are able to retain a large portion of its original axial-load carrying capacity even after being subjected to severe blast loading (i.e. more than 60% in the current research), making them ideal for structures that are high-value targets for terrorists. During the residual axial-load carrying capacity tests, localised buckling failure of the outer steel tubes at mid-span and/or column ends always occurred for square CFDST whereas for circular CFDST, localised buckling failure occurred when the damage level was low and steel rupture happened when the damage level was high. The failure modes were similar to those of CFST members subjected to damage caused by large deformation cyclic loading.

3. Intensive numerical simulations have been carried out through the finite element tool LS-DYNA to investigate the behaviours of UHPCFDST columns under both static and blast loading conditions. The numerical models were firstly calibrated by using a number of laboratory tests and were then validated against a number of tests including the previously mentioned blast tests. In general, good agreement was achieved between the numerical and experimental results – on average, 1% error when validated against the peak lateral load during the three point bending test and 10% error when validated against the peak deflection during the blast test.

4. Based on the proposed numerical models, comprehensive parametric studies have been conducted to study the influence of column dimensions to the blast-resistance. It can be concluded that 1) the increase in explosive charge weight causes a larger mid-span deflection with this effect being more noticeable on axial-load-free columns rather than axially-loaded columns; 2) within a certain limit, the increase in the axial load ratio slightly reduces the mid-span deflection. However, if it increases beyond the critical limit, a significant increase in the mid-span deflection or even structural instability can be caused due to the P-Δ effect; 3) if the area of the hollow section in a UHPCFDST column accounts for less than 25% of the total

cross-sectional area, there are no notable differences in the behaviours of the UHPCFDST columns. Otherwise, a significant increase in the deflection can be observed along with a notable change in the period of oscillation; 4) the increment in inner and outer steel tube thickness both result in smaller mid-span deflections, however, with this effect being more noticeable on outer steel tube than inner; 5) the behaviours of UHPCFDST columns under blast loading are mainly dominated by the shape of outer steel tube whereas the inner steel tube geometry does not have a significant impact

5. Analytical formulae, as functions of column dimension and material properties, are proposed which can be used to quickly construct the pressure-impulse diagrams of UHPCFDST columns. The pressure-impulse diagrams calculated from the proposed analytical formulae are in good agreement with those derived from the numerical simulations with the average error being 2% only.

Recommendations for future work

On top of the current research, further improvement can be made in the future study in the following aspects:

1. Due to time and budget, only a very limited number of parameters are possible to be investigated during the blast experiment. Since the experimental results suggest both square and circular UHPCFDST columns are affected by those parameters in a similar manner, it is therefore recommended that the future study should focus on one cross-section geometry only which allows more parameters to be investigated.

2. In the current research, the explosive is only placed right above the centre of each specimen; however, in situations such as car bombing or suicide bombing, the

explosive is normally detonated near the lower end of a column, therefore the future research could study the effect of explosive location.

3. The LS-DYNA material model used for UHPC in this thesis is obtained by tuning the parameters of a concrete constitutive model that is developed specifically for normal-strength concrete. Although validated against a number of laboratory and blast tests, the model's applicability beyond these validation limits cannot be guaranteed and thus require further investigation.

4. In order to numerically generate pressure-impulse diagram, the failure criterion must be defined. In the current research, a UHPCFDST column is considered failed once its axial load-carrying capacity is halved. It should be noted that the definition of column failure is application specific; therefore the standard adopted herein may not be suitable for other studies. It is recommended that the future study could adopt different damage criteria (e.g. support rotation) and then compare the differences.

5. To construct P-I diagrams, two main assumptions were made: 1) all the applied pressure-time histories were simplified to triangular shape with the peak pressure and impulse kept the same as the original shape; 2) the blast load was assumed to be uniformly distributed along the length of the specimen. The potential issue of having these two assumptions is that when the given blast loading lies within the impulsive loading regime, the peak pressure is usually very large with an extremely short duration. This type of impulsive loading is often resulted from an explosive being detonated at a very close distance, therefore the loading would rapidly decay along the span and in such circumstance and localised damage is usually the governing failure mechanism which conflicts with the aforementioned assumption (2). Improvement can be done in the future by incorporating localised failure into the current model. However, the author believes that this will be extremely time

consuming as the spatial variation of loading needs to be included, thus many more iterations will be required to obtain a P-I diagram.